Polymer electrolytes based on ionic liquids for lithium batteries

Priew Eiamlamai

UNIVERSITÉ DE GRENOBLE

THÈSE

Pour obtenir le grade de

DOCTEUR DE L'UNIVERSITÉ DE GRENOBLE

Spécialité : **Matériaux, Mécanique, Génie civil, Electrochimie**

Arrêté ministériel : 7 août 2006

Présentée par

Priew EIAMLAMAI

Thèse dirigée par **Jean-Yves SANCHEZ** et
codirigée par **Cristina IOJOIU**

préparée au sein du **Laboratoire d'Electrochimie et de Physico-chimie des Matériaux et des Interfaces**
dans **l'École Doctorale I-MEP 2 (Ingénierie – Matériaux, Mécanique, Energétique, Environnement, Procédés, Production)**

Electrolytes polymères à base de liquides ioniques pour batteries au lithium

Thèse soutenue publiquement le **20 février 2015**,
devant le jury composé de :

M. André VIOUX Professeur à l'Institut Charles Gerhardt, Montpellier	Président/Examinateur
M. Thierry HAMAIDE Professeur à l'Université Claude Bernard Lyon 1	Rapporteur
M. François TRAN-VAN Professeur à l'Université de Tours	Rapporteur
M. Jean-Yves SANCHEZ Professeur à l'Université de Grenoble	Directeur de thèse
Mme Cristina IOJOIU Chargé de Recherche au CNRS, LEPMI	Co-directrice de thèse
Mme Laure COINTEAUX Ingénieur de Recherche à Grenoble INP	Invitée

Acknowledgement

It's always hard to acknowledge so many people and their contribution to my PhD research work at Grenoble, as they all deserve my deepest thanks and appreciation for their help.

First and foremost I would like to express the deepest gratitude to my supervisor Professor Jean-Yves SANCHEZ for allowing me to work within his research group, his valuable advices and also for sharing his vision and experiences.

Equally, a very great 'Thank you!' has to go to my co-supervisor, Dr. Cristina IOJOIU. Her expert guidance helped me to overcome the obstacles from the experimental work and made all presentations corrections for thesis and project meeting, as well as the redaction of the manuscript of my thesis work.

My thanks also go to my doctoral dissertation committee, Prof. André VIOUX, Prof. Thierry HAMAIDE, Prof. François TRAN-VAN and Dr. Laure COINTEAUX for reading the manuscript and providing many valuable comments that improve the contents of this dissertation.

I want to thank Jean –Claude LEPRETRE and Fannie ALLOIN for their kind concern and discussion concerning the electrochemical investigation, especially the cyclic voltammetry.

A part of diffusion coefficient and transference number investigation of my research work would not been accomplished without the support of Renaud BOUCHET, Priscillia SOUDANT, Patrick JUDEINSTEIN and in particular Lavinia ASTRATINE who also tested the electrochemical stability of my samples and was always helpful and cheered me up throughout the period of thesis redaction.

I gratefully acknowledge the funding source, The Thai Royal Government, which made my PhD life in France possible. In addition, I thank to SLiM project that allowed me to join in their project and also supported the research work.

I have also been fortunate to have a great group of friends in Grenoble; this includes my classmates during my master degree study at Joseph Fourier University (UJF). I would like to express my thanks to my lab colleagues in ELSA research group for their friendship and help during my thesis work as well as the activities outside the laboratory. And also, all members in

Thai student society in Grenoble from the past to present who shared both good and bad experiences and have had the good memories together over the years.

Finally and most importantly, I wish to thank my “P” family (Peerapong, Pradab and Priu) for their moral support, unending love and for sharing the fun stories from home. That always made me happy during my long stay far from our home and helped to move on from any of the tough moments in my life. Thank you!

Contents

Introduction

The growing market of electric transportation i.e. electric vehicles, EV, hybrid electric vehicles, HEV, Plug-in Hybrid Electric Vehicles, PHEV, motivates a neat improvement of the safety as compared to the worldwide existing 4C (Computer, Cellular Phone, Camcorders, Cordless tools) market. So, solvent-free batteries currently regain attention. This is the case of solid-state batteries, made of inorganic solid components, and of batteries using solvent-free polymer electrolytes.

With regard to the security concerns, solvent free polymer electrolyte films are very attractive in particular those made from poly(oxyethylene) (POE) host polymer. POE has outstanding ability to solvate lithium cation. It suffers however of various handicaps, namely (i) a high crystallinity that penalizes the electrolyte conductivity below the melting temperature (ii) a mechanical strength that vanishes following the polymer electrolyte melting and (iii) a stability in oxidation limited to roughly 3.9 V vs Li/Li^+. In addition to the high performances such as the thermo mechanical, chemical, electrochemical properties, a special attention has to be paid to ion transport. Operation of a battery based on solvent-free polymer electrolyte is partly conditioned by its melting temperature as the conductivity occurs mainly at the amorphous state. The architecture modification of POE is one of the routes to decrease the crystallinity but does not allow overcoming the bottleneck of a low cationic transference number, T^+, in POE electrolytes. The use of commercial ionic liquids is one of the routes to get sufficient conductivities at low temperatures but, once again, T^+ remains low. Furthermore these ionic liquids, which benefit to the conductivity, are based on tetraalkyl ammonium that do not participate in the electrode reactions. We have therefore directed our researches towards lithium-conducting ionic liquids. Hence, this thesis work proposes to address these issues by designing new ionic liquid lithium salts containing the oxyethylene moiety and the perfluorosulfonate/ sulfonimide anion. Consequently, the influences of (i) the number of oxyethylene units (ii) the different chemical structures and (iii) the anion on their intrinsic performances and those of the related polymer electrolytes were investigated.

This is one part of the LEPMI contribution to the 'SLiM' ANR project which has been carried out in collaboration with four academic partners (LEPMI, CMOS : Chimie

Moleculaire et Organisation du solide-Montpellier, IMN : Institut de Matériaux Jean Rouxel-Nantes, and MATEIS : MATEriaux Ingénierie et Science-Lyon).

This manuscript is divided into 4 chapters as follows;

The first chapter will introduce the overview about the secondary batteries, in particular, lithium batteries including the basic aspect and a brief review on different electrolytes. Then, the progresses in the development of 'solid' electrolytes such as polymer electrolytes especially based on poly(oxyethylene) host polymer are mentioned. The key issues from literature reviews initiated the motivation to improve the electrochemical performances i.e. ion conduction and cationic transference numbers of polymer electrolytes as well as the mechanical ones.

The second chapter will be focused on the effect of oxyethylene moiety (mPEG) addition on the aromatic lithium salt ($PhSCF_2CF_2SO_3Li$) which was previously studied by E. Paillard (thesis, INPG, 2008). The key performance like the cationic transference number should be improved and approached to the ideal value 1 by immobilizing or slowing down the anions. The comparative performance of a family of aromatic oligoether lithium salts varying the number of oxyethylene units will be discussed with regard to the characterization data. This chapter also demonstrates the intrinsic properties of liquid-viscous lithium salts.

Apart from the study of a family of aromatic lithium salts in chapter 2, **the following chapter** will also discuss about the influence of oligooxyethylene moiety end-capped with aliphatic lithium salts as well as the difference of anion functional group between sulfonate and sulfonimide on their properties. The aliphatic lithium salts will be incorporated in two different polymer matrix systems to investigate their performances. Additionally the neat salts (without any added polymer or solvent) will be characterized. Moreover, the performance comparison between aromatic and aliphatic lithium salt will be also mentioned. Additionally, it will also comparatively study the influence of the anionic function of the lithium salts prior to their incorporation on mPEG oligomers: thermal, mechanical, electrochemical properties as well as the ion transport properties i.e. conductivity and transference number in the same host polymers as used in both previous parts. Perfluoroalkane sulfonate (LiTPSN) and sulfonimide (LiTPSM) lithium salts are named as the salts which will be used in the chapter and their performance investigation will be presented in the form of the publication as well.

The performance characterization of all salts will be started with the neat salt and followed by the salt dissolved in linear and poly(oxyethylene) network host polymers respectively for each chapter.

The important points carried out from all chapters will be sum up into the **general conclusion** part and some interesting points which could be further deepened will be discussed in the **perspectives**.

The last chapter will present the protocols of synthesis for all materials and the experimental procedures for all characterizations employed to carry out during this thesis work.

I. Literature review

In a domain of the generating and storing electrical energy devices, batteries are always mentioned due to their usability in a variety of applications. They can be found in many vehicles and portable electronic equipments related to our lives in this modern world. However, despite they are expanded to the worldwide market, the development of batteries exhibiting high durability and composed on environmentally friendly components is still under progress. Thus many academic research groups and industrial R&D laboratory are focused on the improvements of lithium battery technology.

Basically, these chemical-electrical energy conversion devices are composed of two electrodes and an electrolyte in a container called “cell”. In general, batteries are categorized to two different types by the ability or inability of the rechargeable process: Primary batteries (non-rechargeable batteries) and secondary batteries (rechargeable batteries).

This chapter will focus on the secondary lithium batteries and in particularly it will give on overview on the main progress in the development of polymer electrolyte. In the first part some basic aspects on lithium batteries are presented followed by a brief review on different electrolytes. The polymer electrolytes based on poly(oxyethylene) and lithium salts are then largely discussed and finally the motivation of my PhD is presented.

I.1. Overview of batteries

General background

Secondary batteries are electrochemical energy storage devices that consist of three key components; a positive electrode (improperly called cathode), a negative electrode (improperly called cathode), and an electrolyte. They directly convert stored chemical energy in electrical energy through electrochemical reactions which are called oxidation and reduction. Moreover, these reactions are electrically reversible, when a voltage is applied to the battery. This point justifies the difference between the secondary batteries which can be recharged many times and the primary batteries which are discarded after using only once. Figure 1.1 represents the diagram of working and component positions of secondary battery during discharge and charge.

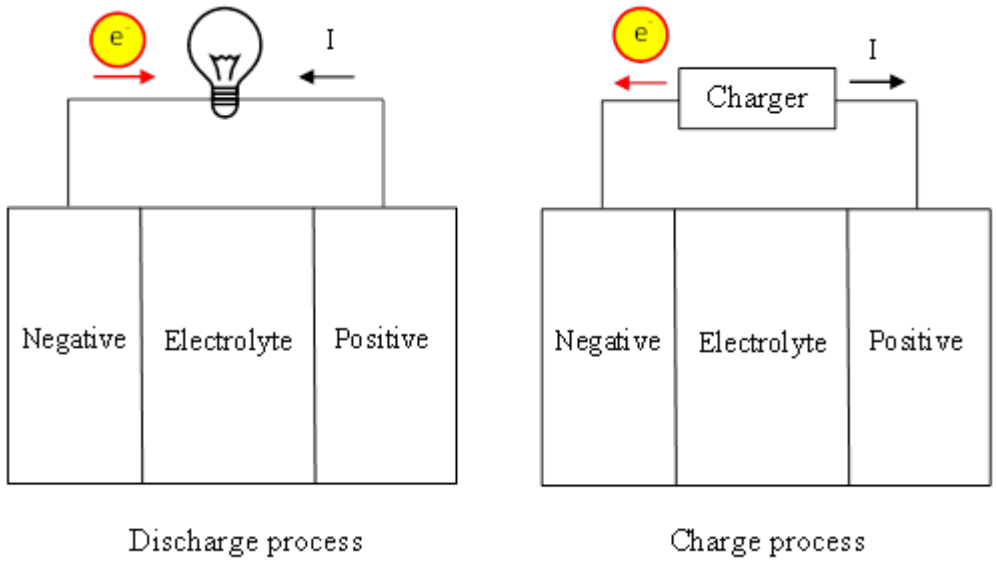

Oxidation: Reductor ⟶ Oxidant + n e^- **Reduction**: Oxidant + n e^- ⟶ Reductor

Figure 1.1. Schematic representation of one battery during the discharge and charge.

During discharge, an oxidation reaction occurs at the negative electrode/electrolyte interface which can be called 'anode'. This produces the positively charged ions (i.e. Li^+) that are moving from anode to cathode while the electrons pass via the external circuit to the positive electrode that can be called cathode. The reduction of positively charged ions (i.e. Li^+)

is carried out at the positive electrode. On the contrary, when the battery is charged, the oxidation – reduction will occur at the reverse direction as the discharging process.

I.2. Advantages and disadvantages of secondary batteries

Over several years, the rechargeable batteries have been available and grown in the battery market because of their, advantages when comparing with the primary. Some examples are presented here down: [1]

- Cost: The secondary batteries are used much longer time because they can be recharged many times while the primary batteries have to be replaced after the first discharge
- Performances: in terms of capacity, energy density (weight & volume) and self-discharge are lower in rechargeable batteries. These later however make continuous progresses and, obviously, the energy supplied by a rechargeable battery during its lifetime significantly exceeds that of non-rechargeable battery.
- Environmental impact: Producing less waste and toxic mineral

But also, they still have some weak points;

- Safety: Even though the rechargeable batteries are less toxic, they still contain some toxic materials. Dangerous trash and special care are still needed for such batteries
- Cost for purchasing at the first time: more expensive than non-rechargeable batteries.

I.3. Fundamental Thermodynamics

In order to understand how a battery works, the fundamental of thermodynamics and electrochemistry must be introduced.

Here, we consider batteries which consist of a lithium metal Li^0 and a vanadium oxide (V_2O_5) as negative and positive electrodes, respectively. These rechargeable batteries were replaced by Lithium-ion batteries from roughly 1992. The alone commercial batteries based on a Li^0 negative are lithium-polymer batteries, LPB, which address electric transportation and stationary applications but, operating at high temperatures are unadapted to electronic devices. LPB use LFP instead of vanadates as positive.

The oxidation reaction occurs at the negative electrode during the discharge:

$Li \longrightarrow Li^+ + e^-$

$E^- = E^0_{Li+/Li} + (RT/F) \ln (a_{Li+}/a_{Li})$

where $E^0_{Li+/Li}$ is a standard potential of Li^+/Li compared with Standard Hydrogen Electrode (-3.1 V/SHE), T is the absolute temperature (K), R is an ideal gas constant (8.314 $Jmol^{-1}\ K^{-1}$), F is the Faraday's constant (96500 $Cmol^{-1}$) and a_i is a chemical activity for the relevant species i, in our case Li

The reduction reaction involves at the positive electrode during the discharge:

$4Li^+ + 4e^- + LiV_3O_8 \longrightarrow Li_5V_3O_8$

$$E^+ = E^0_{4Li^+ + LiV_3O_8/Li_5V_3O_8} + \frac{RT}{F}\ln\left(\frac{a^4_{Li^+} a_{LiV_3O_8}}{a_{Li_5V_3O_8}}\right)$$

The activity of pure solid specie is 1 so, $a_{LiV_3O_8} = a_{Li_5V_3O_8} = a_{Li} = 1$

Redox reaction: $4Li + LiV_3O_8 \longrightarrow Li_5V_3O_8$

- **Theoretical tension**

The theoretical tension of the battery (E^0) is standard electrode potential difference between positive and negative.

$$E^0 = E^0_{LiV_3O_8/Li_5V_3O_8} - E^0_{Li^+/Li}$$

- **Free enthalpy (Gibbs free energy)**

The Gibbs free energy change for the cell reaction is given by this simple relationship:

$$\Delta G^0 = -nFE^0$$

Where n = the charge number of the mobile species involved in the reaction

E = the voltage between the electrodes

F = Faraday's constant

- **Theoretical capacity**

The theoretical capacity of an electrochemical cell is determined by the quantity of electricity involved in the electrochemical reaction. It is denoted Q_{th} and is given by:

$$Q_{th} = xnF \ (Q_{th} \text{ in } C \text{ unit})$$

where x= number of moles of active materials involved in electrochemical reaction, n = number of electrons transferred per mole of reaction and F = Faraday's constant

The capacity is usually expressed in weight (or volume) and not in moles:

$$Q_{th} = \frac{nF}{3600M_r}$$

Where Mr = Molar Mass of active species. The capacity in the above formula is expressed in Ampere-hour per gram (Ah/g)

- **Theoretical energy**

Specific energy is defined as the energy per weight ($Wh.kg^{-1}$). The theoretical specific energy is the maximum energy that can be generated per total mass of cell reactants. The practical specific energy is much lower than the theoretical one and depends on the discharge region because the power varies in the function of the discharge capacity.

I.4. Secondary batteries; comparison of battery technologies

To improve the performances of secondary batteries, various types of such technologies have been developed. The comparison of characteristics of commonly used rechargeable batteries is shown in Table 1.1. Depending on the material of negative electrode they are classified into three types; lead (Pb) based, nickel (Ni) based and lithium (Li) based batteries.

Below is a short summary of comparative of different systems:

Table 1.1 Comparison of the performances of different battery types [2]

System (negative/positive electrodes)	Cell Voltage (V)	Theoretical specific capacity (practical) ($Ah.kg^{-1}$)	Theoretical volume capacity (practical) ($Ah.dm^{-3}$)	Theoretical specific energy (practical) ($Wh.kg^{-1}$)	Theoretical volume energy (practical) ($Wh.dm^{-3}$)	Cycles number
Aqueous electrolyte rechargeable batteries						
Pb/PbO_2	2.1 (2.0)	120 (18)	240 (58)	252 (35)	454 (70)	50-500
Cd/NiOOH	1.35 (1.2)	181 (29)	517 (83)	244 (45)	695 (100)	>500
MH/NiOOH	1.35 (1.2)	178 (63)	570 (200)	240 (75)	768 (240)	> 800
Nonaqueous electrolyte rechargeable batteries						
$Li_xC_6/Li_{(1-x)}CoO_2$	4.1 (4.1)	100 (37)	270 (98)	410 (150)	1013 (400)	> 800
Li/MnO_2	3.5 (3.0)	286 (40)	894 (88)	1001 (120)	3131 (265)	50-200
$*Li/V_XO_Y$	3.5 (2.8)	142 (122)	400 (342)	486 (342)	1396 (963)	200

- In LPB more than 800 cycles were performed with $*Li/V_XO_Y$ at 100% DOD. [3]

Lead and nickel based rechargeable batteries are examples of aqueous based electrolytes, lead acid batteries being available from more than 140 years. Current Pb/PbO_2 batteries are very reliable and less costly than other candidates. Their practical specific energy

is close to 35 Wh/kg. Their charge-discharge cycles vary from 50 cycles to 500 cycles depending on the design of the cell and, probably, to the charging protocols.

Cd/NiOOH, known as Nickel-Cadmium (NiCd) is a well-optimised battery, the most common cell for an alkaline electrolyte system. It was used for longtime even in portable electronic but its market shares dramatically decreased in the last decade. Very robust battery it suffers from two main drawbacks (i) a memory effect that implies a specific charge of the battery and (ii) a detrimental environmental impact related to the use of cadmium. Cd is highly toxic but can be almost quantitatively recycled. This recycling can be easily done with high capacity batteries but it can be feared that some of the small capacity batteries escape to the recycling. Nickel Metal Hydride batteries (NiMH) are also alkaline batteries having approximately the same voltage as NiCd but their practical specific energy increases with regard to NiCd from 45 to 75 Wh/kg. They allow overcoming the issue related to the use of Cd. They suffer two main drawbacks (i) their self-discharge rate is fairly high and (ii) they use rare-earth elements (AB5 or AB2 alloys) whose production is concentrated in China, thus submitted to geopolitical constraints. NiMH cell supplies several hundred charge-discharge cycles and are used in Hybrid Cars as for instance, Toyota Prius.

Rechargeable batteries with non aqueous and more generally aprotic electrolytes have been also widely developed and some of them are already available in the market. In most of them the electrolytes are based on organic solvents, in particular, a lithium salt dissolved in a mixture of ethylene carbonate and linear carbonates as dimethyl carbonate (DMC), diethylcarbonate (DEC), or ethyl methyl carbonate (EMC). These kinds of batteries provide excellent performances but they still needs improvements in term of security and cost. As example, $Li_xC_6/Li_{(1-x)}CoO_2$ cell has very long cycle life and high specific energy but unfortunately these materials are expensive. Additionally, this system raises security problems, which might be amplified by the flammability of the solvents (DMC and EMC have a low Flash Point, F_p), which can result in the cell burning.

A solution to overcome this problem consists in the replacement of Li_xCoO_2 by $LiFePO_4$ (LFP). LFP is safer and less costly than Li_xCoO_2but its redox potential ~3.5 V vs Li/Li^+ is detrimental does not allow obtaining sufficient energy density when lithium graphite is used as a negative electrode. Manganese oxides are also excellent candidates for Li batteries.

$LiFePO_4$ and other transition metal phosphates including vanadium have been proposed as cathode materials. They have promising performances in term of specific capacity, energy

density and cell voltage. In addition, they are cheaper and more environmental friendly than cobalt oxides.

I.5. Lithium batteries

Nowadays, lithium batteries have paid attention and increased global demand for the energy storage domain. The unique properties of lithium element are presented in Table 1.2. Lithium has the highest capacity, the lowest electrochemical potential (-3.04 V/SHE) and provides, for a given positive, the highest energy density.

Two types of lithium batteries have been developed: batteries based on Lithium metal negative, Li^0, and batteries based on graphite, LiC_6 i.e. lithium ion. Shifting from Li^0 to LiC_6 was motivated by the instability of Li^0, especially during charging [4]. There is roughly an order of magnitude between the theoretical capacity of Li^0 and LiC_6 but it must be emphasized than Li^0 is used in large excess with regard to the stoichiometry i.e. often 5 to 7 excess, so the gap in practical capacity strongly decreases. Li^0 has other advantages, namely (i) its electronic conductivity and (ii) its mechanical strength and ductility; these advantages making useless the use of carbon black and polymeric binders and allowing its easy calendaring. Although slightly lower in energy density than lithium metal, lithium-ion is safe, provided certain precautions are met when charging and discharging. In 1991, the Sony Corporation commercialized the first lithium-ion battery. Other manufacturers followed. The energy density of current lithium-ion batteries is typically triple of that of the standard NiCd; some prototypes reaching specific energies around 200 Wh/kg [5].

Table 1.2 Some properties of Lithium

Properties	**Lithium**
Equivalent weight (g/equiv.)	6.94
Reversible potential (V)	-3.045
Electronegativity	0.98
Specific gravity (g/cm^3)	0.53
Theoretical specific capacity (A.h/kg)	3,860

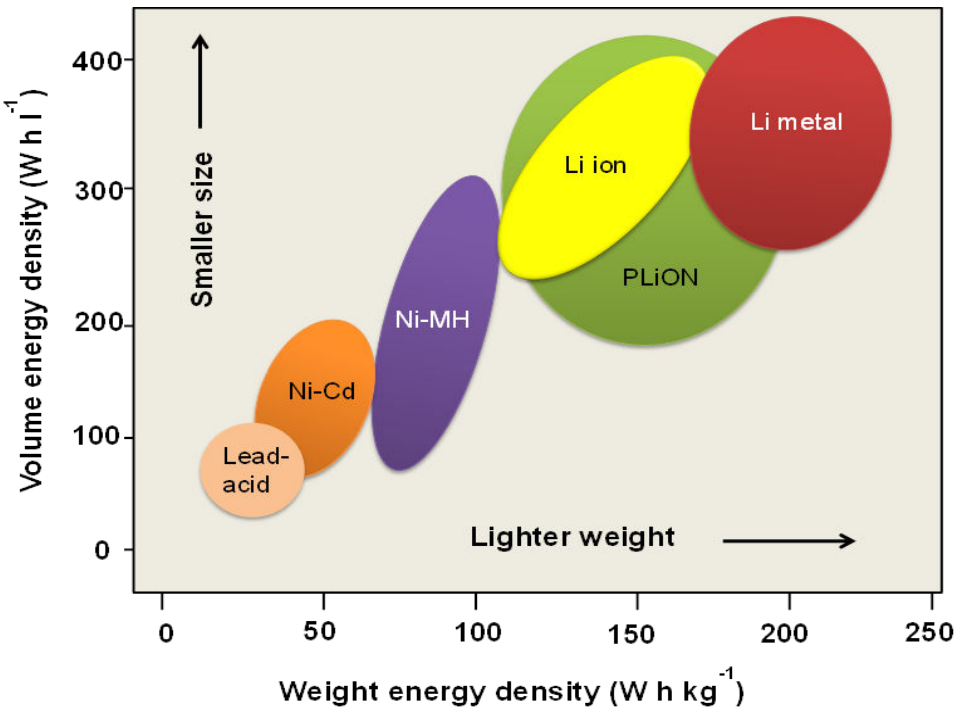

Figure 1.2. Energy density of different types of batteries [6]

Li-ion batteries consist generally of a porous separator, which is soaked with a liquid electrolyte or of a gelled polymer electrolyte, while rechargeable lithium batteries can only operate without liquid organic solvents i.e. solid state batteries made of inorganic materials (electrodes + electrolyte) or polymer batteries based on solvent-free polymer electrolytes. The solvent-free polymer design offers simplifications with respect to fabrication, ruggedness, safety and thin-profile geometry. Unfortunately, the solvent-free lithium-polymer batteries suffer from poor conductivity at low to medium temperatures, operating only around 80°C and, therefore, are unusable in electronic devices.

I.5.1. Lithium-ion batteries

In the figure 1.3 is schematically represented a lithium ion battery.

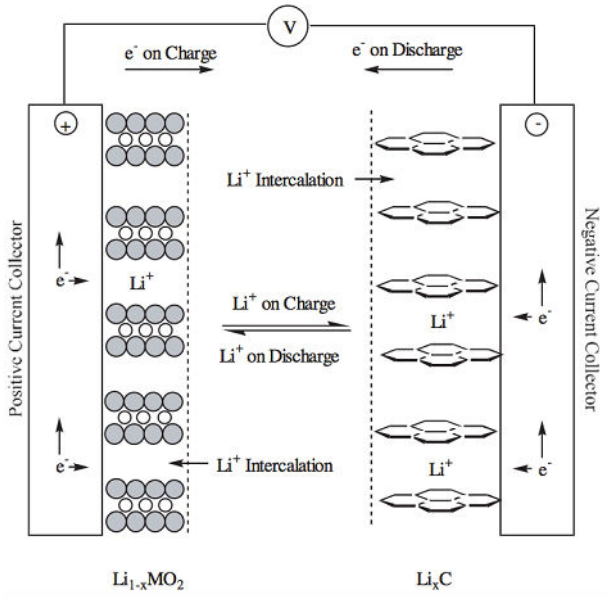

Figure 1.3. Schematic draw of Li-on battery [7].

Typically, the graphite and the transition metal oxide are used as the negative and positive electrodes, respectively. The electrochemical reactions are presented as follows:

Negative electrode half reaction: $Li_xC_6 \longrightarrow xLi^+ + xe^- + C_6$

Positive electrode half reaction: $xLi^+ + xe^- + Li_{(1-x)}CoO_2 \longrightarrow LiCoO_2$

Overall reaction: $Li_xC_6 + Li_{(1-x)}CoO_2 \longrightarrow LiCoO_2 + C_6$

Lithium-ion batteries are divided in two types according the used electrolytes:

- Liquid electrolyte: consisting of a molar solution of a lithium salt in a mixture of organic solvents that filled the porosity of a macroporous separator.
- Polymer gel electrolyte: consisting of a dense polymer swelled by a molar solution of a lithium salt in a mixture of organic solvents

I.5.1.1. Liquid electrolyte

Solvents

Conventional organic solvents for lithium ion batteries are carbonate-based solvents such as ethylene carbonate (EC) and propylene carbonate (PC). These cyclic carbonates have low vapor pressures, thus high Flash Point (Fp), high dielectric constant that favors the ion-pair dissociation but high viscosities that decrease the ion's mobility. Except in the case of some special carbons, PC exfoliates the graphite negative electrode and is therefore not used in Li-ion electrolytes. Thus, combination of cyclic carbonates e.g. EC and acyclic ones e.g. DMC, DEC or EMC are used to obtain high enough dielectric constant while moderating the viscosity. The physical properties of common carbonate solvents are listed in Table 1.3.

Table 1.3 Physical properties of organic solvents [8], [9]

Name	Melting Temperature (°C)	Boiling Temperature (°C)	Viscosity at 25 °C (cP)	Dielectric constant at 25 °C	Solubility parameter $(J\ cm^{-3})^{1/2}$
Ethylene carbonate (EC)	36.4	248	1.86 at 40 °C	89.6 at 40 °C	30.1
Propylene carbonate (PC)	-48.8	242	2.5	66.14	27.2
Dimethyl carbonate (DMC)	2.4	90	0.59	3.12	20.3
γ-butyrolactone (γ-BL)	-43.3	204	1.75	39	25.8

Lithium salts

Lithium salts incorporated in the organic solvent or polymer gel should be highly stable in such medium. In addition, they should provide high conductivities, thermal, chemical and

electrochemical stabilities, non-toxicity and low cost. Several salts are currently used such as $LiPF_6$, $LiAsF_6$, $LiN(CF_3SO_2)_2$, $LiBF_4$, LiBOB and $LiPF_6$ being the most used.

More information will be mentioned in the section of "Incorporation of lithium salt and ionic liquid in polymer electrolytes" (in the section I.8.3).

Liquid electrolytes

These liquid electrolytes can pose some safety concerns; perhaps the most widely reported of these is the flammability and volatility (low Fp) of the solvents. Under the right circumstances, the electrolyte in a Li-ion battery can ignite or even explode [10].

Alkyl carbonates, particularly the linear carbonates are flammable and can vaporize at temperatures that are attainable during battery operation [10], [11]. These kind of electrolytes have caused safety problems for Li-ion batteries and have complicated the deployment of Li-ion batteries for electric and hybrid cars [10], [12].

Also, at temperatures above ~ 60°C, the electrolyte solution used in mostly commercial Li-ion batteries can deteriorate [13]. The dissolved lithium salts can undergo chemical reactions with the solvents at these elevated temperatures, negatively affecting the batteries performance. Because these reactions are irreversible, the electrolytes properties are not fully restored even when the temperature is reduced, and the resulted products can pose additional safety issues.

I.5.1.2. Polymer gel electrolyte (PGE)

Gelled polymer electrolytes, also called ''plasticized polymer electrolytes', preceded polymer electrolytes and were early proposed by Feuillade [14] who patented in 1973 the concept of thin batteries.

Gel electrolytes are obtained by swelling a polymer matrix by the liquid electrolyte. The required properties are high ionic conductivity down to sub-ambient temperature, wide electrochemical stability window (with a stability in oxidation up to 4.5 V vs Li/Li^+) and sufficient dimensional stabilities. Among the host polymers used are homopolymers and copolymers including poly(oxyethylene) (POE) [15], poly(vinyl chloride (PVC) [16], Poly(acrylonitrile) (PAN) [17], polymethacrylonitrile poly(vinylene fluoride) (PVdF) [18] and

poly(vinylene fluoride -co-hexafluoropropylene) [19], [20]. Although the electrochemical stability is mainly governed by the liquid electrolyte contained into the polymer, the latter, as PAN [14], must be source of electrochemical instability. Our laboratory identified the polarized hydrogen of PAN repeat unit as the main source of instability and prepared copolymers of PMAN, where the previous hydrogen is replaced by a methyl group and found a neat improvement of the stability in reduction [21]. Thus, the interfacial resistance vs Li^0 of PAN gelled electrolytes was found to increase by 500% in 5 days while that of PMAN was constant over 10 days [22].

Among the above quoted polymers to be gelled POE has a stability in oxidation limited to 3.9-4V vs Li/Li^+ and above all has poor mechanical strength. Dealing with the halogenated polymers one can fear an instability in reduction (halogen-lithium exchange) and a possibility to undergo, in presence of bases, a dehydrohalogenation (reaction in chain). However the fluorinated polymers can be used in lithium-ion batteries based on graphite negatives [23]. According to their crystallinity of host polymers must be unsuited for a gel application: thus PVdF homopolymer leads once gelled by liquid electrolytes to very poor conductivities [24]. So PVdF homopolymer is well-adapted to a macroporous separator function when PVdF-HFP is unsuited for macroporous separator but suitable as host polymer of gelled polymer electrolytes.

I.5.2.Lithium-polymer batteries

The lithium polymer battery differs from other rechargeable batteries by the electrolyte it uses. The electrolyte is a plastic-like layer, which cannot conduct the electricity, but allows the exchange of ions. The advantages of this electrolyte are a thin film feature, non-volatility, non-flammability and safety. Wright et al. [25], [26] first demonstrated the ion conduction in poly(oxyethylene)/ alkaline salt complexes in 1973. Later, Armand, Duclot and Chabagno proposed polymer as electrolytes for lithium batteries. [27], [28].

These polymer electrolytes are solvent-free thus the accumulators have not the risk of solvent leakage. However, the dry lithium polymer suffers from poor conductivity. For several years now, academic and industrial research groups have unceasingly developed the polymer electrolyte for higher performances. This part will be more developed in the chapter I.8. Before some aspect concerning the role of solvents and the key aspects in the improvement of lithium battery electrolytes are shortly discussed.

I.6. Solvent in electrolytes of lithium batteries

The electrolyte, one of key components of the battery, is a pathway of lithium conduction between two electrodes. How it was presented below, usually, the lithium salt is dissolved in a solvent (organic, polymeric), and the interaction solvent-salt are crucial in determining the electrolyte performances. The main physical role of the solvent are considered as follows:

1. Dissolution of ions in solvent
2. Ion pair dissociation and solvation
3. Ion mobility

In order to understand the nature and the interaction force of solute and solvent in the solution, the dissolution mechanism and ion solvation will be mentioned.

In the fundamental chemistry, when one substance is dissolved into a solvent, a solution is formed. Solvent molecules arrange around solute molecules. Both substances interact each other at the molecule level. In the case of the salt, the solute is an ionic specie and the polar solvent are those with a molecule structure that contain dipoles, thus, the interaction between the solute and the solvent is an ion-dipole electrostatic interaction. The energy of solvation depends on the interaction force, in particularly, in the case of ionic solutes. The interaction force is inversely proportional to the squared distance between solute and solvent molecule. It means that the smaller ion has more interaction force resulting to perform more energy solvation with solvent molecule. As deal with solvents, the solvation by the electrostatic interaction is proportional to the dipole moment (μ) of solvent therefore, polar solvents such as water, nitrile, amide, etc. can strongly solvate ions.

Born proposed [29] the model of solvation of ionic compound by placing a charge in a spherical solvent cavity. The solvation energy is equaled to the electrostatic work for transferring the ion from vacuum to the medium. This is the difference in work to charge the ion in the two environments.

$$W_{Born} = -\frac{q^2 z^2}{8\pi\varepsilon_0}\left(1-\frac{1}{\varepsilon_r}\right)$$

Where q is elemental charge of electron, z is valence of ion concerned, ε_0 is relative permittivity in vacuum and ε_r is dielectric constant of solvent.

Moreover the dielectric constant is as important as the electrostatic interaction between solute and solvent molecules. Polar solvents have been found to have high dielectric constant resulting in polar molecules of these solvent can strongly solvate ions. Thus, the polar solvent can be used for ion solvation.

Thermodynamic dissolution of crystalline material (solute) in the solvent is represented via the cycle of Born Haber as follows:

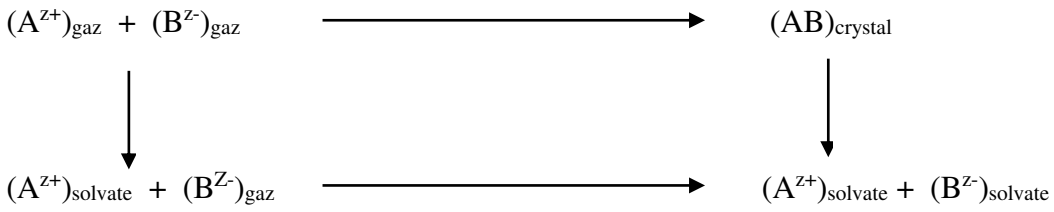

This cycle shows the dissolution of two ions (A^{z+}, B^{z-}). The activities of two species in saturated solution influence to the solubility which is determined by the sum of free enthalpy of solvation two ions.
The free energy of dissolution of a crystalline salt is given by:

$$\Delta G^{\circ}_{diss}(AB) = 2.3\ R.T.pKs = \Delta G^{\circ}_{solv}(A^{z+}) + \Delta G^{\circ}_{solv}(B^{z-}) - \Delta G^{\circ}_{crist}(AB)$$

From the equation of dissolution energy, the solubility is increased if the energy of solvation of ions is higher than that of crystal formation or $\Delta G^{\circ}_{diss} < 0$.

However, this model of Born cannot use to explain for all cases in reality, especially, small ions (radius < 0.1-0.2 nm) because such ions have other factors which should be considered for example; the influence of intense electric field of the neighbor. Therefore, the dielectric constant of ion has to be modified.

Also, the approach of Gutmann is mentioned [30], [31]. The chemical nature of solute and solvent is considered for this specific interaction such as the hydrogen bond formed between the protic solvent and doublet electronic solute donor.

The acceptor-donor interaction (Lewis acidity/basicity) corresponds to the formation of the coordination bond:

- between solvent donor molecule and solute acceptor (cation)

- between solvent acceptor molecule and solute donor (anion)

From this concept, the donor number (DN) and acceptor number (AN) of a good solvent should be thus high for interaction with cation and anion that contribute the dissolution and dissociation of salt.

I.7. Key aspects for the electrolyte improvement

I.7.1. Electrochemical stability

The electrochemical stability of an electrolyte is one of the important parameters when rechargeable lithium batteries are concerned. The instability in the electrolyte is known to show up irreversible reactions. The electrochemical stability window ordinarily expressed for the stability of the electrolyte should be capable of sustaining highly oxidative condition until the positive electrode potential (~ 5 V) and at the same time, until the potential of lithium or lithium graphite for the cathodic stability (0 V vs Li/Li^+). However, solvents and dissolved salts have an influence in the limitation of the stability. Therefore, solvents and salts should be selected to properly use for electrochemical stability investigation.

Acetonitrile is one of solvents commonly used which has good properties in the electrochemical potential domain e.g. moderate dielectric constant, fair donor number and low viscosity. Nevertheless, acetonitrile is replaced by cyclic carbonate compounds such as ethylene carbonate (EC) and propylene carbonate (PC) because of its toxicity and inflammability. Apart from the physical property of EC, it can produce an effective solid electrolyte interphase (SEI) formation on the negative electrode surface to ensure good cyclic stability. The SEI layer is formed by the inorganic and organic electrolyte decomposition product during the first charge for further degradation by blocking the electron transport and allowing the Li ion to pass through it [32]. However, the drawback of EC is its high viscosity and melting point. Linear carbonates are thus added to improve the physical properties of cyclic carbonate. On the other hand, the safety of this mixture is decreased because the mixture can be flammable easier. A co-solvent with a non-flammable additive has to be used for enhancing the security.

In addition to the influence on solvents affecting the electrochemical instability, the salt is also a significant factor. For instance, F. Kita et al. investigated the oxidation stability of

several salts with different fluoroalkyl chain lengths. They found that the oxidation potential of $C_8F_{17}SO_3Li$ (6.5 V) is higher than that of $C_4F_9SO_3Li$ (6.0 V) and CF_3SO_3Li (4.8 V), respectively and also an increase of fluoroalkyl group can provide higher oxidation potential comparing with Li/Li^+ i.e. $(C_8F_{17}SO_2)(CF_3SO_2)NLi$ (6.0 V) > $(C_4F_9SO_2)(CF_3SO_2)NLi$ (5.9 V) > $(CF_3SO_2)_2NLi$ (5.2 V) [33].

I.7.2. Transference number

In the electrolyte system, it consists of the cation (Li^+) and the anion (A^-). The ionic conductivity is defined by the following equation;

$$\sigma = \sigma_{Li^+} + \sigma_{A^-}$$

Transference number is the parameter that denotes the fraction of the current density to the total density carried by one of the ions. It can be related to the conductivity by this relationship [34], [35].

$$T^+ = \frac{\sigma_{Li^+}}{\sigma_{Li^+} + \sigma_{A^-}}$$

Transference number which ideally for lithium battery application should be unity but a value of T^+ is mostly lower than 1. During the operation of the cell, cations migrate to an electrode and anions should move to another electrode at the opposite way. However, there are only cations that react at the electrodes, anions do not involve in these reactions. This can lead to the concentration gradient in the system and limits the power output of the cell. Thus, there is much concern about an increase in concentration polarization and attempt to decrease this phenomenon by the development of salt giving high transference number.

Various techniques are used to investigate the cationic transference number in the electrolyte: namely the potentiostatic polarization (PP) method, the galvanostatic polarization (GP) method [36], the electromotive force (emf) method [37], the determination by Pulse Field Gradient (PFG)-NMR [38] and the impedance measurement [39]. The cationic transference number obtained depends on the technique used.

I.7.3.Conductivity and ionic conduction mechanisms

- Conductivity

The conductivity of the electrolyte is defined to the ability to conduct ions through such electrolyte. It depends on two parameters; those are the number of charge carriers and their mobilities. The number of charge conductors is proportional to the concentration of salt, the dissociation and solvation of solvent and the nature of salt dissolution. The ionic mobility is related to the viscosity of the electrolyte and the interaction between ion and solvent.

The solvation behavior of the solvent in the solution is demonstrated in various types. In the case of the highly concentrated solution or the solvent cannot dissociate the ions completely, the ion-pair phenomenon that does not contribute the current transport is formed depending on the extent of the solvation of the two ions as follows (figure 1.4):

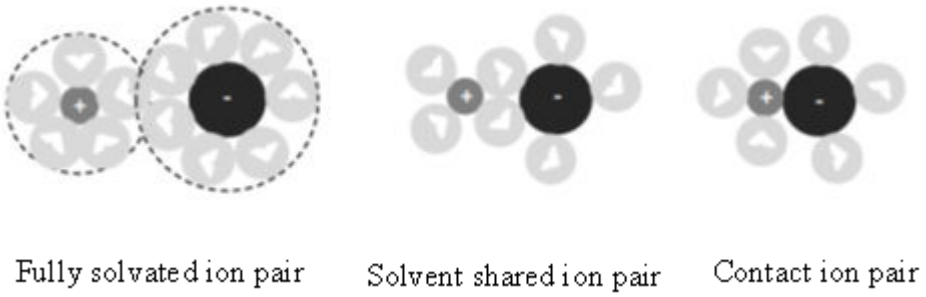

Figure 1.4. Various types of ion pair in the electrolyte solution [40].

Moreover, the formation of aggregate can occur at high concentration of solutes as seen in Figure 1.5. It may be charged and participates to the charge conduction but the performances are much lower than that of the solvated free ion.

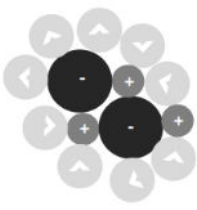

Figure 1.5. Formation of aggregate.

In the case of poly(ethyleneoxide) (POE), the Li^+ migration is done by the polymer chain segmental motions and ion cluster motions. Figure 1.6 shows 4 possibilities of Li cation motion in both intra/inter polymer chain and cluster.

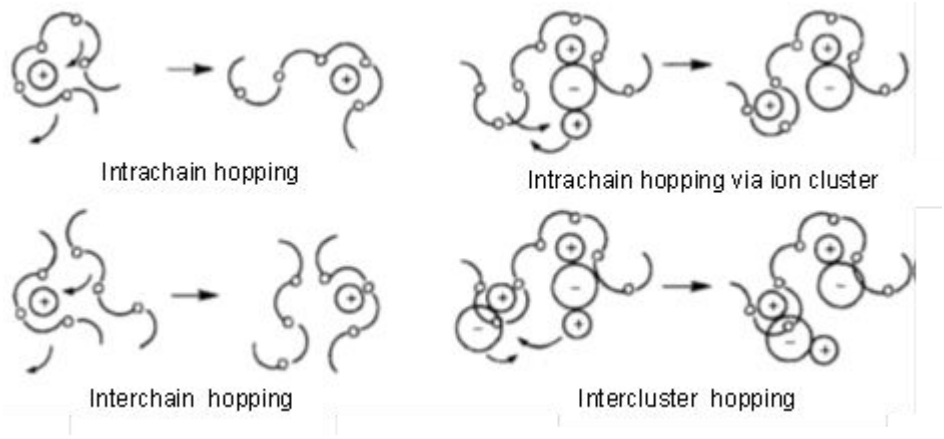

Figure 1.6. Cation migration in polymer electrolyte [41]

- Ionic conduction mechanisms

Mechanisms of ionic transport in the polymer electrolyte can be explained by two models.

a) Arrhenius model

For semi-crystalline polymer electrolytes at temperature below the melting temperature ($T<T_m$) and amorphous system, the conductivity is followed by the Arrhenius law.

$$\sigma = \sigma_0 \, exp\left(\frac{-E_a}{RT}\right)$$

Where σ is the conductivity ($S.cm^{-1}$), σ_0 is pre-exponential factor ($S.cm^{-1}$), E_a is activation energy ($J.mol^{-1}$), R is perfect gas constant ($R = 8.314\ J.mol^{-1}.K^{-1}$) and T is temperature (K).

The variation of conductivity of electrolyte in function of temperature is generally represented by $\log(\sigma) = f(1000/T)$. This equation is usually used for the polymer electrolyte which is at the temperature between $T_g < T < T_m$.

In solid polymer, the movement of polymer chains is quite difficult because of chain entanglement. Thus, the microscopic viscosity of segmental polymer affects to the ion transport. The ionic conduction is carried out effectively when there is a balance of the solvation of ions by the coordinating EO units for promoting the salt dissolution and permitting

the cation mobility. Moreover, the ions migration from one coordinating site to another controlled by the segmental motion is also considered for the ionic conduction.

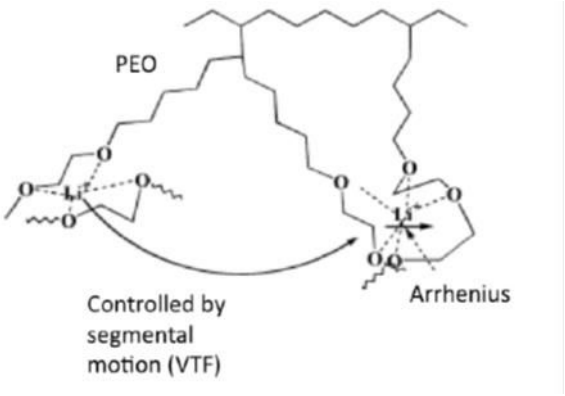

Figure 1.7. Contribution to ion mobility [42].

Another model of H. Vogel, G. Tammann and G.S. Fulcher was proposed to explain the process that is related to the motion of segment of the polymer.

b) Vogel Tammann-Fulcher (VTF) model

Liquid electrolytes [43], gels [44], molten salts [45] and amorphous polymer at above the glass transition temperature ($T > T_g$) has Vogel-Tammann-Fulcher (VTF) [46], [47], [48] dependence and the conductivity is varied in function of temperature as the following relationship:

$$\sigma = \frac{A}{\sqrt{T}}\, exp\left(\frac{-E_a}{R(T-T_0)}\right)$$

where A is a pre-exponential factor related to the number of charge carriers ($S.cm^{-1}.K^{1/2}$), E_a is a pseudo activation energy ($J.mol^{-1}$), T_0 is the ideal glass transition temperature at which ion mobility goes to zero (K). Above T_0, thermal motion of the polymer chains initiates the transport of ions. T_0 is usually found to 50 K below T_g.

At low temperature, the VTF model is dominant and is defined as rate-limiting. When the temperature is increased, the Arrhenius model becomes rate-limiting because the segment of polymer chains has more freedom to move.

At constant pressure and temperature, the conductivity can be related to the ion concentration by this relationship

$$\sigma(T,P) = qc(\mu_+ + \mu_-)$$

where q is the charge, c is the concentration and μ is the mobility of the cation and anion. The mobility is related to the diffusion coefficient (D) through the Nernst-Einstein equation;

$$\mu = qD / kT$$

For anion transport mechanism, the migration principally depends on the free segmental motion or a VTF type at all concentrations and temperatures due to the weak solvation with the polymer host.

I.8. Polymer electrolytes

Up to now, the performance of polymer electrolytes has been continuously improved under the requirement of a variety of applications. For lithium battery electrolytes, a solvation of ions by polymer chain is important requirement that can be related to other characteristics of electrolyte such as the cationic conduction in the term of the conductivity and transference number and the dissolution of salt in polymeric medium.

When the ability to solvate ions of the polymer electrolyte is considered, the acceptor-donor numbers (AN and DN) that are related to the formation of coordination bond between solvent and solute in the system need to be mentioned. Polymers with strong DN such as polyethers, polyamines or polythiols are promising candidates as the electrolyte because electron lone pairs at oxygen, nitrogen or sulfur in such polymers can solvate the lithium cation [49].

Among those high DN polymers, poly(oxyethylene) (POE) based compounds have been studies, because POE forms more stable complexes with inorganic salts and possesses higher solvating power for salt than any other polymers [50].

I.8.1.Poly(oxyethylene) based electrolytes

Poly(oxyethylene) is synthesized via the polymerization of oxyethylene (CH_2CH_2O) monomer by a ring opening mechanism. The monomer molecules are highly strained and possess a triangle structure which favors to open in the presence of polymerization initiators.

The regularity of repeating units allows a high degree of crystallinity of the polymer. Since the experiment of Wright, the studies have been focused on the bulk properties of polymer electrolytes based on the combination of poly(oxyethylene), the most extensively dry solid polymer electrolytes for lithium batteries, with various salts. This led to understand the characteristic and improve the performance of such complex. As the following factors, either the unique characteristic of host polymer or the additives incorporated may affect to the properties of electrolytes.

Regarding the polymer chain length effect, in the case of POE/$LiN(SO_2CF_3)_2$ complex, the mixture of low M_w POE is always viscous liquid whereas the high M_w POE amorphous mixture spends a period of weeks to months to form crystalline regions. In contrast, the crystalline phase formation of $P(OE)_6$-$LiSbF_6$ and $LiAsF_6$ can occur with both low and high MW POE. The influence of the high MW $P(OE)_3$-$LiCF_3SO_3$ on the T_m is not much but for shorter POE chains, T_m is considerable lowered whereas all complexes perform the same pattern of ion coordination [51].

POE has been found to complex with a wide variety of lithium salts. POE-$LiClO_4$ complexes ($M_w = 2\times10^6$) were studied by B.K. Choi et al.[48]. They found that the conductivity was in the range of 10^{-7}-10^{-6} S/cm with the salt concentration (O/Li) ranging between 10 and16 at 20°C. The thermal and ion transport characterization of the system POE_n –$LiPF_6$ were investigated. The conductivity is higher than 10^{-4} S/cm at 70°C with O/Li= 30 but it was around 10^{-8} S/cm at room temperature [52].

As a function of concentration of lithium salt in POE considered, the decreases of conductivity and cationic transference number were observed when the concentration was increased [53]. This was due to the formation of ion pairs instead of the free lithium ions which is more useful for the conduction [54].

POE based polymer electrolyte exhibits very poor ionic conductivity (~10^{-8} S/cm at 40°C) [55] which is a serious barrier in potential technological application. It was widely believed that this obstacle comes from the high degree of crystallinity (~65%) which hinders its ability for ionic conduction. Above the glass transition temperature (T_g), the segmental motion can move faster in the amorphous phase than in the crystalline phase, therefore, the cations migration occurs predominantly in the amorphous phase. Even though Bruce et al. [56] demonstrated that highly crystalline polymer electrolytes exhibit remarkable ionic conductivity although the value was still lower than in the amorphous phase and the understanding about the

phenomenon of ion transport in those crystalline polymer electrolytes is still not completely clear. Later, Q. Liu et al. [57] reported that the conductivity of $P(OE)_6/LiAsF_6$ complex decreases by around 3 orders of magnitude with the molecular weight of POE from 1000 to 6000 Da.

In this context the research was focused on development of modified POE in order to diminish the crystallinity and improved the mechanical properties. Some of these approaches are presented here below.

I.8.2.POE with lower crystallinity degree

One of the strategies to improve the performance of solid electrolyte, in particular the conductivity is a decrease of the crystalline region. Many approaches were proposed to eliminate the crystallinity of polymer electrolyte. Two extensively studied approaches are (i) the modification of POE molecule structure and (ii) the adding material able to interact with the POE decrease its crystallization ability (nanocharge, plasticizer, etc.).

- **Modified POE**
  - Polycondensats

The polycondensation of oligomer of POE with a co-monomer leads to decrease the crystallinity and the melting temperature of POE which commonly exhibit around 65% and 65°C, respectively. Le Nest et al. [58] reported first work about polycondensats by preparing poly(urethane ether) from polyethylene glycol (PEG) end capping with OH group and polyisocyanates. The resulting polymer exhibited an amorphous behavior at ambient temperature. However, the main problem with this synthesis consists that the unreacted PEG and polyisocyanates, that are difficult to remove from the final polymer, are instable to the lithium metal.

Polyurethanes (TPU) with chelating groups was also carried out from 4,4'-diphenylmethane diisocyanate (MDI) , poly(ethylene glycol) (PEG) and imino-diacetic aide (EP-1DM). The hard domain of this polymer not only provided good mechanical properties but also decreases the crystallinity of the polyether. The complex with 0.25 mmol $(g\ TPU)^{-1}$of $LiClO_4$ reaches a conductivity of 1.5×10^{-6} S/cm [59].

Benrabah et al. [60] synthesized poly(amide ether) by polycondensation between an α,ω-diamine poly(oxyethylene -co-oxypropylene) (Jeffamine®diamine) and terephthaloyl chloride. The linear polymer obtained had less crystallinity and its melting temperature was decreased.

Moreover, F. Alloin et al. [61] investigated the thermal behavior of various Mw polymers synthesized by a Williamson reaction. The polycondensation of polyethylene glycol (PEG) and 3-chloro-2-chloromethyl-1-propene provided linear polycondensates with a lower melting point compared to a starting PEG.

- Branch polymer
  - Comb polymer

Watanabe and co-workers [62], [63], [64] first reported the synthesis of comb shaped polymer with both backbone and side chains consisting of ethylene oxide units. Short ether side chain decreased the crystallization and promoted the mobility of polymer segments leading to higher conductivity at room temperature when compared with linear POE matrix. However, it was found the loss of mechanical properties of comb-shape polymers when the number of side chains was increased [65], [66].

Comb-shaped polymers with poly(oxyethylene) side chains blended with POE polymer were designed and these polymer were consist of various types of macromolecules as the backbone including the oxyethylene unit and derivatives [67], [68], [69] aromatic polyether [70]. The conductivity, of complexes based on comb-shaped polymers and $LiClO_4$ was found around 10^{-4} S/cm at room temperature and DSC characterization showed that the copolymer might play a role of plasticizer to increase the free volume and favors the ion conduction.

Due to the presence of flexible amorphous phase, the mechanical properties are reduced. In order to improve the mechanical properties of these solid polymer electrolytes, a new approach is a comb-like network polymer. The expected drop of conductivity caused by crosslinking was well compensated by the introduction of POE side chain as shown in figure 1.8. It provided the conductivity of 1.01×10^{-4} S/cm and the storage modulus of 0.66 MPa at 30°C.

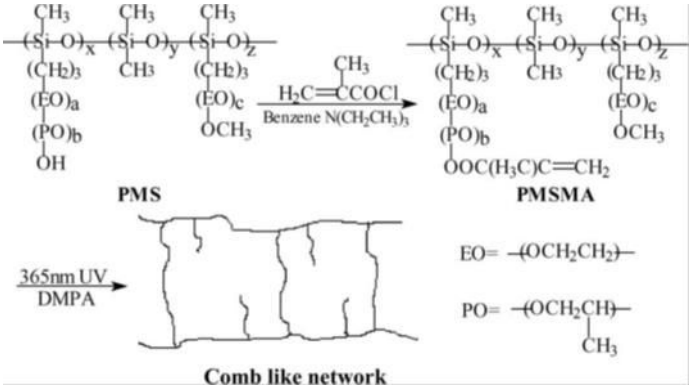

Figure 1.8. Comb-like network polymer electrolyte [71].

- Star shaped polymer

Star shaped polymers have unique structure with multiple chain ends and large free volume. Therefore, they are interesting materials for solid polymer electrolytes. This polymer consists of two main parts; the first part is the core of the molecule often made from siloxane acrylate [72], [73], polyhedral oligomeric silsesquioxane [74] or diepoxide [75] and another important part are the side groups of POE or its derivative. Star-branched polymers in POE/lithium salt system can inhibit the crystallization and improve the ion transport through the matrix by the contribution of side chains. In addition, the core of star-branched polymer can enhance the mechanical strength of the polymer but still low for some electrolytes [75]. The conductivities were around 10^{-5} – 10^{-4} S/cm at 30°C.

Figure 1.9. Star-branched structure; D= core, Θ = reactive site on the core, lines represent POE chains [75].

- Block copolymer

Another approach to improve the multiple properties for POE based polymer electrolyte is the utilization of block copolymers. J. Ji et al. [76] studied the multiple functional diblock POE-b-PE copolymer to enhance the ionic conductivity and mechanical properties. The conductivity was more than 10 times higher than that from the POE/$LiClO_4$ complex. And also,

the mechanical properties were improved 2-6 times compared to POE/$LiClO_4$ electrolyte. Moreover, the XRD results showed that a degree of the crystallinity was obviously decreased and no ion pair formation in the sample. An increase of the amorphous phase by the copolymer provided more free volume for the ion movement. Other analogous material of POE was used for the formation of di-block copolymers such as methoxy capped oligo(ethylene) glycol methacrylate (EGMA). $(PMMA)_x$-b-$(P_nEGMA)_y$ (n=8~9, x/y ratio 3/1) was synthesized through atom transfer radical polymerization (ATRP) and gave the conductivity of 2×10^{-6} S/cm at room temperature when doped with LiTFSI [77].

Polymer electrolytes based on triblock copolymer of POE complexed with different lithium salts have been proposed. PMAN-b-POE-b-PMAN triblock copolymer was prepared by the anionic polymerization with different starting PEGs. The complexes of LiTFSI PMAN-b-POE-b-PMAN copolymers was studied, the interaction between cation and polymer chain was evidenced. PMAN domain exhibited higher salt dissolution ability whereas POE block had stronger cation solvation ability. The conductivity reaching 10^{-5} S/cm at 37°C was still too low for dry polymer electrolytes [78]. H. R. Allcock et al. synthetized poly(phosphazene)-poly(oxyethylene) copolymers. The membranes based on poly(phosphazene)-poly(oxyethylene) copolymers and lithium triflate shown conductivity of 10^{-4} S/cm at high temperature and 7.6×10^{-6} S/cm at room temperature [79]. The polystyrene (PS) and poly(ethylene glycol) methyl ether methacrylate (PME BAB block copolymer was synthesized by T. Niitani et al.. The micro phase separation with a continuous POE phase was observed when the POE content exceeded 70%. The copolymer/$LiClO_4$ complex exhibited the conductivity of 2×10^{-4} S/cm at 30°C and had good electrochemical stability [80].

- Network polymer

Cross-linking of the polymer is another effective way to suppress or decrease significantly the POE crystallization degree. Additionally, the cross-linking is also very beneficial to enhance the mechanical strength of the polymer comparing to the corresponding linear polymer electrolytes. The cross-linking gives to the polymer a rubber-like aspect, large amorphous phase which enhance its ionic conductivity when incorporated with the salts and prevents the creeping behavior of elastomeric materials [81], [82].

Two possible strategies are proposed for the formation of cross-linked polymer electrolytes depending upon the basis on which monomers undergo the chemical reaction. The first strategy

is the polycondensation of di or tri functional monomers. It could be seen in several studies of J. F. LeNest et al. and M. Mastragostino et al. for example; multi-functional reactive molecules such as triisocyanate [83], [84] or triphenylisocyanate [85] and polyether glycol or its derivatives were used as substrates for the formation of network polymers. Another technique is the utilization of the crosslinking agent and macromolecules for instance, phosphate-polyether networks were synthesized by the polycondensation reaction of phosphorus oxychloride ($POCl_3$) with poly(ethylene glycol)/poly(tetramethylene glycol) (PEG/PTMG) (70/30) copolymers to improve ionic conductivity at room temperature without decreasing mechanical properties [86].

The second strategy is the addition reaction of the moderate molecular weight pre-polymer which generally occurs among double or triple-bonded molecule called the post-crosslinking. The post-crosslinking need reactive groups introduced to the polymeric chain. The reactivity and reaction rate of these groups can be controlled by different parameters i.e. temperature, radiation, external reactant (such as moisture, O_2, H_2O, etc) and processing [87].

The polymers containing reactive groups (double bonds) were prepared by F. Alloin et al. [88].The linear Poly(oxyethylene)/ allyl glycidyl ether copolymer obtained from the ring opening polymerization exhibited a lowering of crystallinity and melting temperature when compared to those of POE homopolymer. After the crosslinking, the post cross-linked polymer provided the lower proportion of crystalline phase. The conductivity of the network polymer was 10^{-4} S/cm at 32°C and the mechanical properties were also improved.
Moreover, the three-dimensional networks were synthesized from linear polycondensats of poly(isobutenyloligooxyehtylene) [89] and showed high dimensional and thermal stabilities. Membranes with conductivity of 2×10^{-5} S/cm at 20°C and 10^{-3} S/cm at 80°C (for NPC1000/LiTFSI O/Li=9) were obtained when LITFSI (O/Li=14) was added to this network. However, cationic transference number of only 0.06 was reported for such membranes [90].

I.8.3.Blended-based polymer electrolyte

The second approach for reducing the crystalline phase in polymer electrolyte is the addition of other materials to the POE system such as

- Other polymer (polymer blending)
- Plasticizers
- Inorganic fillers

a. Blended-based polymer electrolyte

The blending of two or more polymers together has been extensively paid attention due to the simplicity of preparation and easy control of the physical properties within the compositional regime. The influences on the electrical, thermal and mechanical properties of polymer electrolytes can also be evaluated from the relative importance of various factors which involve in polymer blends. However, polymer selected for blending system should be concerned in the compatibility that can lead to the phase separation problem. Many POE-based blend systems have been studied e.g. POE/PPO [91], POE/ PVP [92], POE/PAN [93]. The blending of a fully amorphous poly(ethylene oxide-co-propylene oxide) network with POE exhibited a network –type morphology with no obvious microcracks that commonly found in the blend-based polymer and can reduce the crystallization and the melting temperature. At higher than 50 wt% of network polymer mixing, the blended-based polymer electrolytes have an excellent dimensional stability at high temperature. Below 50°C the conductivities were slightly increased due to the adding of network polymers [94]. In additional to such binary blend system, the ternary blends have also been studied. As pointed out by A.M. Rocco and co-workers [95], POE/poly(bisphenol A-co-epichlorohydrin) (PBE) blend polymers which are known to be miscible in all blend compositions due to the intermolecular hydrogen bonds between polymers performed a decrease in a degree of crystallinity and depression of the melting temperature of the system. The complexation of Li cation by both POE and PBE oxygen atoms was confirmed by FTIR evidence. The dissociation behavior of $LiClO_4$ was highly affected to the ionic conductivity of polymer electrolyte at room temperature. However, the conductivity obtained was only 10^{-5} S/cm, probably due to the high T_g of PBE and insufficient number of basic oxygen sites for Li^+ coordination. Low-molecular weight poly(vinyl ethyl ether) (PVEE) was added to improve the performances. Importantly, the

conductivity values of 10^{-3} $\Omega^{-1}cm^{-1}$ (20 wt% $LiClO_4$) at room temperature are the highest values among the literature cited for lithium polymer electrolyte system.

b. Inorganic fillers

One way of enhancing the ion conduction as well as the mechanical properties is the incorporation of inorganic fillers such as nano-particulate ceramics (TiO_2, SiO_2, Al_2O_3, etc), carbon nanotubes, nanaclays (monmorillonite). Therefore, this polymer electrolyte is called composite polymeric electrolyte. POE-$LiClO_4$ based composite polymer electrolyte containing nano-Al_2O_3 as fillers was prepared by E.M. Masoud et al. [96]. The introduction of ceramic fillers did not only reduce the crystallinity and the melting point but increased the dielectric constant that subsequently, increased the conductivity. In the case of nano-clay, the addition of lithium monmorillonite (LiMMT) was proved to decrease the crystallinity of POE which completely disappear above 40 wt% of LiMMT and reduced POE melting temperature. Moreover LiMMT can improve the conductivity, however at high content of LiMMT, the ion mobility decreased due to the self-aggregation. The thermal stability was significant lower than that of the corresponding POE [97].

c. Plasticizers

Increasing the amorphous nature of the polymer electrolyte can be achieved by the addition of plasticizing agents with high dielectric constants relating to enhance the dissociation of ion pair of the salt [98]. Plasticizers commonly used in solid polymer electrolyte system are polar organic solvents i.e. ethylene carbonate, propylene carbonate. These solvent can easily dissolve numerous salts and obtain good conductivity but they are volatile and flammable that may cause a safety concern for lithium battery application [99]. Therefore, non-volatile solvents and low molecular weight polyether are considered as a plasticizer to the matrix polymer [99], [100], [101]

In addition, some salts and ionic liquid can also act as plasticizers.

Ionic liquids

So far, the approach of plasticization has been the conventional way to reduce the crystallinity resulting in an increase of amorphous phase content of the polymer electrolytes. However, the organic solvents widely used as plasticizers lead to the safety issue due to their volatile nature and the reactivity with metal electrodes. Thus, the replacement of such solvents by the addition of room temperature ionic liquids (RTILs) is the promising approach for POE electrolytes.

Ionic liquids are molten salts at room temperature that generally consist of organic cations and organic or inorganic anions. Ionic liquids have been paid attention for their use as an additive for electrolytes in lithium battery application due to their advantages such as non-flammability, negligible vapor pressure, high ionic conductivity and high thermal, chemical and electrochemical stabilities [102]. The combination of a polymer matrix and an ion conducting ionic liquid affects the properties of POE-based electrolytes. A broad and stable amorphous region is increased and creates the free-volume for facilitating the ion conduction [103]. The improvement of conductivity requires low viscosity and high dielectric constant ionic liquid to increase the flexibility to polymer electrolytes and to promote the dissociation of paired ions. Several ionic liquid possessing such properties have been studied for polymer electrolytes. Their performance relies on the component of ionic liquid such as those with cations based on imidazolium [104], pyrrolidium [105], piperidinium [106], morpholinium [19] and quarternary ammonium [107]. Methyl butyl pyridinium (PYR_{14})TFSI is considered a very promising ionic liquid for lithium batteries due to its wide electrochemical window, high ionic conductivity and hydrophobicity. It was examined that the incorporation of PYR_{14}TFSI ionic liquid in POE matrix and crosslinked POE electrolyte effectively prevented the crystallinity of POE. The ternary system of linear POE-LiTFSI-PYR_{14}TFSI and UV cross-linked POE-LiTFSI-PYR_{14}TFSI solid polymer electrolytes were performed, and conductivity of 1.1×10^{-4} S/cm [108] and 3×10^{-4} S/cm at 20°C [109], respectively were reported while the conductivity of pure PYR_{14}TFSI was around 2×10^{-3} S/cm. [110] Moreover, no obvious change of conductivity when the irradiation time increased.

Lithium salts

The performances of an polymer electrolyte depend not only on solvent but also on lithium salt. A strategy for improving the conductivity of polymer electrolyte is the increasing of number of charge carriers by the incorporation of high dissociated salt and adequate salt concentration avoiding the formation of ion pair and aggregation of salt which may obstruct the coordination between cation and polymer chain and subsequently, affect to the ion migration. Suitable salts should possess the large anion with well delocalized negative charge and low basicity leading to good salt dissociation, less ion pairing and high conductivity in POE matrix. Many salts have been developed the main characteristic being presented in Table 1.4.

Among them, those based on bis(trifluoromethyl sulfonyl)imide anion or LiTFSI initially synthesized by M. Armand and C.E.M.F. El Kadiri [111] then commercialized by 3M® [112] has been most extensively studied as charge carrier for solid polymer electrolytes. As discussed earlier, the TFSI anion has unique features with (i) high flexibility of $–SO_2$-N-SO_2- bringing to the plasticizing effect and to lower crystallinity in POE. (ii) A decrease of the interaction between Li^+ and $TFSI^-$ by highly delocalized charge distribution of $TFSI^-$ and, (iii) excellent thermal, chemical and electrochemical stabilities are performed in this outstanding salt.

Another salt in the imide family, bis(fluorosulfonyl)imide $Li[N(SO_2F)_2]$ (LiFSI), has been a rapidly growing interest in lithium as a conducting salt with good anticorrosive properties for Li-ion batteries. However, the salt with high purity cannot be synthesized in an unspecialized laboratory due to its difficulty of preparative process [113]. H. Zhang et al. [114] comparatively studied the performance of LiFSI and LiTFSI salts in poly(oxyethylene) matrix with $M_v = 5\times10^6$ g/mol. Above 60°C, the ionic conductivity of LiFSI was higher than that of LiTFSI one and exceeded 10^{-3} S/cm at 80°C. On the other hand, the transference number of LiFSI/POE electrolyte was 0.14 whereas that of LiTFSI/POE matrix was 0.18. That was expected due to the smaller size of FSI^- bringing out more mobile than the bigger anion like $TFSI^-$. Both FSI^- and $TFSI^-$ anions dominated the plasticizing effect on their polymer electrolyte that might increase the free volume and lead to enhance the ion mobility in polymer matrix. Moreover, POE/LiFSI and POE/LiTFSI complexes were electrochemical stable up to 5.3 and 5.7 V vs Li+/Li, respectively.

Table 1.4: Structure and properties of commonly used lithium salts in polymer electrolytes [115]

Lithium salts	Anions	Main Characteristics
$LiPF_6$		High conductivity, favor SEI formation Decomposes in the presence of moisture and reacts with electrolytes at high temperature resulting in the formation of HF
$LiClO_4$	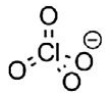	Broad electrochemical stability window Low solubility in carbonate type solvent
$LiBF_4$	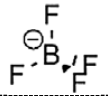	Broad electrochemical stability window Low solubility in carbonate type solvent
LiTFSI	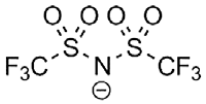	High solubility, conductivity, electrochemical stability Unable to form passivation layer on Al current collectors (Al-degradation and corrosion)
LiFSI	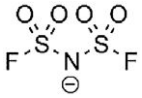	Higher conductivity compared to LiTFSI, high electrochemical stability Unable to form passivation layer on Al current collectors (at the presence of LiCl)
LiBETI	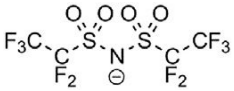	High solubility, conductivity, electrochemical stability Unable to form passivation layer on Al current collectors
LiBOB	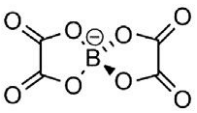	High electrochemical stability and long term stability Form highly resistive SEI-film (low conductivity in comparison to $LiPF_6$ and LiTFSI)
LiDFOB	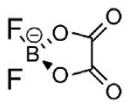	High electrochemical stability and cycling behavior, Able to form passivation layer on Al current collectors Lower solubility in carbonate type solvent compared to LiTFSI and $LiPF_6$ but higher than LiBOB

In addition to the studies on linear polymer electrolytes, the network matrix was also investigated. The matrix of NPC1000/LiTFSI with the salt concentration O/Li =14.5 exhibited

the conductivities of more than 10^{-3} S/cm at 110°C and around 10^{-5} at room temperature [116], [117] while the transference number was approximately only 0.1 to 0.15 at 80°C [90].

Recently new lithium salts have been developed and were incorporated in POE based polymers. Thus E. Paillard et al. [118], [119] synthesized a family of aryl based on perfluorosulfonylimide and perfluorosulfonate lithium salts. They exhibited high chemical and thermal stabilities even the conductivities were insufficient at room temperature. The transference numbers of sulfonate salts (T^+ = 0.4 to 0.55) were higher than those of sulfonylimide ones (T^+ = 0.20 to 0.26) and both values, hosted in POE, were higher when compared to LiTFSI. The ionic conductivities were around 10^{-4} S/cm at 70°C and some of perfluorosulfonate salts had an outstanding stability in oxidation (>5.8 V vs Li/Li^+).

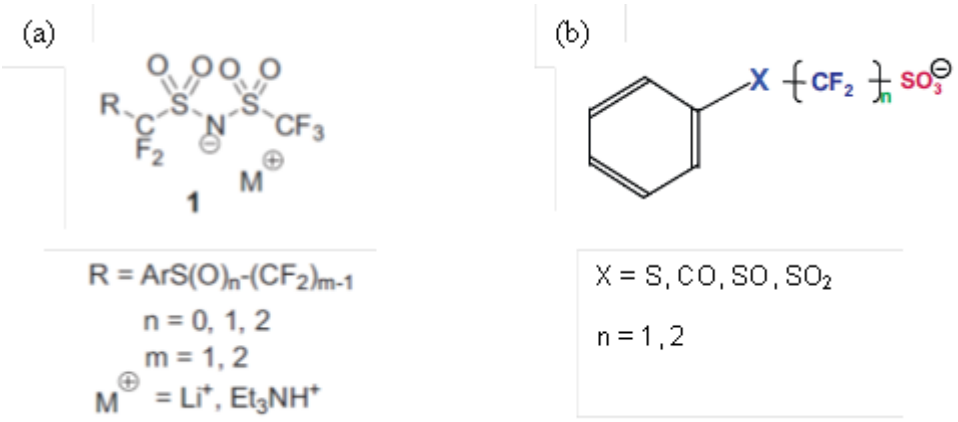

Figure 1.10. General structure of (a) sulfonylimide and (b) sulfonate salts proposed by E. Paillard et al.

Macromolecular single-ion conductors

It is generally accepted that not only the conductivity but also the transference number is the main parameter considered for the polymer electrolyte performance. Practically, the lithium cation transport is coupled to the motion of polymer backbone or segmental motion of polymer chain by coordinating interactions of mobile Li^+ to ether oxygen while the counter anions have weaker interactions with main chains allowing to occur more facile migration of anions compared to cation transport thus, a major drawback of dual ion conduction is the low transference number [110]. Additional, the accumulation of such anions at anode electrode and low diffusion coefficient of Li cations cause the salt concentration gradient which further the concentration polarization and thus the poor performance of the cell [120]. To achieve the high

transference number equaling to unity in theory, the single ion conductor should be prepared, in which the anions are immobilized by covalently linking the anions to the polymeric chains [121]. With such feature, it is expected that only lithium cations mobile in the polymeric matrix. However, the polymer electrolytes obtained from this idea had some issues in the purification because they were involved in several synthetic steps and could not be isolated from the starting materials resulting in the conductivity in the range of 10^{-8} to 10^{-7} S/cm [122]. Single ion conducting concept has been attracted by several research groups, particularly, Watanabe et al., Armand et al. and DesMarteau et al. [118-121]

Polymeric lithium salts of imide anions whose well delocalized negative charges were studied by Watanabe and co-workers [123], [124]. The space length between anionic charges influences to the conductivity and the dissociation of salts. These salts can increase the cationic transference number.

Armand and co-workers [125], [126] prepared the polymer alloys from blending POE with of lithium poly(4-styrenesulfonyl(trifluoromethylsulfonyl)imide polyelectrolyte. The conductivity was still low (7.94×10^{-7} S/cm at 40°C) for practical use in Li-ion batteries even through this polyanion contains the flexible and delocalized nature of the $–SO_2\text{-}N\text{-}SO_2\text{-}CF_3$ providing more amorphous region in polymer matrix. On the other hand, the lithium-ion transference number is almost unity ($T^+ = 0.92$) at 60°C.

Perfluorinated polymer with sulfonylimide group was also studied by DesMarteau and co-workers [127], [128]. Aliphatic and aromatic lithium salt of sulfonylimide anions attached covalently to a polyether oligomers of variable chain length. The highest ambient temperature conductivity of ~10^{-6} S/cm was observed and it reached in the range of 10^{-4}-10^{-3} S/cm at 120°C. Even though, transference numbers were not investigated but the concentration polarization gradient was not found by galvanostatic polarization studies.

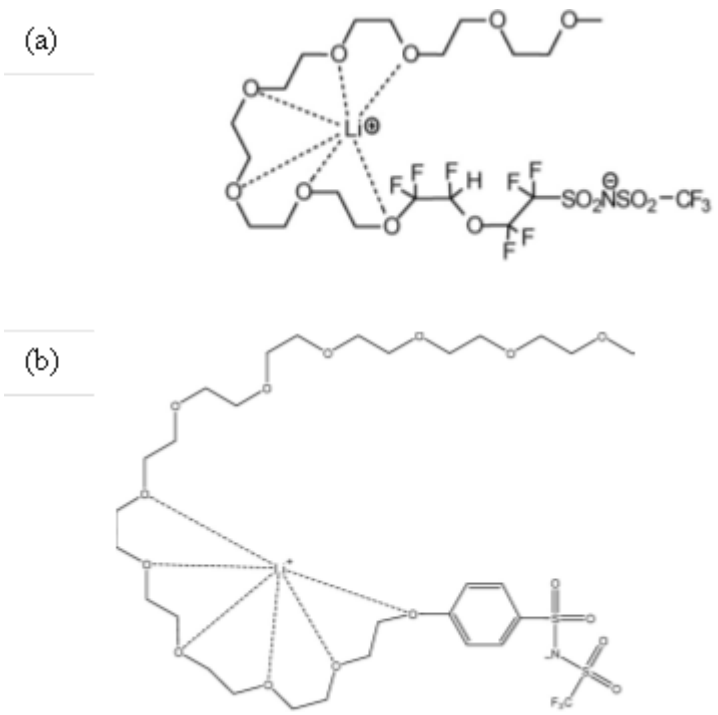

Figure 1.11. Structures of (a) aliphatic and (b) aromatic lithium ionic melts of DesMarteau and co-workers [127], [128]

Besides sulfonylimide anions, polyethers also functionalized with other ionic end groups such as carboxylate, sulfonate and sulfate which were presented in the research work as follows.

Bannister et al. prepared a perfluorocarboxylate anion as a single cation conductor although, this lithium salt was not enough dissociated in polyether matrix resulting in the poor conductivities [129]. In order to decrease the ion paring by using the fluorine atom compound and simultaneously, achieve the high transference number which closing to unity, T. Hamaide and C. Le Deore were trying to blend a large perfluorinated sulfonate lithium salt ($C_8F_{17}SO_3Li$) with a higher molecular weight POE [130]. D. Benrabah et al. studied perfluorosulfonate lithium salts grafting network polyethers. They provided the conductivity of 10^{-7} S/cm and 10^{-6} S/cm at ambient temperature and 72°C, respectively. Besides, the conductivity increased to 10^{-5} S/cm when such lithium salt was incorporated in NPC1000 matrix [131]. K. Ito et al. reported the systhesis of PEG, PPG and PEGME attached with lithium benzenesulfonate on the chain end and the conductivities of such oligomer lithium salts [132]. W. Xu et al. prepared different chain lengths of PEGs end-capped with sulfonate benzoyl group (EO_nPSLi) possessing the self dissociation. The length of ethyleneoxy repeating unit of such lithium salts affected to the ionic conductivity behavior (2.7×10^{-7} S/cm for n=2 and 1×10^{-5} S/cm for n=12 at room temperature,

pure salt) while the conductivities of blend POE/EO_nPSLi complex were in the range of 10^{-8}-10^{-7} S/cm at 25°C. However, the transference number was not mentioned [133].

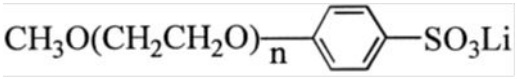

Figure 1.12. Structure of lithium p-[methoxy-oligo(ethyleneoxy)phenylsulfonate.

X. Ollivrin synthesized PEGs end –capped by lithium perfluorosulfonate and obtained high value of conductivity when lithium salts were incorporated in the high molecular weight POE (10^{-3} S/cm at 78°C) [134]. Mono and di-lithium salt based on oligoether sulfate was carried out by C. Chauvin et al. The conductivity reached 6×10^{-5} S/cm at 70°C and was close to 10^{-5} S/cm at 30°C for pure mono lithium salt while pure di-lithium salts exhibited the conductivities of 8×10^{-5} S/cm at 70°C and 2×10^{-5} S/cm at 30°C. The transference numbers of two salts were almost unity at 70°C [135].

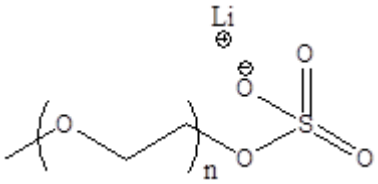

Figure 1.13. Structure of mono lithium salt based on oligoether sulfate.

I.9. Motivation of thesis work

The main objective of my thesis work is to performed polymer electrolytes based on POE and lithium salt complexes with high conductivity at low temperature and good mechanical properties after the melting point of POE. Therefore new salts were synthetized with the aim to improve the interaction between the POE chains and the anion of lithium salt and hence perform POE electrolytes with lower crystallization degree and higher cationic transport number as compared with the polymer electrolytes based benchmarked salts.

In the first part aromatic perfluorosulfonate mono-end caped with polyethylene glycol are synthetized and characterized in POE and POE derivate electrolytes.

The second part is dedicated to the synthesis and characterization of aliphatic perfluorosulfonates and perfluorosulfonimide salt. In order to performed membrane with good mechanical properties POE with double bonds were synthetized and cross-linked by UV irradiation.

The impact of salt structure on the POE and cross-linked POE membrane are study in terms of conductivity, thermal and thermo-mechanical properties, cation transport number.

I.10. References

[1] http://www.ehow.co.uk/about_5397626_advantages-disadvantages-rechargeable-batteries.html, (2014).
[2] C. Chauvin, Thesis, Institut Polytechnique de Grenoble, 2005.
[3] M. Gauthier, A. Bélanger, P. Bouchard, B. Kapfer, S. Ricard, G. Vassort, et al., J. Power Sources. 54 (1995) 163 – 169.
[4] http://batteryuniversity.com/learn/article/is_lithium_ion_the_ideal_battery (accessed July 13, 2014).
[5] C. Arbizzani, F. Colò, F.D. Giorgio, M. Guidotti, M. Mastragostino, F. Alloin, et al., J. Power Sources. 246 (2014) 299 – 304.
[6] J. Tarascon, M. Armand, Nature. (2001) 359.
[7] C. Daniels, J. Besenhard, Handbook of Battery Materials, 2011.
[8] J.Y. Song, Y.Y. Wang, C.C. Wan, Electrochem Soc. (2000) 3219.
[9] B. Scrosati, S. Megahed, Electrochem Soc Shirt Course. (1993).
[10] Q. Wang, P. Ping, X. Zhao, G. Chu, J. Sun, C. Chen, J Power Sources. 208 (2012) 210–224.
[11] M. Holzepfel, C. Jost, A. Prodi-Schwab, F. Krumiech, A. Wursig, H. Buqa, et al., Carbon. (2005) 1488–1498.
[12] E. Quartarone, P. Mustarelli, Chem Soc Rev. (2011) 2525–2540.
[13] J.S. Lee, J.Y. Bae, H. Lee, N.D. Quan, H.S. Kim, H.Kim, J Ind Eng Chem. (2004) 1086–1089.
[14] G. Feuillade, Ph. Perche, J Appl. Electrochem. 5 (1975) 63–69.
[15] P.P. Prosini, S. Passerini, Solid State Ion. 146 (2002) 65 – 72.
[16] E.M. Shembel, O.V. Chervakov, L.I. Neduzhko, I.M. Maksyuta, Y.V. Polischyk, D.E. Reisner, et al., J. Power Sources. 96 (2001) 20 – 28.
[17] B. Kurc, Electrochimica Acta. 125 (2014) 415 – 420.
[18] F. Boudin, X. Andrieu, C. Jehoulet, I.I. Olsen, J. Power Sources. 81–82 (1999) 804 – 807.
[19] K.-S. Kim, S.-Y. Park, S. Choi, H. Lee, J. Power Sources. 155 (2006) 385 – 390.
[20] C.L. Cheng, C.C. Wan, Y.Y. Wang, Electrochem. Commun. 6 (2004) 531 – 535..
[21] N. Chaix, F. Alloin, J.-P. Bélières, J. Saunier, J.-Y. Sanchez, Electrochimica Acta. 47 (2002) 1327 – 1334.
[22] J.-P. Belières, M. Marechal, J. Saunier, F. Alloin, J.-Y. Sanchez, J. Electrochem. Soc. 150 (2003) A14.
[23] J. Saunier, F. Alloin, J.Y. Sanchez, G. Caillon, J. Power Sources. 119–121 (2003) 454 – 459.

[24] J. Saunier, F. Alloin, J.Y. Sanchez, L. Maniguet, J. Polym. Sci. Part B Polym. Phys. 42 (2004) 2308–2317. doi:10.1002/polb.20099.
[25] D.E. Fenton, J.M. Parker, P.V. Wright, Polymer. (1973) 589.
[26] C.C. Lee, P.V. Wright, Polymer. 23 (1982) 681 – 689.
[27] M.B. Armand, J.M. Chabagno, M. Duclot, St Andrews Scotl. (1978).
[28] M. Armand, J.M. Chabagno, M. Duclot, Fast Ion Transport in Solids, Elsevier N. Y. USA. (1979).
[29] B. Trémillon, Electrochimie analytique et reactions en solution, tome 1, Masson, (1993).
[30] V. Gutmann, Coordination chemistry in non aqueous solutions, Springer. (1968).
[31] V. Gutmann, Coord. Chem. Rev. (1975) 107.
[32] E. Peled, J Electrochem Soc. (1979) 2047.
[33] F. Kita, H. Sakata, S. Sinomoto, A. Kawakami, H. Kamizori, T. Sonoda, et al., J. Power Sources. 90 (2000) 27 – 32.
[34] J.O.M. Bockris, A.K.N. Reddy, Mod. Electrochem. 1 – Ion. (1998) 489.
[35] M.M. Hiller, M. Joost, H.J. Gores, S. Passerini, H.-D. Wiemhöfer, Electrochimica Acta. 114 (2013) 21 – 29.
[36] S. Zugmann, M. Fleischmann, M. Amereller, R.M. Gschwind, H.D. Wiemhöfer, H.J. Gores, Electrochimica Acta. 56 (2011) 3926 – 3933.
[37] M. Amereller, T. Schedlbauer, D. Moosbauer, C. Schreiner, C. Stock, F. Wudy, et al., Solid State Chem. (2014) 1–18.
[38] P.M. Richardson, A.M. Voice, I.M. Ward, Electrochimica Acta. 130 (2014) 606 – 618.
[39] Soeresen, P.R., Jacobsen, T., Electrochimica Acta. (1982) 1671–1675.
[40] B.E. Conway, Electrochemical Supercapacitors: Scientific Fundamentals and Technological Applications, Kluwer Acad. Plenum Publ. (1999) 698.
[41] F.M. Gray, Polym. Electrolyte R. Chem. Soc. Camb. (n.d.) 1997.
[42] G. Nazri, G. Pistoia, Lithium Batteries : Science and Technology, (2009).
[43] S.I. Smedly, The interpretation of conductivity in liquids, Plenum Press. (1980).
[44] H.S. Choe, B. Caroll, D.M. Pastiquareillo, K.M. Abraham, Chem Mater. (1997) 369.
[45] C.A. Angell, J Phys Chem. (1964) 218.
[46] H. Vogel, Phys Z. (1921) 645.
[47] G. Tammann, W. Hesse, Z. Anorg, Allg Chem. (1926) 245.
[48] G.S. Fulcher, JAm Chem Soc. (1925) 339.
[49] F.M. Gray, Solid Polymer Electrolytes, in: VCH, New York, 1991: p. 4.
[50] A. Ghosh, P. Kofinas, ECS Trans. (2008) 131–137.
[51] W.A. Henderson, Solid State Ion. 217 (2012) 1 – 5.
[52] B.K. Choi, Y.W. Kim, Electrochim Acta. (2004) 2307–2313.
[53] A. Magistris, P. Mustarelli, E. Quartarone, C. Tomasi, Solid State Ion. 136–137 (2000) 1241 – 1247.
[54] I. Oslen, R. Koksbang, E. Shou, Electrochim Acta. (1995) 1701.
[55] G. Petersen, P. Jacobsson, L.M. Torell, Electrochim Acta. (1992) 1495.
[56] Z. Gadjourova, Y.G. Andreev, D.P. Tunstall, P.G. Bruce, Nature. (2001) 520.
[57] Q. Liu, B. Peng, M. Shen, B. Hu, Q. Chen, Solid State Ion. 255 (2014) 74 – 79.
[58] J.A. Killis, J.-F. LeNest, A. Gandini, H. Cheradame, J Polym Sci. 19 (1981) 1073.
[59] S.M. Lee, C.Y. Chen, C.C. Wang, Y.H . Huang, Electrochim Acta. 48 (2003) 669–677.
[60] D. Benrabah, J.Y. Sanchez, M. Armand, Electrochimica Acta. 37 (1992) 1737 – 1741.
[61] F. Alloin, C.R. Herrero, J.Y. Sanchez, D. Delabouglise, M. Armand, Electrochimica Acta. 40 (1995) 1907 – 1912.
[62] M. Watanabe, A. Nishinoto, Solid State Ion. 79 (1995) 306.
[63] A. Nishimoto, M. Watanabe, Y. Ikeda, S. Kohjiya, Electrochim Acta. 43 (1998) 1177.

[64] A. Nishimoto, K. Agehara, N. Furuya, T. Watanabe, M. Watanabe, Macromolecules. 31 (1999) 1541.
[65] Y. Ikeda, Y. Wada, Y. Mataba, S. Murakami, S. Kohijiya, Electrochim Acta. 45 (2000) 1167.
[66] M. Kono, E. Hayashi, M. Watanabe, J Electrochem Soc. 145 (1998) 1521.
[67] G. Liu, C.L. Reeder, X. Sun, J.B. Kerr, Solid State Ion. 175 (2004) 781–783.
[68] J.S. Chung, H.J. Sohn, J Power Sources. 112 (2002) 671–675.
[69] T. Zheng, Q. Zhou, Q. Li, L. Zhang, H. Li, Y. Lin, Solid State Ion. 259 (2014) 9–13.
[70] A. Vögo, V. Deimede, F. Paloukis, S. G. Neophytides, , J. K. Kallitsis, Mater. Chem. Phys. (2014) 1–10.
[71] H. Jiang, S. Fang, J Power Sources. 159 (2006) 673–678.
[72] Y. Kang, J. Lee, J. I. Lee, C. Lee, J Power Sources. 165 (2007) 92–96.
[73] J.I. Lee, D.W. Kim, C. Lee, Y.Kang, J Power Sources. 195 (2010) 6138–6142.
[74] D.G. Kim, J. Shim, J.H. Lee, S.J. Kwon, J.H. Baik, J.C. Lee, Polymer. 54 (2013) 5812–5820.
[75] M. Marzantowicz, J.R. Dygas, F. Krok, A. Tomaszewska, Z. Florjanczyk, E. Zygadlo-Monikowska, et al., J Power Sources. 194 (2009) 51–57.
[76] J. Ji, B. Li, W. H. Zhong, Electrochim Acta. 55 (2010) 9075–9082.
[77] S.M. Chang, H.W. Liao, C.L. Lin, T.J. Lee, Synth. Met. 154 (2005) 21–24.
[78] J. Saunier, F. Alloin, J.-Y. Sanchez, Electrochimica Acta. 45 (2000) 1255 – 1263.
[79] H. R. Allcock, R. Prange, T. j. Hartle, Macromolecules. 34 (2001) 5463.
[80] T. Niitani, M. Shimada, K. Kawamura, K. Kanamura, J Power Sources. 146 (2005) 386.
[81] J. F. Le Nest, A. Gandini, H. Cheradame, J. P. Cohen-Addad, Macromolecules. 21 (1988) 1117.
[82] J. F. Le Nest, S. Callens, A. Gandini, M. Armand, Electrochim Acta. 37 (1992) 1585.
[83] A. Killis, J.F. LeNest, A. Gandini, H. Cheradame, Solid State Ion. 14 (1984) 231–237.
[84] H. Cheradame, A. Gandini, A. Killis, J.F.L. Nest, J. Power Sources. 9 (1983) 389 – 395.
[85] M.C. Borghini, M. Mastragostino, A. Zanelli, Electrochim Acta. 41 (1996) 2369–2373.
[86] J.-Y. Kim, S.H. Kim, Solid State Ion. 124 (1999) 91–99.
[87] G. Tillet, B. Boutevin, B. Ameduri, Prog. Polym. Sci. 36 (2011) 191–217.
[88] F. Alloin, J.-Y. Sanchez, Electrochimica Acta. 40 (1995) 2269 – 2276.
[89] F. Alloin, J.-Y. Sanchez, M. Armand, J. Power Sources. 54 (1995) 34 – 39.
[90] F. Alloin, D. Benrabah, J.-Y. Sanchez, J. Power Sources. 68 (1997) 372 – 376.
[91] J.L. Acosta, E. Morales, Solid State Ion. 85 (1996) 85–90.
[92] Y.W. Park, D.S. Lee, J Non Cryst. Solids. 351 (2005) 144–148.
[93] B.K. Choi, Y.W. Kim, H.K. Shin, Electrochim Acta. 45 (2000) 1371–1374.
[94] Z. Wen, T. Itoh, T. Uno, M. Kubo, T. Wen, O. Yamamoto, Solide State Ion. 175 (2004) 739.
[95] A.M. Rocco, A. de A. Carias, R.P. Pereira, Polymer. 51 (2010) 5151 – 5164.
[96] E.M. Masoud, A.A. El-Bellihi, W.A. Bayoumy, M.A. Mousa, J Alloys Compd. 575 (2013) 223–228.
[97] M. Erceg, D. Jozić, I. Banovac, S. Perinović, S. Bernstorff, Thermochim. Acta. 579 (2014) 86 – 92.
[98] L.R.A.K. Bandara, M.A.K.L. Dissanayake, B.-E. Mellander, Electrochimica Acta. 43 (1998) 1447 – 1451.
[99] Z. Zeng, B. Wu, L. Xiao, X. Jiang, Y. Chen, X. Ai, et al., J. Power Sources. 279 (2015) 6–12.
[100] L. Yang, J. Lin, Z. Wang, Solid State Ion. 40/41 (1990) 616–619.
[101] I.E. Kelly, J.R.Owen, B.C.H. Steele, J Power Sources. 14 (1985) 13–21.
[102] H. Ohno, Electrochemical Aspects of Ionic Liquids, Wiley New Jersy. (2005).

[103] G.T. Kim, G.B. Appetecchi, M. Carewska, M. Joost, A. Balducci, M. Winter, et al., J Power Sources. 195 (2010) 6130–6137.
[104] B. Garcia, S. Lavallee, G. Perron, C. Michot, M. Armand, Electrochim Acta. 49 (2004) 4583.
[105] J.H. Shin, W.A. Henderson, S. Scaccia, P.P. Prosini, S. Passerini, J Power Sources. 156 (2006) 560.
[106] L.X. Yuan, J.K. Feng, X.P. Ai, Y.L. Cao, S.L. Chen, H.X. Yang, Electrochem Commun. 8 (2006) 610.
[107] T. Sato, T. Maruo, S. Marukane, K. Takagi, J Power Sources. 138 (2004) 253.
[108] G.B. Appetecchi, G.T. Kim, M. Montanino, F. Alessandrini, S. Passerini, J. Power Sources. 196 (2011) 6703–6709.
[109] G.T. Kim et al., J. Power Sources. 195 (2010) 6130-6137.
[110] D.R. MacFarlane, P. Meakim, J. Sun, N. Amini, M. Forsyth, J. Phy.Chem B 103 (1999) 4164.
[111] M. Armand, C.E.M.F. El Kadiri, US 4505997, 1985.
[112] L.J. Krause, W. Lamanna, J. Summerfield, M. Engle, G. Korba, R. Loch, et al., J. Power Sources. 68 (1997) 320–325.
[113] C. Michot, CA 2527802, 2007.
[114] H. Zhang, C.Liu, L. Zheng, F. Xu, W. Feng, H. Li, et al., Electrochim Acta. 133 (2014) 529–538.
[115] M. Grunebaum, M.M. Hiller, S. Jankowsky, S. Jeschke, B. Pohl, T. Schurmann, et al., Prog. Solid State Chem. (2014) 1–21.
[116] J.-Y. Sanchez, F. Alloin, D. Benrabah, R. Arnaud, J. Power Sources. 68 (1997) 43 – 51.
[117] F. Alloin, J.-Y. Sanchez, Electrochimica Acta. 43 (1998) 1199 – 1204.
[118] E. Paillard, F. Toulgoat, R. Arvai, C. Iojoiu, L. Cointeaux, M. Medebielle, et al., J. Fluor. Chem. 132 (2011) 1213 – 1218.
[119] E. Paillard, F. Toulgoat, C. Iojoiu, F. Alloin, J. Guindet, M. Medebielle, et al., J. Fluor. Chem. 134 (2012) 72 – 76.
[120] Ayan Ghosh, Chunsheng Wang, Peter Kofinas, J. Electrochem. Soc. (2010) A846–A849.
[121] M. Armand, Solid State Lonics. 9&10 (1983) 745.
[122] W. Xu, C.A. Angell, Solid State Ion. 147 (2002) 295.
[123] M. Watanabe, Y. Suzuki, A. Nishimoto, Electrochimica Acta. 45 (2000) 1187 – 1192.
[124] M. Watanabe, H. Tokuda, S. Muto, Electrochimica Acta. 46 (2001) 1487 – 1491.
[125] R. Meziane, J.-P. Bonnet, M. Courty, K. Djellab, M. Armand, Electrochimica Acta. 57 (2011) 14 – 19.
[126] S. Feng, D. Shi, F. Liu, L. Zheng, J. Nie, W. Feng, et al., Electrochimica Acta. 93 (2013) 254 – 263.
[127] B.B. Hallac, O.E. Geiculescu, R.V. Rajagopal, S.E. Creager, D.D. DesMarteau, Electrochimica Acta. 53 (2008) 5985 – 5991.
[128] M.B. Herath, S.E. Creager, R.V. Rajagopal, O.E. Geiculescu, D.D. DesMarteau, Electrochimica Acta. 54 (2009) 5877 – 5883.
[129] D.J. Bannister, G.R. Davies, I.M. Ward, J.E. McIntyre, Polymer. 25 (1984) 1291 – 1296.
[130] T. Hamaide, C.L. Deore, Polymer. 34 (1993) 1038 – 1046.
[131] D. Benrabah, S. Sylla, F. Alloin, J.-Y. Sanchez, M. Armand, Electrochimica Acta. 40 (1995) 2259 – 2264.
[132] K. Ito, Y. Tominaga, H. Ohno, Electrochim Acta. (1997) 1561–1570.
[133] W. Xu, X.-Z. Zhang, Z.-H. Deng, Y.-G. Zheng, G.-X. Wan, Solid State Ion. 111 (1998) 219 – 226.

[134] X. Ollivrin, F. Alloin, J.-F. Le Nest, D. Benrabah, J.-Y. Sanchez, Electrochimica Acta. 48 (2003) 1961 – 1969.
[135] C. Chauvin, X. Ollivrin, F. Alloina, J.-F. LeNest, J.-Y. Sanchez, Electrochimica Acta. 50 (2005) 3843 – 3852.

II. Synthesis and characterization of a family of oligoethers end-capped by lithium aryl perfluorosulfonate

II.1. Introduction

Solvent-free polymer electrolytes, which behave both as an ionic conductor and a separator, preventing short-circuits, are used in lithium polymer batteries [1], [2] to overcome the safety issue related to liquid leakage and organic solvent flammability in liquid electrolytes [3], [4]. The main attributions of electrolytes relates to their transport properties such as the ionic conductivity and the transference numbers, which are mainly related to the ion's mobility, salt dissociation and the interactions of the salt with the polymer matrix. Moreover other characteristics for example; a wide electrochemical stability window and good thermo-mechanical properties are also the indispensable properties contributing to the performance enhancement of polymer electrolytes [5]. Due to (i) its commercial availability and (ii) its excellent properties i.e., its cationic solvation ability favored by a high ionicity of the oxygen lone pair (high DN), its flexibility originating from oxyethylene segments supporting the ion transport [6], poly(oxyethylene) (POE), early became the reference host polymer and was extensively studied [7], [8]. Another essential component of electrolyte is the lithium salt that has to present good chemical and electrochemical stabilities, good solubility in the polymer and high dissociation constant. Lithium-trifluoromethansulfonimide (LiTFSI) salt is mostly used because it has good thermal, chemical and electrochemical stabilities and also provides high conductivity [9]; however, its cationic transference number is low [10] when hosted both in linear and cross-linked POE [11].

As mentioned in the bibliographic chapter, the cation diffusion in POE is assisted by the segmental motion of the polymer chain. The mobile Li^+ is strongly coordinated with ether oxygen atoms (high DN) while anions have much weaker interactions (low AN) with polymer chains allowing the anions to diffuse faster than Li^+ and resulting in low cationic transference numbers [12]. Additionally, the existence of higher anionic mobility in the electrolyte leads to the detrimental effect of large salt concentration gradient causing the concentration polarization and limiting the power output of the cell [13].

The designing of bulkier anions with improved interactions with polymer matrix could lead to an increase in cationic transference number.

In previous work our group synthesized the lithium -2-(phenylsulfanyl)-1,1,2,2-tetrafluoroethanesulfonate (Figure 2.1) [14, 16] with fairly high cationic conductivity (1×10^{-4} S/cm at 70 °C) and transference numbers ranging between 0.48 and 0.52 in POE matrix. The perfluoroethane chain (-CF_2CF_2-) contributes to the delocalization of negative charge through the strong electron withdrawing effect causing a good dissociation and dissolution of salt. The thioether function (-S-) increases the flexibility of the molecule but its stability in oxidation was a priori questionable. However, it was previously shown the double substitution of S by aryl and perfluorinated moieties induce an significant enhancement of its electrochemical stability [15] (and any salt degradation was observed up to 4.3 V vs Li/Li^+).

With the aim to increase the cationic transference number and the cationic conductivity we propose to attach the anion $PhSCF_2CF_2SO_3Li$ to a short POE chain (methoxy polyethylene glycol, mPEG). The aromatic ring has the advantage to be easily modified and allow its coupling with mPEG derivates. By attaching the mPEG to the anion of lithium salt we could expect (i) to improve the compatibility between the anion and the POE matrix and thus an increase of cationic transport number, (ii) to decrease the crystallinity of POE matrix, (iii) to benefit from a self-solvation of Li^+ by the oligomeric chain and (iv) to induce a plasticization of the polymer electrolyte and, therefore to increase Li^+ motion. Thus, in this work, lithium salts end-capped by mPEG with different lengths were synthesized.

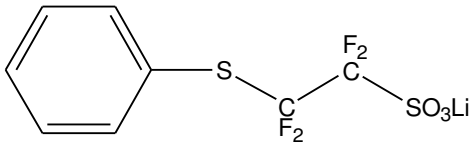

$PhSCF_2CF_2SO_3Li$

Figure 2.1. Chemical structure of Lithium -2-(Phenylsulfanyl)-1,1,2,2-tetrafluoroethanesulfonate.

In this chapter in the first part we discuss on the synthesis and characterizations of mPEG aryl perfluoroalkyl lithium salts (figure 2.2). In the second part the new salts were incorporated in a POE or in a POE derivate matrix and the resulting films were assessed in

terms of thermal, thermo-mechanical, electrochemical properties. Their ion transport ability was studied obviously by measuring the conductivity by impedance spectroscopy but also by measuring their cationic transference numbers by using both electrochemical impedance spectroscopy and Pulsed Field Gradient Nuclear Magnetic Resonance spectroscopy (PFG-NMR).

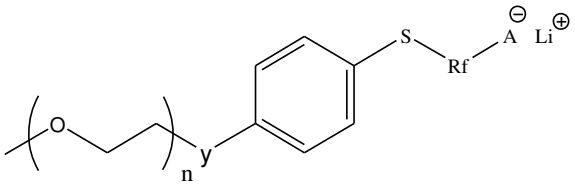

Figure 2.2. Chemical structure mPEG-aromatic.

II.2. Preparation of salts and their characterizations

The aim of this synthesis is to link a mPEG chain to the lithium perfluorosulfonated salt by a nucleophilic substitution, starting from lithium 2-(4-oxydophenylsulfanyl)-1,1,2,2-tetrafluoroethanesulfonate (LiPST) (Figure 3.3 delivered by the SME Eras-Labo).

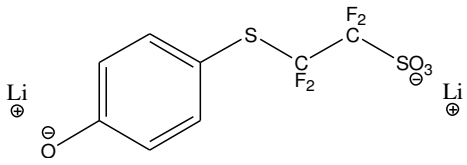

LiPST

Figure 2.3. Chemical structure of lithium 2-(4-Oxydophenylsulfanyl)-1,1,2,2-tetrafluoroethanesulfonate (LiPST).

Two synthesis protocols were used:

1) Nucleophilic substitution of **LiPST** on bromoallyl mPEG (**salt 1**).

2) Nucleophilic substitution of **LiPST** on trifluoromethansulfonate mPEG (**salt 2**)

Prior to synthesize PEG-salts, the reactions were tested on molecules.

II.2.1.Synthesis of salt 1

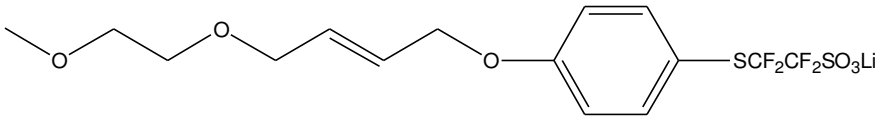

Figure 2.4. Chemical structure of **salt 1**.

The synthesis of **salt 1** was carried out in two main steps (Figure 2.5). Firstly, the hydroxyl function of methoxyethanol was reacted with the dibromobutene via a nucleophilic substitution (SN) to produce **BrmPEG**, followed in the second step by a SN with the **LiPST**.

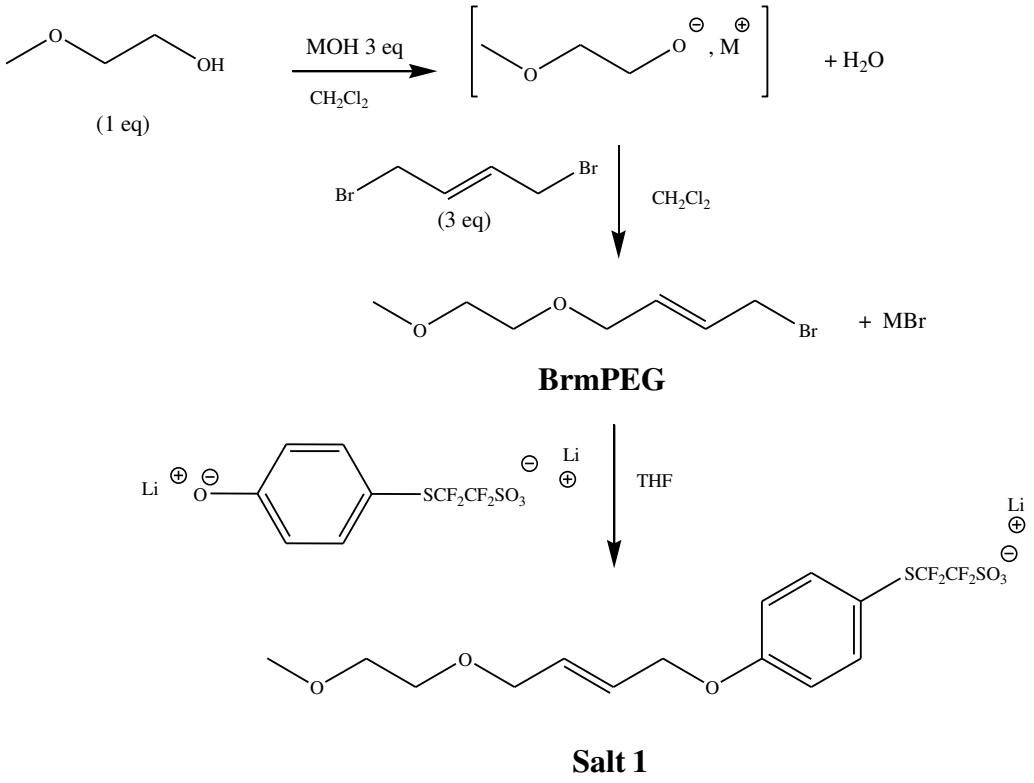

Figure 2.5. Synthesis pathway of **BrmPEG** and **Salt 1.**

Synthesis of **salt 1**.First step

In order to avoid the double substitution of dibromobutene (reaction shown in the Figure 2.6) and to optimize the yield different reaction conditions (base, temperature, solvent) were tested before to find the best protocol Table 2.1.

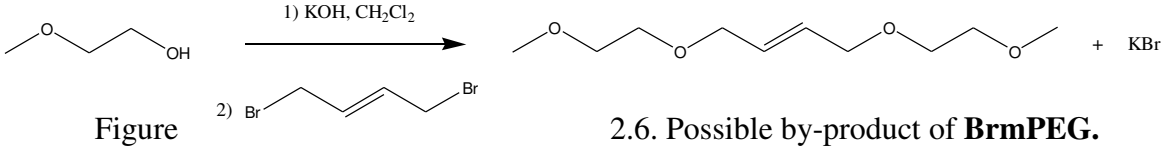

Figure 2.6. Possible by-product of **BrmPEG.**

Table 2.1. Various conditions tested for the formation of intermediate of **BrmPEG**

Entry	Deprotonation			**BrmPEG** formation		% yield
	Base	Solvent	Temperature, reaction time	Solvent	Temperature, reaction time	
1	NaH (1 eq)	THF (in glove box)	RT, 18 h	THF (in glove box)	RT, 24 h	33
2	NaH (1 eq)	THF (in glove box)	50 °C, 18 h	THF (in glove box)	50 °C, 24 h	30
3	KOH (3 eq)	THF	50 °C, 4 h	THF	50 °C, 24 h	27
5	KOH (3 eq)	ACN	50 °C, 4 h	ACN	50 °C, 24 h	8
4	KOH (3 eq)	CH_2Cl_2	50 °C, 4 h	CH_2Cl_2	RT, 16 h	42
6	KOH (3 eq)	CH_2Cl_2	RT, 4 h	CH_2Cl_2	RT, 16 h	66
7	KOH (3 eq) $NBuHSO_4$ (0,1eq)	CH_2Cl_2	RT, 1 h	CH_2Cl_2	RT, 16 h	16

First the reaction was carried out in the glove box; the alcohol deprotonation was performed with NaH but the maximum yield was only 33%. Moreover the increase of reaction temperature from room temperature (RT) to 50°C decreases the conversion in mono-substituted bromobutene.

The solvent seems to have an important impact on the reaction conversion, how it can be seen from Table 2.1. The best conversion into **BrmPEG** was obtained with dichloromethane in which the KOH and potassium alcoolate might have the lowest solubility as compared to other two solvents (acetonitrile ACN, tetrahydrofurane THF). We expected an

increase of conversion by using the tetrabutylammonium bisulfate as phase transfer catalyst [16] but the result was the opposite, only 16 % of **BrmPEG** was isolated.

Finally the precursor of **salt 1** was synthetized by the nucleophilic substitution between the ether alcohol and dibromobutene in the presence of KOH in dichloromethane at ambient temperature.

Synthesis **of salt 1**. Second step

In the second step, the nucleophilic substitution between the resulting monobromo intermediate (**BrmPEG**) obtained in the first step and the LiPST takes place to form **salt 1**.

The presence of a double bond in beta of halogen could both (i) avoid the elimination, competitive to substitution and (ii) accelerate the SN substitution with the phenolate by increasing the nucleofuge (leaving) character of Br.

However to achieve the maximum yield, that was 95%, the reaction was maintained for 3 days at 60°C. For some batches from ERAS labo, the addition of LiH was necessary to increase the conversion from 80% to 95%. This was probably due to the presence of LiPST in phenol form (OH) and not Li phenolate. Nevertheless, after the LiPST was treated with quantitative amount of LiH (figure 2.7) the crude yield, observed by NMR, exceeded 95%.

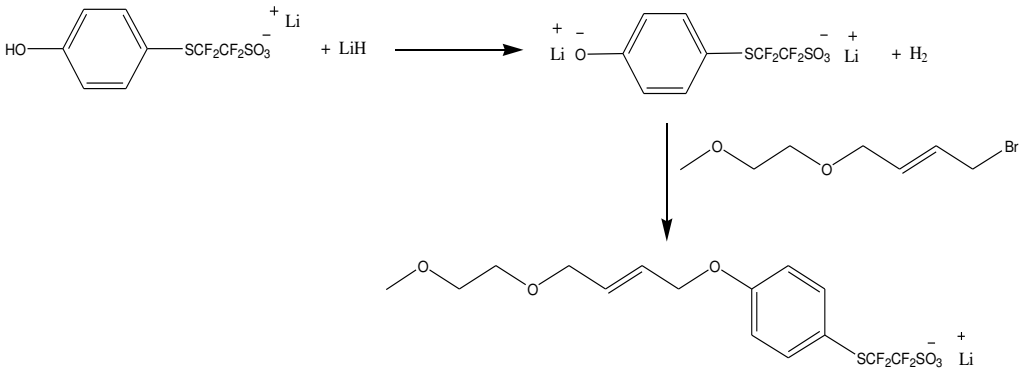

Figure 2.7. Reformation of LiPST by LiH.

NMR characterization

The ^{1}H-NMR spectra of **salt 1** and **BrmPEG** are presented in the figure 2.8. After the substitution of Br from BrmPEG the peak corresponding to the allylic protons shifts from 5.8 (e'f') ppm to 5.9 ppm (e,f) while the peak corresponding to $BrCH_2$, at 3.8 ppm (g'),

disappears and a new peak appears at 4.6 ppm corresponding to CH_2-O-aryl (g). New peaks appear in the range 7.0-7.5 ppm assigned to the aromatic protons (h, i) as well.

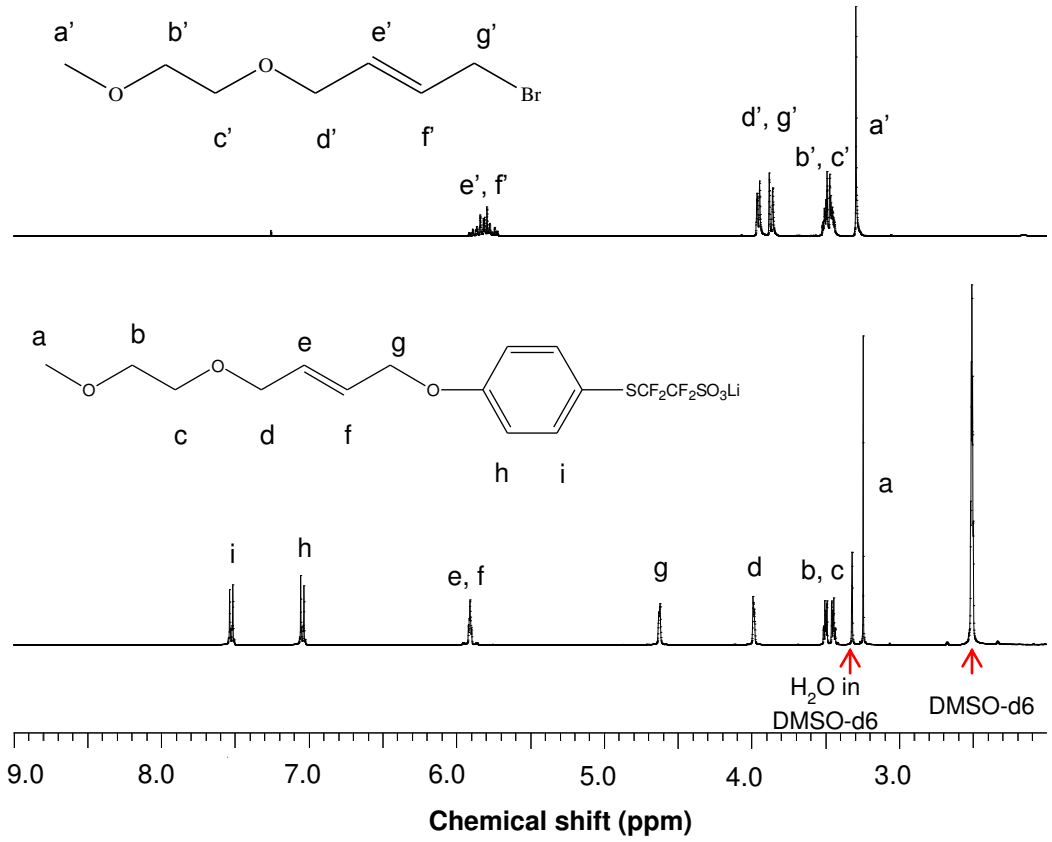

Figure 2.8. Comparative ^{1}H-NMR spectra between (a) substrate (monobromo compound) and (b) product (**salt 1**).

The evolution of the reaction during the second step was followed by ^{19}F-NMR too. In the figure 2.9 the spectra of **salt 1** with LiPST are presented. The peaks corresponding to the **salt 1** are slightly shifted as compared to LiPST. Any other peak is observed in the spectrum 2.9 b that prove the **salt 1** is pure and all the LiPST was reacted or eliminated.

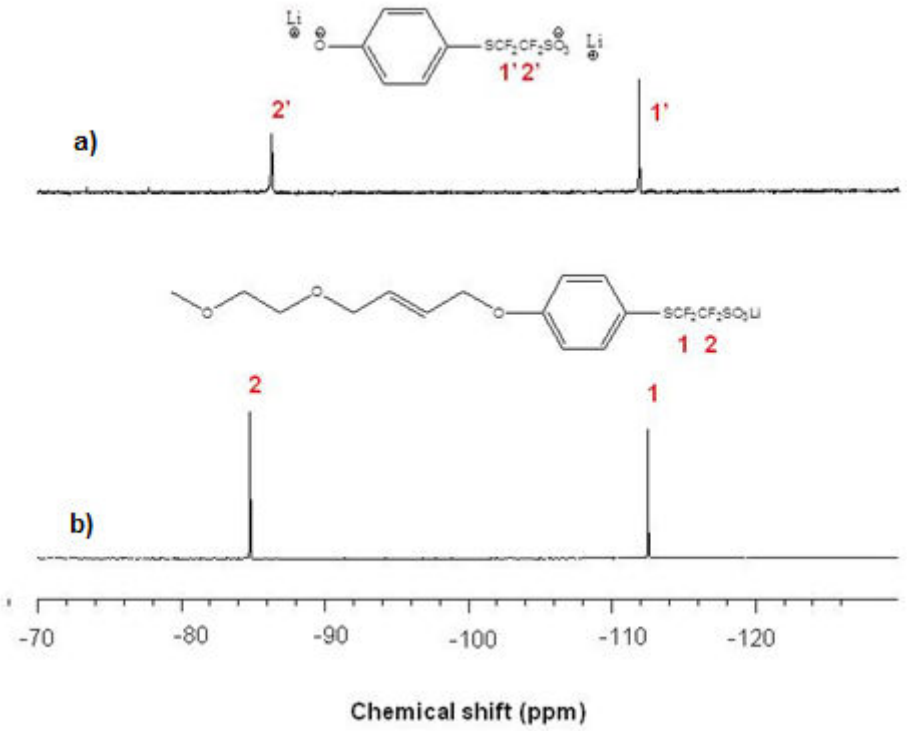

Figure 2.9. Comparative ^{19}F-NMR spectra between (a) reactive and (b) product (**salt 1**).

Elementary analysis

The purity of the salt was also checked by elemental analysis. As shown in the Table 2.2 there is a very good agreement between the calculated and found values for the whole of the analyzed elements.

Table 2.2 Elemental analysis of **salt 1**

Salts	%	C	H	S	F	Li
Salt 1	Calc.	40.91	3.89	14.56	17.26	1.58
	Found.	40.90	3.91	14.30	17.2	1.52

The best total yield in the synthesis of **salt 1** was 63 %. However the reaction time of each step was long. Moreover, the final product contains a double bond that could decrease the electrochemical stability of the salt. The hydrogenation of the double bond can be performed but a new step has to be added in the synthesis of the salt.

II.2.2.Synthesis of salt 2

In order to simplify the synthesis and increase the yield, an alternative protocol was proposed by using a mPEG end-capped by a better leaving group than the Br from allyl bromide, i.e. trifluoromethanesulfonate (CF_3SO_3). The utilization of such leaving group, allows performing the reaction directly on saturated alcohol and good yield might be expected.

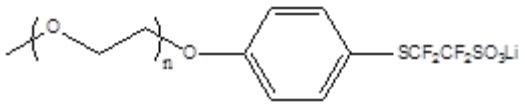

Figure 2.10. Chemical structure of **salt 2**.

The synthesis of the **salt 2** was performed in two steps (figure 2.11). In the first step the reaction between mPEG and triflic anhydride was carried out in the presence of Amberlyst A21® resin in anhydrous dichloromethane, followed in the second step by the reaction of LiPST.

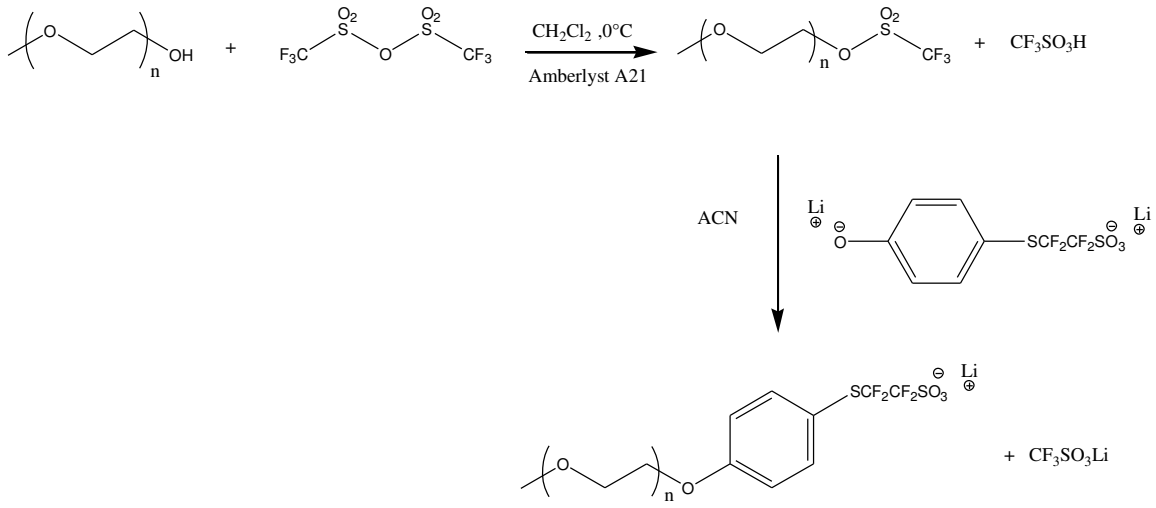

Figure 2.11. Synthesis of **salt 2, n= 1, 3, 7.2 and 16.3.**

Synthesis of **salt 2**. First step

The first step was monitored by ^{1}H and ^{19}F NMR:

In the ^{1}H-NMR spectra the shifting, from 3.6 to 4.5 ppm, of the peak corresponding to protons

CH_2-(OH) proves the transformation of OH into O-SO_3CF_3 (Figure 2.12). The reaction time is 30 min with a yield of 100%. However the product is not very stable, the yellow viscous liquid becomes black if it is kept at room temperature long-time (more than one day) even if is stored in glove box.

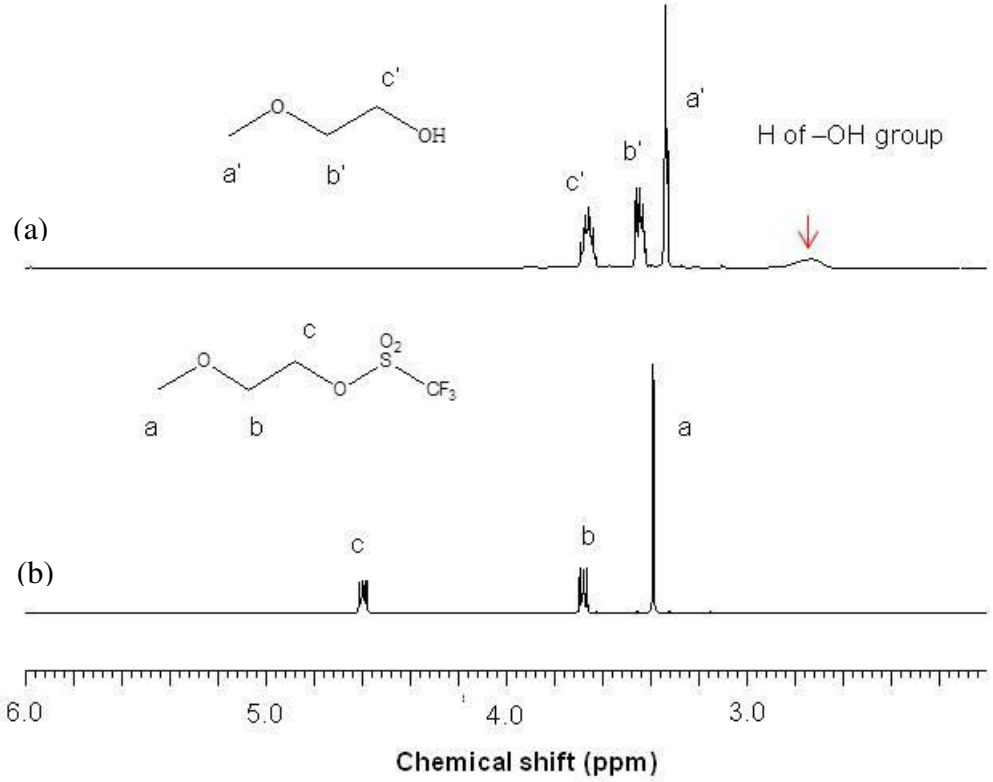

Figure 2.12. Comparative ^{1}H-NMR spectra between (a) reactive (mPEG, n=1) and (b) product (intermediate of **salt 2n1**).

Synthesis of **salt 2**. Second step

The resulting product $CH_3(OCH_2CH_2)_nOSO_3CF_3$ (mPEGSO_3CF_3) was added to a solution of LiPST in anhydrous acetonitrile forming **salt 2** by the nucleophilic substitution. Triflate leaving group was transformed in CF_3SO_3Li and eliminated by flash column chromatography. Due to the excellent leaving group, the reaction time for this step, less than 1 hour, is much lower than for the synthesis of **salt 1**, with a yield close de 90% (by NMR analysis on crude reaction product). The pure product was further isolated by flash column chromatography. However, the total yield of this reaction depends on the mPEG length, i.e. it decreases with the increase of mPEG length and ranged between 50 to 90% (table 2.3).

Table 2.3 Yield % in crude and pure **salt 2** according to the mPEG length

Repeating units of mPEG (n)	% crude yield (from NMR spectra)	% yield (pure product)
1	95	56
3	100	90
7.2	90	67
16.3	85	50

NMR characterization

Figure 2.13 and Figure 2.14 represent the ^{1}H-NMR and ^{19}F-NMR spectra of intermediate $mPEGSO_3CF_3$ and **salt 2n1**. The shift of the triplet from 4.6 ppm (corresponding to the two protons situated on the carbon in α position of sulfonate group) to 4.15 ppm assigned to the two protons of located on C on c position (bonded to phenolate) prove the transformation of $mPEGSO_3CF_3$ in **salt 2n1.** Additionally the evolution of reaction is monitored by the integral of singlet at 3.3 ppm and multiplet at 7.0 and 7.5 ppm corresponding to the three protons of methyl group and four aromatic protons, respectively. The evolution of reaction was monitored by ^{19}F-NMR as well. The peak at -74 ppm disappears whereas two triplets at -85 and -113 ppm appear indicating the successful bonding between the oligoether to the LiPST.

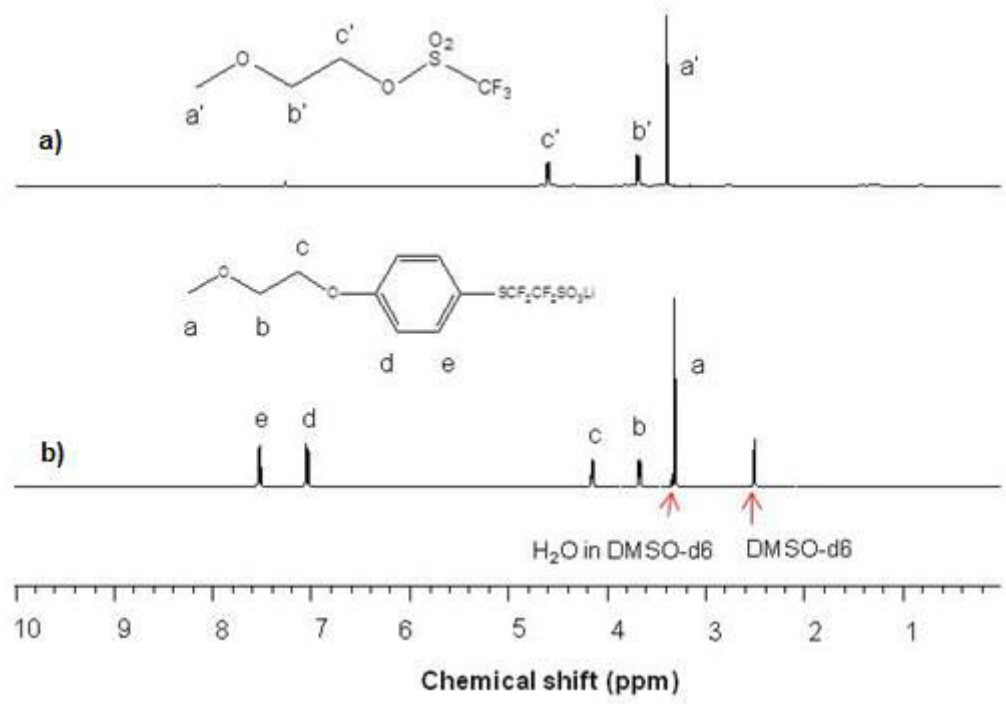

Figure 2.13. Comparative ^{1}H-NMR spectra between (a) intermediate mPEGSO3 and (b) **salt 2n1**.

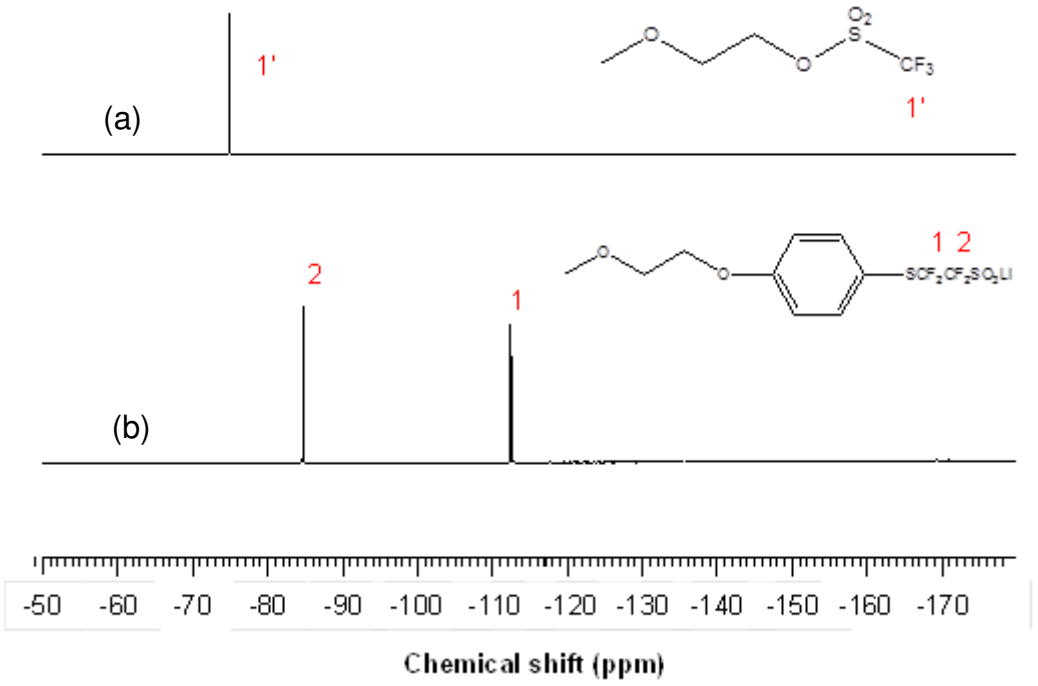

Figure 2.14. Comparative ^{19}F-NMR spectra between (a) intermediate mPEGSO3 and (b) **salt 2n1**.

Elemental analysis

The purity of the salts were checked also by the elemental analysis, the results are gathered in the Table 2.4. The obtained values seem to be very close from the calculated ones and confirm the high purity of the synthetized salts as also shown by ^{1}H and ^{19}F NMR.

Table 2.4 Elemental analyses of **salt 2n1, salt 2n7, salt 2n16**

Salts	%	C	H	S	F	Li
Salt 2n1	Calc.	35.68	2.99	17.32	20.52	1.87
	Found.	35.37	2.9	17.64	20.84	1.8
Salt 2n7	Calc.	43.67	5.57	9.95	11.82	1.09
	Found.	43.57	5.44	9.13	11.54	1.07
Salt 2n16	Calc.	47.86	6.92	6.14	7.29	0.67
	Found.	47.75	7.06	5.93	7.33	0.57

II.2.3.Physical characterizations of salts

II.2.3.1.Thermal characterizations of salts

The characteristic temperatures of the salts, i.e. glass transition temperature (T_g), melting temperature (T_f), degradation temperature (T_d) were measured by Differential Scanning Calorimetry (DSC) and Thermogravimetric Analysis (TGA) respectively. The DSC measurements were performed in the temperature range of -100 to 250°C and the DSC results are presented in Table 2.5.

The Tgs of **salt 1** and **salt 2n1** were impossible to be measured even after the salt melting and quenching, probably due to high ability of the salt to crystallize. For the other **salts 2 with n ≥ 3** the bonding of LiPST on the mPEG leads to an important increase of the glass transition temperature (T_g) as compare to pure mPEG. However their Tg are much lower than that of aromatic lithium salt, $PhSCF_2CF_2SO_3Li$ (without end-capping with mPEG [15], [17]) and decrease with the increase of n.

The **salt 1** and **salt 2 n1** and **n3** are crystalline and the values of T_m are higher than that of $PhSCF_2CF_2SO_3Li$. Moreover, except for the **salt 2 n1** the ΔH is also higher. From these

results, it can be pointed out that the bonding of short mPEG chains on the anion favors the salt organization and reinforce the intermolecular interactions, due probably to the interaction of Li with the oxygen from oligoether. However, for **n7** and **n16** the salts are completely amorphous at room temperature. It is known that five O atoms are necessary for the solvation of Li^+. In the **salt 2 n7** and **n16,** 2 and 11 O atoms respectively are in excess; therefore we assume the mPEG chain can organize differently and lead to amorphous materials.

Table 2.5 Glass transition temperature (T_g) and melting temperature (T_m) of mPEG, **Salt 1**, **salt 2** and $PhSCF_2CF_2SO_3Li$

Samples	T_g (°C)	T_m (°C)	ΔH (J/g)
$PhSCF_2CF_2SO_3Li$[a]	63	118	20
Salt 1	-	162	58
Salt 2n1	-	197	8
mPEG (n=3)[b]	-73	-	-
Salt 2n3	29	130	76
mPEG (n=7.2)[b]	-64	-7	54
Salt 2n7	-11	-	-
mPEG (n=16.3)[b]	-60	22	118
Salt 2n16	-39	-	-

a: data from thesis of E. Paillard, INPG (2008) [17]
b: data from thesis of C. Chauvin, INPG (20005) [18]

The thermal stability was studied by TGA (Figure 2.15). The percentage of weight loss of samples is followed as a function of temperature; the measurements were scanned from 25°C to 500°C under nitrogen with a heat rate of 5°C/min.

Figure 2.15 shows TGA curves of **salt 2** with different chain lengths of mPEG. The onset of weight loss varying from 210 °C to 250 °C and depends on the lengths of mPEG. The decomposition of **salt 2n3** starts at 210°C, similar to that of an aryl lithium perfluorosulfonte salt ($PhSCF_2CF_2SO_3^-Li^+$) [19] while the thermal stability is enhanced for the **salts 2n7** and **2n16**. Taking into account the similar structure of the salts and the degradation temperature of mPEG we suppose that the degradation starts at the same temperature for all the salts but with the increase of mPEG molecular weight, the salts are more dissociated and interact with mPEG chains and probably its resulted degradation fragments, decreasing their volatility.

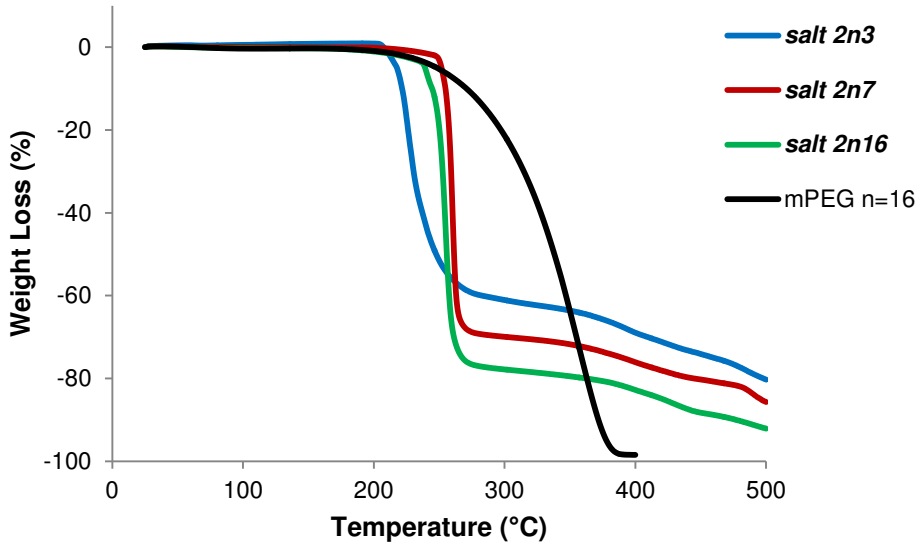

Figure 2.15. Thermogravimetric analysis of aromatic lithium salts.

II.2.3.2. Intrinsic conductivity of salts

The conductivities of the salts were measured by electrochemical impedance spectroscopy in the frequency range of 5 Hz – 13 MHz and temperature range from 20° to 110°C. In this range of temperature only **salt 2 n7** and **salt 2 n16** are in their amorphous state while the others are crystalline and don't present any measurable conductivity. Figure 2.16 shows the conductivity curves of **salt 2n**7 and **salt 2n16** as a function of 1000/T. It can be seen that, the conductivity of **salt 2n16** is higher than that of **salt 2n7** with 2.91×10^{-4} S/cm at 110°C and 7.22×10^{-6} S/cm at 30 °C respectively, despite a higher ionic concentration of the **salt 2n7**. However, to solvate the Li and to dissociate the lithium salt at least five oxyethylene units are necessary. The interaction of Li^+ with several oxygen leads to inter-chains physical cross-linking that could stiffen the system. The increase of molar ratio O/Li contributes both (i) to the solvation of Li^+ and thus the increase of the dissociation, and (ii) to the increase in ions mobility, proved also by the lower T_g in the case of **salt 2n16**. However by analogy with the Li^+ migration, in the case of poly(oxyethylene) (POE), the Li^+ migration from one coordinating site to another is controlled by the segmental motion, that might be higher is the case of **salt 2n7** (lower T_g values).

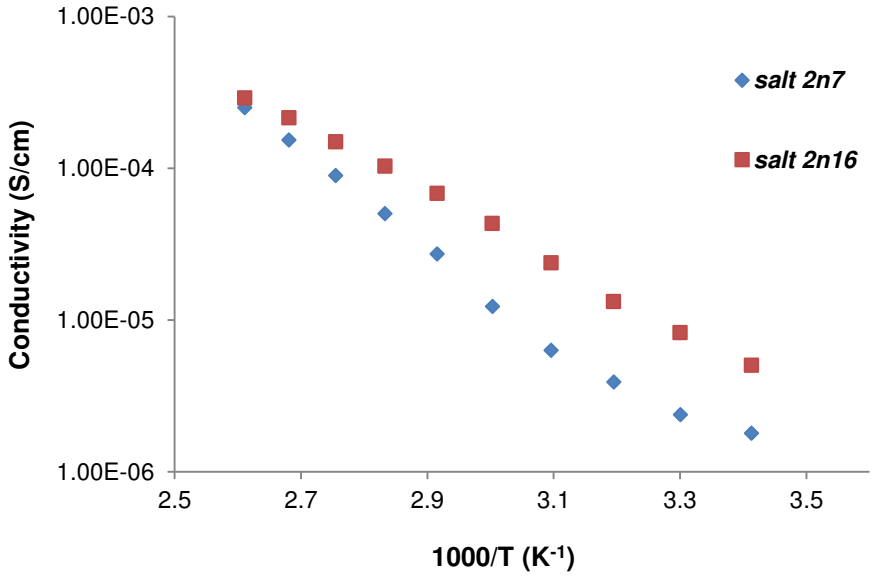

Figure 2.16. Conductivity of aromatic lithium salt in a family of **salt 2**.

II.2.3.3. Diffusion coefficient of salts

The self-diffusion coefficient of anion ($D^{19}F$) and Li^+ (D^7Li) of **salts 2n7** and **n16**, measured by multinuclear Pulse Field Gradient NMR (^7Li and ^{19}F) are gathered in the Table 2.6. It is observed that the diffusion coefficients of anions are lower than that of lithium for both salts. As for comparison of self-diffusion coefficient of both salts, the values of anions (F) are very close while a factor more than 2 is obtained for the diffusion coefficient values of lithium cations. The diffusion coefficient is directly related to the viscosity of the salt and the bulkiness of species that are diffusing. Taking into account the differences in size of mPEG and the close values of diffusion coefficients of anions of both salts it can be supposed that the viscosity of **salt 2n16** is lower than of that of **salt 2n7.** The higher value of diffusion coefficient of Li in the **salt 2n16** is due to higher flexibility and segmental motion of mPEG chain as compared to those of mPEG from **salt 2n7**.

Table 2.6 Comparison of diffusion coefficients determined by PFG-NMR at 383K

	Salt 2n7	**Salt 2n16**
$D^{19}F(cm^2s^{-1})$	0.69×10^{-7}	0.67×10^{-7}
$D^{7}Li(cm^2s^{-1})$	1.22×10^{-7}	1.52×10^{-7}
σ_{Nernst} (Scm^{-1})	4.95×10^{-4}	4.07×10^{-4}
σ_{exp} (Scm^{-1})	2.52×10^{-4}	2.91×10^{-4}
% dissociation	51	71

With the help of self-diffusion coefficients the conductivities can be calculated (σ_{calc}) by using Nernst-Einstein equation.

$$\sigma_{Nernst} = \frac{F^2 C\ (D_+ + D_-)}{RT} \tag{4}$$

Where F Faraday constant (9.6485×10^6 Coulomb/mol), R gas constant (8.31446 J/(K mol), C ionic molar concentration mol.

However, this equation is valid for the infinitely dilute solution. For our salts, it is sure the calculated values are not correct but it permits the comparison between the two salts.

In order to calculate the ionic molar concentration (C), we first calculate the salt density by using the next formula: [18]

$$\rho_{salt} = \frac{M_{PEG}}{M_{PEG} + M_{LiPST}} * \rho_{PEG} + \frac{M_{LIPST}}{M_{PEG} + M_{LiPST}} * \rho_{LiPST} \tag{5}$$

where M_{PEG} et ρ_{PEG} the molecular weight and density of mPEG used in the synthesis of **salt 2**, M_{LiPST} is the molecular weight of LiPST et ρ_{LiPST} is the density of LIPST measured with a pycnometer (2.4915 g/cm^3). The values of density of different salts are gathered in Table 2.7 and the calculated values of conductivity of **salt 2n7** and **n16** are presented in Table 2.6.

	Density (g/cm^3)	Concentration (mol/cm^3)
Salt 2 n1	**2.20**	**5.94×10^{-3}**
Salt 2 n3	**1.99**	**4.35×10^{-3}**
Salt 2 n7	**1.75**	**2.73×10^{-3}**
Salt 2 n16	**1.51**	**1.45×10^{-3}**

Table 2.7 Density and molar concentration of **salt 2**

The NMR provides the diffusion coefficient of a specie but it does not discriminate between the charged and neutral species (dissociated anion-cation or ion pairs), while the ionic conductivity measure the diffusion of only the charged species. Hence, by the ratio between σ_{exp} and σ_{calc} (equation (5)),, the dissociation degrees can be inferred (Table 2.5).

$$\%\ dissociation = \frac{\sigma_{exp}}{\sigma_{Nernst}} \times 100 \quad (6)$$

For both salts values of 51 % and 71 % were calculated for **salt 2n7** and **salt 2n16** respectively. These results indicate a higher dissociation of **salt 2n16** as compared with **salt 2n7.** The higher dissociation degree can explain the higher conductivity of **salt 2n16** despite a lower lithium concentration.

II.2.3.4. Cationic transference number

One of the factors affecting the performances of lithium salt is the transference number. The ideal transference number is $T^+ = 1$, that means the conductivity is done only by the migration of Li^+. But for most of the salts the migration of the anion is much higher than that of cation and the existence of anionic mobility in the electrolyte leads to the detrimental effect of large salt concentration gradient causing the concentration polarization and limiting the power output of the cell.

The intrinsic cationic transference numbers were determined here starting from diffusion coefficients using the next equation (7), where D^+ is D^7Li and D^- is $D^{19}F$.

$$T^+ = \frac{D^+}{D^+ + D^-} \quad (7)$$

The cationic conductivities are calculated with the equation: $\sigma^+ = T^+\sigma$ where σ is experimental conductivity. (Table 2.8)

Table 2.8 Comparison of intrinsic cationic transference numbers and cationic conductivities of **salt 2n7** and **salt 2n16** investigated by PFG-NMR at 383K

Salt	O/Li	σ (S/cm)	T^+	σ^+ (S/cm)
Salt 2n7	7.2	2.52×10^{-4}	0.64	1.61×10^{-4}
Salt 2n16	16.3	2.91×10^{-4}	0.72	2.09×10^{-4}

From the result in Table 2.8, the transference number of **salt 2n16** ($T^+ = 0.72$) exhibits higher value than that of **salt 2n7** ($T^+ = 0.64$). The cationic conductivities reached 2.09×10^{-4} S/cm for **salt 2n16**, higher than for **salt 2n7** i.e. 1.61×10^{-4} S/cm. These results are different from those reported by C. Chauvin [18] for POE oligomer mono-end capped by sulfate group (CH_3-O (-CH_2-CH_2-O)$_n$-OSO_3Li for which they reported a higher T^+ for the salts with shorter mPEG (n= 7 $T^+ = 0.58$, n=16 T^+=0.46).

II.2.3.5. Electrochemical stability of salts

The cyclic voltammetry measurements (figure 2.17) were performed in ACN + 0.1 M $TEABF_4$ as support electrolyte, scan rate of 10 mVs^{-1} at 20°C. The salt was dissolved in the electrolyte with a concentration of 5 mmol/L. The oxidation wall of the **salt 2** starts at 4.25 V versus Li/Li^+ and seems to be independent of the chain length of mPEG and very close to that of $PhSCF_2CF_2SO_3Li$ (4.3 V) [17]. Moreover, the stability seems to be slightly higher than that of POE that is known to be close to 3.9 V versus Li/Li^+. This result is a good surprise and is in line with theoretical calculations performed by Chauvin et al. [18] Concerning the **salt 1** its stability seems to be slightly lower, a first shoulder appear to 3.9 V versus Li/Li^+ probably due to the presence of the double bond. However, all synthesized salts seem to be enough stable for an utilization in lithium polymer batteries.

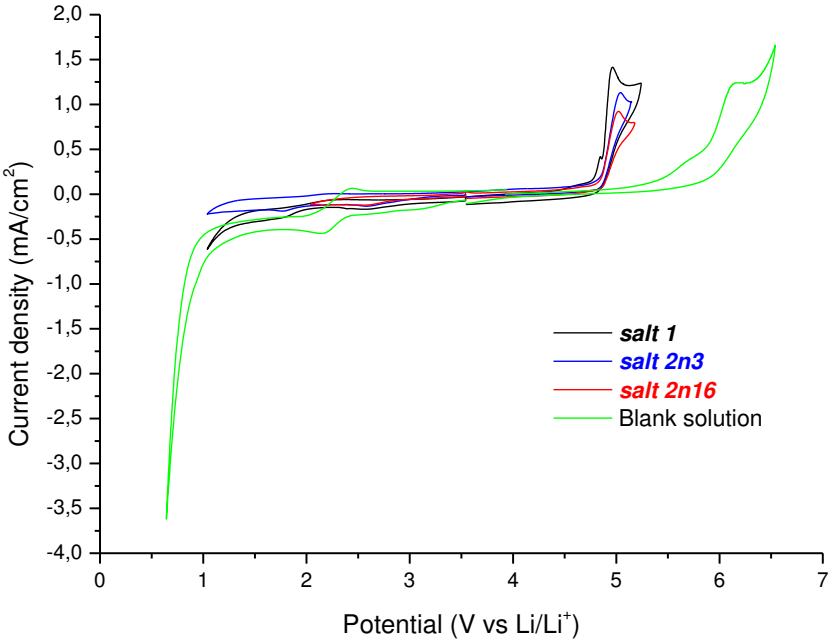

Figure 2.17. Cyclic voltamperometry of **salt 1**, **salt 2n3** and **salt 2n16** at 5 mmol/l in ACN + $TEABF_4$ (0.1 M), scan rate: 10 mVs^{-1} at 20°C on platinum as working electrode.

Table 2.9 Oxidation potential of different salts in the solution of $TEABF_4$

Salt	Oxidation potential (V vs Li/Li^+)
Supporting electrolyte (CH_3CN + $TEABF_4$)	5.3
Salt 1	3.9
Salt 2n1	4.25
Salt 2n3	4.25
Salt 2n7	4.25
Salt 2n16	4.25

II.3. Polymer electrolytes based on linear POE and salts 1 and 2

Films with different amounts of **salt 1** and **2** were elaborated by casting in glove box in argon by dissolving both POE (M_w = 300,000 g/mol) and salt in anhydrous acetonitrile. After the solvent evaporation, membranes were dried at 50 °C under vacuum for 2 days and they were then kept in the glove box for further characterizations. The membrane's thickness is 100-150 μm approximately. The thermal, thermo-mechanical properties were studied by DSC, ATG and dynamic mechanical analysis (DMA) and the ion mobility was evaluated through ionic conductivity and diffusion coefficients measurements.

II.3.1. Thermal characterization

POE is a semi-crystalline polymer. T_g, T_m and the melting enthalpy (ΔH_m) of POE electrolytes depend on salt concentration and on salt- POE interactions. Therefore the host polymer was blended with different amounts of salt, the concentration, as usual, being expressed by the ratio O/Li, where O represents the number of structural oxyethylene (OE) units for 1 mole of Li salt. For the calculation of O/Li we took also in account the OE units of the anions and we used the next formula (8):

$$\frac{O}{Li} = \frac{m_{POE}}{m_{salt}}\frac{M}{44} + n \qquad (8)$$

Where m_{POE} is the weight of POE; m_{salt} is the weight of the salt, M the molecular weight of the salt, n the number of OE structural units in the salt (mPEG), 44 represent the molecular weight of OE.

In table 2.10 are gathered T_g, T_m, and ΔH_{POE} of the electrolytes based on the linear commercial POE (M_w = 300,000 g/mol) and on **salt 1** and **salt 2**, used at various concentrations. In the column O/Li into brackets we give also the O/Li taking in account only the OE from POE.

Two series of measurements were performed. First, all the samples were submitted to two heating scans, in the first scan the samples, that was kept at least for a month in the glove

box, were heated from -100 °C to 100 °C and we measured the T_{g1}, T_{m1}, ΔH_{m1}, then it was cooled down at -100 °C with a ramp of 20 °C/min and heated once again to 100°C (T_{g2}, T_{m2}, ΔH_{m2}). In the second series, the samples were quenched, therefore the pans containing the samples placed in a well closed recipient were heated at 80°C on a heater outside of the DSC device and, after 10 min, the pans were put in the DSC at -100°C to get the characteristic temperatures of the quenched samples (T_{gq}, T_{mq}, ΔH_{mq}).

First we discuss the results obtained in the first series. T_m measured for the first and the second cycles are very close for all the electrolytes, which means that the crystallization kinetics are very fast; the salt does not delay the crystallization phenomena.

Regarding the impact of the salt on T_g, from the first and second scans, similar values were obtained excepted for the **salt 1**, where the values for the first cycle seems to be surprising lower. Moreover the T_{gs} of the electrolytes based on **salt 1** are lower, for the whole of the concentrations, than those of the electrolytes based on **salt 2n1**.

The interaction of Li^+ with several oxygen leads to inter-chains physical cross-links that stiffens the polymer electrolyte evidenced by a T_g increase [18]. The lower values for the complexes based on **salt 1** could be explained by (i) a lower dissociation of the **salt 1** or (ii) a higher ability of the anion to plasticize the POE electrolytes as compared to **salt 2n1**. The difference on T_g between the first and second scan without significant modification on Tm and ΔH_{POE} indicate a better dissociation of the salt after the first heating scan. Thus, it can be assumed in the second scan due to the heating and the melting of the POE more salt are disaggregated, dispersed in POE matrix and interact with POE in amorphous state. Hence, the T_g values are increased for the second scan. But the formed complexes are probably not stable and in time the salt reform aggregates (this could explain the lower T_g in the first scan). The behavior of **salt 1**/POE is similar to that of $PhSCF_2CF_2SO_3Li$/POE [14].

Concerning the impact of the concentration, for almost all the studied series the highest T_g seems to be for O/Li =20. At higher Li salt concentration (O/Li =12, O/Li=16) it could be expected a higher T_g value due to a higher density in physical crosslinking. The opposite results (lower T_g for O/Li =12, O/Li=16) are probably due to the salt aggregation and partial dissociation of lithium salt.

Regarding the impact of the size of anion, for the same O/Li ratio, we observe a slightly decrease of T_g with increase of mPEG chain length. However the **salt 2n16** presents two T_g, that means two amorphous phases.

The T_g decrease with the increase of mPEG lengths can be explained by (i) the ratio O/Li that involves the OE from POE (Table 2.10) (ii) the plasticizing effect of the anion. To support the 1st explanation, it must be assumed that Li^+ interacts mostly with the OE belonging to the salt when the mPEG chain is long enough. In that case the POE density in physical cross-links is decreased and the stiffness of the polymer electrolyte decreases. To support the 2nd explanation it must be emphasized that the anion's tail acts as an external plasticizer. A 3rd explanation might be invoked: a decrease of T_g that could be expressed by the well-known Flory-Fox semi-empirical relationship. However the semi-crystalline nature of the polymer does not allow a quantitative prediction to be done. However if anion's tail acts as an external plasticizer with lengthening of the anion tail a decrease in crystallization content might be expected. Contrarily it can be seen, from the table 2.10, a reverse behavior with an increase in ΔH_m and % crystallinity with the chain lengthening.

The crystallinity percentage is directly proportional to ΔH_m and is calculated according to eq. (9) where ΔH_0 is the melting enthalpy per unit weight of 100% crystalline POE, which is 205 J/g [20] and w is the weight fraction of POE in the sample.

$$X_c = \frac{\Delta H_m}{\Delta H_0 .w} \times 100 \quad (9)$$

The increase of crystallinity with the anion size means the amount of amorphous phase in POE is lower and these results sustain the hypothesis that Li^+ prefers to interact with the oxygen atoms from the anion. Moreover, for the **salt 2n16** the crystallinity degree seems to be very close to that of pure membrane that allows assuming that Li^+ interacts mostly with the O from mPEG anion.

The melting temperatures increase slightly with the increase of O/Li for all the studied series. The lengthening of mPEG anion seems to have no effect on Tm; however the values remain lower than that of the POE host.

Now if we analyze then second series we observed the T_{gq} has much lower values as compared to those obtained on the first series (T_{g1} and T_{g2}). Concerning the Tm the values

seem to be slightly lower. However for all the quenched membrane a crystallization peak was observed during the heating scan.

Table 2.10 Glass transition temperature (T_g) and melting temperature (T_m) of POE/**salt 1** and POE/**salt 2** complexes ($_1$ = the 1st cycle, $_2$ = the 2nd cycle)

Samples	O/Li ((O/Li)-n))	T_{g1} (°C)	T_{g2} (°C)	$T_{g(q)}$ (°C)	T_{m1} (°C)	T_{m2} (°C)	$T_{m(q)}$ (°C)	ΔH_{POE1} (J/g)	ΔH_{POE2} (J/g)	$\Delta H_{POE(q)}$ (J/g)	% crystallinity ($1^{st}/2^{nd}$/q)
POE	-	-	-63	-	70	69	-	125	127	-	61/62
POE/ **Salt 1**	12 (11)	-32	-23	-	53	53	-	34	34	-	17/17
	20 (19)	-39	-16	-44	62	62	55	75	74	90	36/34/44
	30 (29)	-49	-25	-50	60	60	60	108	105	113	52/51/55
POE/ **Salt 2n1**	16 (15)	-32	-32	-41	60	55	61	44	37	142	21/18/69
	20 (19)	-11	-11	-39	61	60	59	92	87	82	45/42/40
	30 (29)	-14	-14	-47	62	62	54	92	90	63	45/44/31
POE/ **Salt 2n3**	16 (13)	-34	-35	-	55	55	-	67	65	-	33/32
	20 (17)	-14	-14	-41	58	58	57	74	71	74	36/35/36
	30 (27)	-15	-17	-48	61	61	53	96	89	67	47/43/32
POE/ **Salt 2n7**	20 (13)	-18	-18	-40	57	56	56	89	87	98	44/42/48
	30 (23)	-28	-27	-49	60	60	58	96	83	98	47/41/48
	40 (33)	-	-	-52	61	61	60	126	117	126	61/57/61
POE/ **Salt 2n16**	40 (24)	-26; 7	-22; 7	-50; 7	59	59	59	123	115	107	60/56/52
	50 (34)	-33; 4	-36; 5	-54	59	59	61	122	119	146	60/58/71
	60 (44)	11	14	-51	61	61	61	128	128	189	62/62/92

ΔH_{POE} fusion enthalpy calculated by mass of POE host polymer; q : sample heated at 80°C and introduced on DSC (TA) at -100°C.

II.3.2.Thermal stability

The weight losses of different POE/salt complexes are presented in figure 2.18 as a function of temperature. The onset of weight losses of POE/**salt 2n3** and POE/**salt 2n7** start at 266 °C and 278 °C respectively and both complexes show higher thermal stability than those of the pure salts but much lower than that of pure POE. We assume that the thermal stability increase of the salts, when they are embedded in POE matrix might be due to the formation of

fragments during the degradation, that are less volatile due to the interaction with the POE. The weight loss takes place in two steps (figure 2.18b). However during the first step the weight loss is much higher than the amount of salt contained by the POE electrolytes, which means that the salt's degradations induce that of POE at much lower temperature than the pure POE.

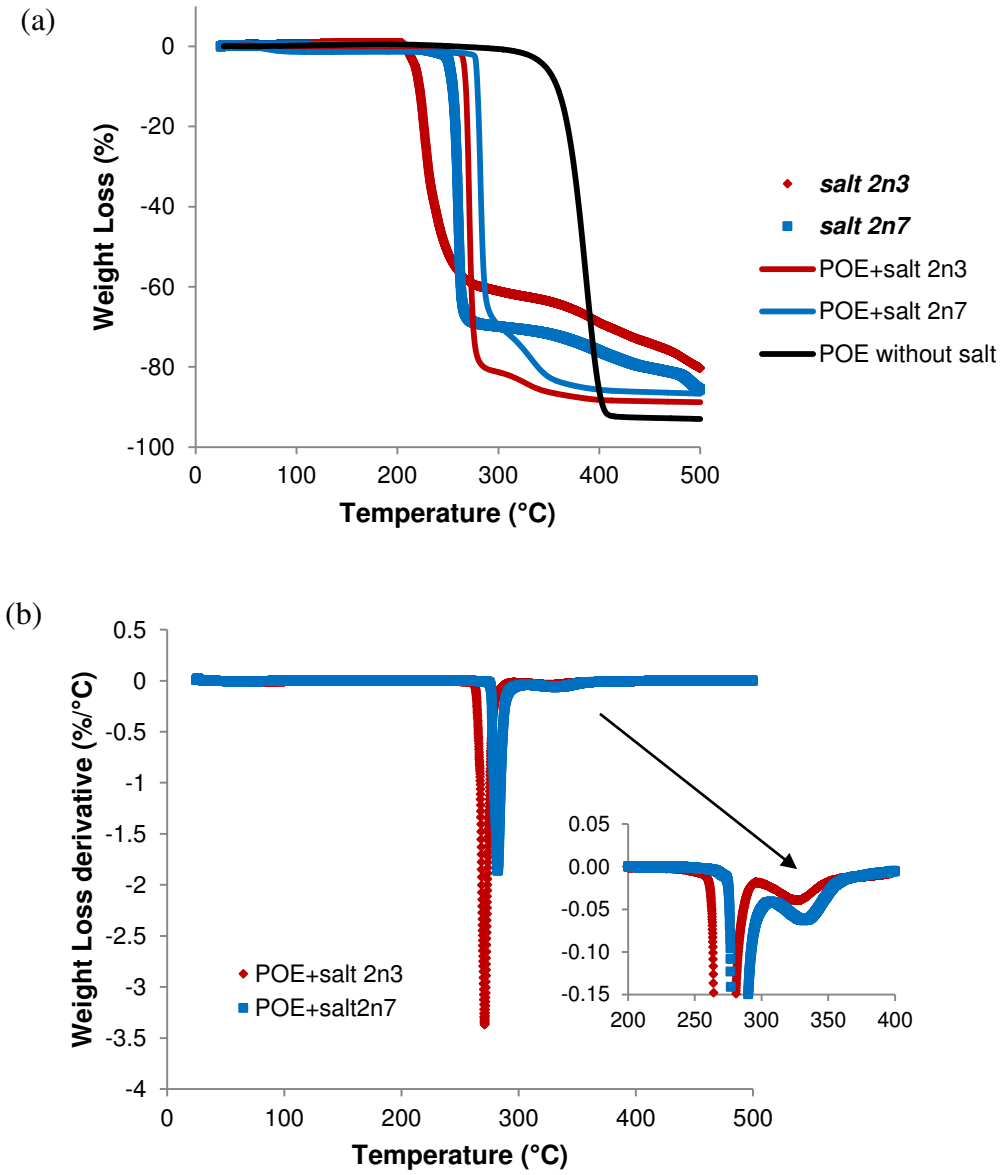

Figure 2.18. (a) TGA curves for **salt 2n3, 2n7** and POE+**salt 2n3** and **salt 2n7** complexes (O/Li=20) and (b) first derivatives of POE+**salt 2n3** and **salt 2n7.**

II.3.3.Thermo-mechanical properties

Dynamic mechanical analysis (DMA) is particularly useful for measuring the storage modulus and the transitions temperatures in polymers. Figure 2.19 (a) shows the variation in storage modulus at 1 Hz as a function of temperature for POE electrolytes at the concentration O/Li= 20. The elastic storage modulus E' at -100°C was normalized at one constant value (approximately 3 GPa) with the aim of minimizing the effect from the difference of the thickness of each sample.

If we compare the curve of pure POE, POE**/salt 1** and POE**/salt 2n1 electrolytes** we observed that (i) the T_α of POE is lower than the electrolytes one, (ii) the T_α of membrane based on POE**/salt 2n1** is the highest (iii) the POE electrolytes melt at similar temperature but lower than pure POE. The T_α are associated with the T_g, nevertheless the values of T_g obtained by DSC and DMA are very different due to the conditions of measurements. The T_α of POE + **salt 2n1** is 10°C lower than that of POE + **salt 1** and about 20°C higher than that of POE The results corroborate those obtained by DSC in the first heating scan, where the T_g of POE< POE+**salt2n1<** POE+**salt 1**.

(a)

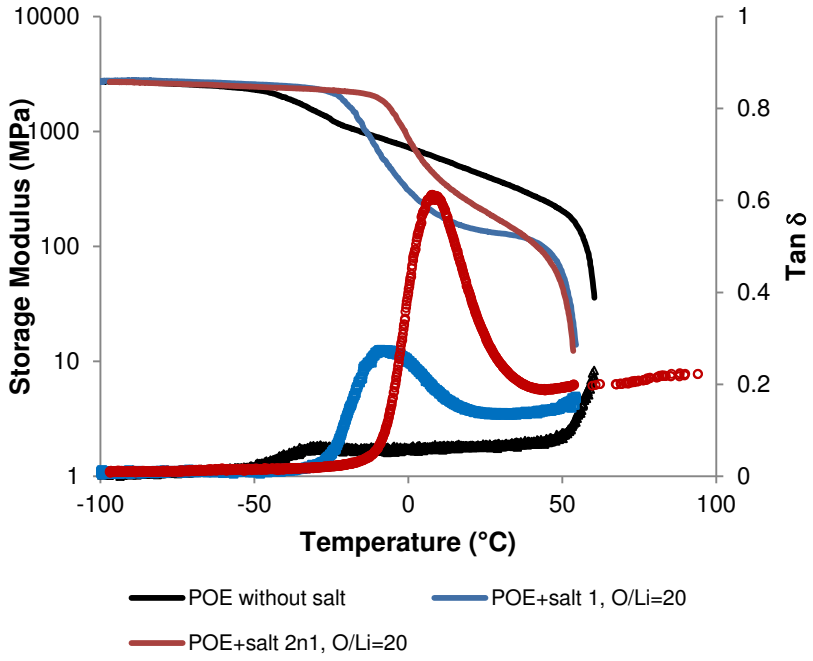

(b)

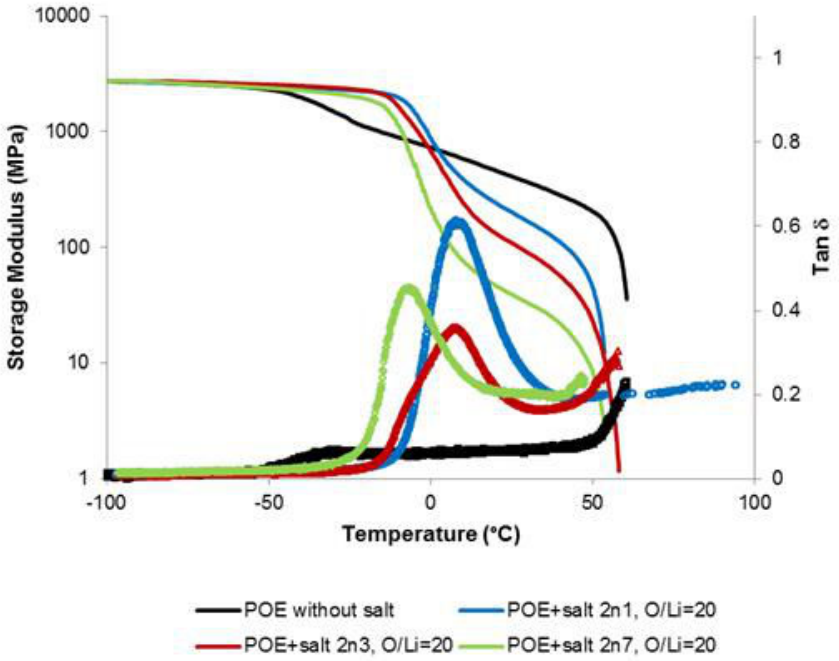

Figure 2.19. Mechanical properties of aromatic lithium salts at the concentration (O/Li) =20 (a) storage tensile modulus (E') and (b) loss angle tangent tan δ in a function of temperature.

Regarding the impact of the chain length of mPEG (n=1, 3, 7) on thermo-mechanical properties we observe that the drop in storage modulus and in T_α, appears at lower values with

the anion lengthening. These results are in agreement with those obtained by DSC. All the E' drop dramatically at temperatures close to 60°C, which correspond to the POE melting point.

Nevertheless, the behavior of electrolytes POE + **salt 2n16** is different of the other POE electrolytes based on **salt 2** having lower mPEG lengths. The figure 2.20, on the evolution of storage modulus and tanδ with the temperature, two thermal transitions appear. The first one is very close to that of pure POE membrane while the second one is much higher. The presence of two T_{α}, corresponding to the amorphous phases, underlines the presence of phase separation with the formation of two percolated phases. Similar results were obtained by DSC and support the hypothesis that the Li^+ of the salt interacts mainly with the O from mPEG attached to the anion and the salt is phase separate. Indeed, oligomers are often incompatible with their polymers of high molecular weight. The end-capping of the oligoether by a Lithium ion pair should act as a compatibilizer. If Li^+ however interacts mostly with its own oligoether tail rather than with the POE long chain, these oligomers might become immiscible with the host polymer and lead to a partial phase separation.

However the DSC T_g observed for the first and second heating of POE + **salt 2n16** seems to be higher than that of the pure **salt 2n16**. We can explain partially this higher value by the high crystallinity of the POE matrix; as DSC shown that the degree of crystallinity of POE host polymer is close to that of pure POE. The Li salt phase is therefore constrained by the crystalline phase explaining the higher T_g.

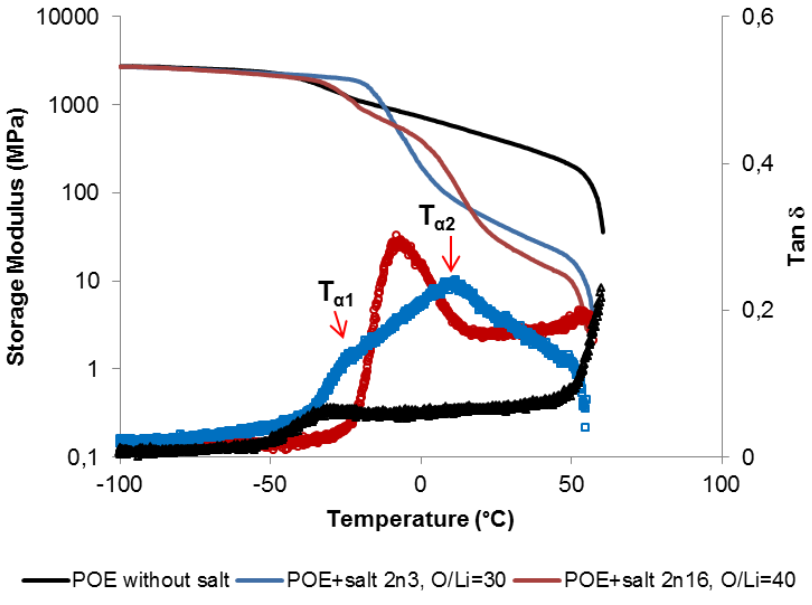

Figure 2.20. DMA curves of POE/**salt 2n3** and **salt 2n16**.

II.3.4.Conductivity

The conductivities were measured in the temperature range of 20-70 °C by impedance spectroscopy, in the heating and cooling cycles. The conductivities were measured after stabilizing for 1 hour the sample at each temperature. The maximum temperature was 70°C in order to minimize the membrane creeping. In the figure 2.21 the evolution of conductivities as a function of 1000/T on both heating and cooling cycles for membranes based on POE/**salt 1**, POE/**salt 2n1** and POE/**salt 2n16** are represented. All the conductivity curves show a specific shape for the POE electrolyte, i.e. below melting point, the conductivities followed the classic Arrhenius law, at the melting point the conductivity increase very fast to reach than a plateau where conductivities follow the VTF law. At temperatures lower than T_m, the conductivities on the cooling cycles are higher than those measured on the heating cycles due to (i) surfusion phenomena, (ii) presence of a lower amount of POE in crystalline phase and (iii) a better contact between the POE electrolyte and the blocking electrodes after the polymer melting.

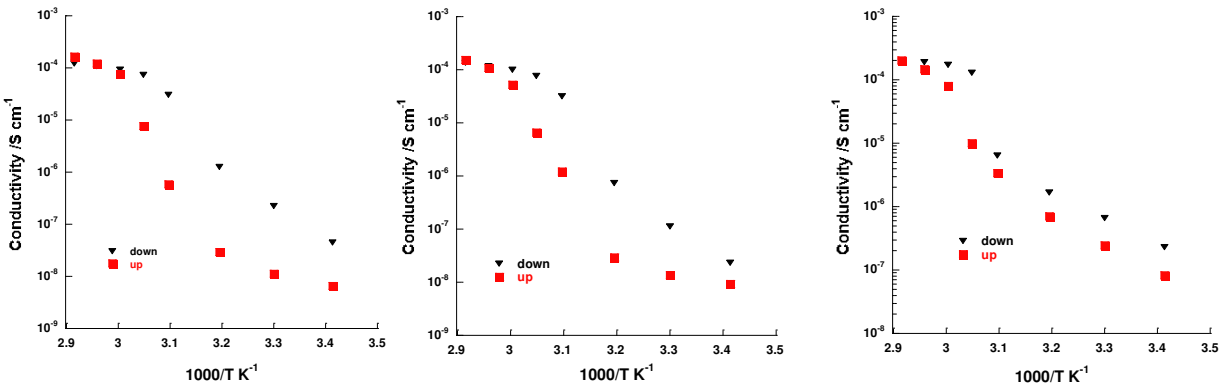

POE/ **salt 1** (O/Li =20) POE/ **salt 2n1** (O/Li =20) POE/ **salt 2n16** (O/Li =40)

Figure 2.21. Comparison of conductivity of polymer electrolyte on heat scan (up) and cooling scan (down).

However, from the figure 2.21 we can observe that the gap between up and down is much higher in the case of **salt 1** as compared to **salt 2n16**, while **salt 2n1** is in between. For the **salt 1** we have evidenced by DSC an increase of T_g after the first heating scan and we supposed a better homogeneity of the electrolyte after the POE fusion. This could explain the higher conductivity differences between up and down as compared to **salt 2n1**. For the **salt 2n16**, by DSC we shown that POE has almost the same crystallinity than the neat POE membrane, the low difference between the conductivities on heating and cooling cycles allows to suppose

that the crystalline phase has a moderate impact on the ionic conductivity and corroborate with the hypothesis the Li interact preferentially with the O from mPEG chain.

For the next discussion we consider the conductivities on the down cycle in order to suppress the thermal history of the membrane.

A decrease in the value of T_g contributes to easy movement of the polymer chains and as a result an increase in the conductivity is expected [21]. As comparing the complexes with lower T_g and similar lengths of mPEG, i.e. membranes based on POE+**salt 1** with those based on POE+**salt 2n1** the conductivities of both membranes are similar above crystallization temperature while after the crystallization the values are lower for POE+**salt 2n1** (figure 2.22a). The higher conductivities values of complexes POE+**salt 1** after the membrane crystallization corroborates with DSC studies, for that a lower T_{g2} was obtained.

The Arrhenius plots of POE electrolytes with lithium salt with different chain lengths are presented in the figure 2.22b. The ration O/Li is 30 for n=1, 3, 7 while for n=16 O/Li =40. The measurements of the conductivity for a membrane POE+**salt 2n16** O/Li =30 were not possible because the membrane is too soft and creeps even at room temperature. In the figure 2.22 c the conductivities of membranes based on POE+ **salt 2n7** and POE **+ salt2 n16** at same O/Li (40) are compared.

A slight increase of the conductivities was observed with the increase of the mPEG lengths. We suppose that this increase is due to the contribution of EO from mPEG to the solvation and mobility of Li^+. The mPEG is more flexible and mobile (length much lower than the entanglement threshold) as compared to the EO units from POE. Moreover, by DMA and DSC phase separation between the salt and POE was evidenced for the electrolytes POE+**salt 2n16**. Hence, the short chain length of mPEG and thus absence of chain entanglements as compared to POE might decrease the local viscosity in the conducting domains. However the increase of mPEG chain length has to decrease the anion conductivity due to the increase of steric hindrance. This impact of the size of anion will be studied on the next part related to the self-diffusion coefficients.

Regarding the conductivity of the POE+**salt 2n16** with that of POE+**salt 2n7** at the same concentration (O/Li = 40), the conductivity of the former is 40% higher than that if the latter. However, for O/Li =40 the weight ratio POE+**salt 2n16** is approximately 1:1 while is for **salt 2n7** it is 1:0.63.

The conductivity seems to be even higher than that of pure salt. This can be explained by the contribution of POE in its melted state to the solvation and mobility of Li^+.

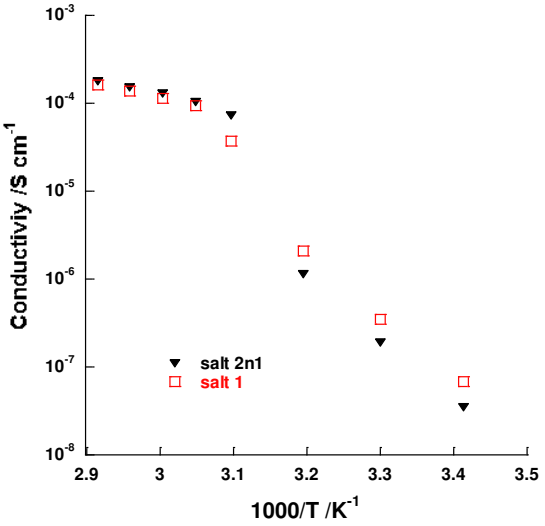

a) POE/ **salt 1 and POE/sal2n1** (O/Li =20)

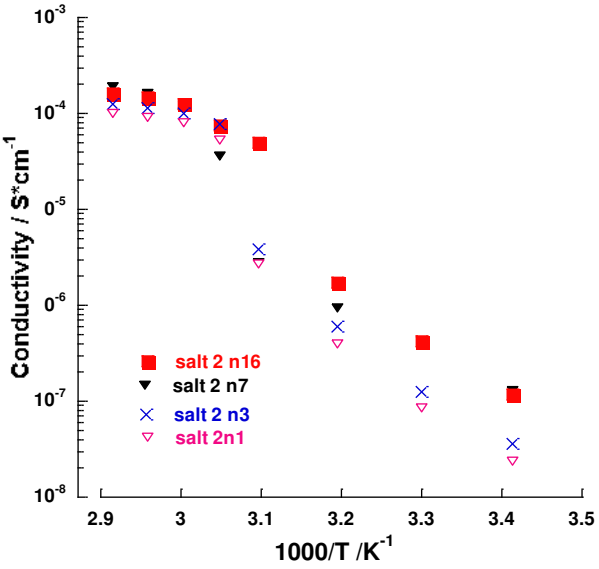

b) POE/ **salt 2 n =1,3,7** (O/Li =30) and **n=16** (O/Li =40)

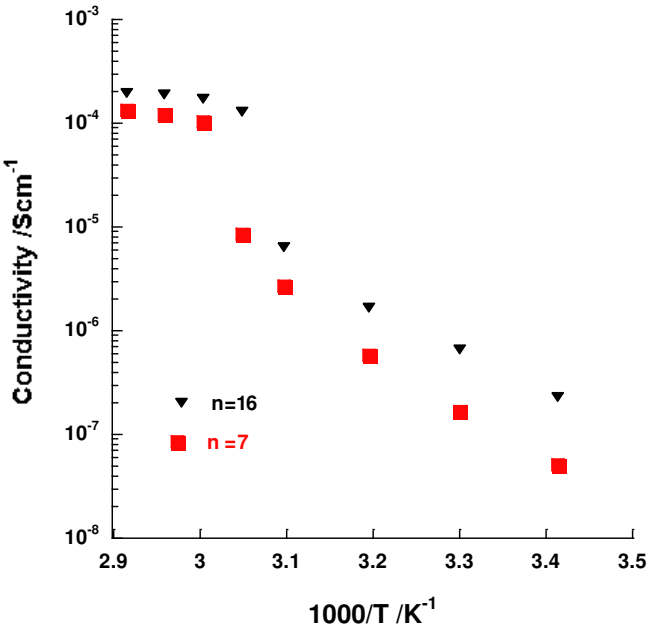

c) POE/ **salt 2 n =7,16** (O/Li =40)

Figure 2.22. Comparison of conductivity of POE/**salt 2** with various chain lengths.

In the figure 2.23 the impact of the ratio O/Li on the conductivities, for the electrolytes (a) POE+**salt 2n1**, (b) POE+**salt 2n3** and (c) POE+s**alt 2n16,** are represented. For the electrolytes based on **salt 2n1** and **salt 2n3** the higher conductivity is obtained for n=20. The conductivity depends on the salt concentration; addition of higher amount of salt means theoretically increase of ion concentration which might improve the conductivity but also decrease in mobility. Increasing the salt concentration from O/Li= 20 to 16 induces for both electrolytes (figure 2.23 a and b) a decrease in conductivity. The decrease in salt concentration (from O/Li=20 to O/Li=30) induces also a decrease in conductivity. This means that, as often, the conductivity vs salt concentration passes by a maximum that might be close to O/Li = 20. In the case of POE +s**alt 2n16** a salt concentration increase must increase the concentration in ionic species contributing to the conductivity even if the dissociation decreases with the salt concentration according to the theory of weak electrolytes. But contrary to POE + **salt 2n1** and POE + **salt 2n3**, the mobility should not be penalized by a salt concentration increase. Unfortunately, the electrolytes creeping did not allow assessing to salt concentrations exceeding O/Li= 40. Nonetheless, the conductivities increase from O/Li= 60 to O/Li= 40.

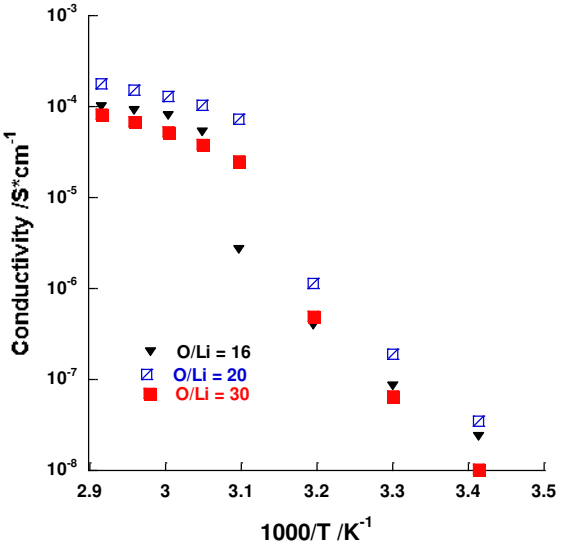

a) POE + **salt 2n1**

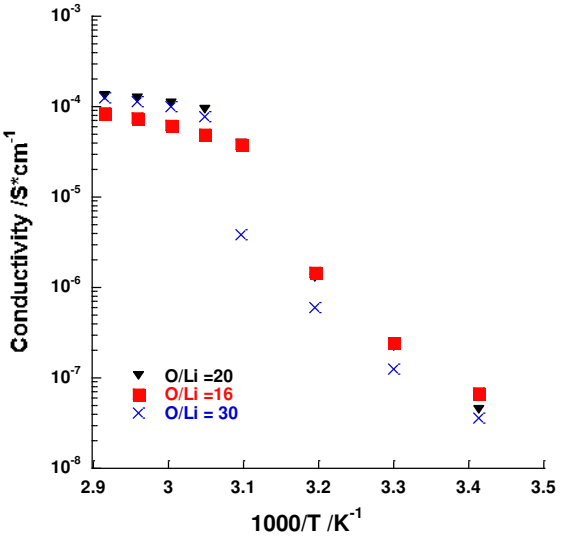

b) POE + **salt 2n3**

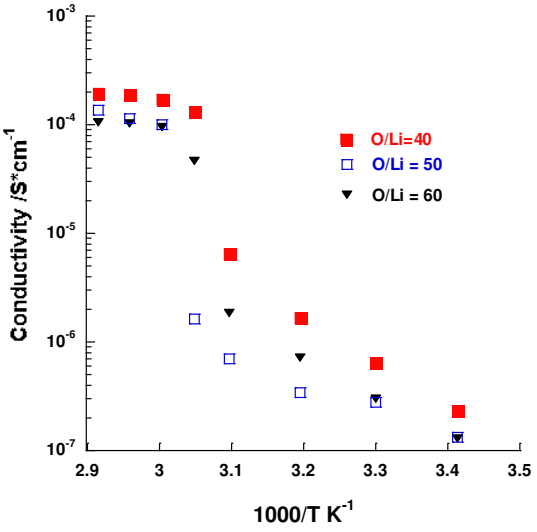

c) POE + **salt 2n16**

Figure 2.23. Comparison of conductivity of POE/**salt 2** with various O/Li.

II.3.5.Diffusion coefficients

The diffusion coefficients of the different species, Li^+ and anion determined by multinuclear Pulsed Field Gradient ^{7}Li-NMR and ^{19}F-NMR respectively are presented in Table 2.11.

Table 2.11 Comparison of diffusion coefficients for the different polymer electrolytes POE/**salt 1** and **2**) determined by PFG-NMR at 110°C

POE/Salt	**Salt 1**	**Salt 2n1**	**Salt 2n3**	**Salt 2n7**	**Salt 2n16**
O/Li	30	30	30	30	40
D ^{19}F($cm^2\ s^{-1}$)	1.15×10^{-7}	1.64×10^{-7}	1.55×10^{-7}	1.25×10^{-7}	1.02×10^{-7}
D ^{7}Li($cm^2\ s^{-1}$)	0.85×10^{-7}	1.20×10^{-7}	1.35×10^{-7}	1.42×10^{-7}	1.45×10^{-7}
σ_{Nernst} (S $cm^{-2}mol^{-1}$)	4.6×10^{-4}	6.7×10^{-4}	6.9×10^{-4}	5.3×10^{-4}	$3.7.\times10^{-4}$
σ_{exp} (S cm^{-1})	3.32×10^{-4}	2.96×10^{-4}	2.94×10^{-4}	3.07×10^{-4}	3.41×10^{-4}
% dissociation	71	44	42	59	91

From Table 2.11 it can be observed that the self-diffusion coefficients of anion and Li^+ are lower for POE+**salt 1** than for POE+**salt 2**. However, it was shown previously that conductivities are very close at temperatures higher than the POE crystallization temperature at the same concentration. Regarding the **salt 2**, first it can be pointed out that the self-diffusion coefficient of anion is higher in the POE+salt as compared to the pure salt. An increase of factor close to 2 and 1.5 is observed in the case of **salt 2n7** and **salt 2n16** respectively while the values of D^{7}Li are much closer (in pure salt and POE electrolytes). The higher values of the anion self-diffusion coefficients in POE membrane could be explained by the interactions of Li^+ with the O atoms of the melted POE and thus an increase of mPEG chain mobility. However the values of diffusion coefficients decrease with the increase of mPEG chain length (from n=1 to n=16). Contrarily, the self-diffusion coefficients of Li^+ increase with the increase of the mPEG chain lengths, due certainly to the higher mobility of mPEG chain as compared to POE chain. The higher n is the higher weight content of salt in

the POE electrolyte and the higher probability for Li^+ to interact with more O atoms belonging to more mobile mPEG.

As we already mentioned the Nernst–Einstein equation is valid for the infinitely dilute state, in our case we use it only to compare the values obtained with different POE electrolytes. To measure the conductivities at 110°C (in order to compare the experimental conductivity with that obtained by Nernst–Einstein equation) we have used the same cell that was used for the pure salts (**salt 2n 7** and **salt 2n16**), i.e. a dip-type glass cell with two platinum electrodes at a constant distance while, at this temperature the utilization of stainless disc electrodes in a Swagelok cell was impossible because of the films creeping that affects the thickness or even leads to short circuit. However there is a good concordance between the conductivities measured with both types of cells.

From Table 2.11 it can be observed that the experimental conductivities, of electrolytes based on **salt 2**, increase slightly with the lengthening of mPEG while those calculated using Nernst–Einstein equation decrease. This behavior might reveal a higher dissociation of the salt based on the longest mPEG. However, the obtained values for the % dissociation are too high, from our point of view.

II.3.6.Cationic transference number and cationic conductivity

One very important parameter for the performances and safety of the lithium batteries is the cationic transport number. In this manuscript the T^+ values were determined employing both, pulsed NMR spectroscopy and electrochemical impedance spectroscopy methods.

T^+ inferred by NMR is obtained from diffusion coefficients of anion and cation, even though NMR cannot discriminate between, on the one hand, the free ions and solvent-separated ion pairs that contribute to the conductivity and, on the other hand contact ion pairs that are electrically neutral.

The electrochemical measurements are based on the method developed by Sorensen and Jacobsen [22]. According to the method by Sorensen and Jacobsen, the lithium transport number can be extracted from a single impedance experiment. In this work symmetrical lithium test cells: Lithium/ solid polymer electrolyte/ Lithium were used for electrochemical experiments. The acquired electrochemical impedance spectrum comprises the electrolyte resistance (R_e) and the two electrode/electrolyte interfaces. In general, in the high frequency

region are detected the processes related to ion transport within the bulk electrolyte and it can be easily observed that this component changes substantially. At low frequencies, the Nyquist plot for impedance of the symmetric plane cell Lithium/electrolyte/Lithium containing two ionic mobile species is characteristic of lithium ions transport limitation by diffusion through electrolyte. This solid state lithium ion diffusion is known as Warburg diffusion [23]. The cells were carefully prepared in an argon glove box in order to avoid degradations of lithium metal foil and the presence of humidity in the electrolyte. Both electrodes (anode and cathode) are made of thin lithium foils which have a thickness of approximately 65 µm, while a polypropylene layer was used as insulator. Also the polymer electrolyte thickness thickness (l), important, must be known before and after the impedance measurements). The cell elaboration (the lamination process) and further impedance measurements modify the membrane thickness. For this reason, the membrane thickness after impedance represents the 'real' thickness which is used for calculation of diffusion coefficient. The value of diffusion coefficient can be easily detected while using the characteristic (solid state) diffusion time τ [24].

$$\tau = l^2 / D \qquad (12)$$

where l is the inter-electrode distance (polymer electrolyte thickness) and D is the ambipolar diffusion coefficient [25].

In the case of symmetrical electrochemical cells, Li/electrolyte/Li, the lithium metal electrodes are considered as blocking electrodes for the anion and non-blocking for the lithium cation. For this reason, the diffusion impedance (Warburg diffusion, W_d) is given by:

$$W_d = R_e \mu_2/\mu_1 \qquad (13)$$

Where μ_1 is the lithium cation mobility, μ_2 is the anion mobility and R_e is the electrolyte resistance. This leads to the final equation for transference number, T^+:

$$T^+ = R_e / (R_e + W_d) \qquad (14)$$

Prior to impedance measurement a potential of 40 mV is applied. All measurements were done at high temperature i.e. 110 °C, as the high temperature generates fast ion movement and in order to match with PFG NMR data. The complexes of POE+ lithium salt were maintained to 20 h isotherm in order to be sure the film is stable. After 20 h only 5 % weight loss was shown.

The cationic conductivities of the electrolyte were calculated from the equation (15).

$$\sigma^+ = T^+\sigma \quad (15)$$

The cationic transference numbers and cationic conductivities are presented in Table 2.10. The values of T^+ measured by PFG-NMR, range from 0.42 to 0.59. All POE/**salt 1** and **2** electrolytes exhibit higher T^+ than that obtained with POE/LiTFSI electrolytes. In the case of **salt 2**, the lengthening of mPEG induces an increase of T^+. However, the incorporation of **salt 2n7** and **salt 2n16** in POE results in lower cationic transference number as compared to the pure salt. This is certainly due to the participation of POE to the Li^+ mobility.

Excepting the **salt 2n7** the T^+ obtained by EIS technique are close to 0.5 (ranging between 0.5 and 0.55) and for the salts **salt 1, salt 2n1, salt 2n3,** the values are higher than those obtained by PFG-NMR. The PFG-NMR measured both the diffusion of dissociated ion-pair and contact ions pairs. For contact ion-pairs anion and cation diffuse at the same rate: therefore the cationic contribution of these ion-pairs is 0.5. If the salt has a low T^+ as LiTFSI, the undissociated ion pairs increase artificially T^+. Conversely if the salt has a high T^+, the undissociated ion-pairs will lower artificially T^+.

Table 2.12 Transference number (T^+), conductivity (σ) and cationic conductivity (σT^+) for **salt 1** and **salt 2** in POE matrix with two different investigating methods at 110°C

Complex	O/Li	σ (S/cm)	PFG-NMR		EIS	
			T+	σ^+ (S/cm)	T^+	σ^+ (S/cm)
Salt 2n7	-	2.52×10^{-4}	0.64	1.61×10^{-4}	-	-
Salt 2n16	-	2.91×10^{-4}	0.72	2.10×10^{-4}	-	-
POE/LiTFSI	30	1.24×10^{-3}	0.28	3.47×10^{-4}	0.12	1.74×10^{-4}
POE/**PhSCF$_2$CF$_2$SO$_3$Li***	30	$1.8\times10^{-4*}$	-	-	0.48*	$8.6\times10^{-5*}$
POE/**Salt 1**	30	3.32×10^{-4}	0.42	1.40×10^{-4}	0.55	1.82×10^{-4}
POE/**Salt 2n1**	30	2.96×10^{-4}	0.42	1.26×10^{-4}	0.50	1.51×10^{-4}
POE/**Salt 2n3**	30	2.94×10^{-4}	0.46	1.35×10^{-4}	0.53	1.73×10^{-4}
POE/**Salt 2n7**	30	3.07×10^{-4}	0.53	1.63×10^{-4}	0.26	0.8×10^{-4}
POE/**salt 2n16**	40	3.41×10^{-4}	0.59	2.01×10^{-4}	0.51	1.74×10^{-4}

* measured at 70°C [17]

II.4. Film elaboration based on POE network (NPC) electrolyte based on salt 1 and 2

As previously discussed, the films based on semi-crystalline POE electrolytes exhibit a low conductivity below their melting temperature and very poor mechanical properties after this melting. This is detrimental both, for the performances (conductivity, thickness, ohmic drop) and for the safety of lithium polymer batteries. Therefore, many research groups have proposed modified POE matrix in order to increase both the content of amorphous phase and the mechanical strength after the POE melting [2], [26], [27], [28], [29], [30]. In this manuscript we selected an unsaturated polyether (polycondensat) obtained by Williamson type polycondensation. This reaction is performed by reacting poly(ethylene glycol) (Mw =1,000) with 3-chloro-2-chloromethyl -1-propene in the presence of KOH. Once casted the electrolyte films, the polymer are cross-linked by an UV photo-initiation of their double bonds.

II.4.1.Polycondensat synthesis (LPC)

Unsaturated polyethers were prepared by a Williamson type polycondensation as shown in Figure 2.24. Poly(ethylene glycol) (Mw =1,000) and 3-chloro-2-chloromethyl -1-propene were used as the starting materials, the reaction take place in presence of grinded KOH without any added solvent at 40°C for 48 hours. The linear polycondensat (LPC) was purified by ultrafiltration (cut-off: 3,000 Dalton) in order to remove the reaction product, KCl, the excess of KOH, and all the oligomers having a molecular weight lower than 3,000 g/mole. As the entanglement threshold in POE is close to 3,400 g/mole we can assume that even the uncross-linked chains will be entangled into the network

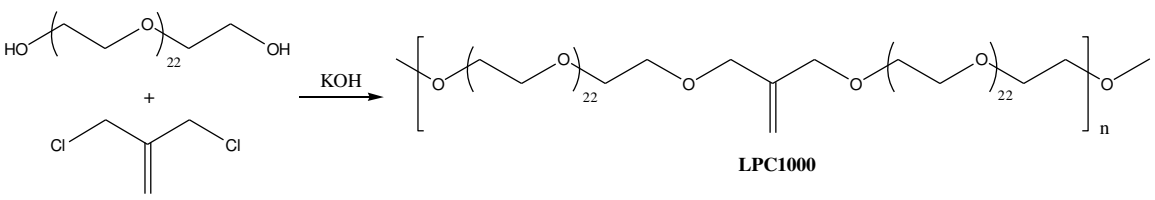

Figure 2.24. Synthesis of linear polycondensat (LPC).

The unsaturated polyether was characterized by Size Exclusion Chromatography (SEC) and M_w = 73,470 g/mole, M_n = 26740 g/mole and $I = M_w/M_n = 2.7$ were obtained.

II.4.2.Membrane preparation

The cross-linked films (NPC) were obtained by the UV irradiation of the casted films. The LPC, the salt, the initiator (IRGACURE® 2959, CIBA) were dissolved in acetonitrile in the glove box. The resulting electrolyte was poured into a Teflon plate. After the solvent evaporation, the cross-linking under UV radiation was carried out for 30 seconds or 1 minute. The resulting network polycondensat electrolytes (NPC) were then dried under vacuum at 60 °C for 72 h and carefully stored in the glove box.

The membranes with the average thickness of 200-300 µm were characterized by various methods to study and understand their physical, chemical, mechanical and electrochemical behavior (discussed in the following section).

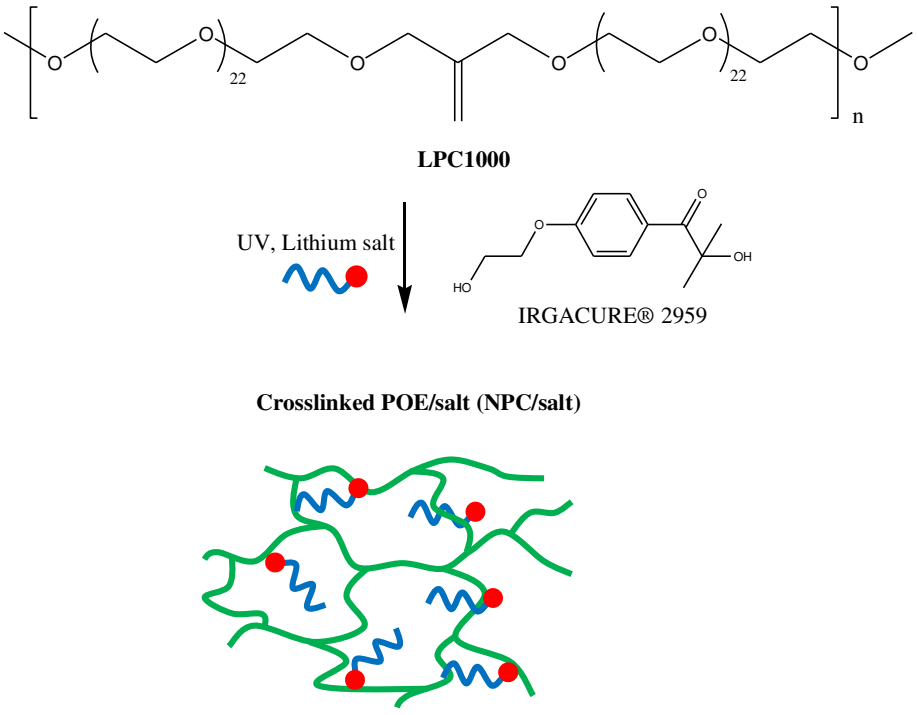

Figure 2.25. Schematic draw of Crosslinked POE (NPC).

II.4.3.Thermal characterizations

Table 2.13 summarizes the T_g, the T_m and the ΔH obtained by DSC measurements for the host polymer NPC and its electrolytes. The T_{g1}, T_{m1}, ΔH_1 were measured after the first heating from -100°C to 60°C and the T_{g2}, T_{m2}, ΔH_2 were measured during the second heating after a 1st heating up to 60°C followed by a quenching (cooling ramp 50°C/min). The thermograms showed a crystallization peak before the fusion of crystalline phase, sometime the peaks are overlapping, therefore the values of T_m was taken at peak. The samples still exhibited the semi-crystalline behavior but the melting temperature decreased as compared to POE and to the 1st heating.

For NPC+salt complexes, at the same salt concentration and irradiation time we did not observe a significant and coherent evolution of T_g with the increase of the mPEG chain length from n=1 to n=7 or with the increase of O/Li ratio. However for **salt 2n16** the T_g seems to be at least 4°C higher as compared to other NPC +other salts and additionally another T_g is observed at 7°C. This behavior is similar to that observed for POE +**salt 2n16** and shows the presence of two amorphous phases.

Concerning the melting temperature and enthalpy a significant decrease was observed for the second scan as compare to the first scan. However, similar to the membrane based on POE the values of ΔH seem to increase with the increase of n of mPEG. Nevertheless the values of ΔH for longer mPEG are higher than of NPC without salt. These results prove the presence of salt into membrane can modified the value of ΔH of NPC. Moreover, in the case of membranes based on NPC the presence of salt could affect the crosslinking reaction, and thus the ΔH value. The ΔH of 100% NPC crystalline is not known therefore the % crystallization was not calculated.

Table 2.13 (a) Glass transition temperature (T_g) melting temperature (T_m) and fusion enthalpy (ΔH) of NPC/**salt 1** and NPC/**salt 2** electrolytes at different cross-linking times 30s

Sample	O/Li (O/Li-n)	T_{g1} (°C)	T_{g2} (°C)	T_{m1} (°C)	T_{m2} (°C)	ΔH_{NPC1} (J/g)	ΔH_{NPC2} (J/g)
NPC	∞	-52	-64	44	38	58	38
NPC/**Salt 2n1**	20(19)	-40	-59	39	31	37	17
	30(29)	-36	-59	42	34	54	29
NPC/**Salt 2n3**	12(9)	-31	-63	36	28	27	6
	20(17)	-38	-64	36	30	22	13
	30(27)	-35	-66	40	32	42	27
NPC/**Salt 2n7**	20(13)	-38	-66	39	32	33	27
	30(23)	-37	-63	41	36	48	40
	40(33)	-38	-65	37	36	26	31
NPC/**Salt 2n16**	30(14)	-31; 7	-67; 7	45	39	73	94
	35(19)	-31; 7	-63; 4	45	38	63	76
	40(24)	-37	-66	48	36	64	54

The increase of irradiation time from 30 s to 1 min in the case of NPC films does not induce significant modification of T_g, while T_m and ΔH are significantly decreased. The longer irradiation time should enhance the cross-linking density that usually induces a T_g increase. In our case, obtaining the same T_g can be explained by the significant crystallinity decrease, which counterbalances the stiffening produced by higher crosslinking density. Indeed the

formation of the cross-linking bridges creates disorder and prevents the crystallization of the POE segments of NPC.

Concerning the effect of irradiation time on NPC+**salt 2** complexes, a slight increase of T_g was observed for the sample irradiated 1 min as compared to those irradiated 30s.

Similarly to the results obtained on the sample irradiated for 30s, no correlation between the lengths of mPEG chain or O/Li ratio and the T_g values can be established. Moreover, for the electrolytes based on **salt 2n1, 2n2** and **2n7** important decreases of T_m and ΔH values were observed following a longer irradiation time. For the electrolytes based on **salt 2n16** the values of ΔH and T_m for the samples irradiated at different times are close.

Table 2.13 (b) Glass transition temperature (T_g) melting temperature (T_m) and fusion enthalpy (ΔH) of NPC/**salt 1** and NPC/**salt 2** complexes in different cross-linking times 1 minute

	O/Li (O/Li-n)	T_{g1} (°C)	T_{g2} (°C)	T_{m1} (°C)	T_{m2} (°C)	ΔH_{1NPC} (J/g)	ΔH_{2NPC} (J/g)
NPC	∞	-51	-64	32	21	40	33
NPC/**Salt 2n1**	20(19)	-37	-64	35	26	14	6
	30(29)	-49	-68	34	34	46	34
NPC/**Salt 2n3**	12(9)	-28	-63	35	26	13	2
	20(17)	-47	-61	35	27	24	13
	30(27)	-48	-62	32	18	5	5
NPC/**Salt 2n7**	20(13)	-38	-62	34	26	12	4
	30(23)	-41	-60	40	33	40	29
	40(33)	-35; 14	-62	41	31	38	27
NPC/**Salt 2n16**	30(14)	-32	-58	45	38	96	94
	35(19)	-32	-60	45	38	83	76
	40(24)	-31	-60	45	38	68	70

ΔH_{NPC}: fusion enthalpy calculated by mass of NPC host polymer
O/Li-n: the O/Li taking in account only the OE from NPC.

II.4.4.Thermal stability

Figure 2.26 shows the TGA curves of **salt 2n3** , POE + **salt 2n3** , NPC+ **salt 2n3** , and NPC. Similarly to the POE + salt electrolytes we observed an increase of T_d when the salt is incorporated in NPC matrix and its values are much lower than that of pure NPC matrix. It could see that POE electrolyte exhibited a slightly higher thermal stability as compared with

electrolytes based on NPC but the stability of host polymers free of salt is in agreement with these data. This result is surprising as a network is a polymer of infinite molecular weight and its thermal stability should be higher than that of a unidimensional polymer. However the thermal stability of all these materials is overestimated and TGA does not allow detecting degradation products if there chain lengths are high enough to prevent their evaporation. Then, the TGA experiments were performed in inert gas and not in air. So, the main conclusion of these TGA records is that the weight loss of the salt is delayed when the salt is blended to host polyether in relation with the possible interaction of the degradation products with the host polymers.

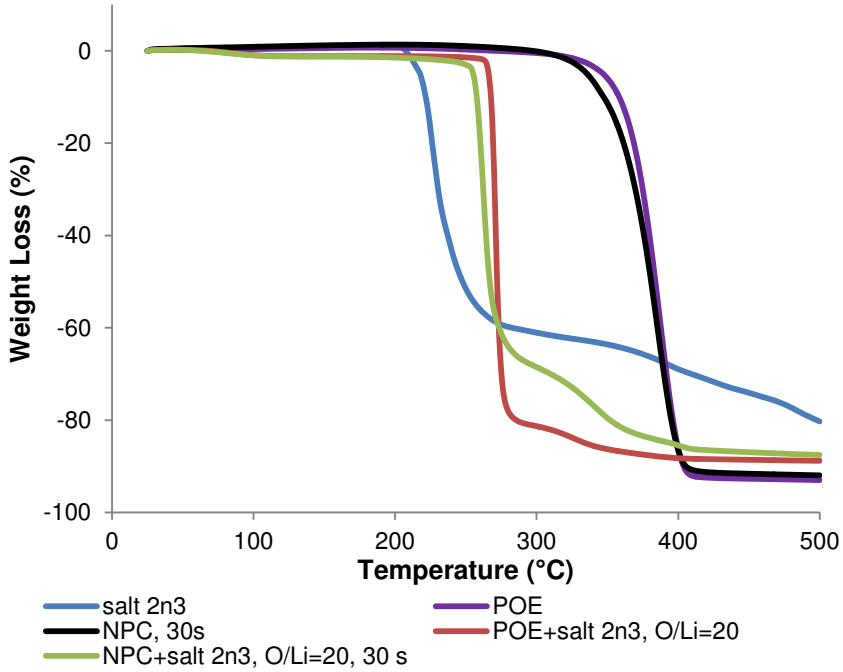

Figure 2.26. Influence of different host polymers on the thermal stability of complex at the concentration O/Li = 20.

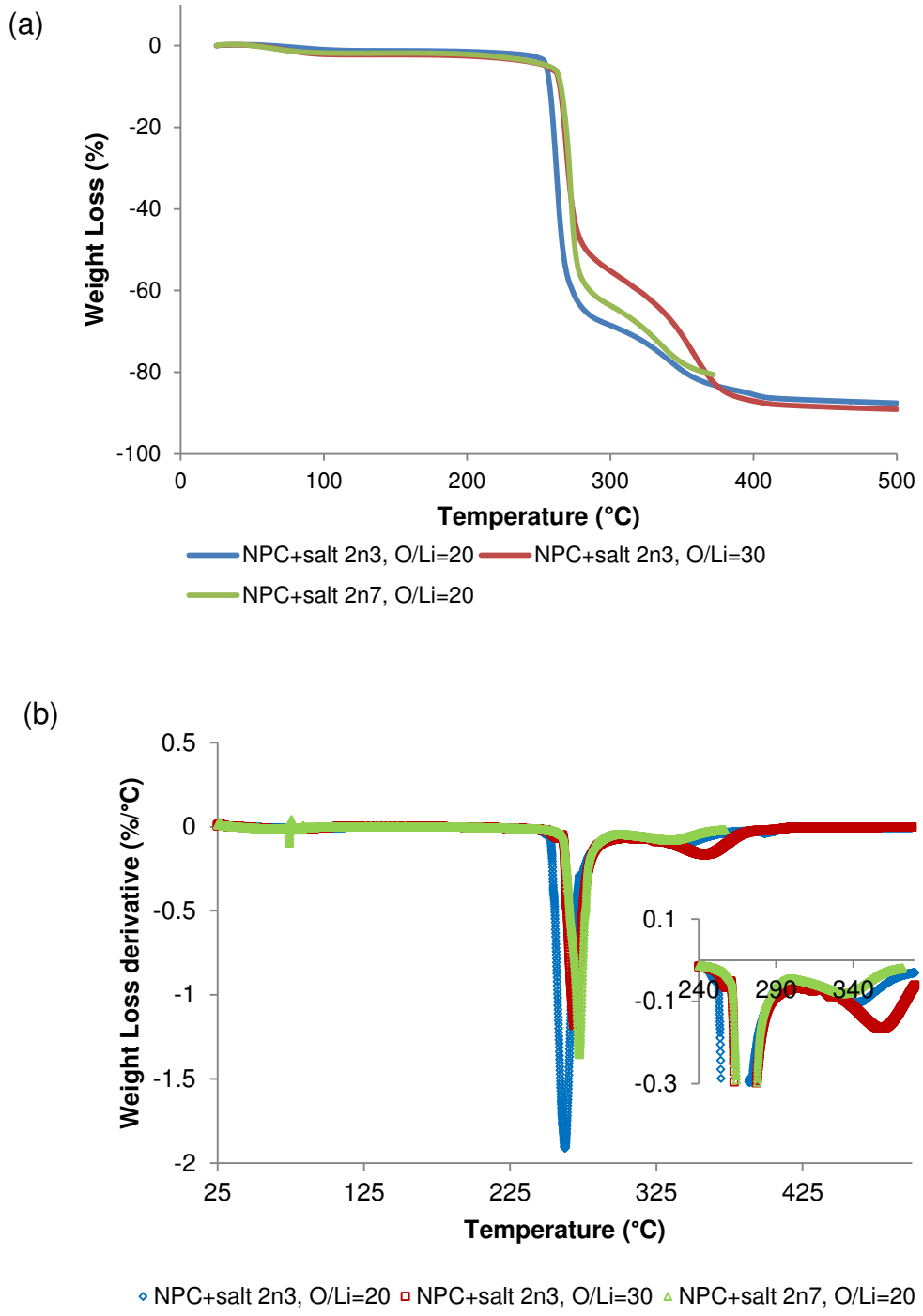

Figure 2.27. (a) Weight loss (%) of NPC/**salt 2n3**, **2n7** complexes as a function of temperature and (b) their first weight loss derivatives.

The weight loss temperatures of NPC complexes increases with the increase of mPEG chain lengths of the salt, starting at 257 °C and 267 °C, in nitrogen, for NPC/**salt 2n3** and NPC/**salt 2n7** at O/Li =20, respectively. This phenomenon was also observed when the longer lithium salt was incorporated in POE host polymer. The weight loss takes place in two steps.

However in the first step more than 60% weigh is lost that is much higher than the weight of the salt. With regard to the salt concentration, the highest salt content exhibits slightly lower thermal stability as shown in the figure 2.27 for NPC/**salt 2n3** for O/Li= 20 and 30 concentrations. We can suppose that the salt concentration impacts on the degradation ; similar results being previously obtained by C. Chauvin et al. [31]

II.4.5.Mechanical properties

The mechanical properties are improved when the linear POE is replaced by the cross-linked one, NPC, as represented in figure 2.28. At low temperature, the storage modulus of NPC membrane is higher than that of POE due to the strength of cross-linked architecture. However, relaxation temperature (T_α) associated to T_g for NPC membrane appears at slightly lower temperature as compared to POE membrane. Above the melting temperature the NPC membrane present rubbery plateau, that indicates a behavior of cross-linked elastomer, whereas the storage modulus of linear POE matrix drops to 0 MPa.

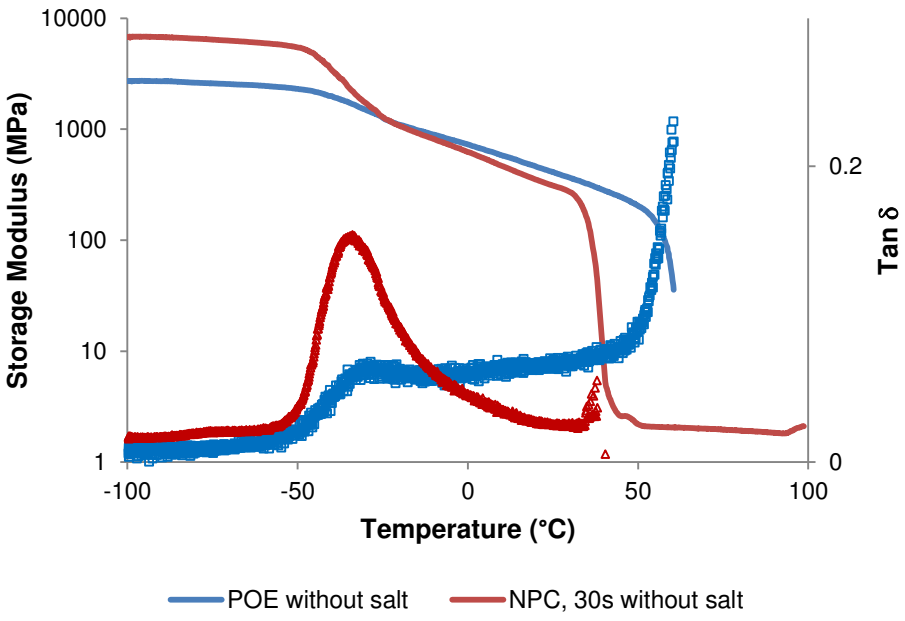

Figure 2.28. Comparison of mechanical properties between POE and NPC host polymers (crosslinking time of 30 seconds for NPC complex).

Irradiation time

As we can see from the figures 2.29, a longer irradiation time induces a slight decrease of the transition α, T_α, associated to T_g and of the storage modulus between T_α and T_m. This is certainly due to the decrease of crystallinity of host the polymer as evidenced by DSC. This can be explained by an increased disorder generated by a more complete crosslinking, which reduces both the crystallinity and melting point. Moreover, longer irradiation time leads to higher crosslinking degree, evidenced through the DMA by the greater values of the storage modulus on the rubbery plateau, E' increasing from 2 to 5 MPa.

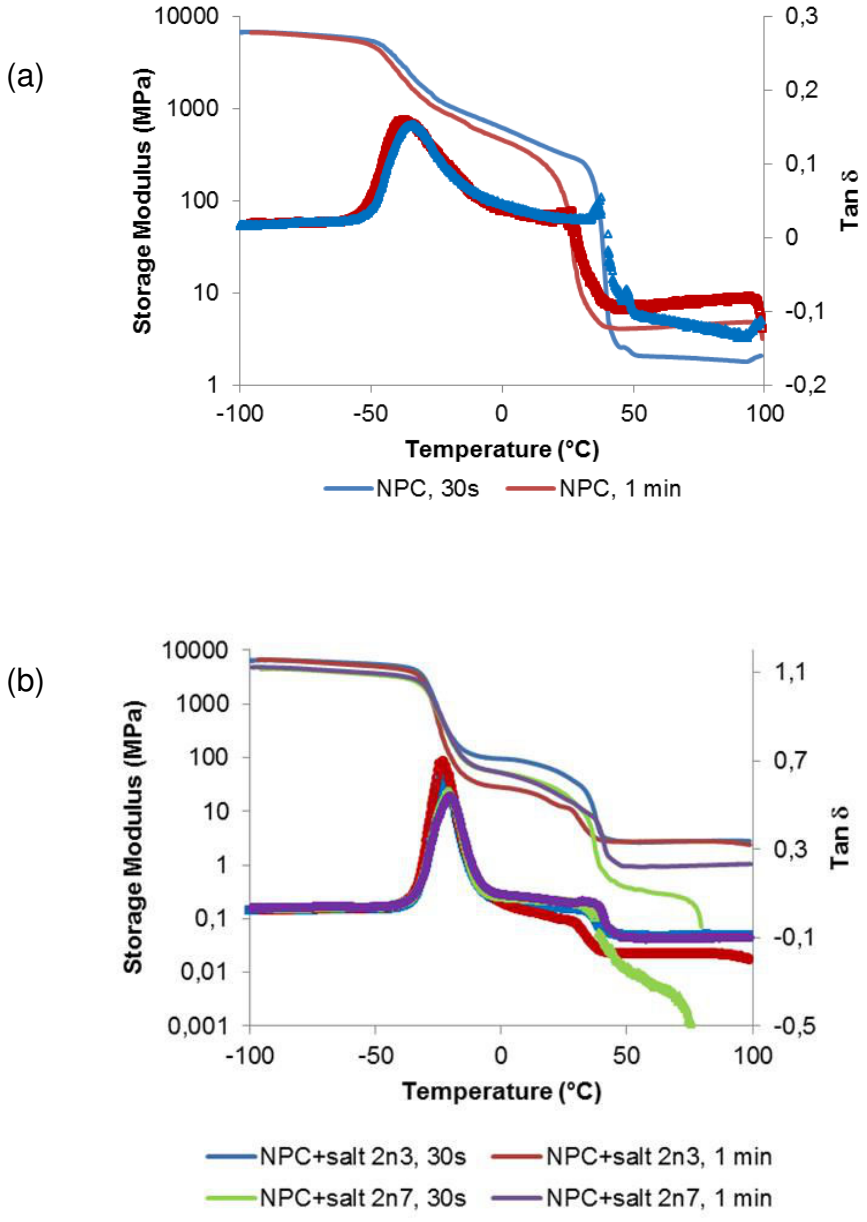

Figure 2.29. Effect of irradiation time on mechanical properties of NPC membrane (a) NPC without salt, (b) NPC+ **salt 2n3** and NPC + **salt 2n7**. (O/Li=30)

Concerning the salt doped NPC membranes the behavior is dependent on the salt structure (figure 2.29 b). Thus in the case of **salt 2n7** the increase of irradiation time seems to have any significant impact on the relaxation temperature but the value of storage modulus on rubbery plateau is twice higher. Moreover, the storage modulus drop related to the melting temperature is lower for the membrane irradiated for 1 min as compared to the membranes irradiated for 30 s, indicating a lower crystallization degree of host polymer for the first. These results corroborate the DSC results. In the case of the membranes based on NPC +**salt 2n3** the same effect was observed as for free NPC membranes, i.e. a decrease of storage modulus values between the T_α and Tm and higher storage modulus on the rubbery plateau.

Length of mPEG

The doping of NPC with a salt affected both the alpha relaxation and the storage modulus on rubbery plateau (figure 2.30). The T_α values of the NPC + **salt 2n3** and **n7** are lower than that of NPC + **salt 2n1.** Moreover, the peaks corresponding to α relaxation are very intense and thin in the case of membranes based on the **salt 2n1, salt 2n3 and salt 2n7** as compare to NPC membrane**.** These results indicate a greater content of amorphous phase with more homogenous domains size in NPC electrolytes as compared to pure NPC. Regarding the storage modulus on the rubbery plateau the NPC + **salt 2n3** give the highest values that means the higher reticulation degree. The membrane based on NPC + **salt 2n16** exhibits a surprising behavior. This membrane has two relaxation temperatures and the values of both of them are higher than those of all membranes studied here. This behavior underlines the presence of two amorphous phases. The surprising high value can be partially explained by the high crystallization degree of NPC matrix evidenced by DSC measurements. A similar behavior was reported in this manuscript for the membranes POE+ **salt 2n16**. The second Tα could correspond to **salt 2n16** confined in NPC crystallized phase.

None rubbery plateau was observed for the electrolytes NPC+**salt 2n16.** However the films are insoluble in acetonitrile, which proves the formation of a NPC (cross-linked polycondensate LPC)**.** To explain the total absence of rubbery plateau we can assume that NPC phase doesn't well percolate. The NPC content in the membrane (O/Li = 30) is only 47% w/w.

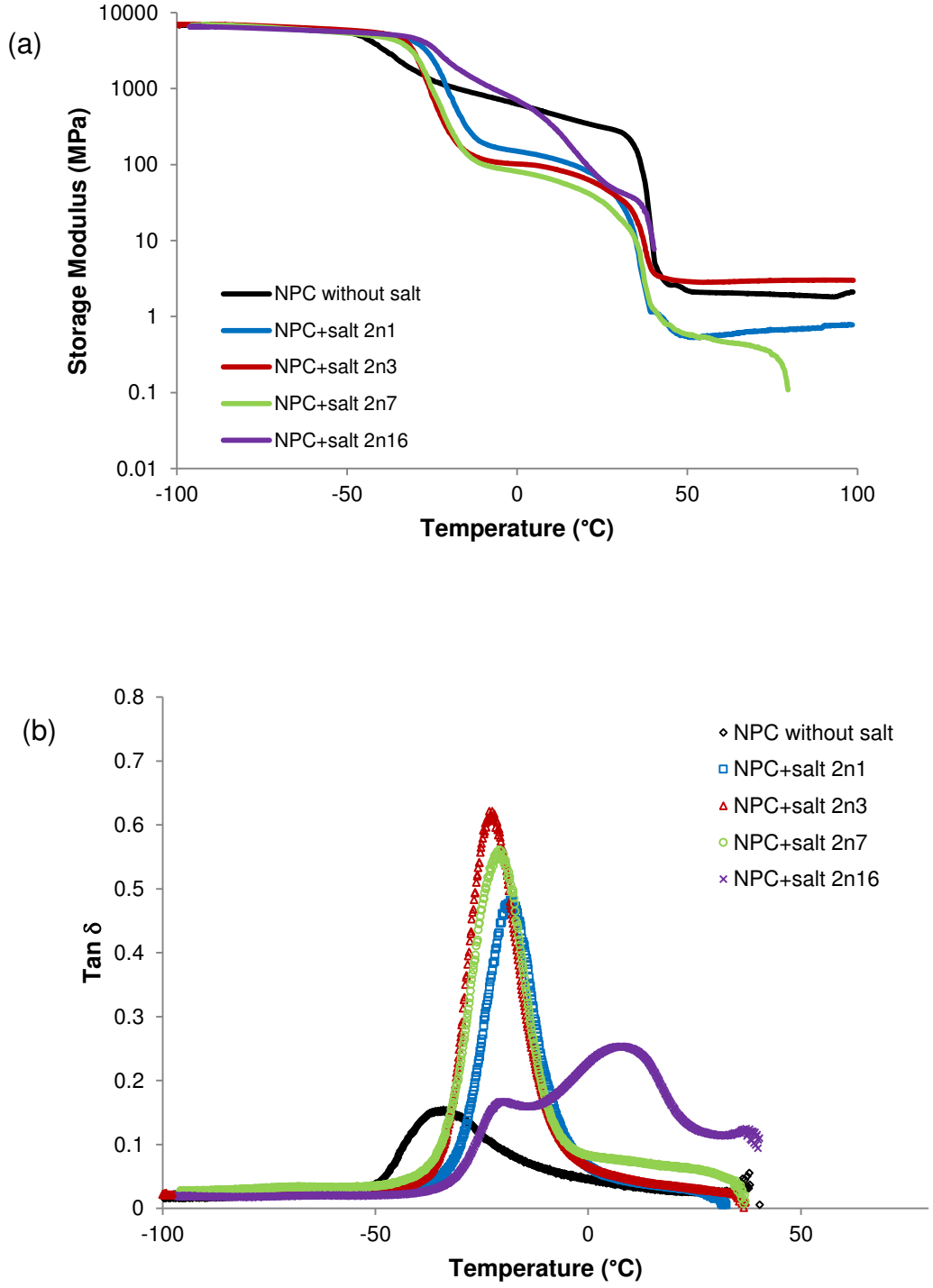

Figure 2.30. (a) Storage modulus vs temperature for various **salt 2** incorporated in NPC host polymer at O/Li= 30, irradiation time 30 seconds, (b) their Tan δ.

The membranes NPC + **salt 2n16** show a similar behavior for different O/Li.

II.4.6. Conductivity

Host polymer

The effects of the host polymer (POE, NPC) on the conductivities of the electrolytes, based on **salt 2n3** and **salt 2n16**, are compared in figure 3.31. The conductivities of the electrolytes based on **salt 2n3 +** POE and **salt 2n16 + POE** are slightly higher than those of membranes based on NPC above the melting temperature T_m while, below T_m, the conductivities of NPC based electrolytes are roughly 10 times higher. The much lower crystallinity and Tm of NPC explain this conductivity gain at low temperatures.

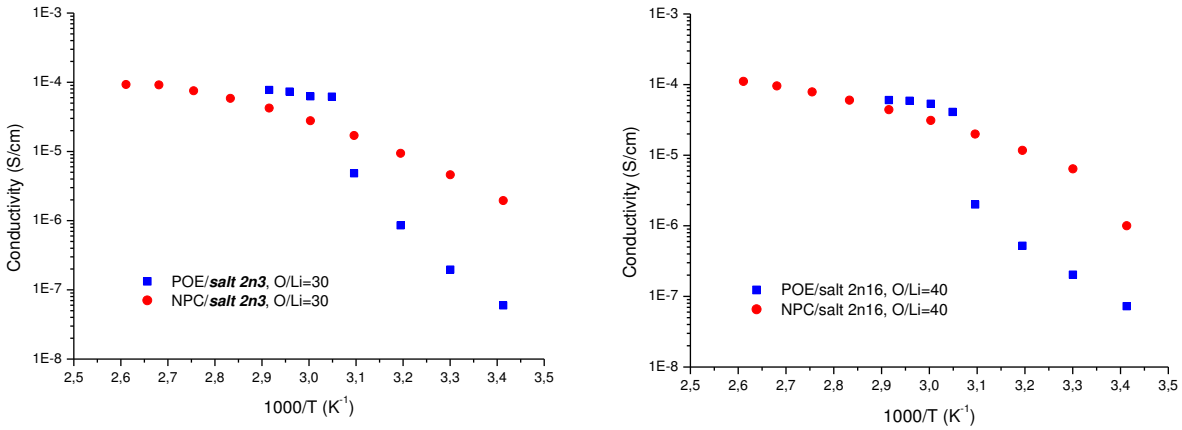

Figure 2.31. Conductivities vs 1000/T for (a) **salt 2n3** O/Li=30 and (b) **salt 2n16** O/Li=40 in POE and NPC matrix.

Up and down

The conductivities were measured in the temperature range 20 -110°C in heating-cooling cycle, first (up) the temperature was increased and then it was decreased (down). In the figure 2.32 we can see, at temperatures higher than 40°C, that conductivities perfectly superimpose on curves up and down. These results prove that: (i) the thickness of the membrane is very stable despite the performing of the measurements at temperatures much higher than the NPC T_m (between 30 and 40°C) (ii) the cross-linking degree of the membrane was unaffected by the high temperature. The membranes were heated for an hour at 110°C and at this temperature it could be expected a thermal polymerization of the residual uncross-linked double bonds, and thus an increase of the crosslinking density. The higher crosslinking degree

leads usually at to a decrease of conductivity (as we show below for the membranes irradiated for a longer time). This means that the membranes are thermally stable up to at least 110°C.

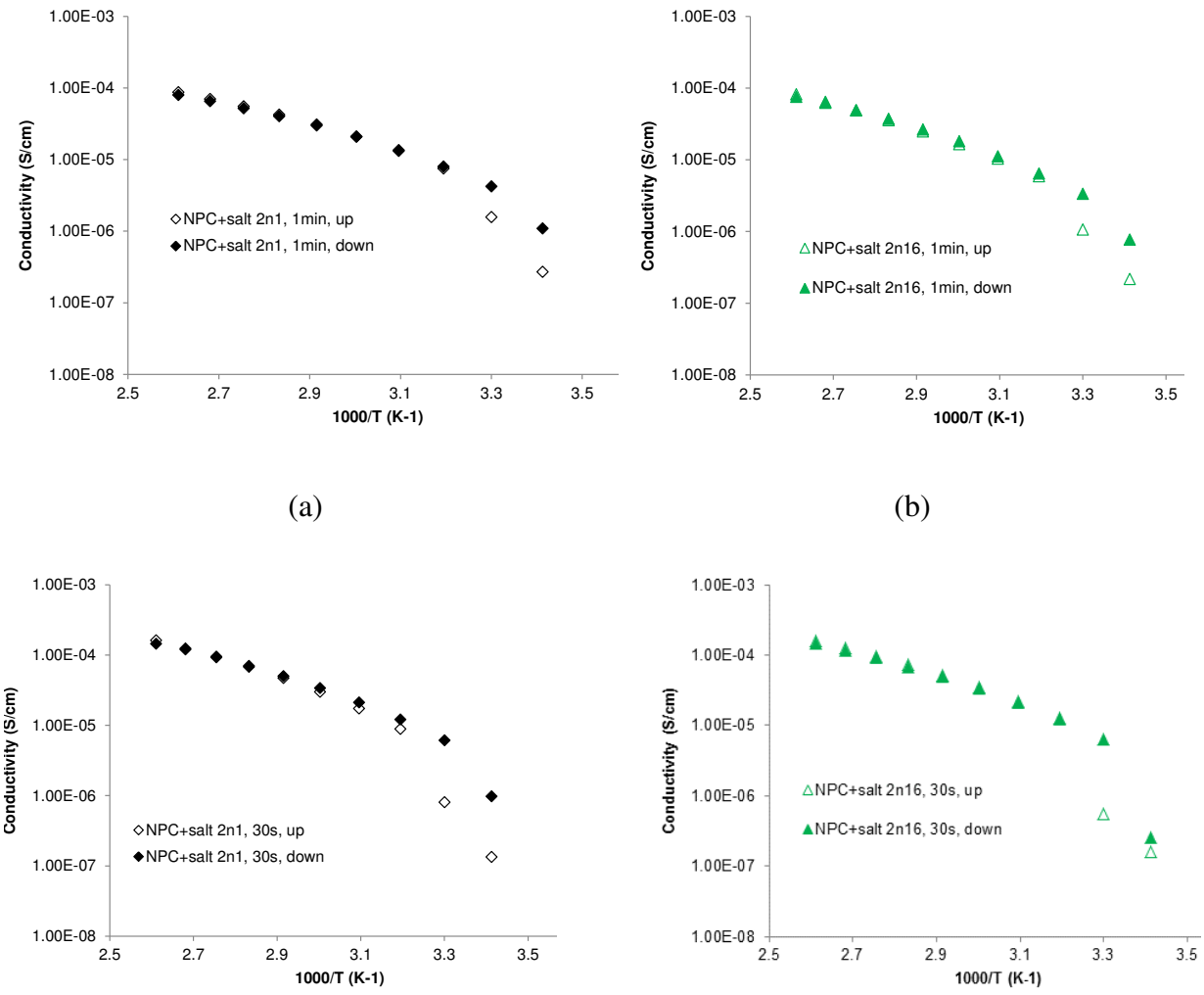

(a) (b)

(c) (d)

Figure 2.32. Conductivities vs 1000/T for (a) **salt 2n1** irradiation time 1 min, (b) **salt 2n16** irradiation time 1 min, (c) **salt 2n1** irradiation time 30s and (d) **salt 2n16** irradiation time 30s in NPC matrix, O/Li 30.

mPEG chain lengths

The temperature dependence of the ionic conductivity for complexes based on NPC + salts with different chain PEG lengths is represented in Figure 2.33 (a and b). In both figures we can see that conductivities are close, in the whole temperature range, for all the electrolytes whatever the mPEG lengths. However, for the membranes irradiated 30 s the conductivity of

the electrolyte NPC + **salt2 n16** is slightly higher than the other ones that superimpose. On the other hand, the conductivities of all the electrolytes, irradiated for 1 min, superimpose.

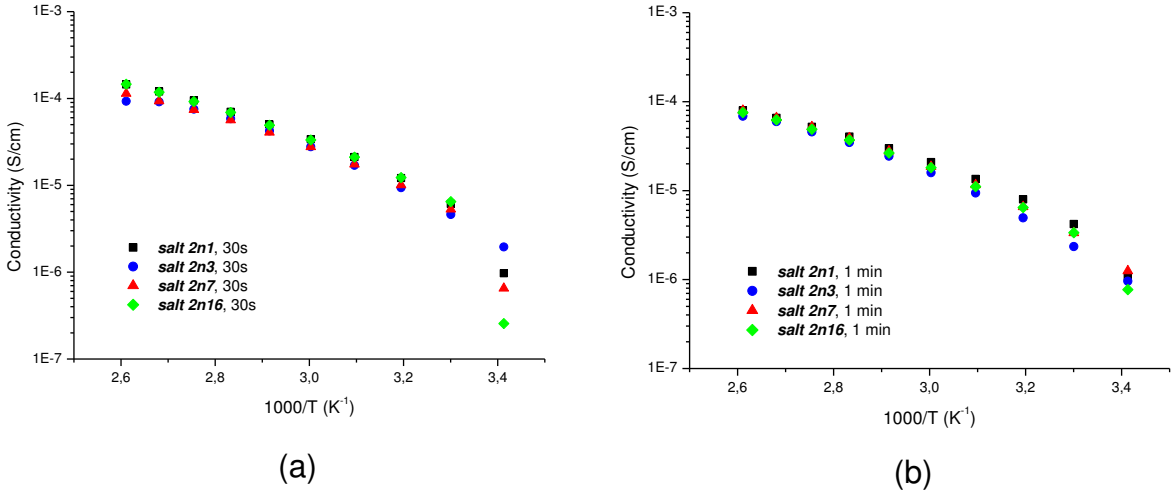

Figure 2.33. Conductivities vs reciprocal temperature for various chain length of **salt 2** in NPC matrix at the concentration O/Li=30 with irradiation times of 30 seconds and 1 minute.

Irradiation time

From the graph 2.34, which represents the influence of the irradiation time on the conductivity, a conductivity decrease can be observed upon an increase in irradiation time that can be ascribed to an increase of crosslink density. All the membranes, irradiated for 1 min, exhibit conductivities of ~10^{-6} S/cm at room temperature and 7×10^{-5} S/cm at 110°C. These values are however lower than the conductivities of NPC/$PhSCF_2CF_2SO_3Li$ prepared by E. Paillard [17]. However, the membranes were processed in different conditions (irradiation time, light intensity, lamp power).

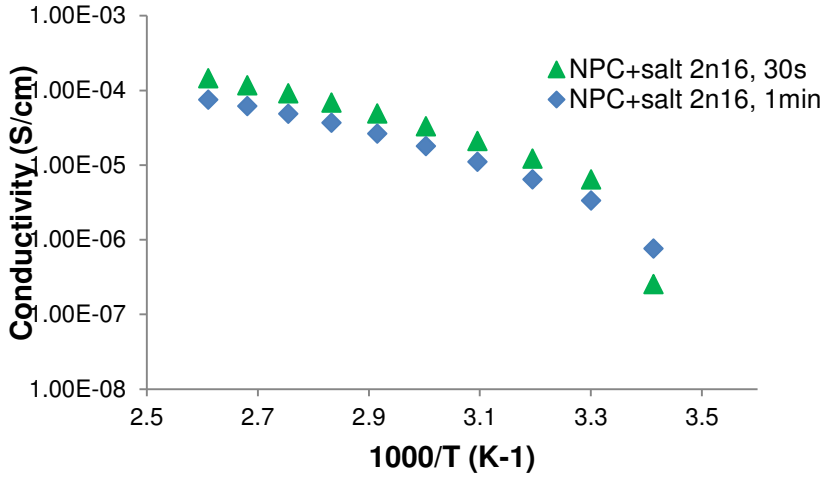

Figure 2.34. Conductivities vs reciprocal temperature for two irradiation time of **salt 2n16** in NPC matrix at the concentration O/Li=30.

The ratio O/Li

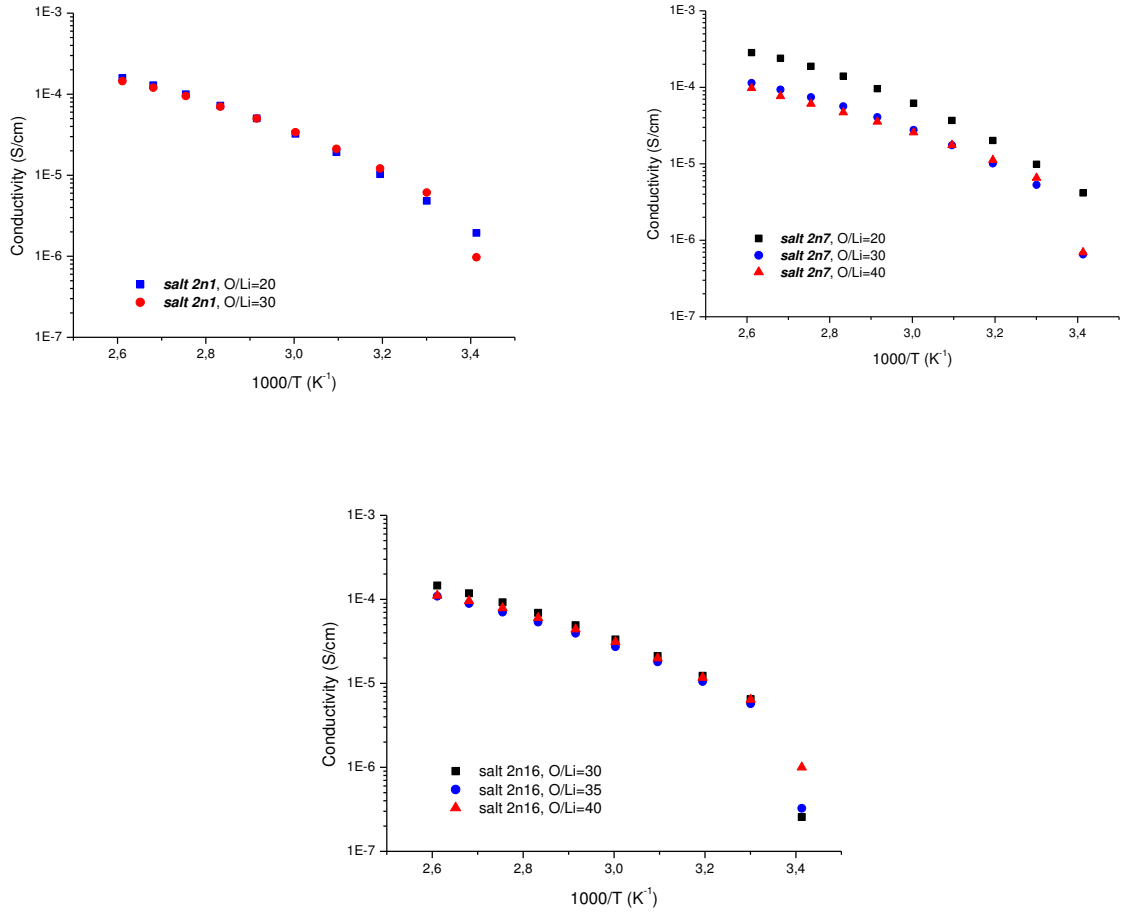

Figure 2.35. Conductivities vs reciprocal temperature for each chain length of **salt 2** in NPC matrix at various concentration O/Li=30 with the crosslinking time 30 seconds.

Except the **salt 2n7** for which O/Li =20 give the best conductivities, for the other complexes (NPC + **salt 2** (**n1, n3, n16** and **salt 1**) the O/Li has low impact on the conductivities. This is probably due to the crosslinking degree that can change as a function of salt concentration.

II.4.7.Diffusion coefficients and cationic transference numbers

The self-diffusion coefficients, of anion and Li^+, determined by PFG-NMR at 110°C are gathered in the table 2.14. The self-diffusion coefficients of anion in NPC membranes seem to be less dependent of the size of anion as compared to membranes based on POE. Additionally the values of self-diffusion coefficients in NPC membranes are close or higher as compared to those determined in POE electrolytes. Moreover, the highest values were obtained for the electrolytes that shown the highest storage modulus on the rubbery plateau (Figure 2.30). Regarding, the self-diffusion coefficients of Li^+, they increase with the increase of anion size and this behaviour is similar to the POE electrolytes. However, this increase is much higher in the case of NPC membrane and the value of the self-diffusion coefficient in the electrolytes based on NPC+**salt 2n16** is more than 3 times higher than that of POE +**salt 2n16** one. These results are very surprising; all the more so since the conductivities NPC based electrolytes are lower than those of on POE ones. These higher values of diffusion coefficient and much lower conductivities can be explained by a lower dissociation degree of the salts in NPC host polymer than in POE, how it can be seen from the Table 2.14

Table 2.14 Comparison of diffusion coefficients and transference numbers for different **salt 2** in NPC at 110°C. O/Li=30 irradiation time=30s at 110°C

NPC/Salt	Salt 2n1	Salt 2n3	Salt 2n7	Salt 2n16
D ^{19}F ($cm^2 s^{-1}$)	1.39×10^{-7}	1.61×10^{-7}	1.40×10^{-7}	1.55×10^{-7}
D ^{7}Li ($cm^2 s^{-1}$)	0.93×10^{-7}	1.75×10^{-7}	2.08×10^{-7}	4.70×10^{-7}
T^+	0.40	0.52	0.60	0.75
σ_{exp} ($S\ cm^{-1}$)	1.45×10^{-4}	1.19×10^{-4}	1.24×10^{-4}	1.46×10^{-4}
σ^+ ($S\ cm^{-1}$)	5.80×10^{-5}	4.83×10^{-5}	6.84×10^{-5}	1.10×10^{-4}
σ_{Nernst} ($S\ cm^{-2}mol^{-1}$)*	5.26×10^{-4}	7.71×10^{-4}	8.11×10^{-4}	1.48×10^{-3}
%dissociation	28	15	15	10

* We suppose to NPC has the lower density than the POE.

II.5. Conclusion

Salts

- Five salts were successfully synthetized by the modification of 2-(phenylsulfanyl)-1,1,2,2 –tetrafluoroethane sulfonate with the mPEG.
- Only two salts can be considered as ionic liquids (T_m<100°C), i.e. the **salt 2n7** and the **salt 2n16**.
- The T^+ and the conductivities increase with the increase of n of PEG.
- The thermal stability of the salts are higher than of 2-(phenylsulfanyl)-1,1,2,2 –tetrafluoroethane.
- The electrochemical stability is better than the POE and comparable to of 2-(phenylsulfanyl)-1,1,2,2 –tetrafluoroethane lithium salt.

Polymer electrolytes

- Polymer electrolytes were prepared by blending the synthesized salt with the linear (POE) or cross-linked (NPC) host polymer.
- In the of POE electrolytes the increase of mPEG lengths of the salt induce:

- a decrease of T_g,
- increase of conductivity,
- increase of T^+ (determinate by NMR)
- increase of dissociation salt degree

DMA, DSC show the presence of two amorphous phases in the case of POE+**salt 2n16**

The conductivities and Li self-diffusion coefficients sustain the hypothesis the OE from mPEG have an important contribution to the Li^+ conduction.

- In the of NPC electrolytes the increase of mPEG lengths influence less significantly the T_g and the conductivity as compared to POE electrolytes. In contrast the T^+ and the values of diffusion coefficients are higher for all the complexes based on NPC+ salts as compared to POE+salts while the conductivities at 110°C are lower. Consequently the salt in NPC seems to be less dissociated.
- The conductivity of electrolytes based NPC are 10 times higher at low temperature as compared to those of POE while at high temperature is 2 to 3 times lower.
- Contrary to POE electrolytes, NPC provides sufficient mechanical properties to prevent the creeping.

II.6. References

[1] Y. Aihara, J. Kuratomi, T. Bando, T. Iguchi, H. Yoshida, T. Ono, et al., J. Power Sources. 114 (2003) 96 – 104.
[2] Y. Kobayashi, S. Seki, Y. Mita, Y. Ohno, H. Miyashiro, P. Charest, et al., J. Power Sources. 185 (2008) 542 – 548.
[3] Q. Wang, P. Ping, X. Zhao, G. Chu, J. Sun, C. Chen, J. Power Sources. 208 (2012) 210 – 224.
[4] M. Holzapfel, C. Jost, A. Prodi-Schwab, F. Krumeich, A. Würsig, H. Buqa, et al., Carbon. 43 (2005) 1488 – 1498.
[5] C.A. Vincent, 1959–2009, Solid State Ion. 134 (2000) 159 – 167.
[6] M. Armand, J.M. Chabagno, M. Duclot, Fast Ion Transport in Solids, Elsevier N. Y. USA. (1979).
[7] Z. Wen, T. Itoh, T. Uno, M. Kubo, T. Wen, O. Yamamoto, Solid State Ion. 175 (2004) 739 – 742.
[8] Y. Kumar, S.A. Hashmi, G.P. Pandey, Solid State Ion. 201 (2011) 73 – 80.
[9] D. Benrabah, J.-Y. Sanchez, M. Armand, Solid State Ion. 60 (1993) 87 – 92.
[10] H. Zhang, C. Liu, L. Zheng, F. Xu, W. Feng, H. Li, et al., Electrochimica Acta. 133 (2014) 529 – 538.
[11] F. Alloin, D. Benrabah, J.-Y. Sanchez, J. Power Sources. 68 (1997) 372 – 376.

[12] S. Guhathakurta, K. Min, Polymer. 51 (2010) 211 – 221.
[13] D. Benrabah, S. Sylla, F. Alloin, J.-Y. Sanchez, M. Armand, Electrochimica Acta. 40 (1995) 2259 – 2264.
[14] E. Paillard, F. Toulgoat, C. Iojoiu, F. Alloin, J. Guindet, M. Medebielle, et al., J. Fluor. Chem. 134 (2012) 72 – 76.
[15] E. Paillard, F. Toulgoat, J.-Y. Sanchez, M. Médebielle, C. Iojoiu, F. Alloin, et al., Electrochimica Acta. 53 (2007) 1439 – 1443.
[16] O. Seitz, H. Kunz, Angew Chem Int Ed Engl. (1995) 803–805.
[17] Elie Paillard, Institut Polytechnique de Grenoble, 2008.
[18] Christophe CHAUVIN, Institut Polytechnique de Grenoble, 2005.
[19] E. Paillard, F. Toulgoat, C. Iojoiu, F. Alloin, J. Guindet, M. Medebielle, et al., J. Fluor. Chem. 134 (2012) 72 – 76.
[20] M. Erceg, D. Jozić, I. Banovac, S. Perinović, S. Bernstorff, Thermochim. Acta. 579 (2014) 86 – 92.
[21] M. Kumar, S.S. Sekhon, Eur. Polym. J. (2002) 1297.
[22] Soeresen, P.R., Jacobsen, T., Electrochimica Acta. (1982) 1671–1675.
[23] D. Aurbach, J Power Sources. (2000) 206–218.
[24] J Phys Chem B. (1997) 4630–4640.
[25] M. Rosso, Electrochimica Acta. (2006) 5334–5340.
[26] H. Cheradame, A. Gandini, A. Killis, J.F.L. Nest, J. Power Sources. 9 (1983) 389 – 395.
[27] X. Ollivrin, N. Farin, F. Alloin, J.-F.L. Nest, J.-Y. Sanchez, Electrochimica Acta. 43 (1998) 1257 – 1262.
[28] X. Ollivrin, N. Farin, F. Alloin, J.-F.L. Nest, J.-Y. Sanchez, Electrochimica Acta. 43 (1998) 1257 – 1262.
[29] D. Benrabah, J.Y. Sanchez, M. Armand, Electrochimica Acta. 37 (1992) 1737 – 1741.
[30] M. Watanabe, H. Tokuda, S. Muto, Electrochimica Acta. 46 (2001) 1487 – 1491.
[31] C. Chauvin, F. Alloin, P. Judeinstein, D. Foscallo, J.-Y. Sanchez, Electrochimica Acta. 52 (2006) 1240 – 1246.

III. Aliphatic Lithium Salts based on Sulfonate and Sulfonylimide Oligoether

III.1. Introduction

In the previous chapter, a family of aryl-perfluorosulfonate lithium salt end-capped with oligoether (mPEG) was studied. The presence of the mPEG in the structure of salt has a moderate impact on crystallinity degree of host polymer but higher polymer electrolyte T^+ and cationic conductivities were obtained as compared to the salt without mPEG. Indeed the presence of aromatic ring in the structure of the salt usually (i) increases the viscosity of the salt and (ii) could modified the interaction of the salt with the host polymer as compare to aliphatic salts [1]. Thereafter, it will be interesting to design aliphatic salt end-capped with mPEG and study the impact of the bonding of mPEG on anion on the performances of polymer electrolytes. Moreover, thanks to the higher ability of sulfonimide lithium salt (LiTFSI) to dissociate and form polymer electrolyte with high conductivity and very low T^+, as previously reported in many works [2], [3], [4] it will be interesting to study how the introduction of mPEG moieties affect the performances of membranes based on sulfonimide salt.

This chapter is divided in 2 parts: (i) in the first part we present as a publication the characterization of 2 salts, i.e. LiTPSM and LiTPSN (figure 3.1) in polymer electrolytes based on POE and cross-linked POE, (NPC).

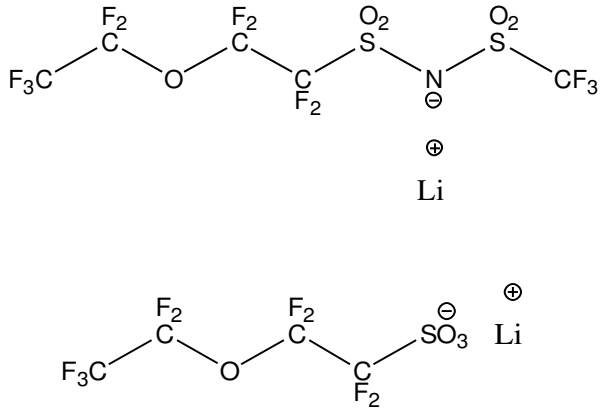

Figure 3.1. Chemical structures of (a) LiTPSM and (b) LiTPSN.

(ii) in the second part the anion LiTPSM and LiTPSN were modified (mono-end caped) with mPEG with different lengths (figure 3.2.). The resulted salts were characterized in pure state or in polymer electrolytes based on POE and POE derivate (cross-linked POE – NPC). Along this part comparisons with the aromatic salt (chapter 2) were performed.

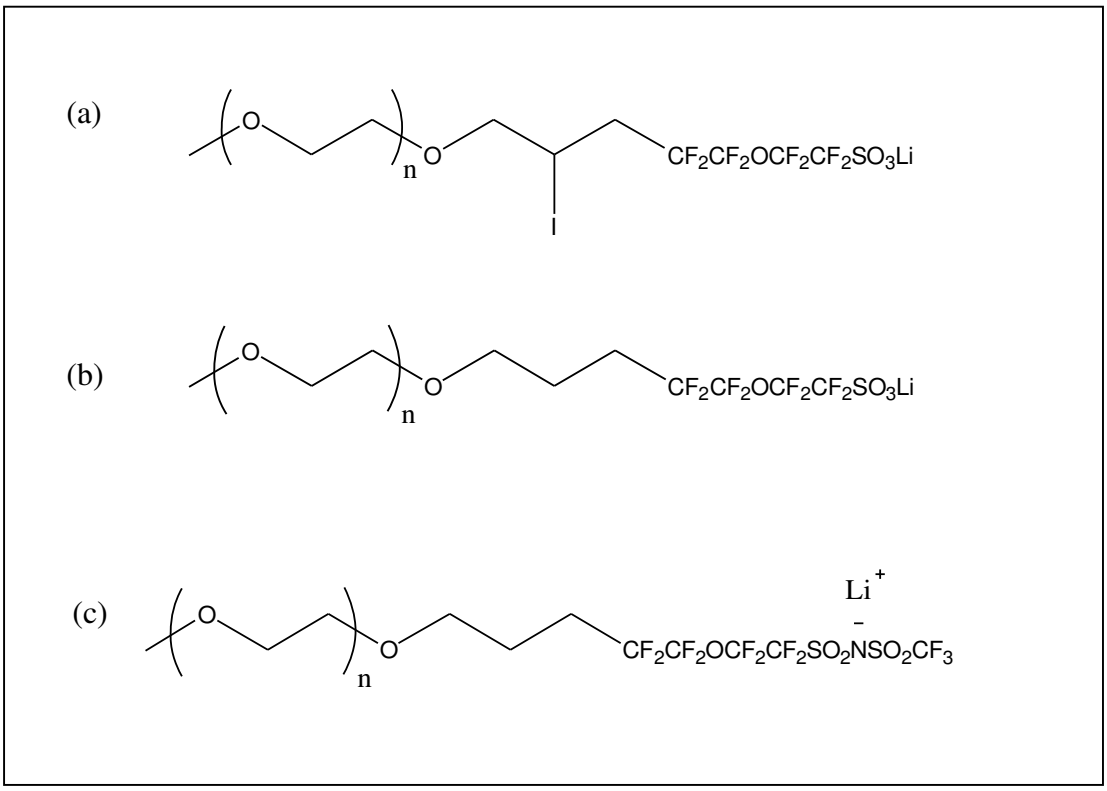

Figure 3.2. Three families of aliphatic lithium salts (a) **salt 3,** n=1, (b) **salt 4** n=1 and 3 and (c) **salt 5,** n=3.

III.2. Publication

Polymer electrolytes based on flexible perfluoroalkanesulfonylimide and sulfonate lithium salts hosted in linear and crosslinked poly(oxyethylene)

P. Eiamlamai[1,2], C. Iojoiu[1,2], P. Judeinstein[3], L. Astratine[1,2] , A. Thiam[1,2], J.-Y. Sanchez[1,2]

1) Univ. Grenoble Alpes, LEPMI, F-38000 Grenoble, France
2) CNRS, LEPMI, F-38000 Grenoble, France, 1130 Rue de la Piscine, 38402, St. Martin d'Hères, France
3) R.M.N. en Milieu Orienté, Institut de Chimie Moléculaire et des Matériaux d'Orsay (ICMMO), UMR8182, Bâtiment 410, Université Paris-Sud, 91405 Orsay Cedex, France

Key words: POE; PEO; Lithium salt; lithium battery, Polymer electrolyte; Ionic conductivity; Transference numbers

Abstract

Perfluoroalkanesulfonimide and perfluoroalkanesulfonate lithium salts endowed with a flexible ether moiety were synthesized. The performances of their polymer electrolytes were assessed in linear and cross-linked host polymers. Their conductivities, stabilities, and transference numbers, make these salts promising for lithium polymer batteries. The Pulse Gradient NMR study allowed highlighting distinctly different diffusion coefficients according whether a linear POE or a cross-linked one is used.

1. Introduction

Lithium battery production deals mostly with Li-ion batteries able to operate at sub zero ambient temperatures. Initially oriented towards the nomad electronic applications, which require cyclability down to 250 K, Li-ion batteries are also excellent candidates for electric transportation i.e. EV (Electric Vehicles), HEV (Hybrid Electric Vehicles) and PHEV (Plug-in Electric Vehicles). All these lithium batteries incorporate a liquid electrolyte made of a lithium salt dissolved in mixtures of organic aprotic solvents, often cyclic and acyclic

carbonates. In order to overcome some safety issues related to the use of flammable solvents i.e. with low F_p (Flash point) their replacement by ionic liquids was proposed [1] Whatever the liquid electrolyte selected it requires, for safety purpose, the use of a dense or a macroporous polymer. The former leads to gelled polymer electrolytes, which were early reported by Feuillade et al. forty years ago [2], while the later, widely used in commercial lithium-ion batteries, are made of polyolefins and commercialized under registered marks such as Celgard®. Another technology, which is oriented towards the use of solvent-free polymer electrolytes SFPE, was found successful in terms of both performances and safety [3]. Unsuited for nomad electronic application, SFPE based batteries address the EV and stationary markets [4], [5]. In SFPE, the host polymer must be a multifunctional polymer endowed with abilities in (i) salt dissolution/solvation (ii) ion's mobility via segmental motion and (iii) in electrodes separation to prevent the battery from short-circuits. P.Wright early reported [6], [7] about the ionic conductivity, of blends made of poly(oxyethylene) POE and salts, and pointed out a conductivity increase above the melting point of the crystalline phase. The deciding contribution of the amorphous phase in the ionic conductivity was later confirmed by NMR measurements [8]. It must be however pointed out that highly concentrated solutions of lithium superacid salts can exhibit an appreciable ionic transport in their crystalline phase [9]. Nonetheless the conductivity maxima remain much lower than those obtained in amorphous SFPE and, on the other hand, high salt concentrations are detrimental to the battery operation. Thus, the ideal SFPE host polymer should be amorphous with glass transition temperatures as low as possible and sufficient thermomechanical performances to be shaped into thin films. To fulfill these contradictory requirements, 3D-solvating host polymers are the best compromise. So, from the pioneering works of Cheradame et al. [10] on polyurethane-ether cross-linked polymer electrolytes, a variety of networks were reported. Thus, M.Watanabe et al. [11] reported 3D materials obtained by free-radical polymerization of macromonomers consisting of OE/OP oligomers end-capped by (meth)acrylate functions. C. Schoeneberger et al. [12] reported the use of POE-grafted polysaccharides cross-linked by isocyanates. Alloin et al. reported [13] the synthesis, by anionic ring-opening polymerization, of oxyethylene/allyl-glycidyl-ether random copolymers and of the resulting cross-linked electrolytes, which provide conductivities exceeding 1 mS/cm at 70°C.

In parallel to the research efforts to tailor new host polymers alternative to the highly crystalline homopolymer POE, another approach has dealt with the invention of new lithium

salts as for instance Lithium bis(oxaloborate) LiBOB [14], or aromatic lithium salts [15]. Bis(trifluoromethanesulfonyl)amide or (trifluoromethanesulfonyl)imideim properly called Bis(trifluoromethanesulfonyl) imide, $(CF_3SO_2)_2NLi$ abbreviated LiTFSI, which provides a neat enhancement of ionic conductivity in a variety of host polymers [16]**.** Among the advantages of LiTFSI can be mentioned (i) its impact on crystallinity and melting temperatures of semi-crystalline host polymers that it decreases (ii) its lesser effect on the glass transition temperature of polymer electrolytes i.e. the so-called plasticization and (iii) its high thermal, chemical and electrochemical stability. LiTFSI suffers however of two main drawbacks. One of the drawbacks is, a low cationic transference number when dissociated into poly(oxyethylene) based host polymers [17]. The second one deals with the corrosion of the Aluminum current collector that it induces, at high voltage, which prohibited its use in most of the lithium-ion batteries. This second issue was recently overcame thanks to the use of suitable acyclic fluorinated carbonates [18]. Following the performances of TFSI anion, methide salt $(CF_3SO_2)_3CLi$, was also investigated and provided in POE slightly more conducting polymer electrolytes but the molar mass of the salt is probably too high [19]. In order to improve the performances of sulfonamide, (pentafluoroethanesulfonyl)imide $(C_2F_5SO_2)_2NLi$, called LiBETI [20] but the performances don't exceed LiTFSI ones. Dissymetric sulfonylimides were also proposed but if the anion dissymmetry is an asset, the increase in apolar difluoromethylene groups, CF_2, is not an asset [21]. In order to increase the number of CF_2 while avoiding this drawback, and to increase the flexibility of the anion, perfluoroether was selected. Thus, 2 flexible salts were prepared and investigated i.e. the lithium 1,1,2,2-tetrafluoro-2-(perfluoroethoxy)ethanesulfonate, LiTPSN, and the lithium[tetrafluoro-2-(pentafluoroethoxy)ethane]-trifluoromethanesulfonimide, LiTPSM (Figure 1). The Lewis basicity of the lone pair of the ether function is impoverished by the perfluoralkylene groups meaning that, even if it should slightly improve the polarity, it should not participate to the solvation of Li^+. It might be feared that the oxygen atom decrease the electron-withdrawing effect of the perfluoroalkylene ether moiety. Oxygen is however, just after fluorine, the most electronegative element. Due to the position of the ether function, this inductive effect cannot be counterbalanced by the resonance electron-donating effect. Thus pentafluoroethoxy moiety should lead to a strong electron-withdrawing effect, which is expected to benefit both to the decrease of the anion's negative charge density and to a high oxidative stability. This contribution reports on the performances of these salts hosted in both linear POE and in cross-linked polyether as host polymers.

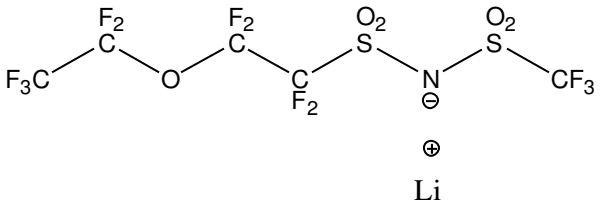

(a)

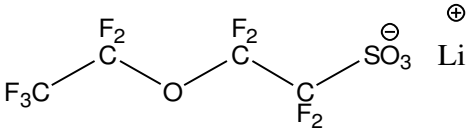

(b)

Figure 1. Chemical structures of (a) LiTPSM and (b) LiTPSN

2. **Experimental**

2.1. Materials and solvents

High molecular weight poly(oxyethylene) (POE) (M_w =300,000 g/mol) from Acros Organics was dried at 80°C during 48h before to be use in the glove box. Lithium bis(trifluoro-methanesulfonyl)imide (LiTFSI) and Lithium hydroxide monohydrate were purchased from Sigma-Aldrich. Acetonitrile for the membrane preparation was distilled before to be used.

2.2. Salts synthesis

LiTPSN synthesis

LiTPSN synthesis was carried out by the neutralization of perfluoro(2-ethoxyethane) sulfonic acid in aqueous solution with lithium hydroxide (scheme 1). In a typical procedure, the Perfluoro(2-ethoxyethane) sulfonic acid (20 mmol, 3.3 ml) was added in an aqueous solution of lithium hydroxide monohydrate (2M) (60 mmol, 30 ml). The mixture was stirred at room temperature for 2 h. After water evaporation, the residue was dissolved in dried acetonitrile, filtered and concentrated under vacuum. The operation was repeated 3 times in order to remove all LiF. LiTPSN salts were further dried at 80 °C, respectively for 48 h under vacuum

before storing in a dry glove box. The LiTPSN, a white solid, was obtained with a net yield of 83%. The purity of LiTPSN was verified by ^{19}F-NMR spectroscopy and elemental analysis.

LiTPSN ($C_4F_9LiO_4S$): ^{19}F NMR $(CD_3)_2SO_2$): -83.30 (t, J= 16 Hz., 2F), -87.91 (s, 3F), -89.39 (t, J= 16Hz., 2F), -119.33 (s, 2F)

Anal. Calcd. C, 14.92; F, 53.10; Li, 2.16; S, 9.96; Found: C, 15.08; F, 52.92; Li, 2.15; S, 9.74

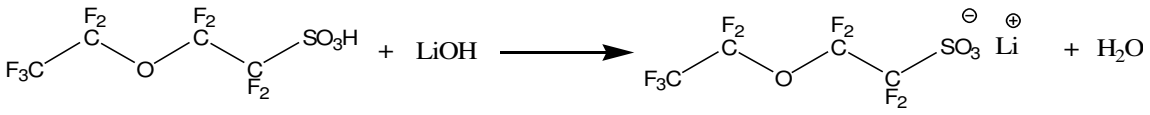

Scheme 1. Lithium 1,1,2,2-tetrafluoro-2-(perfluoroethoxy)ethanesulfonate salt (LiTPSN) preparation.

LiTPSM salt synthesis

The LiTPSM salt was purchased by ERAS-labo.

The synthesis of LiTPSM was carried out in 3 steps (scheme 2).

LiTPSM synthesis was carried out by three steps as presented in Scheme 2. To a solution of anhydrous 1,2-dichloroethane and perfluoro(2-ethoxyethane) sulfonyl fluorides (13 mmol, 4.14 g) under inert atmosphere, was added freshly distilled benzylamine (65 mmol, 7.1 ml). The mixtrure was stirred at 50 °C during 20 h and was followed by thin layer chromatography (TLC) and ^{19}F NMR until sulfonyl fluoride completely disappeared. At room temperature, an aqueous HCl solution (10%) was added, and the mixture was extracted with dichloromethane. The organic phases were dried over $MgSO_4$, filtered and evaporated. The residue was purified by column chromatography on silica gel with gradient eluent (Pentane/AcOEt 1/0 to 4/1) to obtain a benzyl sulfonamide (13 mmol, 5.27 g). The second step, a solution of dichloromethane and benzyl sulfonamide, under inert atmosphere, was added DIEA (13 mmol, 2.3 ml) Then triflic anhydride (19.5 mmol, 3.3 ml) was added at 0°C, the mixture was stirred for 30 min at constant temperature then 1 h at room temperature (followed by TLC and ^{19}F NMR). Then the products were evaporated, and the residue was dissolved in hot pentane and the supernatant was isolated. The solvent was evaporated and the benzyl

trifluoromethanesulfonamide was obtained. The third step, a suspension of benzyl trifluoromethanesulfonamide (12.8 mmol, 6.88 g) in ethanol (60 ml) was stirred during 8 h at room temperature until the solution was completely soluble. An aqueous solution of lithium hydroxide monohydrate (12.87 mmol, 540 mg) was added and the mixture was stirred at room temperature overnight. After the solvent removal, the white residue was dissolved in diethyl ether, filtered and concentrated under vacuum. The residue was washed with cyclohexane, filtered and concentrated under vacuum to afford 4.5 g of LiTPSM salt as solid. LiTPSM salts was storing in a dry glove box.

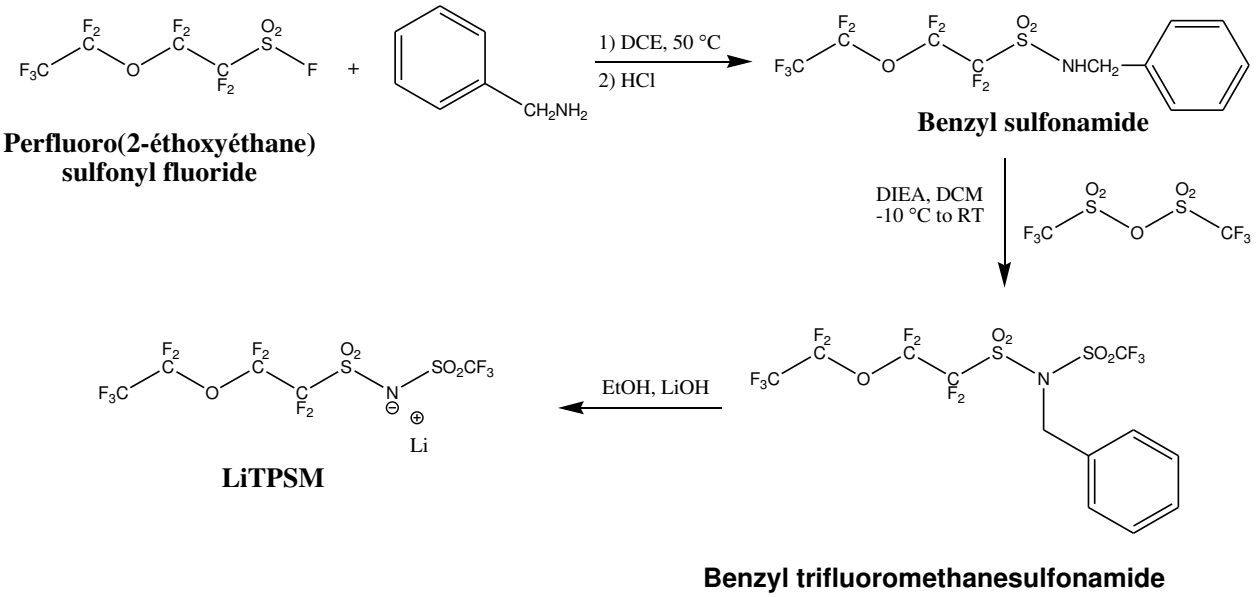

Scheme 2. Synthesis of lithium[tetrafluoro-2-(pentafluoroethoxy)ethane]-trifluoromethanesulfonimide salt (LiTPSM).

^{19}F NMR $(CD_3)_2SO_2$): -79.08 (s, 3F), -81.52(t, J= 18 Hz, 2F), -86.34(s, 3F), -88.25(t, J=18 Hz, 2F), -117.29(s, 2F);

Anal. Calcd. C, 13.25; F, 50.21; Li, 1.53; N, 3.09; S, 14.15; Found: C, 13.29; F, 47.48; Li, 1.52; N, 3.16; S, 13.03

2.3. Linear polycondensat (LPC1000) preparation

Linear unsaturated polycondensates prepared by following the procedure of F. Alloin et al. [22], as shown in scheme 3.

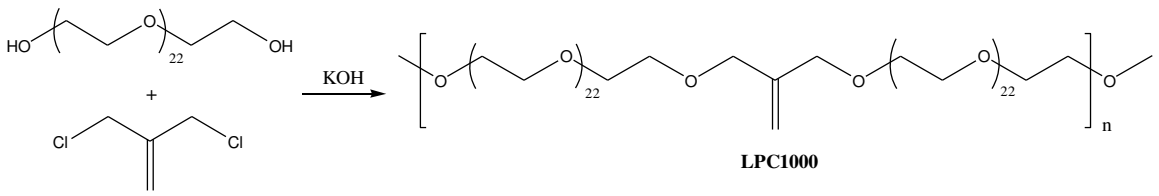

Scheme 3. Synthesis of linear polycondensat (LPC)

The mixture of polyethylene glycol (PEG) with M_w = 1000 and a four-fold excess of ground KOH were stirred at 40°C for 4 hours and 3-chloro-2-chloromethyl-1-propene (CCMP) was then added dropwise. After stirring for 48 hours, the resulting solution was dissolved in deionized water and neutralized by concentrated HCl solution until pH = 7. The inorganic by-products (KOH, KCl) were eliminated by the ultrafiltration and the water was removed by lyophilization for 3 days. The polycondensate obtained was further characterized and kept in the glove box.

The linear polycondensat (LPC1000) was characterized by steric exclusion chromatography (SEC) and $\bar{M}_w$ = 73470, $\bar{M}_n$ = 26740 and $I = \overline{M_w}/\overline{M_n} = 2.7$.were obtained.

2.4. Polymer electrolytes preparation

Polymer electrolytes based on POE

The films based on POE were prepared in a glove box by dissolving both POE and the salt in acetonitrile. The resulting solution was stirred overnight and subsequently casted on a Teflon plate. Solvent evaporation process was done in the glove box for 18h. The membrane was then dried under vacuum at 60°C for 48 h and further stored in the glove box under argon.

Polymer electrolytes based on NPC

The film based on NPC were prepared in the glove box by dissolving the salt, NPC and the photoinitiator (IRGACURE® 2959, CIBA) in acetonitrile. The resulting electrolyte was poured into a Teflon plate. After the solvent evaporation, the films were submitted to the UV irradiation by using a UV light generator with 0.866 mW and P300 MT Power supply, Fusion UV system, Inc. in order to polymerize the allylic bond and perform cross-linked

network. The films were irradiated 30s. The resulted NPC membranes were then dried under vacuum at 60 °C for 72 h and carefully stored in the glove box.

The lithium salt concentration in the both films (based POE on NPC) is indicated by the number n = O/Li, which actually corresponds to the oxyethylene/lithium molar ratio. [15]

2.5. NMR measurement

^{19}F NMR (282 MHz) spectra were run on a Bruker Advance 400 spectrometer, and obtained using DMSO-d6. Chemical shifts (δ) are given in ppm vs. $CFCl_3$ (^{19}F), used as internal references. Coupling constants J are reported in hertz (Hz). Multiplicities are reported as follows: s = singlet, t = triplets.

2.6. Thermal analysis

Glass transition temperatures, T_g, and melting temperatures, T_m, were measured in nitrogen flow using a DSC 1- Mettler -Toledo. In a typical procedure, the samples maintained in glove box for at least one month were submitted to two heating cycles. In the first samples were cooled down to -100°C and heated at 5°C/min up to 100°C, and T_{g1}, T_{m1} and ΔH_1 were measured. Then the samples were cold down with 50°C/min at -100°C and T_{g2}, T_{m2} and ΔH_2 were measured during the second heating from -100°C to 100°C. The T_g were taken as the inflection point of specific heat increment at the glass-rubber transition while T_m was taken in the top of peak of the melting peak. Around 10 mg of sample were placed in a DSC aluminium crucible in glove box.

Thermogravimetric measurements were carried out with a TGA/SDTA Mettler-Toledo STARe software version 12.10 thermal analyzer. A few milligrams of the sample were heated from room temperature up to 500 °C at 5°C/min under nitrogen flow.

2.7. Dynamic mechanical analysis

The thermo-mechanical properties of the different membranes were determined using a TA Instruments DMA2980. The setup measured the complex tensile modulus E*, i.e. the storage component E' and the loss component E", as well as the ratio of the two component, i.e. tan δ (=E'/E"). Measurements were performed in isochronal conditions at the frequency of 1 Hz. Strain magnitude was fixed at 0.01% of the sample length and 150% force track. The temperature was varied in the temperature range of -100 °C - 100 °C at a heating rate of 3 °C / min.

2.8. Conductivity measurements

Conductivities were measured by electrochemical impedance spectroscopy using an HP 4192A Impedance Analyzer in the low frequency range 5 Hz – 13 MHz. The membrane was placed between two stainless steel electrodes in a Swagelok cell with Teflon o-rings and spacers. Measurements were done on successive increase and decrease of temperature in the range 20 °C - 70 °C (from 20 °C – 110 °C for NPC/salt complex). The temperature was equilibrated for 1 hour before each measurement.

2.9. Transference number

The transference number was estimated from two methods; an electrochemical impedance spectroscopy technique (EIS) and Pulsed Field Gradient NMR (PFG-NMR) technique.

The electrochemical measurements are based on the method developed by Sorensen and Jacobsen [23]. According to the method by Sorensen and Jacobsen, the lithium transport number can be extracted from a single impedance experiment. In this work symmetrical lithium test cells: Lithium/ solid polymer electrolyte/ Lithium were used for electrochemical experiments. The acquired electrochemical impedance spectrum comprises the electrolyte resistance (R_e) and the two electrode/electrolyte interfaces. In general, in the high frequency region are detected the processes related to ion transport within the bulk electrolyte and it can be easily observed that this component changes substantially. At low frequencies, the Nyquist plot for impedance of the symmetric plane cell Lithium/electrolyte/Lithium containing two ionic mobile species is characteristic of lithium ions transport limitation by diffusion through electrolyte. This solid state lithium ion diffusion is known as Warburg diffusion [24]. The cells were carefully prepared in an argon glove box in order to avoid degradations of lithium metal foil and the presence of humidity in the electrolyte. Both electrodes (anode and cathode) are made of thin lithium foils which have a thickness of approximately 65 µm, while a polypropylene layer was used as insulator. Also the polymer electrolyte thickness (l), important, must be known before and after the impedance measurements. The cell elaboration (the lamination process) and further impedance measurements modify the membrane thickness. For this reason, the membrane thickness after impedance represents the ‘real’ thickness which is used for calculation of diffusion coefficient. The value of diffusion coefficient can be easily detected while using the characteristic (solid state) diffusion time τ [25].

$$\tau = l^2 / D$$

where l is the inter-electrode distance (polymer electrolyte thickness) and D is the ambipolar diffusion coefficient [26].

In the case of symmetrical electrochemical cells, Li/electrolyte/ Li, the lithium metal electrodes are considered as blocking electrodes for the anion and non-blocking for the lithium cation. For this reason, the diffusion impedance (Warburg diffusion, W_d) is given by:

$$W_d = R_e \mu_2/\mu_1$$

Where μ_1 is the lithium cation mobility, μ_2 is the anion mobility and R_e is the electrolyte resistance. This leads to the final equation for transference number, T+:

$$T^+ = R_e/ (R_e+W_d) \quad (14)$$

Prior to impedance measurement a potential of 40 mV is applied.

The Pulsed Field Gredient-NMR is another technique used for determining the diffusion coefficient. The magnitude of the pulsed field gradient was varied between 0 and 55 G cm^{-1} (sinus shaped pulsed gradient); the diffusion time Δ between two pulses was fixed at 500 ms and the gradient pulse duration δ was set between 3 and 22 ms depending on the diffusion coefficient of mobile species. This allowed us to observe the attenuation of spin echo amplitude over a range of at least 2 decades leading to a good accuracy (≤5%) of the self-diffusion coefficient values. They were determined from the classic relationship $\ln(I/I_0) = \gamma^2 D g^2 \delta^2 (\Delta - \delta/3)$ where g is the magnitude of the two gradient pulses, γ is the gyromagnetic ratio of the nucleus under study and I and I_0 are respectively the area of the signal obtained with or without gradient pulses. The measurement was carried out at high temperatures of 110 °C. The cation transference number is obtained from this relationship (1):

$$T^+ = \frac{D_+}{D_+ + D_-} \quad (1)$$

where D_+ is the self diffusison coefficient of the cation and D_- the self-diffusion coefficient of the anion. All measurements were done at high temperature i.e. 110 °C, as the high temperature generates fast ion movement and in order to match with PFG-NMR data.

3. Results and discussion

3.1. Thermal characterizations

3.1.1. Calorimetric measurements

DSC analyzes are essential as they allow assessing the ability of new salts to decrease the crystallinity of POE and favor the segmental mobility.

a) POE electrolytes

Table 1

Glass transition temperature (T_g) and melting temperature (T_m) of POE/LiTPSM and POE/LiTPSN complexes (1= the first cycle, 2= the second cycle after cooling with 50 °C/min)

Samples	O/Li	T_{g1} (°C)	T_{m1} (°C)	ΔH_{1POE} (J/g)	T_{g2} (°C)	T_{m2} (°C)	ΔH_{POE2} (J/g)
LiTPSM[a]	-	-	193	-			
LiTPSN[b]	-	123	157	-			
PEO	∞	-	70	126	-62	58	105
POE/LiTFSI	12	-32	47	111	-42	41	6
	20	-32	58	107	-51	50	68
	30	-	66	173	-55	53	84
POE/LiTPSM	16	-38	63	53	-54	35	10
	20	-38	66	61	-53	51	64
	30	-38	61	69	-52	54	78
POE/LiTPSN	12	-	66	92	-43	59	90
	20	-	68	135	-51	56	100
	30	-	66	155	-55	63	112

ΔH_{POE} : fusion enthalpy calculated by mass of POE host polymer

As usual, the crystallinity contents and the T_g values obtained using highly crystalline polymer electrolytes are poorly reproducible and strongly depends on the experimental conditions (Table 1). Indeed, the T_g that should reflect, at the amorphous state, the ionic mobility of a solvent-free polymer electrolyte through the chain's segmental motion is

subjected to the effect of the crystalline phase that constrains the amorphous one. DSC data of POE/LiTPSM and POE/LiTPSN electrolytes are reported in Table 1 and compared with those of POE matrix and of POE/LiTFSI, O/Li=20 and O/Li=30. It can be observed that despite the flexibility induced by the ether function, LiTPSN induces neither a significant decrease in crystallinity content nor a decrease in melting temperatures. Contrarily, LiTPSM has a more important effect both on crystallinity and T_g. Indeed, as increasing the salt concentration decreases the crystallinity it also decreases the constraining suffered by the amorphous phase. This leads to the surprising effect that the most concentrated sample (O/Li=16) exhibits the lowest T_g (T_{g2}), while the contrary effect was observed on the LiTFSI and LiTPSN due to the interaction of POE with Li^+.

b) NPC electrolytes

Table 2

Glass transition temperature (T_g) and melting temperature (T_m) of NPC/LiTPSM and NPC/LiTPSN complexes

	O/Li	T_{g1} (°C)	T_{m1} (°C)	ΔH_{1NPC} (J/g)	T_{g2} (°C)	T_{m2} (°C)	ΔH_{2NPC} (J/g)
NPC	∞	-52	44	58	-64	38	38
NPC/LiTFSI	12	-45	-	-	-53	-	-
	20	-49	22	22	-53	21	5
	30	-44	40	34	-58	33	31
NPC/LiTPSM	12	-46	-	-	-66	-	-
	20	-46	36	13	-59	29	12
	30	-45	39	34	-58	30	30
NPC/LiTPSN	12	-42	37	19	-54	29	16
	20	-38	40	26	-55	33	23
	30	-39	37	42	-58	34	55

In NPC, melting temperature and crystallinity are strongly decreased with regard to the homopolymer POE and, therefore, the DSC data are much more reproducible and credible.

However the same restrictions about the impact of the crystalline phase on the T_gs can be made. Thanks to the low crystallinity and Tm of NPC, the salt LiTPSN can lead to amorphous polymer electrolytes from 29 to 34°C, according to the salt concentration. LiTPSM, once again, has more effect on both parameters and provide crystallinity and Tm at least equal to those obtained with LiTFSI. A first heating up to 60°C followed by a rapid quenching and a second heating allowed decreasing or suppressing the crystallization and therefore accessing to T_g more representative of the polymer segmental mobility, above T_m. Thus T_g ranging from – 58 to – 66°C were obtained with LiTPSM. As compared to LiTFSI, LiTPSM leads to slightly lower T_g in particular at high salt concentration. It was reported [27] from conformational ab initio calculations that the energy barrier in the rotation around the SNS bonds of LiTFSI, close to 10 JK/mole, is very low allowing an easy rotation of the $TFSI^-$ anion. Even if the same calculation were not performed on LiTPSM it can be assumed for the related anion an energy barrier close to $TFSI^-$. The higher plasticizing effect of LiTPSM could be ascribed partly to the dissymmetry around the sulfonamide moiety but above all to the additional flexibility around the perfluoroether function.

3.1.2. Thermal stability

Thermal degradation temperatures were determined in nitrogen, the figure 2 (a, b and c) represents the TGA thermograms of (a) salts, (b) salts and POE films, (c) salts and NPC films respectively.

For the salts, the onset of weight loss starts at 340°C for both flexible salts as shown by Figure 2a , a value close to that of LiTFSI (340°C) but lower than that of CF_3SO_3Li (425 °C) under a nitrogen atmosphere [28].

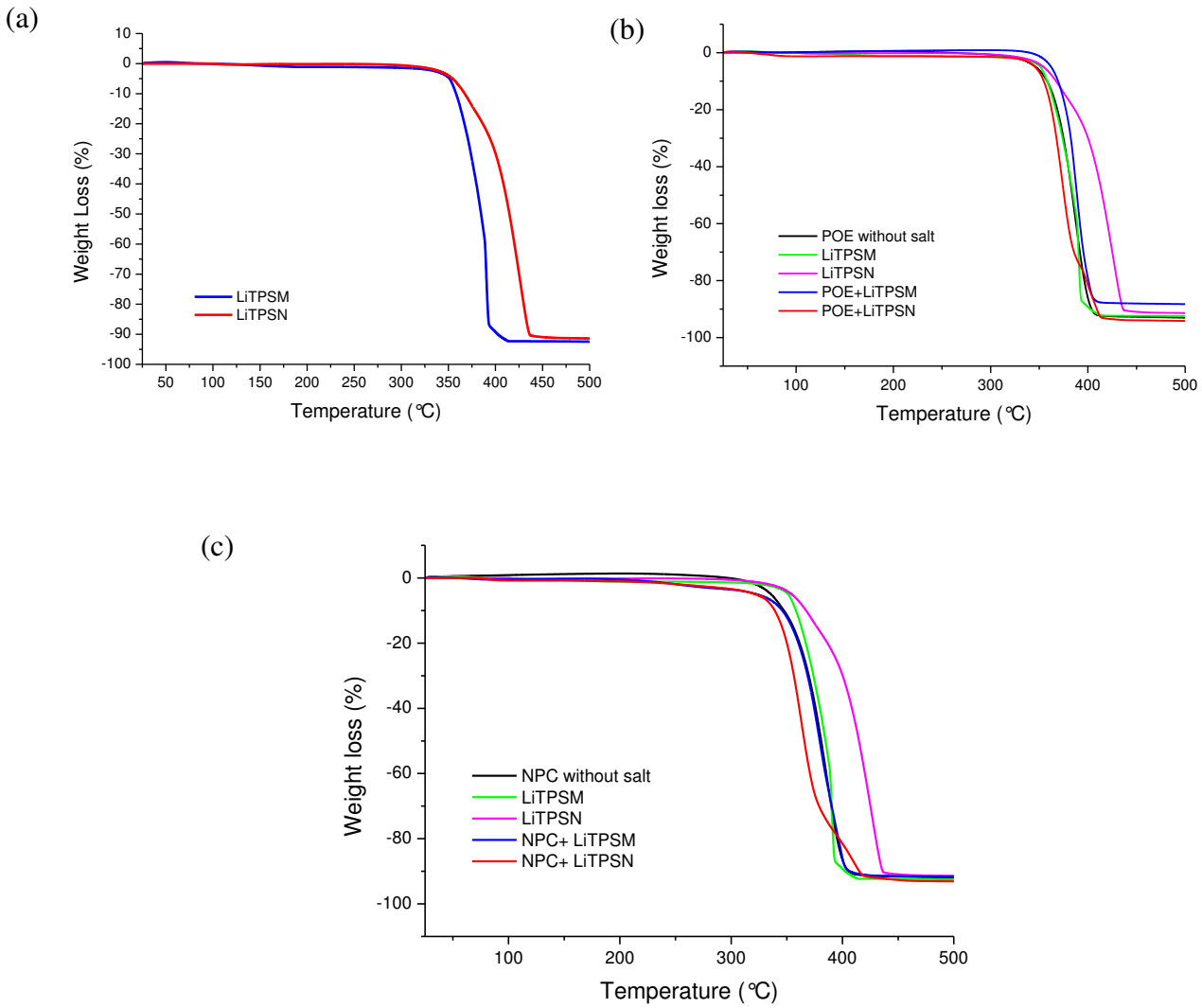

Figure 2. Thermogravimetric analysis of (a) LiTPSM and LiTPSN salts; (b) salt, POE and POE electolytes (O/Li =30) (c) salt, NPC and NPC electrolytes at O/Li= 30.

The onsets of weight loss are very close for LiTPSM and LiTPSN but the weight loss is faster in the case of the former. It might therefore be assumed that degradation occurs around the sulfonamide group. As for the slight decrease in thermal stability of LiTPSM vs LiTFSI and LiTFSN vs lithium triflate they might be ascribed to the perfluoroether function. It must be however emphasized that both flexible salts are much more stable than $LiPF_6$ and could enhance the safety of liquid electrolytes.

Concerning the stability of films based POE, figure 2b, 2c gathers the TGA records of POE and NPC electrolytes as compared to POE, NPC and salts. The onsets of the weight loss for electrolytes start at temperatures close to POE, NPC respectively. It must be recalled that these weight losses (i) are observed in inert gas and (ii) exceed distinctly the operating

temperature of lithium polymer batteries and even, in case of short-circuits the melting temperature of lithium metal.

3.2. Thermo-mechanical characterizations

The knowledge of the thermo-mechanical behavior of a polymer electrolyte in the operating temperature range of a battery is essential. Polymer electrolytes endowed with high mechanical strength can indeed benefit to battery performances in slimming the electrolyte film, thus in decreasing the ohmic drop while improving the safety. This is an indisputable asset provided the reinforcements do not result in a significant conductivity decrease.

3.2.1. POE electrolytes

The Figure 3 compares, at 1 Hz, the thermal evolution of the storage modulus of POE and its electrolytes at the concentration O/Li =20. Such evolutions are expected for linear semi-crystalline polymers with a glassy plateau interrupted by a transition α and followed by a second plateau slightly decreasing with temperature, which is related to the reinforcement induced by the crystalline phase. Regarding the mechanical strength of the films, the whole of the DMA curves shows that E' drops sharply around 60°C i.e. above the melting temperature of the samples. Thus, POE and its polymer electrolytes lose their solid aspect to become viscous gels above Tm i.e. in the operating range of the batteries. As LiTPSM and LiTFSI impact more on the crystalline phase than LiTPSN, the E' drop at T_α of their electrolytes is much more pronounced as well as the slope d(E')/dT along the crystallinity-induced plateau. Due to the salt-matrix interactions T_α increases, with regard to the host polymer, following the salt dissolution, as evidenced by the maxima of tang δ. Although Tα are supposed to roughly represent the T_g of polymers, T_α values exceeding significantly, by 12 (LiPSN) to ~25°C (LiTPSM, LiTFSI, POE) the T_g (DSC), were determined. This discrepancy must be ascribed (i) to the different type of characterization and (ii) to the thermal history of the samples. Thus, in order to avoid or to limit the constraining of the amorphous phase by the crystalline that artificially increases T_g, DSC analyses were performed with a first heating of the samples up to their total fusion followed by a cooling at 50°/mn; the T_g being measured in a second scan. This is not a quenching as the cooling is not fast enough to prevent the crystallization of the melted sample but the crystalline phase content is decreased. The amorphous phase is therefore less constrained in the second measurement than in the pristine sample leading to lower T_g, which reflect more the segmental motion ability of the polymer. As for the DMA

measurements, a 1st heating scan would obviously modify the mechanical properties of the polymer and therefore were performed on the pristine sample.

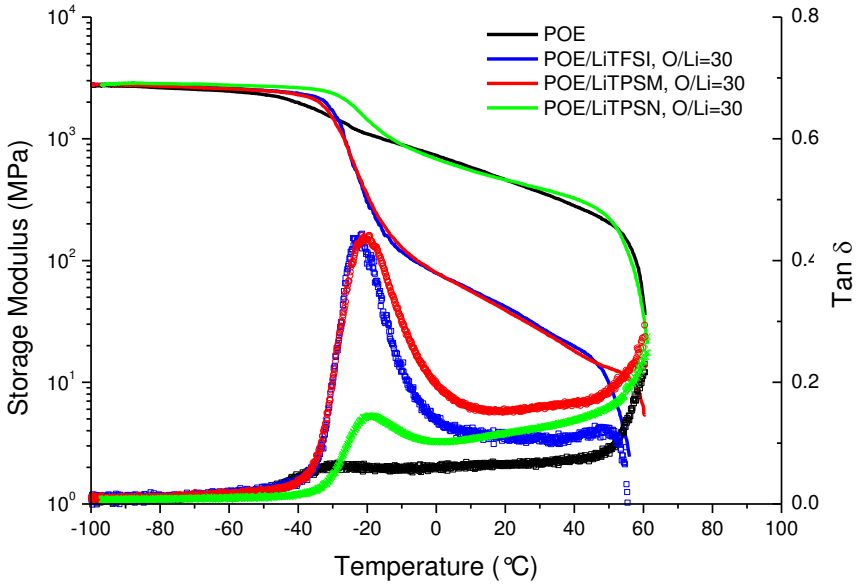

Figure 3. Storage tensile modulus (E') and loss angle tangent tan δ vs temperature at 1 Hz for POE, POE/LiTPSM, POE/LiTPSN and POE/LiTFSI electrolytes at O/Li=30.

3.2.2. NPC electrolytes

Figure 4 gathers the DMA curves of NPC and its electrolytes benchmarked with NPC/LiTFSI ones. Due to the tridimensional nature of NPC, the DMA curves differ in their shape and in their characteristic temperatures from those based on linear POE. The whole of the records show a much narrower crystallinity-induced plateau and the maintaining, through a rubbery plateau, of storage modulus much higher than those obtained with linear POE. The maxima of tan δ curves allow accessing to accurate determination of T_α. The latter are significantly higher than the T_g obtained by DSC, from 20 to more than 30°C with regard to their DSC determination during the 1st or the 2nd heating scan. A slightly higher Tα is obtained for NPC/LiTPSN electrolytes as compared to NPC/LiTPSM ~LiTFSI ones. The E' drop at T_α is much more pronounced for LiTPSM and might be ascribed to a higher disorder induced by the dissymmetric and flexible anion. E' values, on the rubbery flat plateau, range between 1 and 3 MPa, up to at least 100°C.

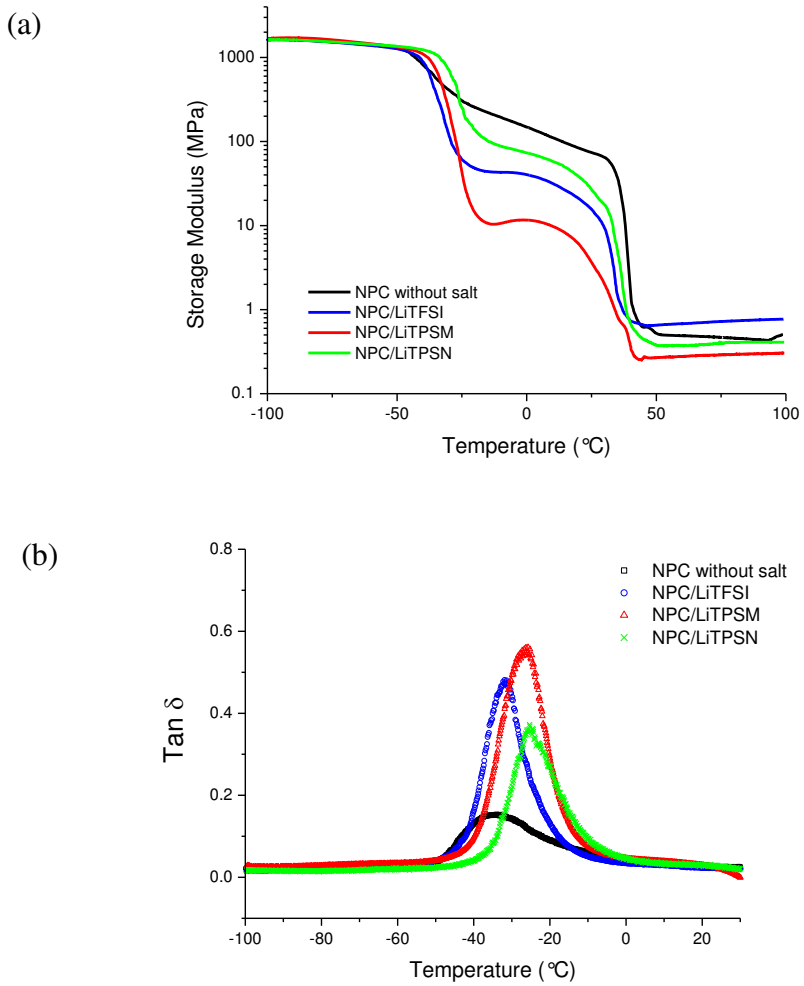

Figure 4. (a) Storage tensile modulus (E') and loss angle tangent tan δ vs. temperature at 1 Hz for NPC, NPC/LiTPSM, NPC/LiTPSN and NPC/LiTFSI complexes, (b) their Tan δ.

3.3. Conductivity measurements

The comparison of the ionic behavior of LiTFSI, LiTPSM and LiTPSN was performed in linear POE and in the cross-linked host polymer NPC.

3.3.1. Conductivities of POE electrolytes

Figure 5 shows the conductivities vs reciprocal temperature obtained with POE electrolytes. The ionic conductivities of analyzed samples were measured between 20°C and 70°C downwards. This allows improving electrode/electrolyte surface area contact but leads to overestimated values in semi-crystalline host polymer as linear POE. Indeed at 70°C the samples become amorphous and some salts, delaying the polymer crystallization, provide conductivities higher than those obtained with the same sample at its equilibrium state. The

highest conductivities, 5×10^{-4} S/cm at 70°C and 2.6×10^{-6} S/cm at 20°C, were obtained with POE/LiTPSM at O/Li= 16. This must be related to a decrease in crystallinity corroborated by the lower fusion enthalpy and T_m values. Additionally, the thermal conductivity evolution of LiTPSM and LiTPSN electrolytesis obviously different owing to the plasticizing effect and to a greater negative charge delocalization on sulfonimide anion [29] as compared to sulfonated anion leading to higher conductivities. At the same concentration (O/Li=20), POE/LiTPSM exhibited higher conductivities than those obtained for POE/LiTPSN but still lower than those obtained for POE/LiTFSI. If conductivity comparisons in linear POE are unavoidable, owing to its commercial availability and to the tremendous amount of papers, the conductivity accuracy and the reproducibility strongly depend (i) on the thermal history of the sample (stabilization time at each temperature, rate of cooling) and (ii) on the geometric factor with a possible creeping of the sample at high temperatures.

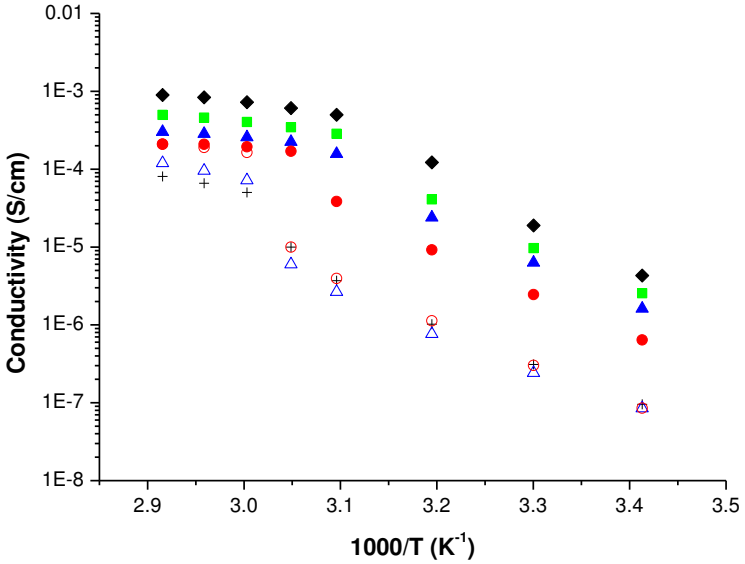

Figure 5. Comparison of conductivity as a function of salt concentration in POE/LiTPSM complexes: (■) O/Li = 16, (▲) O/Li= 20, (●) O/Li= 30 and in POE/LiTPSN complexes: (+) O/Li=12, (△) O/Li= 20, (○) O/Li=30 as compared with POE/LiTFSI complex (◆) O/Li=20.

3.3.2. Conductivities of NPC electrolytes

Contrary to POE, NPC host polymer allows the investigation of polymer electrolytes to be performed in a wide temperature range. Thus, the low crystallinity and melting points allow measuring the conductivities, in the amorphous state, down to ambient temperatures

while the cross-linking allows measuring accurate conductivities at high temperatures without fearing a possible creeping. In Figure 6 are compared the Arrhenius plots of LiTPSM, LiTPSN and LiTFSI NPC electrolytes. It must be emphasized that the physical appearance of the films i.e. dimensional shape and thickness was found unaffected by their heating up to 110°C. The best conductivities reached at 20 °C, 1.6×10^{-5} S/cm and at 110 °C, 7.2×10^{-4} S/cm were obtained for the composition O/Li=20 of NPC/LiTPSM electrolyte. However the data obtained at O/Li =12 are very close to the previous one, while those obtained at O/Li =30 are fairly disappointing. From the benchmarking done with NPC/LiTFSI it can be inferred that LiTPSM and LiTFSI behave similarly, with slight advantages at high temperatures for LiTFSI and at lower temperatures for LiTPSM. NPC/LiTPSN films exhibited the highest conductivities, 3.9×10^{-6} S/cm at 20°C and 3.4×10^{-4} S/cm at 110°C, for the composition O/Li=12. At 20°C the conductivity data reveal, for the compositions O/Li = 20 and 30, a partial crystallization of the LiTPSN samples. As the glass transition temperatures of NPC/LiTPSN are in the same range than those of the sulfonamide electrolytes, the conductivity gap might be related to the higher delocalization of the negative charge in both TPSM and TFSI anions. As expected, the use of NPC host polymer instead of linear POE allows more accurate and exploitable conductivities to be obtained.

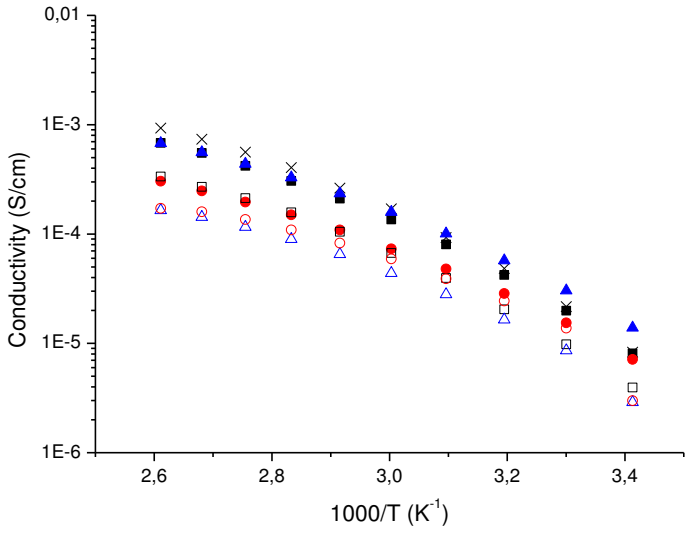

Figure 6. Temperature dependence of the ionic conductivity of NPC electrolytes based on different salts; NPC/LiTPSM electrolytes (■) O/Li=12, (▲) O/Li=20, (●) O/Li=30, NPC/LiTPSN electrolytes (□) O/Li=12, (△) O/Li =20, (○) O/Li= 30 compared with NPC/LiTFSI electrolyte (×) O/Li=12.

3.4. Transference numbers

In addition to ionic conductivities, the cationic transference numbers, T^+, are important parameters to appreciate the electrolyte performances; low cationic transference numbers impacting the performances of a rechargeable lithium batteries [30]. Ion transport was characterized, at 110°C, in both POE and NPC electrolytes using two techniques; Pulse Field Gradient NMR (PFG-NMR) and Electrochemical Impedance Spectroscopy (EIS). The characterizations dealt with the salt concentration, O/Li = 20. Thereafter, the cationic conductivities i.e. $\sigma^+ = \sigma T^+$ were calculated. All data are reported in Table 3.

3.4.1. PFG-NMR.

The self-diffusion coefficients ^7Li, ^{19}F of the different species, Li^+ cation, perfluorosulfonimide and perflurosulfonate anions, host polymer respectively were measured at 110°C and are collected in Table 3.

Table 3
Comparison of diffusion coefficients determined by PFG-NMR at 110°C, O/Li = 20
(a): calculated using the same density that the electrolytes based on linear POE

	POE		NPC	
	LiTPSM	LITPSN	LiTPSM	LiTPSN
D ^{19}F ($cm^2\ s^{-1}$)	4.4×10^{-7}	1.62×10^{-7}	5.25×10^{-7}	1.73×10^{-7}
D ^7Li ($cm^2\ s^{-1}$)	8.5×10^{-8}	5.8×10^{-8}	5.2×10^{-7}	9.7×10^{-8}
	($\pm0.05\times10^{-8}$)	($\pm1.5\times10^{-8}$)		($\pm1.2\times10^{-8}$)
T^+	0.16	0.26	0.5	0.36
σ_{Nernst} ($S\ cm^{-1}$)	1.56×10^{-3}	7.05×10^{-4}	3.1×10^{-3}(a)	1.4×10^{-3}(a)
σ_{exp} ($S\ cm^{-1}$)	4.33×10^{-4}	1.33×10^{-4}	7.21×10^{-4}	1.65×10^{-4}
% dissociation	28	19	23	11.8

Scrutinizing the data gathered in Table 3 allow inferring reveals that TPSM anion

despite its higher molar weight exhibits higher mobility than its sulfonated analog TPSN. The diffusion coefficient of TPSN anion in NPC is slightly increased (~8%) with regard to POE matrix, the same tendency being observed for TPSM (~12%). This means that despite the tridimensional nature of NPC, its segmental mobility is slightly higher than that of linear POE. Regarding Li^+ diffusion coefficients in POE, the cation diffusion is slower, from roughly 30%, in LiTPSN/POE than in LiTPSM/POE. As Li^+ is a hard acid and the polyethers as POE and NPC are hard bases the HSAB theory predicts a very strong Li^+-polyether interaction which can be counterbalanced by the anion-cation interaction.

The cationic transference numbers T^+ are lower than 0.5 for both salts when the salts are hosted in POE. Moving from POE to NPC host polymers results for both salts in a T^+ increase, moderate for LiTPSN (38 %) high for LiTPSM (~300 %).

For free ions and solvent-separated ion pairs, the Nernst–Einstein equation may be used to calculate ionic conductivity, σ_{Nernst}, from the diffusion coefficients of the cation and anion eq. (2)

$$\sigma_{Nernst} = \frac{F^2 C\ (D_+ + D_-)}{RT} \tag{2}$$

And also, the degree of dissociation can be calculated from the equation (3).

$$\%\ dissociation = \frac{\sigma_{exp}}{\sigma_{Nernst}} \times 100 \tag{3}$$

From the values of σ_{Nerst} and σ_{exp} presented in Table 3, the estimated dissociation degree is ≤ 0.5, with an advantage for LiTPSM. The degrees of dissociation are lower in NPC than in POE. This result seems questionable as NPC and POE have a very similar chemical nature as (i) the average number of oxyethylene repeat units between 2 cross-links exceeds 22 and (ii) as the conductivities obtained by impedance spectroscopy are very close.

3.4.2. T^+ comparison from EIS and PFG-NMR

The results from EIS and NMR are collected in Table 4.

Table 4 Transference number (T^+), conductivity (σ) and cationic conductivity (σT^+) for LiTPSM, LiTPSN, LiTFSI in POE and NPC matrix with two different investigating methods at 110°C

Complex	O/Li	σ (S/cm)	PFG-NMR		EIS	
			T^+	σ^+ (S/cm)	T^+	σ^+ (S/cm)
POE/LiTFSI	30	1.34×10^{-3}	0.28	3.75×10^{-4}	0.14	1.88×10^{-4}
POE/LiTPSM	20	4.33×10^{-4}	0.16	6.93×10^{-5}	0.19	8.22×10^{-5}
	30	3.17×10^{-4}	0.20	6.34×10^{-5}	0.19	6.02×10^{-5}
POE/LiTPSN	20	1.33×10^{-4}	0.26	3.45×10^{-5}	0.50	6.65×10^{-5}
	30	1.94×10^{-4}	0.36	6.98×10^{-5}	0.46	8.92×10^{-5}
NPC/LiTFSI	20	4.52×10^{-4}	0.29	1.33×10^{-4}	0.16	7.23×10^{-5}
NPC/LiTPSM	20	7.21×10^{-4}	0.50	3.59×10^{-4}	0.17	1.22×10^{-4}
NPC/LiTPSN	20	1.65×10^{-4}	0.36	5.94×10^{-5}	0.40	6.60×10^{-5}

From EIS measurements, T^+ values ranging between 0.14 and 0.5 were obtained according to the salt used. In some cases as NPC/LiTFSN there is a very good agreement between the values obtained by impedance and those calculated from the diffusion coefficients. Once again, T^+ are higher with LiTPSN based electrolytes than with LiTPSM. The gap between the T^+ calculated from PFG-NMR and those obtained from EIS is related to the type of analysis. Thus, PFGNMR does not discriminate between on the one hand contact ion-pairs that are electrically neutral and, on the other hand, free-ions and solvent separated ion-pairs that both contribute to the electrolyte conductivity. In POE the highest σ^+ was obtained with LiTFSI while in NPC host polymer, the highest $\sigma^+$was obtained with LiTPSM.

4. Conclusion

New lithium salts based on perfluoroethersulfonate and dissymmetric

perfluoroethersulfonimide anions, hosted in linear and tridimensional, were thoroughly characterized. Generally polymer electrolytes are used in a wide range of salt concentration. However, the best performances are obtained, in lithium battery, for medium to fairly low salt concentrations. Furthermore, decreasing the salt concentration allows cost-cutting to be performed as the lithium salts are expensive. We have therefore mainly focus our polymer electrolyte study on 2 concentrations (O/Li = 20 and 30). The best conductivities in POE commercial host polymer were obtained for electrolytes based on the dissymmetric sulfonamide. However, thanks probably to the flexibility brought by the ether function, the conductivities obtained with the perfluorosulfonate salt are much higher, at 70°C, than those already reported for lithium triflate [31]. In a perspective or post-lithium-ion batteries based on sodium or on alkaline-earth metals e.g. magnesium, it should be interesting to assess the capability of this flexible perfluorosulfonate anion to induce both high conductivities and cationic conductivities. Using as host polymer NPC allows significantly (i) reinforcing the mechanical strength of the polymer electrolytes (ii) decreasing the crystallinity and Tm of the polymer electrolyte and (iii) increasing the ambient temperature conductivities as compared to commercial POE. The conductivity of NPC electrolytes based on both salts could be still improved in terms of conductivity, by decreasing the crosslink density, while their mechanical strength could be distinctly increased by the use of Nano Crystalline Cellulose [32]

These results are still limited as compared to hundreds of published papers dealing with LiTFSI and, owing to the data here reported, these new salts deserve to be investigated not only in solvent-free polymer electrolytes but also in liquid and gelled electrolytes. Furthermore the potential of these new anions must be assessed in ionic liquids and, in particular, in proton-conducting ionic liquids for High Temperature PEM Fuel Cells. The starting commercial sulfonyl fluoride could be easily produced at large scale as it can be derived from one of the monomer used to synthesize perfluorosulfonic acids, while the perfluorosulfonamide (TPSM) synthesis can use trifluorosulfonic anhydride [33]

Acknowledgements

This work was supported by the Agence Nationale de la Recherche (ANR 2011 BS08 003 01)

References

[1] P. Isken, C. Dippel, R. Schmitz, R.W. Schmitz, M. Kunze, S. Passerini, et al., Electrochimica Acta. 56 (2011) 7530–7535.
[2] G. Feuillade, Ph. Perche, J Appl. Electrochem. 5 (1975) 63–69.
[3] M. Gauthier, A. Bélanger, P. Bouchard, B. Kapfer, S. Ricard, G. Vassort, et al., J. Power Sources. 54 (1995) 163 – 169.
[4] K. Murata, S. Izuchi, Y. Yoshihisa, Electrochimica Acta. 45 (2000) 1501 – 1508.
[5] V.D. Noto, S. Lavina, G.A. Giffin, E. Negro, B. Scrosati, Electrochimica Acta. 57 (2011) 4 – 13.
[6] D.E. Fenton, J.M. Parker, P.V. Wright, Polymer. 14 (11) (1973) 589.
[7] P.V. Wright, Br Polym. J. 7 (1975) 319.
[8] C. Berthier, W. Gorecki, M. Minier, M.B. Armand, J.M. Chabagno, P. Rigaud, Solid State Ion. 11 (1983) 91 – 95.
[9] Z. Stoeva, I. Martin-Litas, E. Staunton, Y. G. Andreev, P. G. Bruce, J AM CHEM SOC. 125 (2003) 4619–4626.
[10] A.Killis, J-F.Le Nest, H.Cheradame, MakrolChemRapid Comm.1 (1980) 595.
[11] M. Watanabe, H. Tokuda, S. Muto, Electrochimica Acta. 46 (2001) 1487 – 1491.
[12] C. Schoenenberger, J.F. Le Nest, A. Gandini, Int. Symp. Polym. Electrolytes. 40 (1995) 2281–2284.
[13] F. Alloin, J.-Y. Sanchez, Electrochimica Acta. 40 (1995) 2269–2276.
[14] J. Barthel, M. Schmidt, H.J. Gores, J Electrochem Soc. 145 (1998) L17–L20.
[15] E. Paillard, C. Iojoiu, F. Alloin, J. Guindet, J.-Y. Sanchez, Electrochimica Acta. 52 (2007) 3758 – 3765.
[16] S. Sylla, J.-Y. Sanchez, M. Armand, Electrochimica Acta. 37 (1992) 1699 – 1701.
[17] F. Alloin, D. Benrabah, J.-Y. Sanchez, J. Power Sources. 68 (1997) 372 – 376.
[18] J. Kalhoff, D. Bresser, M. Bolloli, F. Alloin, J.-Y. Sanchez, S. Passerini, ChemSusChem. 7 (2014) 2939–2946.
[19] D.Benrabah, D.Baril, J-Y.Sanchez, M.Armand, G.Gard, J.Chem. Soc. Faraday Trans. 89 (1993) 355–359.
[20] L. Conte, G. Gambaretto, G. Caporiccio, F. Alessandrini, S. Passerini, J. Fluor. Chem. 125 (2004) 243 – 252.
[21] O.E. Geiculescu, S.E. Creager, D.D. DesMarteau, in : T. Nakajima, H. Groult (Eds.), Fluorinated Materials for Energy Conversion, Elsevier (2005), pp. 223–251 (Chapter 10)
[22] F. Alloin, J.-Y. Sanchez, M. Armand, J. Electrochem. Soc.141 (1994) 1915.
[23] P.R. Soeresen, T. Jacobsen, Electrochimica Acta. 27 (1982) 1671–1675.
[24] D. Aurbach, J Power Sources. 89 (2000) 206–218.
[25] M.D. Levi, D. Aurbach, J. Phys. Chem. B. 101 (1997) 4630–4640.
[26] M. Rosso, Electrochimica Acta. 51 (2006) 5334–5340.
[27] R.Arnaud, D.Benrabah, J-Y.Sanchez, J Phys Chem. 100 (1996) 10882–91.
[28] Z. Lu, L. Yang, Y. Guo, J. Power Sources. 156 (2006) 555–559.
[29] D. Benrabah, R. Arnaud, J.-Y. Sanchez, Electrochimica Acta. 40 (1995) 2437 – 2443.
[30] M. Doyle, T.F. Fuller, J. Newman, Electrochimica Acta. 39 (1994) 2073 – 2081.
[31] D. Benrabah, S. Sylla, F. Alloin, J.-Y. Sanchez, M. Armand, Electrochimica Acta. 40 (1995) 2259–2264.
[32] M.A.S. Azizi Samir, F. Alloin, J.-Y. Sanchez, N. El Kissi, A. Dufresne, Macromolecules. 37 (2004) 1386–1393.
[33] F. Toulgoat, B.R. Langlois, M. Médebielle, J.-Y. Sanchez, J. Org. Chem. 73 (2008) 5613–5616.

III.3. Preparation and characterizations of aliphatic oligoether lithium salts

In order to study the performance of aliphatic lithium salts based on sulfonate/sulfonimide mono end-capped mPEG and to compare with the salts LiTPSM and LiTPSN we selected to modify the 1,1,2,2,-tetrafluoro-2-(1,1,2,2,-tetrafluoro-2-iodoethoxy)ethane sulfonyl fluoride. It is well known the iodoperfluoalkyl is able to perform an addition reaction on allylic double bond (figure 3.3) [5]. Then the SO_2F from R_F can be transformed in SO_3Li by hydrolysis or in sulfonimide Li.

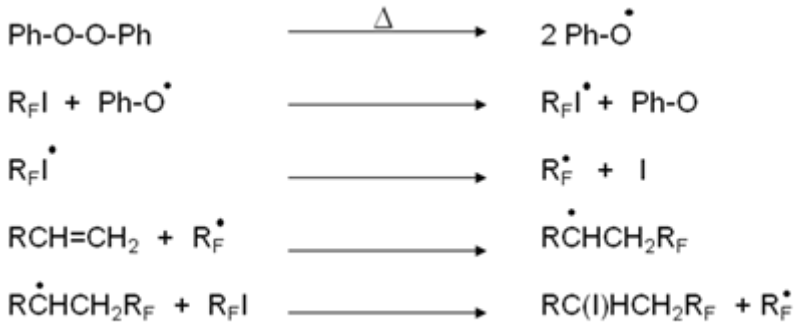

R_F is CF_2CF_2-O-$CF_2CF_2SO_2F$

Figure 3.3. Mechanism for free radical addition on allylic double bond [5].

The fluorinated part of these salts is similar to that of salt LiTPSM and LiTPSN.

The synthesis of these salts needs a precursor that is an allyl mono-ended mPEG.

Synthesis of allyl monoended mPEG precursor

The allyl ether precursors were obtained by Williamson synthesis from mPEG and allyl bromide via the nucleophilic substitution reaction (figure 3.4). The alcohols with different number of repeating oxyethylene units are deprotonated by the NaH at 40°C in anhydrous tetrahydrofurane at room temperature. Allyl bromide was added dropwise at 0°C in order to limit the side reactions. The temperature of solution was heated to 40 °C and the reaction progress was monitored by ^{1}H-NMR.

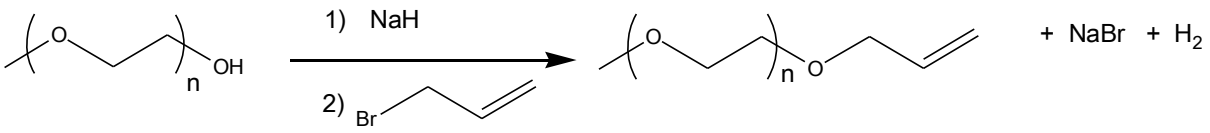

Figure 3.4. Schematic of allyl ether precursor synthesis for n ≥ 3.

The figure 3.5 represents the spectrum of mPEG and Allyl-mPEG. The transformation of mPEG in Allyl-mPEG is showed by the shifting of the peak corresponding to the protons from position a (CH_3) from 3.1 ppm to 3.3 ppm and the multiplet peaks corresponding to protons of oxyethylene appear at 3.5 ppm instead of 3.3 ppm. Moreover, new peaks appear at 3.9, 5.1 and 5.8 ppm corresponding to protons of methylene (d) and allyl (e,f). All proton signals represented in figure 3.5 (b) indicates the successful formation of allyl ether precursors.

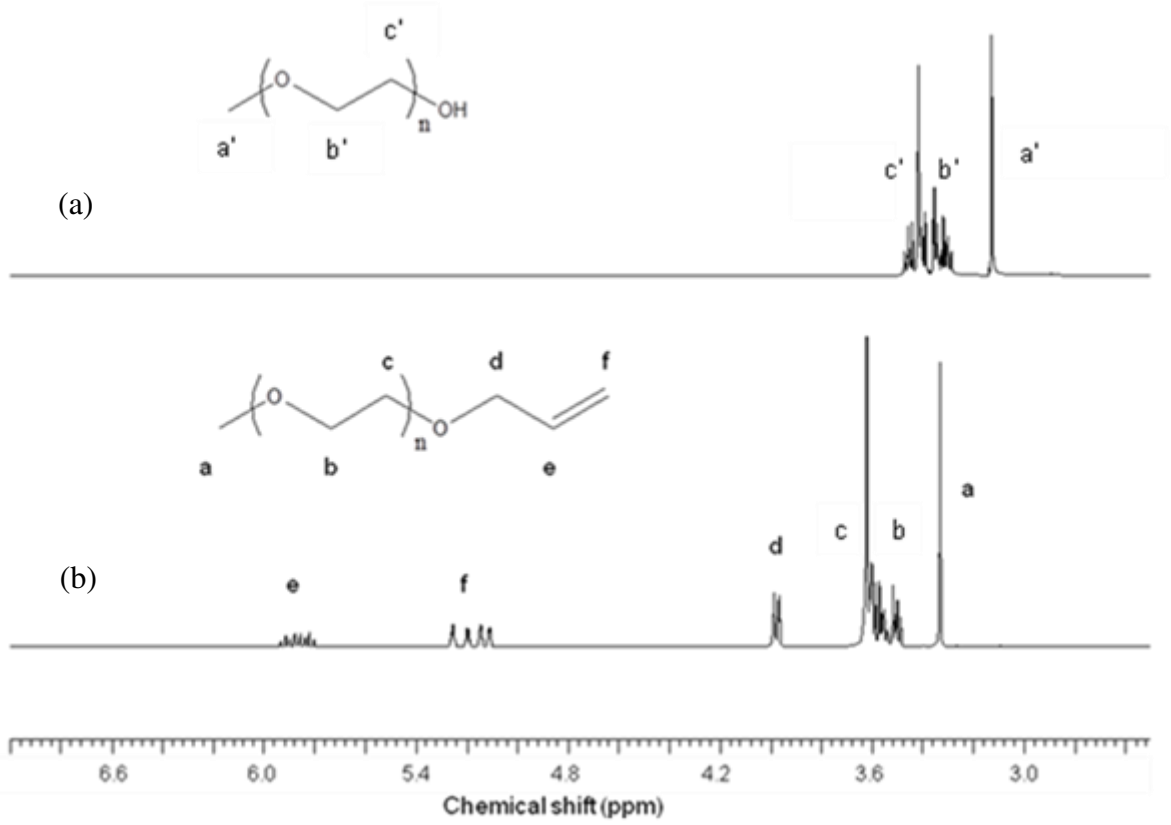

Figure 3.5. ^{1}H-NMR spectra of (a) alcohol starting material (mPEG) (b) allyl ether precursor (Allyl-mPEG), n=3.

The crude yield of reaction was 100%, the resulted product is a solid or a liquid, depending on the chain length of molecule. In order to separate, the Allyl-mPEG from by-product (white precipitate NaBr) and excess of bromoallyl the mixture resulted after the

evaporation of THF was washed with water and extracted in diethylether. The net yield depends on the length of mPEG and the results are gathered in the Table 3.1.

Table 3.1 Percentage yield obtained for each chain length of mPEG

n	% crude yield	% net yield
1	100	60
3	100	85
7	100	85
16	100	62

III.3.1.Synthesis of Salt 3

Salt 3 was carried out by the radical addition reaction of allyl oligoether (figure 3.6) on 5-Iodoperfluoro-3-oxapentanesulfonyl fluoride using benzoyl peroxide as an initiator [6], [7] to form mPEG-SO_2F follow by the hydrolysis reaction to form the **salt 3** .

The synthesis of mPEG-SO_2F takes place with net yield of 66 %. As side products we found small quantity of by-product resulted by the polymerization of Allyl-mPEG or by dimerization of 5-Iodoperfluoro-3-oxapentanesulfonyl fluoride. The side products, the benzoyl peroxide and the excess of 5-Iodoperfluoro-3-oxapentanesulfonyl fluoride were removed by flash column chromatography.

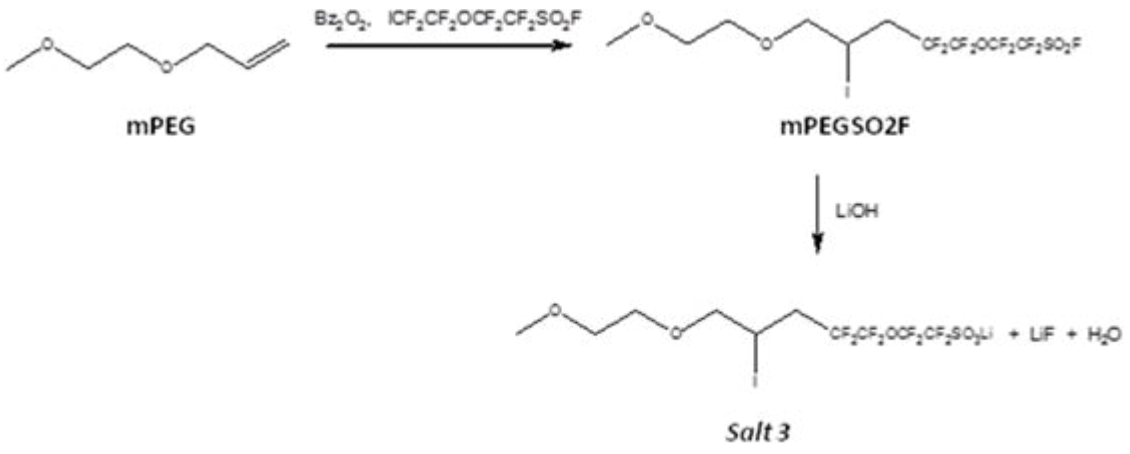

Figure 3.6. Synthesis of **salt 3.**

The ^{1}H NMR spectrum of $mPEGSO_2F$ is represented in the figure 3.7. As comparing with Allyl-mPEG it can be observed the peaks corresponding to the protons from allyl disappear and a new peak, as multiplet, appears at 4.2 ppm corresponding to the proton of CH-I (e). New peaks appear, like multiplets, at 2.6 and 3.0 ppm corresponding to two protons of carbon bonded to CF_2 and CHI (f). We note the peak corresponding to the protons in d and f positions are multiplets with a very complicate shape. This was also reported by other authors [8], [9], [10] and we assume this is due to the presence of stereocentre (CHI) and the formation of different diastereomers. Hence the protons from d and f positions are diastereotopic.

Furthermore, ^{19}F-NMR spectra, represented in Figure 3.8 indicates the formation of $mPEGSO_2F$ by the shift of the peak corresponding to $-CF_2-I$ from -65 ppm to -112 ppm assigned to CF_2 bonded to CH_2. Also the peaks corresponding to the other F from other carbons (2', 3',4') shift with some ppm after the addition reaction while the peak of SO_2F located at 45.8 ppm shift only with 0.5 ppm (45.3 ppm).

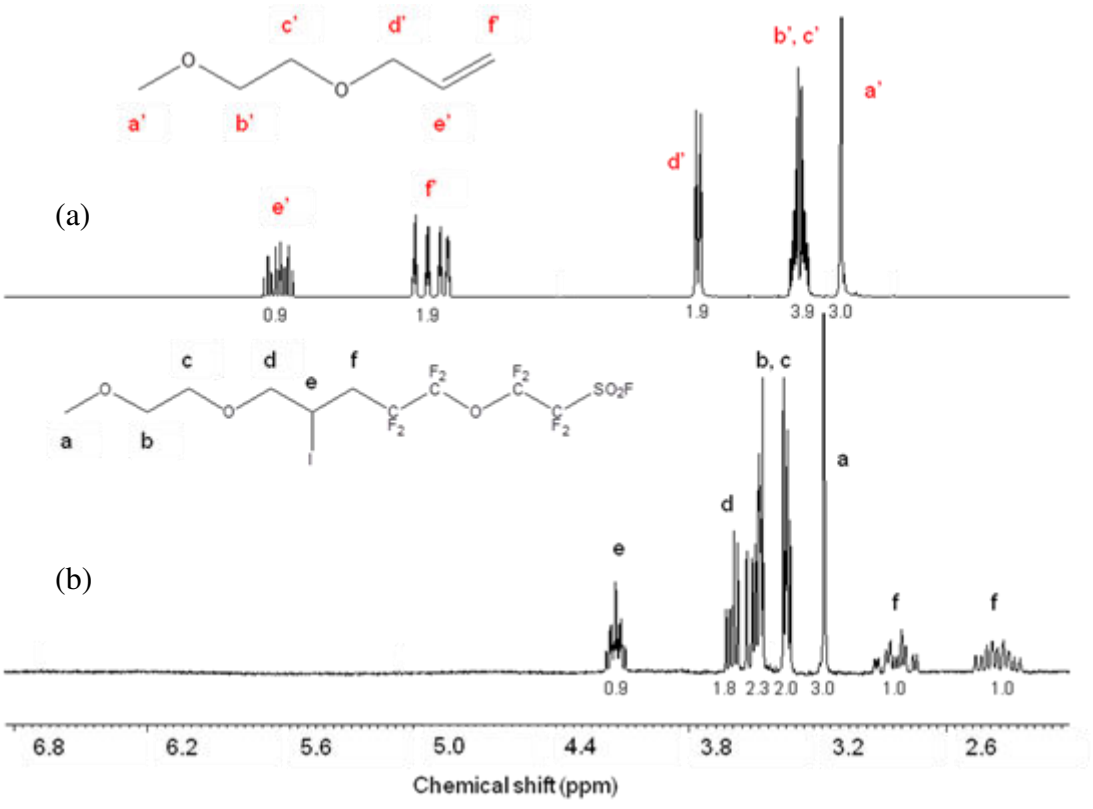

Figure 3.7. ^{1}H NMR spectra of (a) allyl ether precursor and (b) intermediate of **salt 3** in $CDCl_3$.

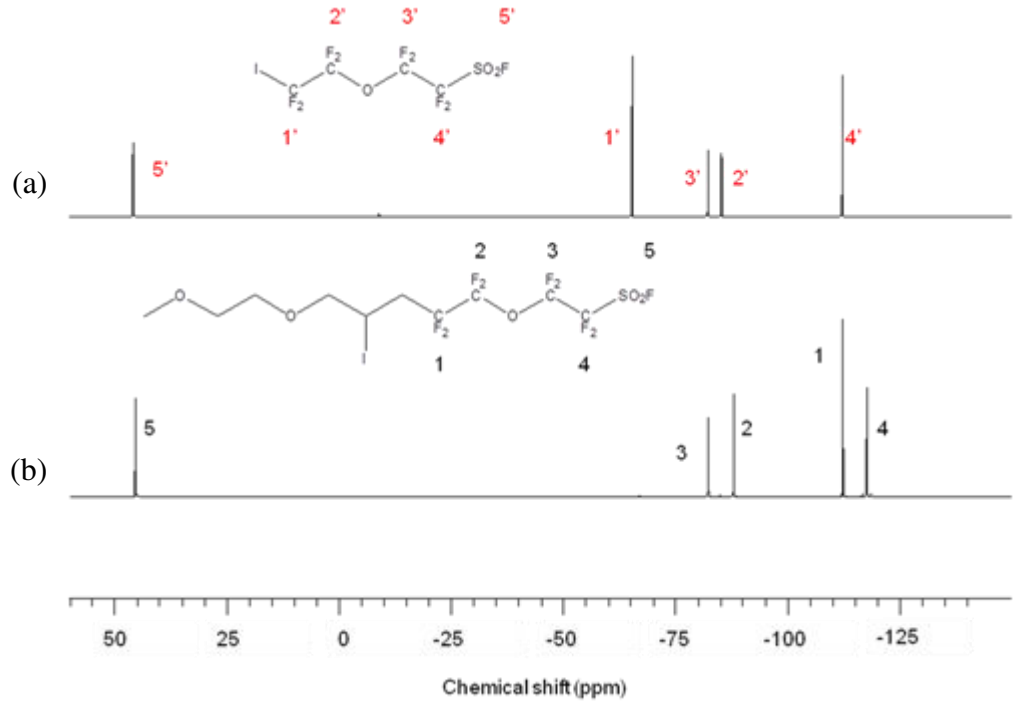

Figure 3.8. ^{19}F-NMR spectra of (a) 5-Iodoperfluro-3-oxapentanesulfonyl fluoride and (b) intermediate of **salt 3** in $CDCl_3$**.**

In order to obtain the lithium salt, the $–SO_2F$ was transformed in $–SO_3Li$ in THF with LiOH at ambient temperature (Figure 3.9). The success of transformation was checked by the disappearance of the peak at 46 ppm on ^{19}F-NMR spectrum corresponding to the F from SO_2F as shown in Figure 3.9. The peak NMR spectra were performed in acetone, while the obtained product in SO_3Li form (**salt 3**) is not more soluble in chloroform. In acetone solvent the F in 1 position appears like multiplet in ^{19}F-NMR spectrum, probably due to the protons in f positions that are diastereotopic.

Additionally, there is a slightly shift of peaks in ^{1}H-NMR as seen in Figure 3.10.

The transformation of SO_2F in SO_3Li carried out in basic condition and a deiodination reaction could be expected (figure 3.11) that might lead to the formation of double bonds. However, in ^{1}H-NMR (Figure 3.10), any peak corresponding to the double bonds was detected. Another possibility is a part of iodine was replaced with OH but the elementary analysis does not sustain this hypothesis (Table 3.2), the iodine found in the composition is slightly higher than expected one.

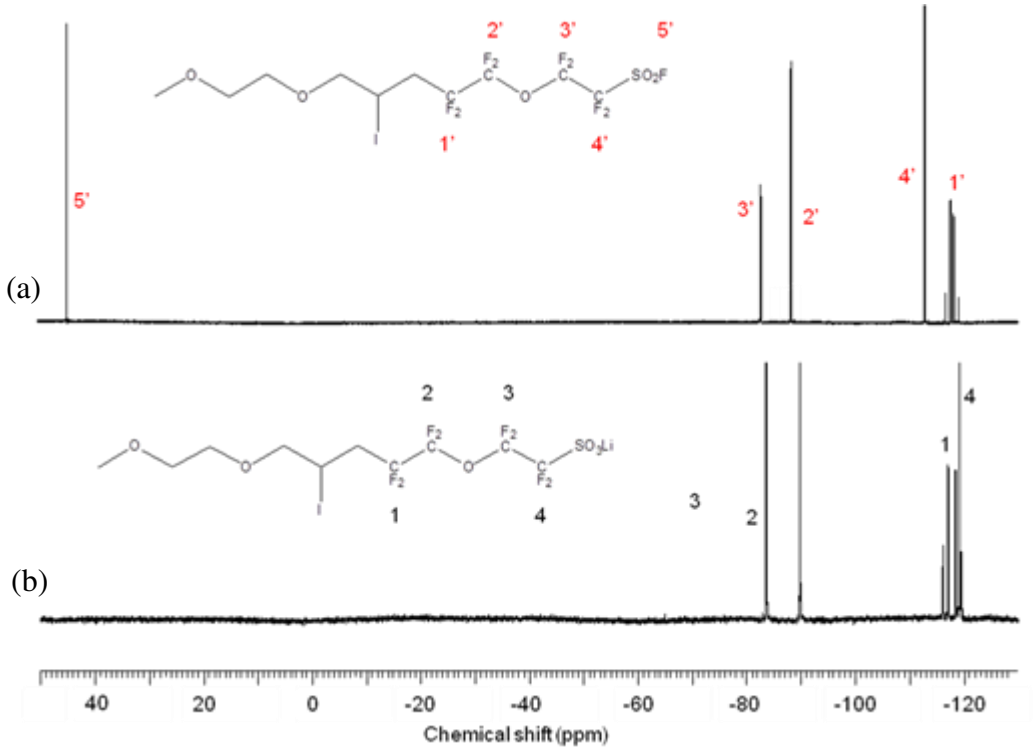

Figure 3.9. ^{19}F-NMR spectra in acetone of (a) mPEGSO$_2$F and (b) **salt 3** in acetone-d6**.**

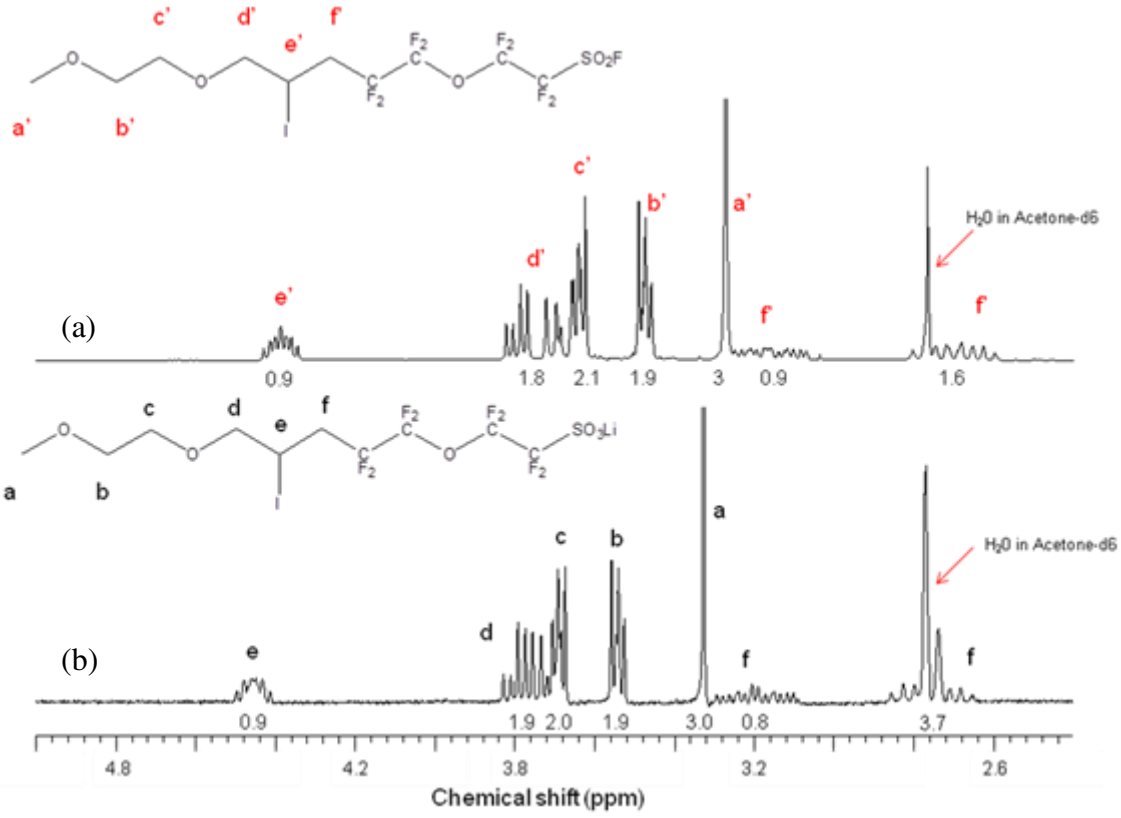

Figure 3.10. ^{1}H-NMR spectra of (a) intermediate of **salt 3** and (b) **salt 3.**

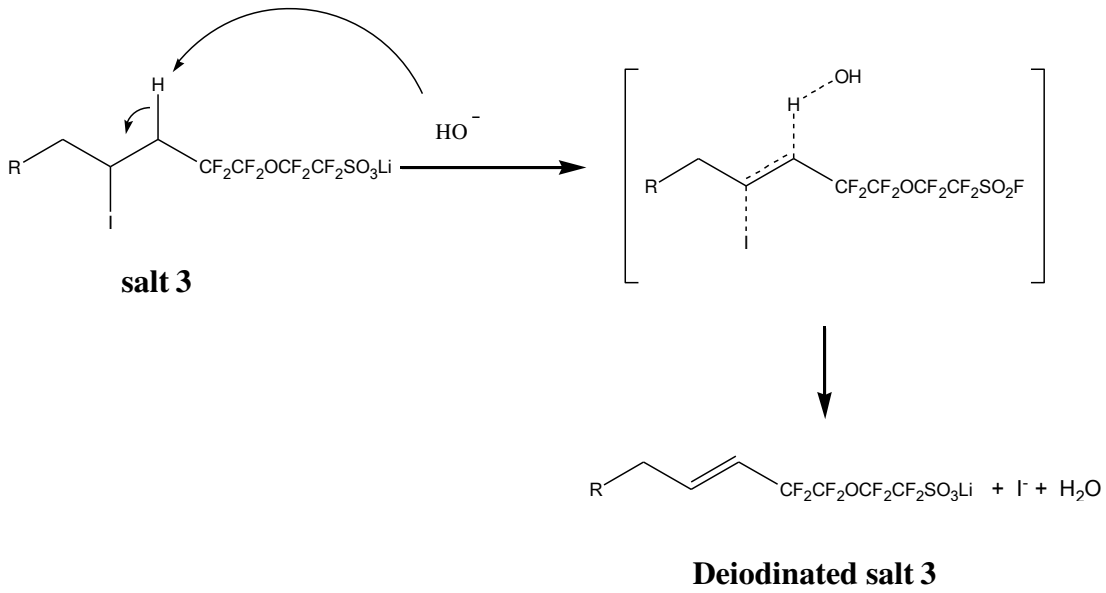

Figure 3.11. Deiodination of **salt 3** (R = $CH_3OCH_2CH_2O$-). [11]

Elementary analysis

Table 3.2 Elemental analysis of **salt 3**

Element	C	H	F	Li	S	I
Calc.	21.99	2.21	27.83	1.27	5.87	23.24
Found	22.02±0.3	2.60±0.3	27.89	1.1	5.65	23.55

III.3.2.Synthesis of Salt 4

The presence of iodine in the structure of salt can affect its chemical and electrochemical stability. Therefore, the **salt 4** was obtained by the substitution of iodine with hydrogen. The synthesis of **salt 4n1** was performed by intermolecular perfluoroalkylation of alkenes in presence of tris-(trimethylsilyl)silane $(Me_3Si)_3SiH$ and benzoyl peroxide (figure 3.12) followed by the transformation of SO_2F in SO_3Li.

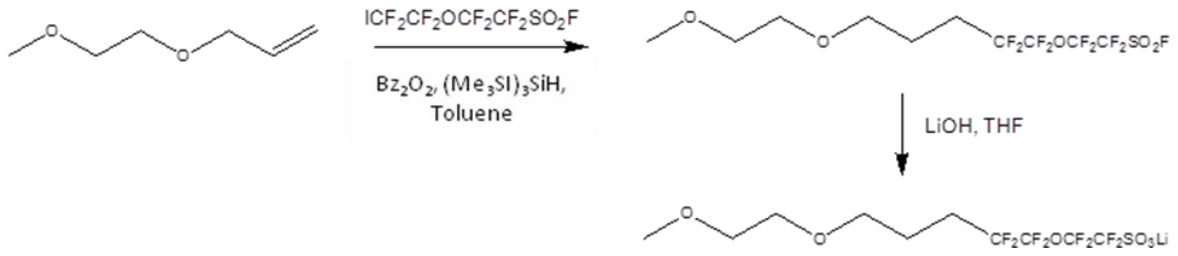

Salt 4

Figure 3.12. One pot reaction and lithiation of **salt 4**.

The mechanism of the $(Me_3Si)_3SiH$-mediated intermolecular perfluoroalkylation of alkenes is depicted in the Scheme represented in Figure 3.13 [12]. The $(Me_3Si)_3Si$• radical (produced peroxide decomposition) abstracts the halogen atom (iodine) from R_fX. This Rf• radical reacts faster with the alkene than with the silicon hydride, affording the perfluoroalkylated radical adduct 10. The perfluoroalkylated radical adduct 10 abstracts hydrogen from the silane, affording the perfluoroalkyl-substituted alkane 11, and regenerating the silyl radical, thus propagating the chain. The electrophilicity of Rf• radicals is the dominant factor giving rise to their high reactivity. The stronger carbon-carbon bond that forms when Rf • versus R• radicals add to an alkene is a driving force for the radical addition (the greater exothermicity of the Rf• radical addition is expected to lower the activation energy).

Dolbier et al. [13] have found that perfluorinated radicals were much more reactive than their hydrocarbon counterparts in addition to normal, electron rich alkenes such as 1-hexene (40 000 times more reactive) in organic solvents, and that H transfer from $(Me_3Si)_3SiH$ to a perfluoro-n-alkyl radical such as $n\text{-}C_7F_{15}CH_2CH\bullet C_4H_9$ was 110 times more rapid than that to the analogous hydrocarbon radicals.

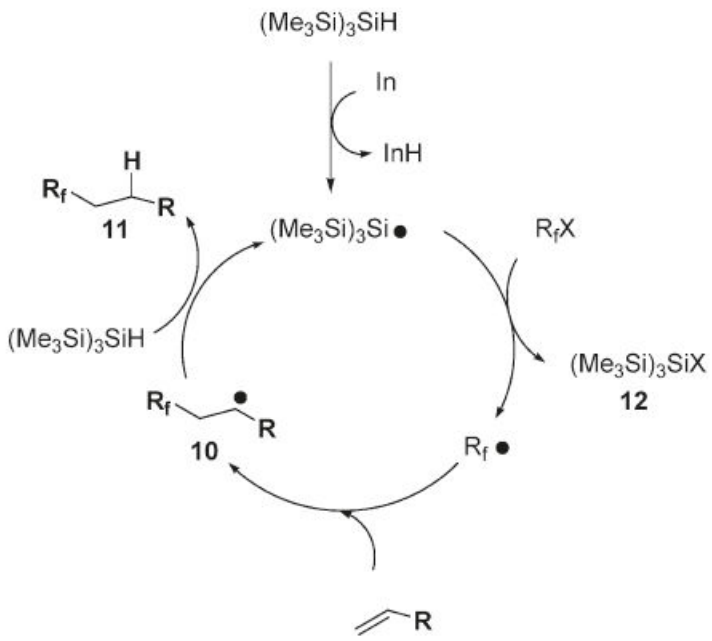

Figure 3.13. Mechanism for Radical Carbon-Carbon Bond Formation Reactions from Alkenes and Perfluoroalkyl Iodides mediated by $(Me_3Si)_3SiH$

The intermediate ($mPEGHSO_2F$) of **salt 4n1** was recovered by distillation and then by reaction with LiOH the **salt 4n1** was obtained.

However for $n \geq 3$ the distillation was not more possible the purification of $mPEGHSO_2F$ by extraction or flash column chromatography give not good results probably due the similar polarity of different products present in the reaction mixture. In order to improve it we proceed first to the transformation of $mPEGSO_2F$ in **salt 4** (SO_3Li) and then perform the purification. However, the purification is quite difficult and the yield net was lower than 30%.

Therefore in the second time we performed the synthesis of **salt 4** by hydrogenation of **salt 3** with $(Me_3Si)_3SiH$. The **salt 4n1 (3, 7, 16)** was purified and then was submitted to hydrogenation reaction (Figure 3.14).

The ^1H-NMR spectra (figure 3.15) represents the comparison between the **salt 3** and **salt 4** intermediate. The disappearance of multiplet at 4.3 ppm which corresponds to proton of CHI (e') and the apparition of a new peak 1.3 ppm prove the transformation of CHI in CH_2. Moreover the protons from the carbon close to CF_2 shift from 2.6 and 3 ppm at 2.1 ppm.

The modification of SO_2F in SO_3Li was monitored by ^{19}F-NMR. The disappearance of peak at 45 ppm belonging to SO_2F and the slight shift of CF_2 peak from 112 ppm to 118 ppm was

shown in ^{19}F-NMR spectrum in figure 3.16. This can indicate the successful formation of **salt 4n3**.

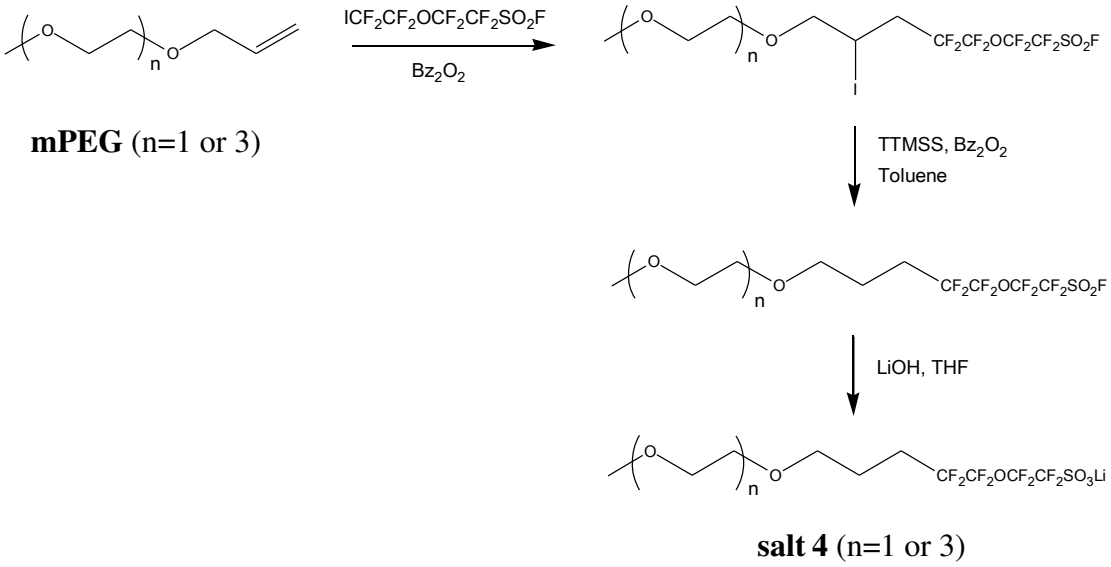

Figure 3.14. Syntheses of **salt 4n1** and **salt 4n3.**

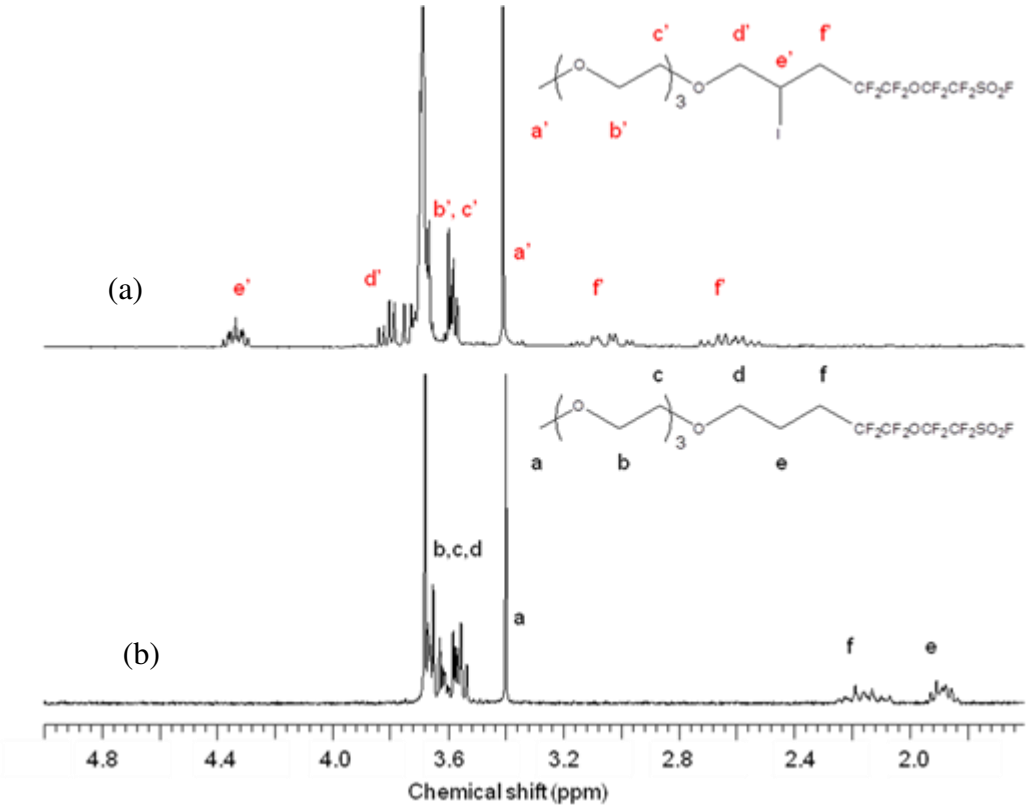

Figure 3.15. ^{1}H NMR spectra of (a) **salt 3n3**-SO_2F and (b) **salt 4n3** after the replacement of I with H in $CDCl_3$.

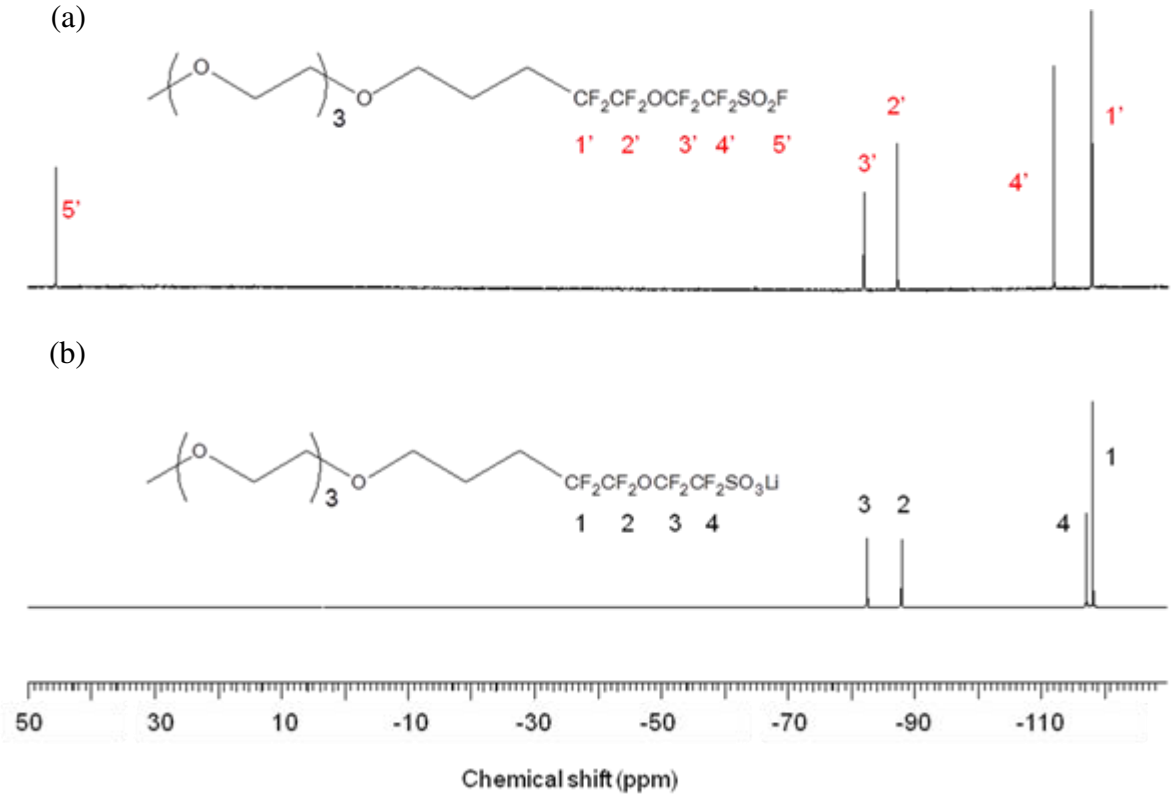

Figure 3.16. ^{19}F NMR spectra of (a) intermediate of **salt 4n3** and (b) **salt 4n3** in acetone –d6.

The synthesis of **salt 4n1 and salt 4n3** were obtained with a net yield around 53%.

For the synthesis of **salt 4** with n= 7 and 16 we did not succeed to improve the yield. During the purification by column chromatography almost all product was loss. Therefore, the study on the **salt 4n7** and **salt 4n16** were not carried out in the further characterization.

III.3.3.Salt 5

As reported in the bibliographic part, the performances of sulfonylimide anions are more attractive due to the feature of $TFSI^-$ anion. This anion function provides a large delocalization of its negative charge contributing the ion pair dissociation and the high flexibility. Therefore, the lithium salt of aliphatic sulfonylimide oligoether is synthesized by transforming the sulfonyl fluoride into sulfonylimide group as shown in the following schematic (Figure 3.17).

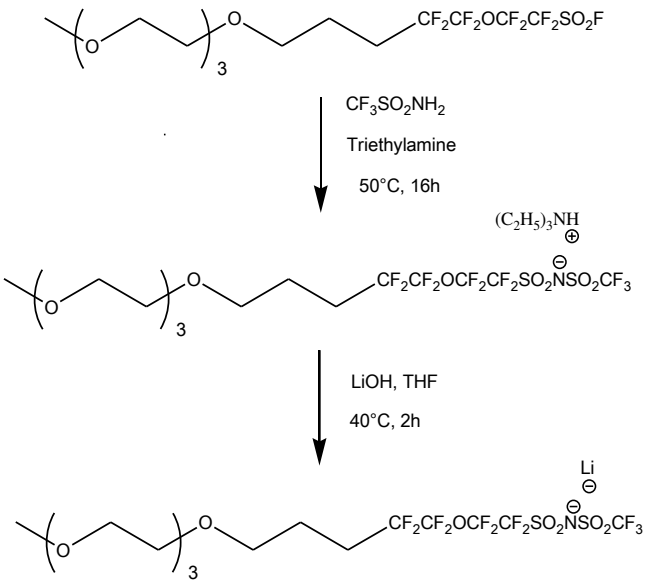

Salt 5n3

Figure 3.17. Synthesis of **salt 5n3.**

The sulfonyl fluoride oligoether n= 3 is reacted with trifluoromethanesulfonamide in the presence of triethylamine in acetonitrile according to a procedure for synthesis of lithium sulfonylimide monomers [14], [15]. The residue after the solvent evaporation is dissolved in dichloromethane, washed by distilled water many times to remove the excess of trifluoromethanesulfonamide and the side product, sulfonate triethylammonium salt (figure 3.18). This side product can be formed by the hydrolysis of SO_2F with water traces from solvent [14]. This competitive reaction simultaneously occurs with the formation of sulfonylimide triethylammonium salt. This assumption is indicated by the 4 peaks at -82, -88, -117 and -118 ppm on the ^{19}F-NMR spectrum (figure 3.19 (a)). The triethylammonium salt of the main product is concentrated and followed by the cation exchange with a solution of LiOH. The ^{1}H-NMR spectrum in figure 3.20 shows the disappearance of protons on methyl and methylene carbon of sulfonylimide triethylammonium salt at 1.3 and 3.1 ppm respectively.

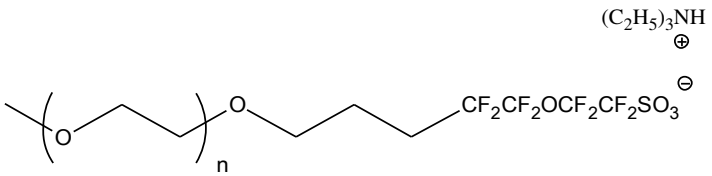

Figure 3.18. Possible formation of sulfonate triethylammonium salt from competitive reaction.

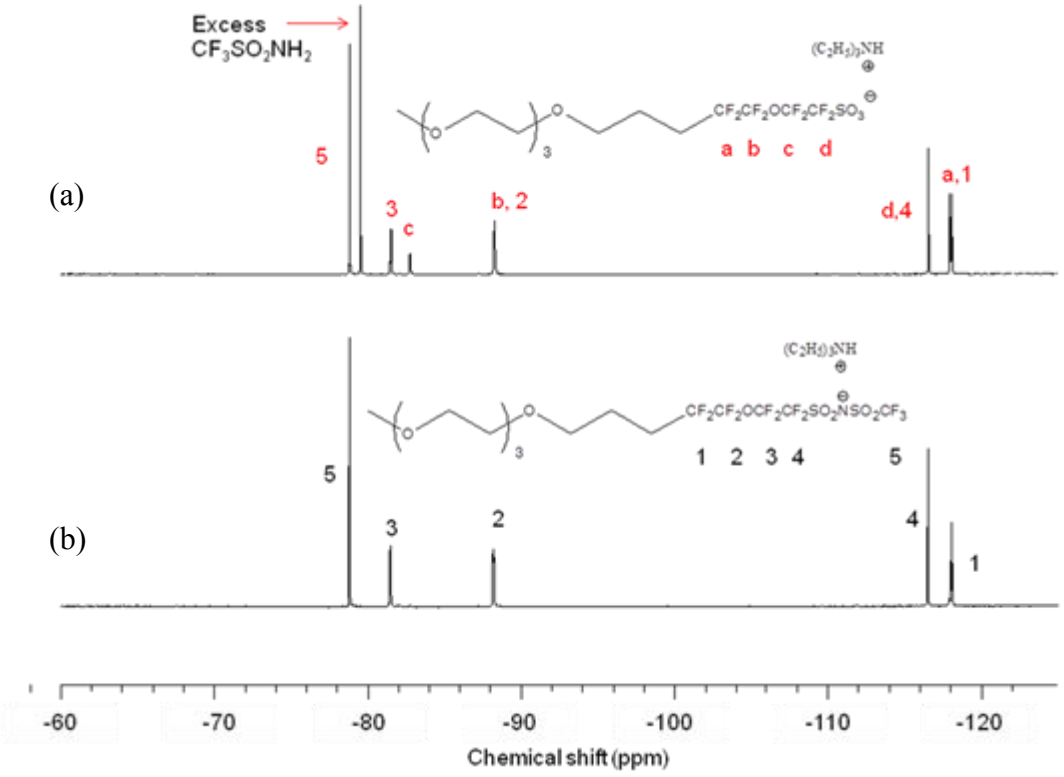

Figure 3.19. ^{19}F spectra of (a) mixture of sulfonate triethylammonium salt and sulfonylimide triethylamonium salt (b) sulfonylimide triethylammonium salt in DMSO-d6.

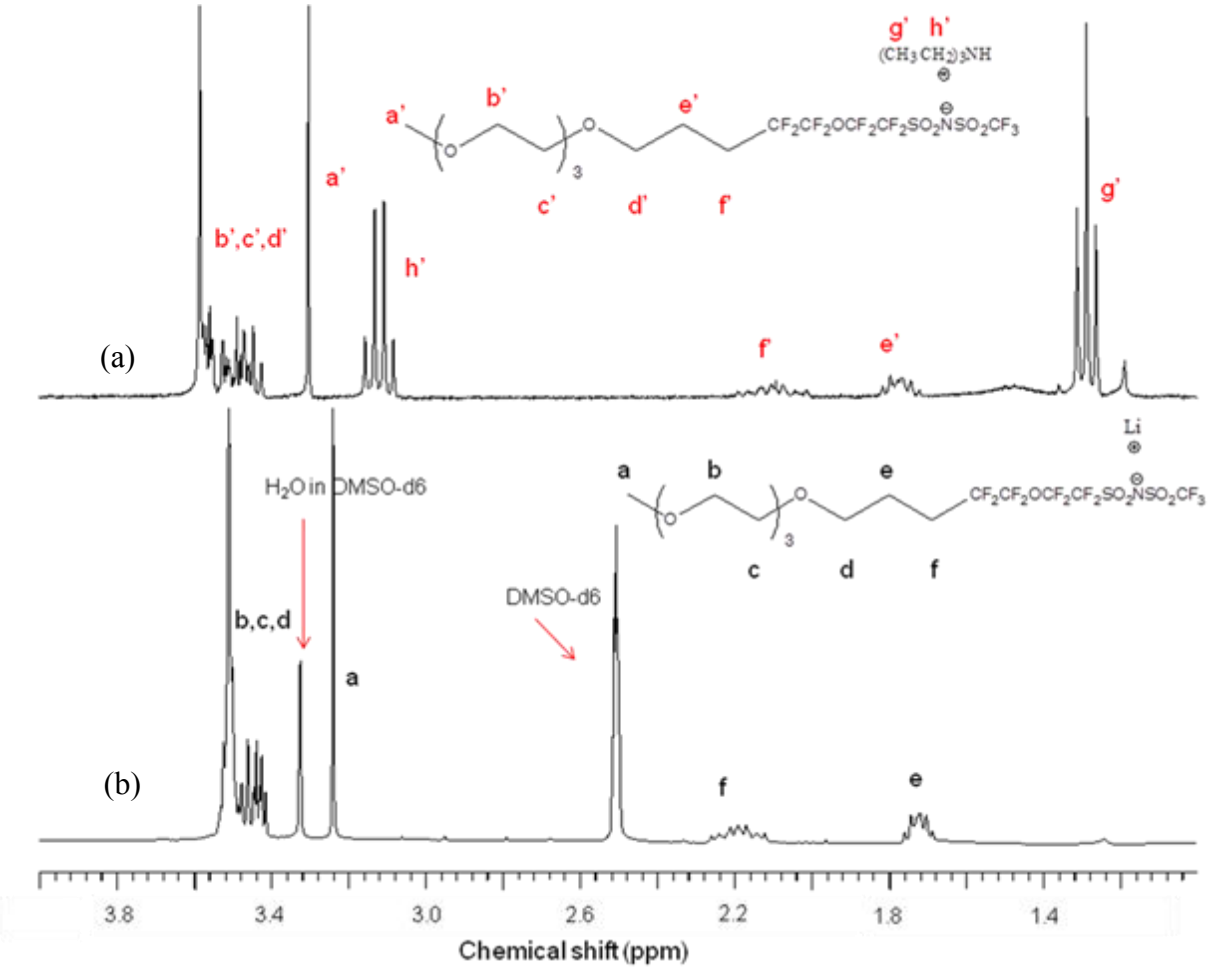

Figure 3.20. ^{1}H spectra of (a) sulfonylimide triethylammonium salt (b) **salt 5n3** in DMSO-d6**.**

III.3.4. Characterizations of salts

III.3.4.1. Thermal Properties

a. DSC analyses

The T_g, T_m and ΔH of different salts synthesized are gathered in the Table 3.2. The salt LiTPSM and LiTPSN were added for comparison.

Table 3.2 Glass transition temperature (T_g), melting temperature (T_m) and ΔH of aliphatic lithium salts modified mPEG.

Samples	Chemical Structure	T_g (°C)	T_m (°C)	ΔH (J/g)
LiTPSN	$CF_3CF_2OCF_2CF_2SO_3Li$	123	157	10
Salt 3n1	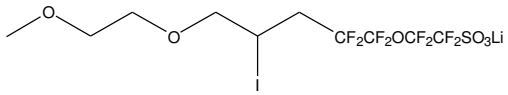	30	126	28
Salt 4n1	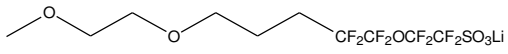	8	130	58
Salt 4n3	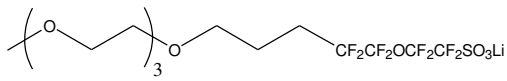	-8	102	7
LiTPSM	Li^+ $CF_3CF_2OCF_2CF_2SO_2\overset{-}{N}SO_2CF_3$	not detected	192	50
Salt 5n3	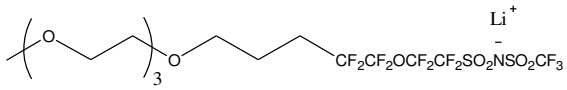	-33	-	-

Concerning the sulfonated salts, the bonding of a mPEG to the perfluorulfonated anion leads to a significant decrease of T_g and T_m values. The presence of bulky and polar iodine in the salt structure seems to increase the T_g (**salt 3n1**) as compare to the **salt 4n1** where the I was replaced by H (**salt 4n1**) while the melting point and the ΔH are higher for the last salt. The presence of I might increase the viscosity of the salt and prevent its fully organization. However, the increase of n from 1 to 3 **(salt 4n3**) leads to an important decreases of both temperature, T_g and T_m as well as ΔH. The same phenomena were observed in the case of **salt 2** (see chapter 2).

As regarding the salts based on sulfonimide the bonding of mPEG n=3 to the anion leads to a salt completely amorphous. This is contrarily to the pristine salts, where the salt LiTPSM has higher T_m as compared to LiTPSN. The higher Tm for the first (LiTPSM) can be explaining

by a higher dissociation degree of the salt and thus stronger interaction between the chains forming the crystals. For the **salt 5n3** we suppose adding of mPEG, create disorder due to the interaction of Li^+ with the O from mPEG, and this disorder should be most important as compare to the **salt 4n3** due to the anion asymmetry.

As compared with the **salt 2n3** (chapter 2) the thermal characteristic and especially the T_g are much lower for aliphatic perfluorsulfonated salts, (**salt 4n1** as compared to **salt 2n1**, **salt 4n3** as compared to **salt 2n3**)

b. Thermal stability

Figure 3.21 shows TGA curves of aliphatic lithium salts i.e. **salt 3n1**, **salt 4n3** and **salt 5n3**, and for comparison the **salt 2n3**(aromatic salt) **and LiTPSM, LiTPSM** were added in the figure. Also in order to evaluate if the presence of mPEG in the salt structure decrease the thermal stability as compared to the salt, we added mPEG n=16 (we choose n=16 to avoid the evaporation before degradation). The temperature of TGA measurements were carried out from 25°C to 500°C under argon.

The onset of weight loss starts at 232 °C up to 292 °C and leads to 35 and 70 wt% weight losses for **salt 3n1** and **salt 4n3** respectively.

The presence of I in the structure of the salt (**salt 3n1**) decreases drastically the thermal stability as compared to **salt 4** (when I was replaced by H). However, the onset of weight loss is slightly higher than that of aromatic salt (i.e. **salt 2n3**). Regarding the impact of the mPEG bonded to the anion on the stability of the salt, we can see, by comparing the TGA curves of LiTPSN and LiTPSM with those of **salt 4n3** and **salt 5n3**, the onsets of weight loss are lower in the case of the last salts but higher to the onset of mPEG degradation. Hence we can conclude the weight losses of the **salt 4n1**, **4n3** and **5n3** start with mPEG degradation. The formed fragments have to interact with the Li^+ therefore the weight loss onset is higher than that of mPEG n16.

However, the stability of all the salts are enough good for the application lithium batteries.

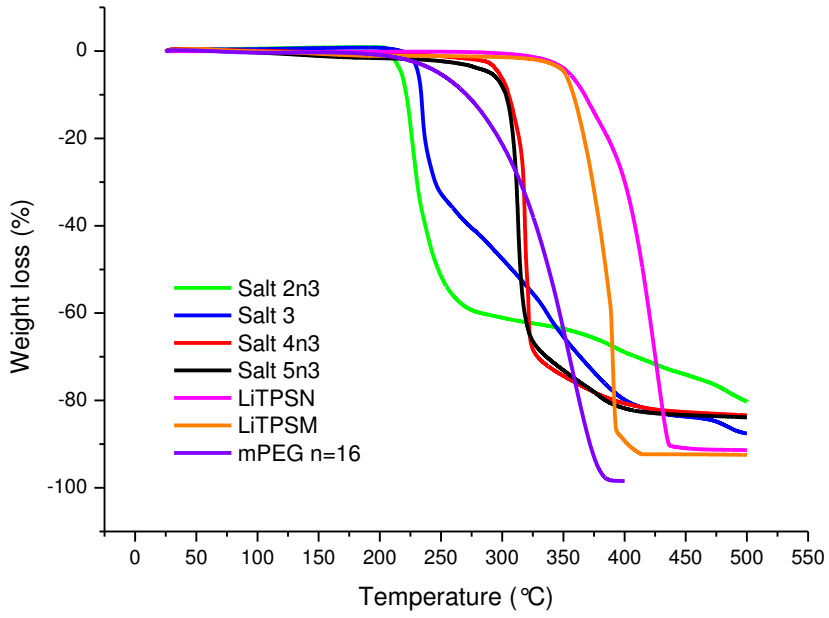

Figure 3.21. Thermogravimetric analysis of aromatic (**salt 2n3**) and aliphatic (**salt 3**, **salt 4n3** and **salt 5n3**) lithium salts.

III.3.4.2. Intrinsic conductivity of salts

The intrinsic conductivities were measured for the **salt 4n3** and the **salt 5n3** and are represented in the Figure 3.22 as a function of temperature (1000/T). At 30 °C the **salt 4n3** exhibits a conductivity of 5.08×10^{-6} S/cm and 4.10×10^{-4} S/cm at 110°C. This value is comparable with that of **salt 2n16**, higher than that of **salt 2n7** (see chapter 2) and much higher than that of the oligoether sulfate salt (POEMSLi164: CH_3-$(OCH_2CH_2)_3$-OSO_3Li) which has been reported (10^{-7} S/cm) by C. Chauvin [16]. The replacement of Oxydophenylsulfanyl)-1,1,2,2-tetrafluoroethane (in the case of **salt 2**) with more flexible moiety i.e. 1,1,2,2,-tetrafluoro-2-(1,1,2,2,-tetrafluoro-2-ethoxy)ethane might to decrease significantly the viscosity and thus increase the conductivities.

As comparing the **salts 5n3** and **salt 4n3** with same n of mPEG, the salt based on sulfonylimide (**salt 5n3**) provides higher conductivity than that based on sulfonate one (**salt 4n3**) with 6.11×10^{-4} S/cm at 110°C and 4.05×10^{-5} S/cm at 30 °C. This result can be explained by the lower viscosity of the salts, as shown by the DSC (lower T_g) but also by the dissociation degree of salt based n on sulfonimide might be higher.

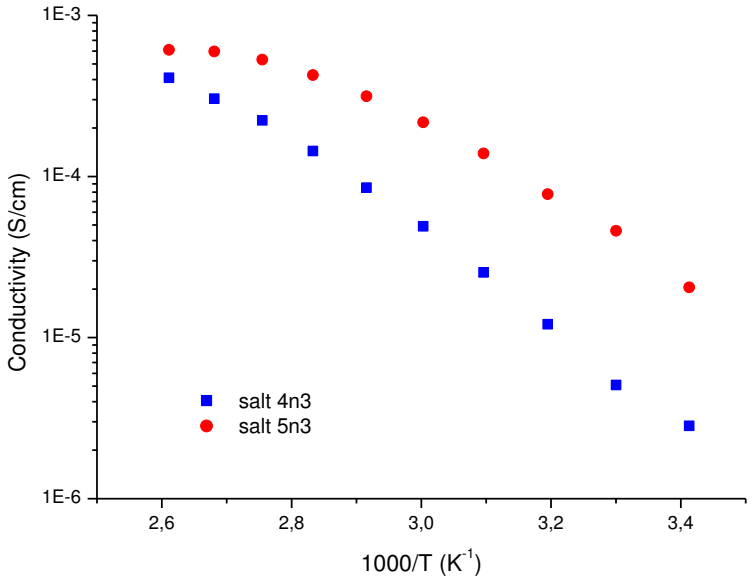

Figure 3.22. Conductivity of aliphatic lithium salts.

III.3.4.3. Diffusion coefficient

The self-diffusion coefficient was measured by multinuclear Pulsed Field Gradient NMR (^{7}Li, ^{19}F and ^{1}H) and all results are gathered in Table 3.3. The diffusion coefficients of anion ($D^{19}F$ – D^{-} fluorine) are lower than those of cation, Li^{+}, ($D^{7}Li$, D^{+}) for both **salt 4n3** and **salt 5n3**. C. Chauvin [17] reported opposite results on aliphatic sulfate oligoether lithium salt (CH_3-$(OCH_2CH_2)_3$-OSO_3Li), where the D^{-} is higher. However, we obtained similar results reported in the chapter 2 on the **salt 2n7** and **salt 2n16**. The values of both, i.e. self-diffusion coefficient of anion, D^{-} and Li^{+}, D^{+} of the **salt 5n3** are higher than those of the **salt 4n3**. The diffusion coefficient is directly related to the viscosity of the salt and the bulkiness of species that are diffusing. Taking into account the size of anion is even higher in the case of **salt 5n3** we can suppose the viscosity of this salt is lower

The dissociation degree of **salt 4n3** and **salt 5n3** are calculated by the ratio of the conductivity obtained from the experiment and the conductivity calculated by applying the Nernst-Einstein equation. As expected result lower dissociation degree is obtained for the **salt 4n3** as compared with the **salt 5n3.**

Table 3.3 Comparison of diffusion coefficients determined by PFG-NMR at 383K

	Salt 4n3	**Salt 5n3**
$D^{19}F$ (cm^2s^{-1})	0.29×10^{-7} ($\pm0.02\times10^{-7}$)	0.43×10^{-7}
$D^{7}Li$ (cm^2s^{-1})	0.39×10^{-7} ($\pm0.10\times10^{-7}$)	0.7×10^{-7}
Density (g/cm^3)	1.61	1.65
Concentration (mol/cm^3)	3.17×10^{-3}	2.58×10^{-3}
σ_{Nernst} (Scm^{-1})	6.30×10^{-4}	8.54×10^{-4}
σ_{exp} (Scm^{-1})	4.10×10^{-4}	6.11×10^{-4}
% dissociation	65	72

III.3.4.4. Transference numbers

The cationic transference numbers, T^+, are calculated with the self-diffusion coefficient of anion ($D^- = D^{19}F$) and cation ($D^+ = D^{7}Li$) determinate by PFG-NMR by using the next relationship: $T^+ = \frac{D^+}{D^+ + D^-}$.

The cationic conductivities are also calculated from $\sigma^+ = T^+\sigma$.

It is observed that the cationic transference number of **salt 5n3** is higher than that of **salt 4n3**. This behavior is in contrast to the salt incorporated in POE membranes where the sulfonylimide/POE complex has much lower T^+ than the sulfonate one [4]. The lower T^+ is generally due to both the strong interaction of Li^+ with the O from OE and the poor interactions between the anion and the POE host polymer. Here, Li^+ diffuse thanks to the segmental motion of mPEG. The lithium is solvated by 5 O, in the case of the both salts the number of O is lower (n=3 from OE + 1 from methoxy), that means at least 2 mPEG are involved in the solvatation of a Li^+. The higher T^+ for the **salt 5n3** could be explaining by the higher dissociation degree of the **salt 5n3**.

The cationic conductivities calculated reach 2.34×10^{-4} S/cm for **salt 4n3**, lower than **salt 5n3** providing 3.79×10^{-4} S/cm.

Table 3.4 Comparison of intrinsic cationic transference numbers and cationic conductivities between sulfonate and sulfonylimide mPEG lithium salts (**salt 4n3** and **salt 5n3)** at 383K

Salt	O/Li	σ (S/cm)	T^+	σ^+ (S/cm)
Salt 4n3	3	4.10×10^{-4}	0.57	2.34×10^{-4}
Salt 5n3	3	6.11×10^{-4}	0.62	3.79×10^{-4}

III.3.4.5. Electrochemical stability

The anodic oxidation potentials were measured by cyclic voltammetry. Platinum wires (diameter = 0.2 mm) were used for working and counter electrodes using $Ag/AgNO_3$ as reference electrode. Tetraethyl ammonium tetrafluoroborate in acetonitrile was used as the supporting electrolyte. Table 3.5 gathered the values of onset oxidation peak potentials obtained by cyclic voltamperometry with a rate of 10 mV/s.

The **salt 3** shows the lower stability in oxidation. The oxidation wall of the **salt 3** starts at 4.5 V and is lower than those of salt LiTPSN (4.9 V). The replacement of I by H induce an increase of the oxidation potential with 0.3V. Despite the presence of OE units that are known to present oxidation stability close to 3.9 V versus Li/Li^+, the oxidation stability of salts seems to be higher than that of POE. Similar results were obtained for the **salt 2** (chapter 2). These results are a good surprise and are in line with theoretical calculations performed by Chauvin et al.[16]

The chain lengths of the mPEG perform any impact on the oxidation potential. The oxidation potential of the **salt 5n3** (4.7 V) is slightly lower than that of **salt 4n3**.

However, all synthetized salts seem to be enough stable for an utilization in lithium polymer batteries.

Table 3.5 Oxidation potential of different salts in the solution of $TEABF_4$

Salt	Oxidation potential (V vs Li/Li^+)
Supporting electrolyte (CH_3CN + $TEABF_4$)	5.3
LiTPSN	4.9
Salt 3n1	4.5
Salt 4n1	4.8
Salt 4n3	4.8
LiTPSM	4.8
Salt 5n3	4.7

III.4. Elaboration and characterization of membrane based on POE host polymer doped with mPEG aliphatic lithium salt

Practically, lithium electrolytes are obtained by the incorporation of lithium salt in a host polymer (solid electrolyte for lithium polymer batteries) or by dissolving of a salt in a solvent (liquid electrolyte for lithium ion batteries). In this current work, similar to chapter 2 and first part of chapter 3 the salts are mixed with the linear POE or with polycondensat.

Characterization of membrane based on linear POE host polymer doped with aliphatic lithium salt

III.4.1.Thermal characterizations

The glass transition temperature (T_g), the melting temperature (T_m) and the fusion enthalpy (ΔH) of polymer electrolytes, based on aliphatic perfluorosulfonate lithium salts modified by mPEG (**salt 3**, **salt 4** or **salt 5**) and linear POE (M_w = 300,000 g/mol), were measured by DSC. All data are gathered in Table 3.6.

To evaluate the impact of mPEG on the thermal behavior of polymer electrolytes based on salt mono-end caped with mPEG the thermal characteristics of POE/LiTPSN and POE/LiTPSM, O/Li =20 were added in the table.

The POE was blended with different amount of salt, expressed by the ration O/Li, where O represents the number of structural oxyethylene (OE) units for a Li salt. For the calculation of O/Li we take in account the OE from the anion and we use the next formula:

$$\frac{O}{Li} = \frac{m_{POE}}{m_{salt}}\frac{M}{44} + n \quad (1)$$

Where m_{POE} is the weight of POE; m_{salt} is the weight of the salt, M the molecular weight of the salt, n the number of OE structural unit in the salt, 44 represent the molecular weight of OE.

In the column O/Li, in brackets, we give also the O/Li taking in account only the OE from POE.

Two series of measurements were performed. First, all the samples were submitted to two heating scans, in the first scan the samples, that were conserved at least a month in the glove box, were heated from -100°C to 100°C and we measured the T_{g1}, T_{m1}, ΔH_{m1}, then it was cooled down at -100°C with a ramp of 20°C/min and further heated once again to 100°C (T_{g2}, T_{m2}, ΔH_{m2}). In the second series, the samples were quenched, therefore the pans containing the samples placed in a well closed recipient, were heated at 80°C on a heater outside of the DSC devise and after 10 min the pans were removed in the DSC at -100°C (T_{gq}, T_{mq}, ΔH_{mq}).

First, if we analyze the results obtained on the first series, we observed the T_g values are higher than that of pure POE and the values enhance with the salt concentration in the electrolyte. This is a general behavior for the electrolytes based on lithium salt/POE complexes, the T_g increase due to the interactions of Li cation with OE moieties. The interaction density (physical crosslinking) might to increase with salt concentration affecting the mobility of chains and thus increase the T_g.

By comparing the T_m and T_g for the first and the second heating scan, in the second lower values were obtained for all the complexes. These results are different from the electrolytes based on aromatic salts (chapter 3, T_g, T_m, ΔH very close in the first and second

scan) and suggest the aliphatic salt delate the crystallization phenomena. To explain this different behavior we can suppose a better interaction between the POE and the aliphatic salt.

Regarding the impact of the size of anion, for the same O/Li ration, we observe a slightly decrease of T_g values with increase of mPEG chain (**salt 4** n=1 and n=3), this results is similar to those reported on **salt 2** (chapter 2).

The crystallinity percentage is directly proportional to ΔH_m and is calculated according to eq. (2) where ΔH_0 is the melting enthalpy per unit weight of 100% crystalline POE, which is 205 J/g [18] and w is the weight fraction of POE in the sample.

$$X_c = \frac{\Delta H_m}{\Delta H_0 .w} \times 100 \quad (2)$$

We observed, similar to the **salt 2** an increase of Tm and of crystallinity with the n of PEG. Also the lower T_m and crystallinity were obtained for the **salt 5n3**.

The values of melting temperatures and the crystallinity degree increase slightly with the increase of O/Li for all the studied salts.

For the quenched sample the T_g, T_m are lower as compared with T_{g1} and T_{g2}, Tm_1 and T_{m2} and follow the same trend (decrease with the n, decrease of T_g with the O/Li, increase of T_m with the O/Li).

Table 3.6 Glass transition temperature (T_g) and melting temperature (T_m) of POE/**salt 3n1**, **salt 4n1**, **salt 4n3** and **salt 5n3** complexes

Samples	O/Li (O/Li-n)	Tg_1 (°C)	Tg_2 (°C)	$Tg_{(q)}$ (°C)	Tm^*_1 (°C)	Tm^*_2 (°C)	$Tm^*_{(q)}$ (°C)	ΔH_{1POE} (J/g)	ΔH_{2POE} (J/g)	$\Delta H_{POE(q)}$ (J/g)	% crystallinity ($1^{st}/2^{nd}$ /q)
POE	∞	-	-63	-62	70	69	58	126	127	105	61/62/51
POE/LiPSTN	20	-	-21	-51	68	63	56	135	101	100	66/49/49
POE/LiPSTM	20	-38	-37	-53	66	60	51	61	50	64	30/24/31
POE/ **Salt 3n1**	20(19)	-28	-46	-46	63	57	55	66	60	61	32/29/30
	30(29)	-27	-48	-51	65	60	55	76	69	97	37/33/34
	40(39)	-26	-49	-54	66	62	58	119	99	104	58/48/45
POE/ **Salt 4n1**	12(11)	-33	-34		50	52		103	64		50/31
	20(19)	-33	-35	-38	65	59	58	86	71	129	42/34/33
	30(29)	-44	-39	-45	68	61	61	124	90	133	60/44/45
POE/ **Salt 4n3**	16(13)	-25	-34	-49	62	47	57	98	66	106	48/32/52
	20(17)	-29	-38	-52	63	58	57	124	99	67	61/48/43
	30(27)	-29	-41	-54	65	60	61	156	121	120	76/59/58
POE/ **Salt 5n3**	20(17)	-30	-33		60	55		59	52		29/25
	30(27)	-32	-36	-56	60	57	55	74	65	125	36/32/30

Tm was taken at peak

The weight loss of different POE/salt complexes is presented in figure 3.23 as a function of temperature. It is observed in the thermogram the degradation of electrolytes based on **salt 3** takes place in many degradation steps (at least, 3 steps) for the total weight loss. The percentage weight loss is 80 %, and it start at 260 °C. How already shown on study

of the salt degradation, the degradation temperature of the salt increase significantly when the I is replaced by H (**salt 4n1**, **salt 4n3**). The degradation temperature of the polymer electrolytes follows the same order as that reported on the salts. Indeed the weight loss starts at higher temperature when the salt is incorporated in the POE. Thus, the weight loss of POE/**salt 4n1** starts at 320 °C while POE/**salt 4n3** starts at 340 °C, the last close to the POE host polymer.

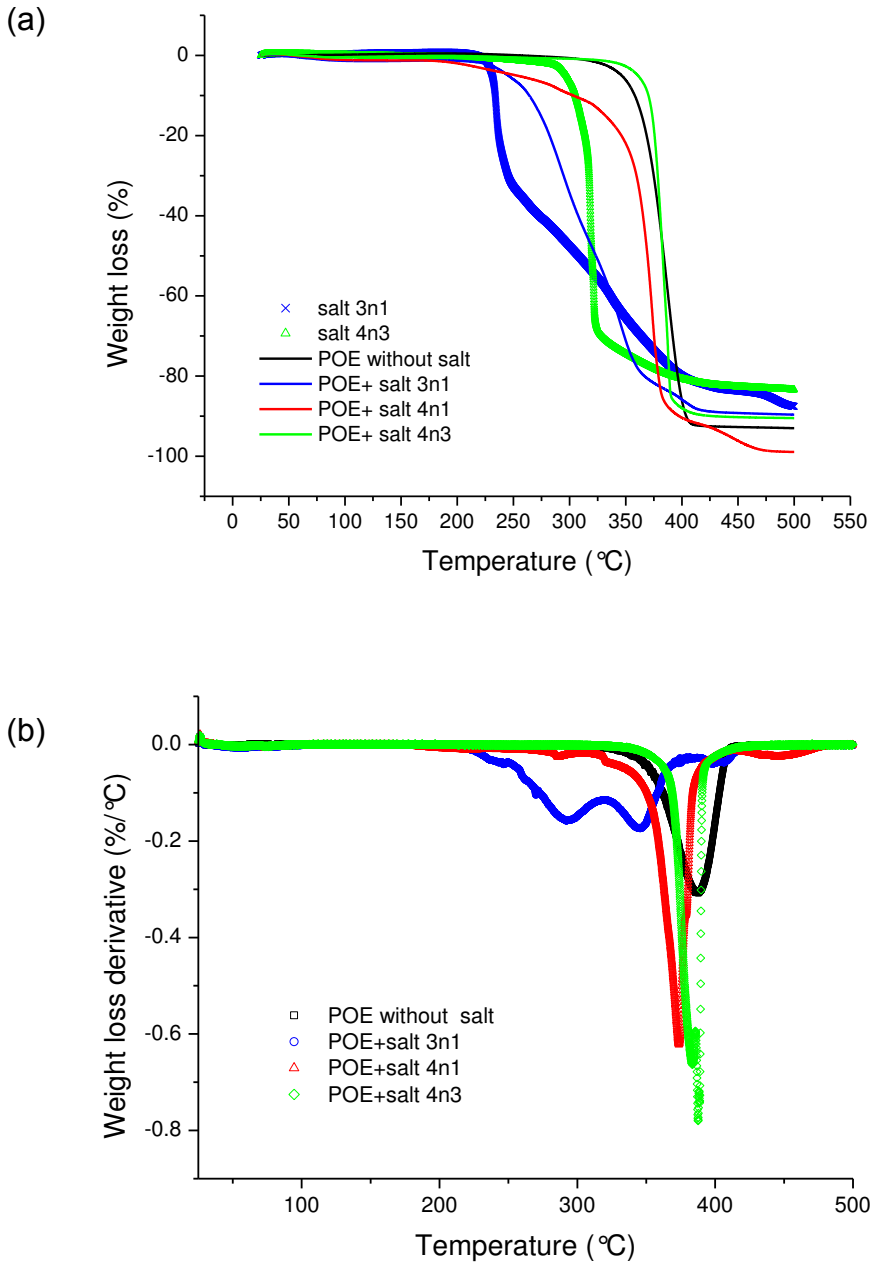

Figure 3.23. (a) Thermogravimetric curves of various POE/aliphatic salt membranes at O/Li =30, under argon with heating rate of 5 °C/min and (b) their first weight loss derivatives.

III.4.2.Mechanical properties

Figure 3.24 (a) shows the variation of storage modulus at 1 Hz as a function of temperature for POE, POE/**LiTPSN** and POE/**salt 4** (n=1 and n=3) for ratio O/Li= 20. The elastic storage modulus E' at -100°C was normalized at one constant value (approximately 3 MPa) with the aim of minimizing the effect from the difference of the thickness of each sample.

If we compare the curve of pure POE (Figure 3.24.a), POE/**salt LiTPSN,** POE/**salt 4n1** and **POE/salt 4n3** we observed (i) the T_α of POE is lower than that of the membranes based on salts, (ii) the T_α of electrolyte POE/ **LiTPSN** is the highest (iii) the T_α of electrolytes POE/ **salt 4** are lower than that of POE/LiTPSN and decrease slightly with the increase of n from mPEG (iv) the electrolytes based on **LiTPSN** melt at similar temperature as POE while the electrolytes based on **salts 4** salts melt at lower temperature (v) the storage modulus drop dramatically after the T_α in the case of electrolyte POE/**salt 4n1** and **4n3** while it the case of POE/LiTPSN is similar to POE. All these observation leads to the conclusion the bonding of a mPEG to the anion change significantly the interactions salt- host polymer (POE). The dramatic decrease of storage modulus after T_α can be explaining by a higher content of amorphous phase due to the contribution of the salt.

The results corroborate with those obtained by DSC in the first heating scan, where the T_g of POE<POE+**LiTPSN**< POE+**salt4n1**<POE+**salt 4n3** while T_m and ΔH are opposite (POE> POE+**LiTPSN** >POE+**salt4n1**>POE+**salt 4n3)**

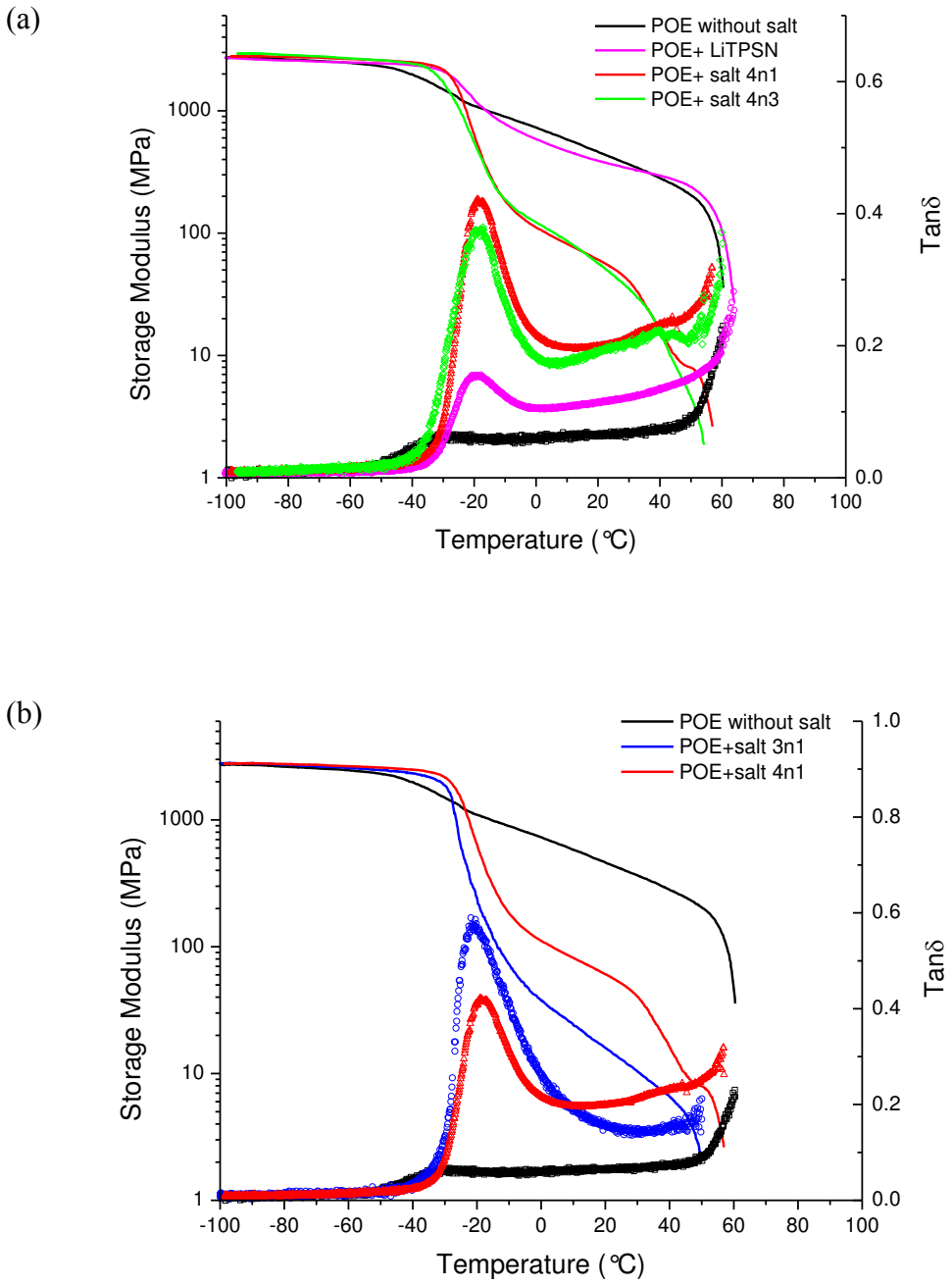

Figure 3.24. Storage modulus and tan δ in a function of temperature for (a) POE, POE+ LiTPSN, POE +**salt 4n1**, POE +**salt4n3** and (b) POE+**salt 3n1** and POE+**salt 4n1** at O/Li=20.

The same behavior is observed for the **salt 3n1**, however the storage modulus and the T_α are slightly lower as compared to those of **salt 4n1**.

As regards the impact of the bonding of mPEG on the **salt 5n3** (comparison between the POE +LiTPSM and POE+**salt 5n3**) the effect is minor as compare with that obtained on sulfonate.

Moreover, the Tα and storage modulus increase when mPEG n=3 is bonded to the salt, in this is opposite as compared to the behavior of salt based on aliphatic sulfonate (**salt 3** and **salt 4**). It should be mentioned the LiTPSM impact much more the thermo-mechanical properties of POE as compare to the LiTPSN how it can be seen from the figure 3.25.

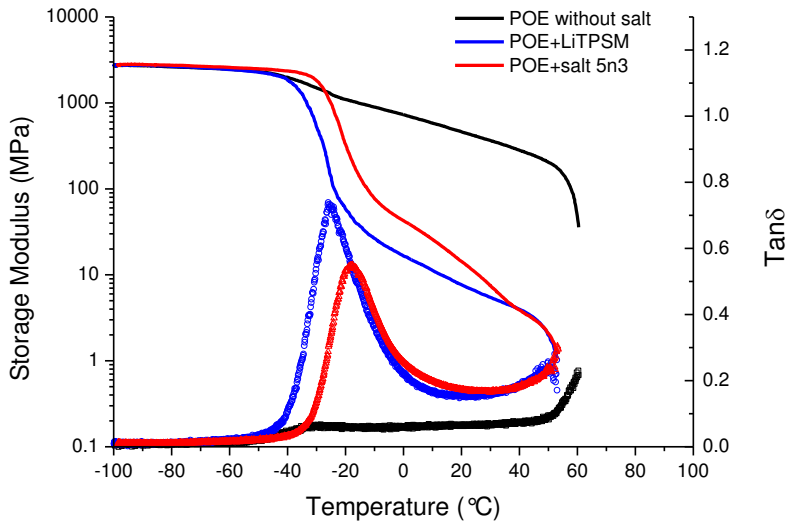

Figure 3.25. Storage modulus and tan δ in a function of temperature for (a) POE, POE+ LiTPSM, POE +**salt 5n3** at O/Li= 20.

Now, if we compare the POE electrolyte based on the **salt 2n3** (aromatic salt chapter 2) with POE electrolyte doped with **salt 4n3** (same anion and same mPEG lengths) (figure 3.26) we can conclude the moiety between the anion and the mPEG influence significantly the T_α and the T_m, i.e. lower values were obtained for the aliphatic salts. This behavior point out that the presence of aromatic ring in the salt induce both (i) a higher stiffness of the complex (POE/salt) and (ii) lower impact on crystallization degree of the POE host polymer.

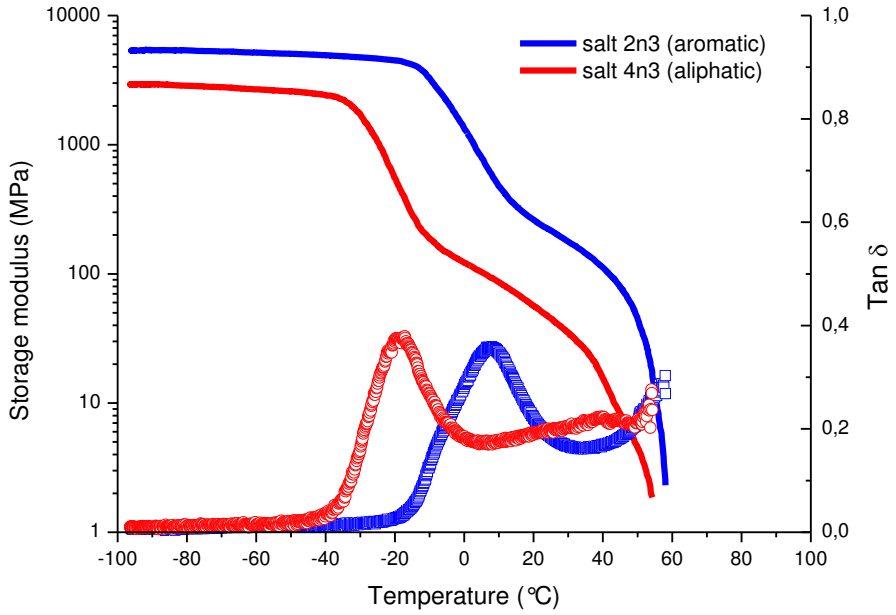

Figure 3.26. Comparison of mechanical properties between aromatic **(salt 2n3)** and aliphatic **(salt 4n3)** lithium salts at the concentration (O/Li) =20.

III.4.3.Conductivity

The conductivity as function of 1000/T of different polymer electrolytes based on aliphatic Li salts modified with mPEG are presented in the Figure 3.27 (a,b,c,d). To evidence the impact of the mPEG the Arrhenius plots of salt LiTPSN and LiTPSM are added. The figure 3.27 (a) pointed out that both mPEG modified salts (**salt 3n1**, and **salt 4n1**) show greater conductivities for both concentration (O/Li =20 and O/Li 30) as compared to the electrolyte based on POE+LiTPSN. The best conductivity value is 3.3×10^{-4} S/cm at 70 °C for POE/**salt 4n1** electrolyte at O/Li= 20 which is slightly higher than that of POE/**salt 3n1** electrolyte. For both salts (**salt 3n1** and **salt 4n1**) the conductivities of electrolytes are slightly higher for O/Li =20 as compared to those of O/Li=30.

Similar to mPEG modified sulfonic salt, the bonding of mPEG to LiTPSM anion improve their conductivities, thus the polymer electrolytes based on **salt 5n3** give higher conductivities than those of electrolytes based on LiTPSM (Figure 3.27 b). Concerning the increase of n of mPEG, greater conductivity was obtained in the case of **salt 4** when n was increased from 1 to 3 (figure 3.27 c), especially after the recrystallization temperature. This

behavior is in agreement with the DSC results where a lower T_g was obtained for the polymer electrolytes based on **salt 4n3** and is similar to that reported on the **salt 2** on chapter 2.

Now if we compare the electrolytes of mPEG modified sulfonimide (**salt 5**) and sulfonate (**salt 3**, **salt 4**) the first exhibits higher conductivities. However, the gap between the conductivities at different temperatures are much lower than observed between the electrolytes based on salts LiTPSN and LiTPSM (figure 3.27 d).

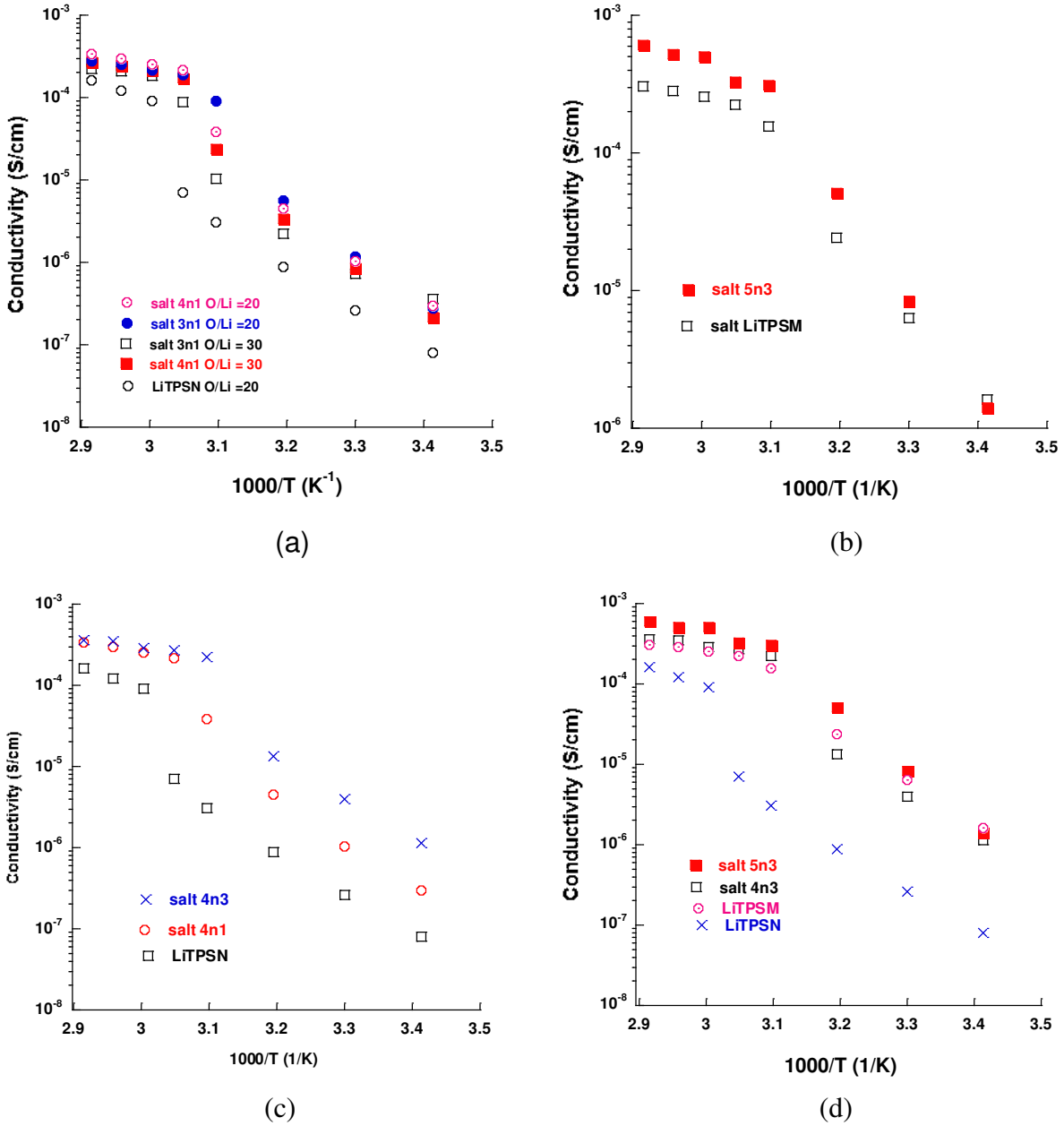

Figure 3.27. Comparison of conductivity of polymer electrolyte: (a) POE/ **salt 3n1** and POE/ **salt 4n1**, O/Li = 20 and 30 and POE/LiTPSN O/Li =20; (b)) POE/ **salt 5n3** and POE/**LiTPSM** at the concentration, O/Li = 20 (c) POE/ **salt 4n3,** POE/ **salt 4n1** and POE/**LiTPSN,** O/Li = 20 (d)) POE/ **salt 5n3,** POE/ **salt 4n3, POE/LiTPSM** and POE/**LiTPSN,** O/Li = 20.

In figure 3.28 the Arrhenius plots of two electrolytes, i.e. POE/**salt 2n3** and POE/**salt 4n3** are represented. Both salts contain the same mPEG (n =3) bonded to perfluorosulfonate anion. The electrolytes of **salt 4n3** exhibit at least 2 times higher conductivities than polymer electrolyte of **salt 2n3**. These results point out the presence of aromatic ring in the structure of the salt might increase the viscosity of the polymer electrolyte and thus decrease the conductivities. This hypothesis is sustained by the results on the DSC and DMA analysis.

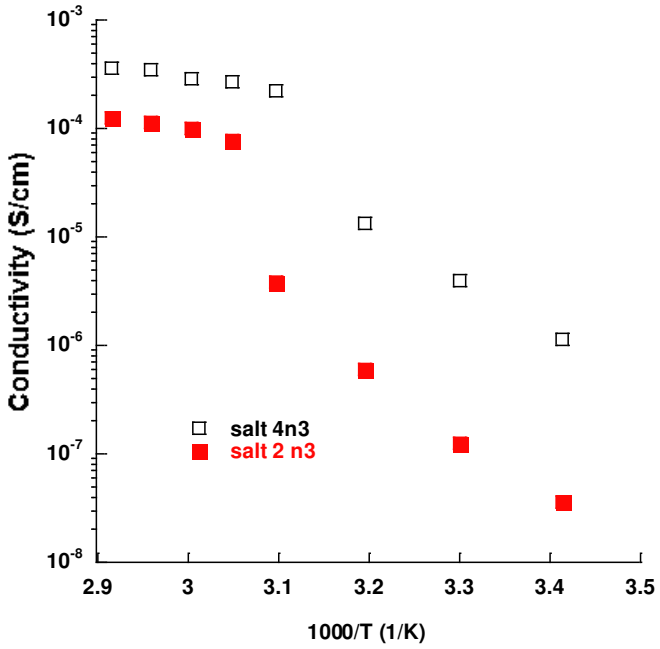

Figure 3.28. Comparison of conductivity of POE/**salt 2n3** and POE/**salt 4n3** at the concentration, O/Li = 20.

III.4.4.Diffusion coefficient

The self-diffusion coefficients of anion D^- ($D^{19}F$) and of Li^+, D^+ (D^7Li) in POE polymer electrolyte determined by PFG-NMR are gathered in the table 3.7. To evaluate the impact of mPEG on the diffusion coefficients the salt LiTPSM and LiTPSN were added in table 3.7.

It can be seen the diffusion coefficients of anions are higher than those of Li^+ for all the salts. However the values of D^- decrease when the anion LiTPSM or LiTPSN is modified with mPEG. The values decrease with the increase of anion size, thus the lowest value in the case of perfluorinated salt are done by **salt 4n3** and **salt 3n1**. As regarding the self-diffusion coefficient of the lithium, excepting the **salt 3n1**, higher values were obtained when the anion

is modified with mPEG. The lower diffusion of anion in the case of electrolyte based on **salt 3n1** is probably due to the interaction of Li with the I from the anion. It is surprising to observe the D^+ values of **salt 4n1**, **4n3** and **5n3** are very close. This result point out the D^+ is independent on the length and nature of anions discussed here (sulfonate or sulfonimide). We mention also the self-diffusion coefficient of both anion and cation of aliphatic salt polymer electrolytes are higher as compared to those of aromatic salt (**salt 2**, chapter 2).

Table 3.7 Comparison of diffusion coefficients of different polymer electrolytes determined by PFG-NMR at 110°C

POE/Salt	**LiTPSM**	**LiTPSN**	**Salt 3n1**	**Salt 4n1**	**Salt 4n3**	**Salt 5n3**
O/Li	30	30	30	30	30	30
D $^{19}F(cm^2\ s^{-1})$	3.9×10^{-7}	2.49×10^{-7}	1.98×10^{-7}	2.40×10^{-7}	2.00×10^{-7}	3.00×10^{-7}
D $^{7}Li(cm^2\ s^{-1})$	1.00×10^{-7}	1.4×10^{-7}	1.27×10^{-7}	1.7×10^{-7}	1.8×10^{-7}	1.7×10^{-7}
σ_{Nernst} (S cm^{-1})	1×10^{-3}	8.9×10^{-4}	7×10^{-4}	8.9×10^{-4}	7.9×10^{-4}	9.7×10^{-4}
σ_{exp} (S cm^{-1})	3.2×10^{-4}	1.9×10^{-4}	4.7×10^{-4}	4.6×10^{-4}	4.7×10^{-4}	6.5×10^{-4}
%dissociation	30	22	67	51	59	66

By applying the Nernst–Einstein equation, starting from the self-diffusion coefficient we can calculate the conductivity. The densities of different salts were obtained by applying the same equation (equation 5 from chapter 2).

$$\rho_{salt} = \frac{M_{PEG}}{M_{PEG} + M_A} * \rho_{PEG} + \frac{M_A}{M_{PEG} + M_A} * \rho_{LiPST} \quad (5)$$

where M_{PEG} et ρ_{PEG} the molecular weight and density of mPEG used in the synthesis of **salt**, M_A is the molecular weight of anion (LiTPSN or LiTPSM) et ρ_A is the density of LiTPSN or LiTPSM measured with a pycnometer (1.80 and 1.83 g/cm^3 respectively). The values of density of different salts are gathered in Table 3.8 and the calculated values of conductivity of **salt 4n3** and **5n3** are presented in Table 3.7.

	Density (g/cm^3)	Concentration (mol/cm^3)
Salt 3 n1	**1.86**	**3.40×10^{-3}**
Salt 4 n1	**1.56**	**3.72×10^{-3}**
Salt 4 n3	**1.61**	**3.17×10^{-3}**
Salt 5 n3	**1.65**	**2.58×10^{-3}**

Table 3.8 Density and molar concentration of **aliphatic salt**

How we already mentioned the Nernst–Einstein equation is valid for the infinitely dilute state, in our case we use it only to compare the values obtained on different membranes. To measure the conductivities at 110°C (in order to compare the experimental conductivity with that obtained by Nernst–Einstein equation) we have used the same cell that was used for the pure salts (**salt 4n3** and **salt 5n3**), i.e. a dip-type glass cell with two platinum electrodes at a constant distance while at this temperature utilization of the stainless disc electrodes in a Swagelok cell was not possible because the membranes are flowing and affect the thickness or even leads to short circuit. However there is a good concordance between the conductivities measured with the two types of cells.

From table 3.8 it can be observed the experimental conductivities, of complexes based on mPEG modified salts are higher than that of corresponding salts without mPEG. Moreover, the higher dissociation degree seems to be obtained for the salt based **salt 3n1** that contained iodine function and for the **salt 5n3** based on perfluorsulfoimide. As in chapter 2 a slightly higher dissociation degree of the salt based on longer mPEG is observed. Also the values obtained for **salt 4n3** is higher than that obtained for **salt 2n3**.

III.4.5.Cationic transference number and cationic conductivity

One of the factors affecting the performances of lithium salt is the transference number.

In this chapter the T^+ values were determined employing both, pulsed NMR spectroscopy and electrochemical impedance spectroscopy methods.

The T^+ analyzed by NMR is obtained from diffusion coefficients of anion and cation, even though there is inconvenient; cannot discriminate between the dissociated species and ion pairs. The intrinsic cationic transference numbers were determined here starting from diffusion coefficients using the next equation (3), where D^+ is D^7Li and D^- is $D^{19}F$.

$$T^+ = \frac{D^+}{D^+ + D^-} \quad (3)$$

The cationic conductivities are calculated with the equation: $\sigma^+ = T^+\sigma$ where σ is experimental conductivity. (Table 3.9). The electrochemical measurements are based on the method developed by Sorensen et Jacobsen [19], the method was described in the chapter 2.

Table 3.9 Transference number (T^+), conductivity (σ) and cationic conductivity (σT^+) for **salt 3n1**, **salt 4n1**, **salt 4n3** and **salt 5n3** in POE matrix with two different investigating methods at 110°C

Complex	O/Li	σ (S/cm)	PFG-NMR		EIS	
			T+	σ^+ (S/cm)	T^+	σ^+ (S/cm)
POE/LiTPSM	30	$3.6x10^{-4}$	0.20	$0.7x10^{-4}$	0.19	0.68×10^{-4}
POE/LiTPSN	30	1.9×10^{-4}	0.36	0.7×10^{-4}	0.46	0.87×10^{-4}
POE/**salt 3n1**	30	4.7×10^{-4}	0.39	1.8×10^{-4}	0.35	1.65×10^{-4}
POE/**salt 4n1**	30	4.6×10^{-4}	0.40	1.84×10^{-4}	-	-
POE/**salt 4n3**	30	4.7×10^{-4}	0.44	2.1×10^{-4}	0.60	2.06×10^{-4}
POE/**salt 5n3**	30	6.5×10^{-4}	0.35	2.3×10^{-4}	0.22	1.43×10^{-4}

In the case of sulfonate anion the T^+ increase with the increase of n of mPEG. However despite the higher molecular weight of anion of **salt 3n1**, the T^+ is lower than that of **salt 4n1**. Moreover, by electrochemical measurements the T^+ of the **salt 3n1** seems to be lower than that of the salt LiTPSN. The presence of iodine in the salt structure has slow down the migration of Li. We can note also the T^+ values of LiTPSN and **salt 4n3** are higher when they are calculated from electrochemical measurements as compared to NMR, while for the LiTPSM and **salt 5n3** the reverse is obtained.

The bonding of mPEG to the anion leads to polymer electrolytes with better cationic conductivities and it seems the values are close or even higher than that obtained with POE and TFSI (1.74×10^{-4} S/cm).

III.5. Membrane elaboration based on NPC host polymer doped with aliphatic lithium salt

The cross-linked films (NPC) were obtained by the UV irradiation of the casted films. In this part, we selected to study only the **salt 4n3** and **5n3**. Thus the NPC membranes were performed by the irradiation of a film (30 s and 1 min) obtained after the evaporation of acetonitrile (in the glove box) from the mixture of LPC, **salt 4n3** or **5n3** and initiator (IRGACURE® 2959, CIBA).

The membranes were characterized by various methods to study and understand their physical, chemical, mechanical and electrochemical behavior (discussed in the following section).

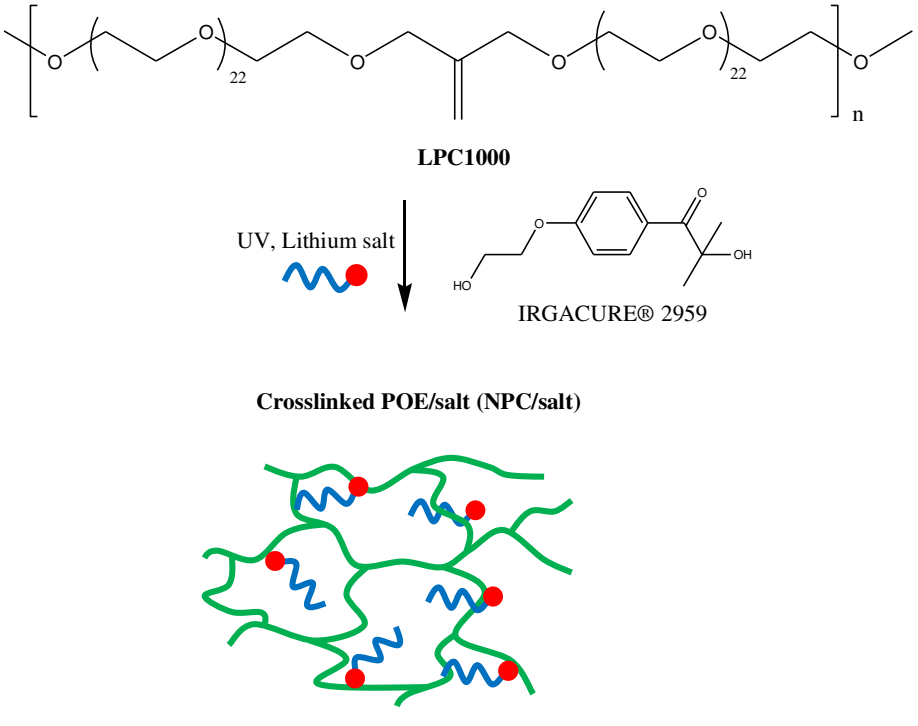

Figure 3.29. Schematic draw of Crosslinked POE (NPC).

III.5.1.Thermal characterizations

Table 3.10 summarizes the T_g, the T_m and the ΔH obtained by DSC measurements for the host polymer NPC and its electrolytes. All the data presented in this table were measured during the first heating from -100 to 60 °C (T_{g1}, T_{m1}, ΔH_1) and the second heating after a 1st

heating up to 60°C followed by a quenching (cooling ramp 50°C/min) (T_{g2}, T_{m2}, ΔH_2). The thermograms showed a crystallization peak before the fusion of crystalline phase. The samples still exhibited the semi-crystalline behavior but the melting temperature decreased as compared to POE and to the 1st heating.

For NPC+ salt complexes, at the same salt concentration and 30 s irradiation time we observed lower T_g, T_m and ΔH for the electrolytes based on **salt 5n3** for the both heating cycles. The T_g and Tm values of electrolytes are higher respectively lower than the pure NPC.

The polymer electrolytes irradiated more time, i.e. 1 min show lower T_g and T_m as compared with those irradiated 30 s. The longer irradiation time should enhance the cross-linking density that usually induces a T_g increase. In our case, obtaining T_g with lower values can be explained by the significant crystallinity decrease, which counterbalances the stiffening produced by higher crosslinking density. Indeed the formation of the cross-linking bridges creates disorder and prevents the crystallization of the POE segments of NPC.

The evolution of the T_g with the concentration doesn't follow the same trend as the electrolytes based on POE, i.e. increase of T_g with the decrease of O/Li. This can be explaining by the fact the crosslinking density might be affected by the salt concentration.

Table 3.10 (a) Glass transition temperature (T_g) melting temperature (T_m) and fusion enthalpy (ΔH) of NPC/**salt 4n3** and **salt 5n3** complexes in the cross-linking times 30s

	O/Li (O/Li –n)	Tg_1 (°C)	Tg_2 (°C)	Tm_1 (°C)	Tm_2 (°C)	ΔH_{1NPC} (J/g)	ΔH_{2NPC} (J/g)
NPC	∞	-52	-64	44	38	58	38
NPC/**salt 4n3**	20(17)	-43	-55	39	32	35	28
	30(27)	-44	-53	40	32	38	28
	40(37)	-43	-63	39	30	52	44
NPC/**salt 5n3**	20(17)	-49	-63	29	23	0	16
	30(27)	-48	-63	39	32	35	27
	40(37)	-49	-62	40	33	41	33

Table 3.10 (b) Glass transition temperature (T_g) melting temperature (T_m) and fusion enthalpy (ΔH) of NPC/**salt 4n3** and **salt 5n3** complexes in the cross-linking times 1minute

	O/Li (O/Li-n)	Tg_1 (°C)	Tg_2 (quenching) (°C)	Tm_1 (°C)	Tm_2 (°C)	ΔH_{1NPC} (J/g)	ΔH_{2NPC} (J/g)
NPC	∞	-51	-64	32	21	52	33
NPC/**salt 4n3**	20(17)	-46	-64	38	26	23	18
	30(27)	-45	-65	39	33	52	31
	40(37)	-45	-64	32	33	40.	39
NPC/**salt 5n3**	20(17)	-49	-61	34	20	2	11
	30(27)	-50	-63	39	32	14	12
	40(37)	-53	-62	38	32	19	11

O/Li-n: the O/Li taking in account only the OE from NPC.
ΔH_{1NPC} and ΔH_{2NPC} : fusion entralpy calculated by the consideration of NPC mass in the first and second cycles respectively

Figure 3.30 shows the TGA curves of **salt 4n3**, NPC+ **salt 2n3**, NPC+ **salt 5n3.** Similarly to the POE + salt electrolytes we observed an increase of T_d when the salt is incorporated in NPC matrix and its values are close to that of pure NPC matrix.

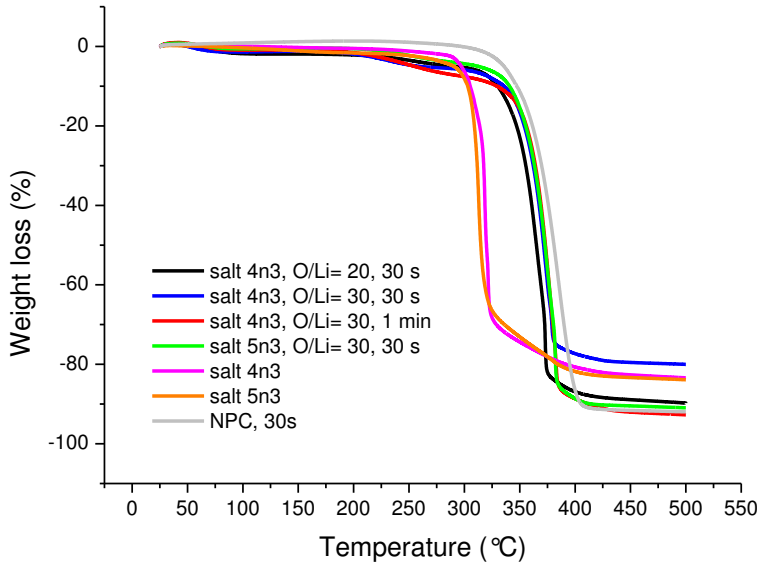

Figure 3.30. TGA curves for NPC/**salt 4n3** and NPC/**salt 5n3** complexes.

It was found the salt concentration and irradiation time do not affect the decomposition of the sample.

III.5.2.Mechanical properties

Figure 3.31 (a, b) shows the variation of storage modulus at 1 Hz as a function of temperature for different NPC electrolytes in order to put in evidence the impact on mPEG (a,b), of the irradiation time (c) and anion nature (d). By analyzing the figure 3.31 (a) we observed the mPEG bonded to the anion (LiTPSN) induces a decrease of storage modulus after the T_α, the value of T_α as well storage modulus on plateau (after the NPC melting). The impact on T_α and storage modulus before the melting point is similar to that of POE, however the impact of the mPEG bonded on the anion is less dramatic. However the Tm seems to be not affected by the presence of mPEG.

Concerning the impact of mPEG on the mechanical behavior of electrolytes based on LiTPSM (figure 3.31 b) anion the curves are very similar before the rubbery plateau. On the rubbery the storage modulus is almost 0.5 MPa for the NPC+LiTPSM electrolyte while for NPC +**salt 5n3** is more than 1 MPa. Hence for the polymer electrolytes based on **salt 5n3** we can suppose a higher crosslinking degree.

If we compare the irradiation time, the membranes irradiated 1 min show higher storage module after the NPC melting (on the rubbery plateau) and thus how expected a higher crosslinking degree (figure 3.31c).

(a)

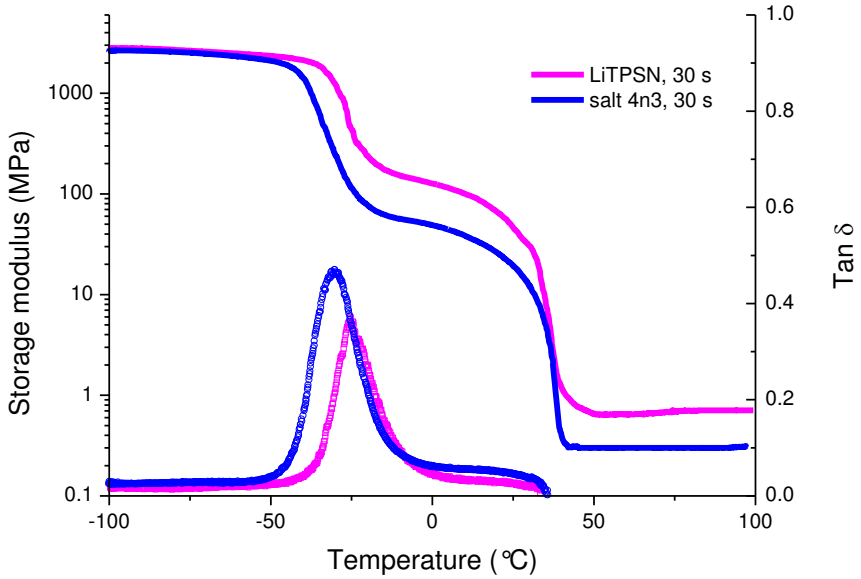

(b)

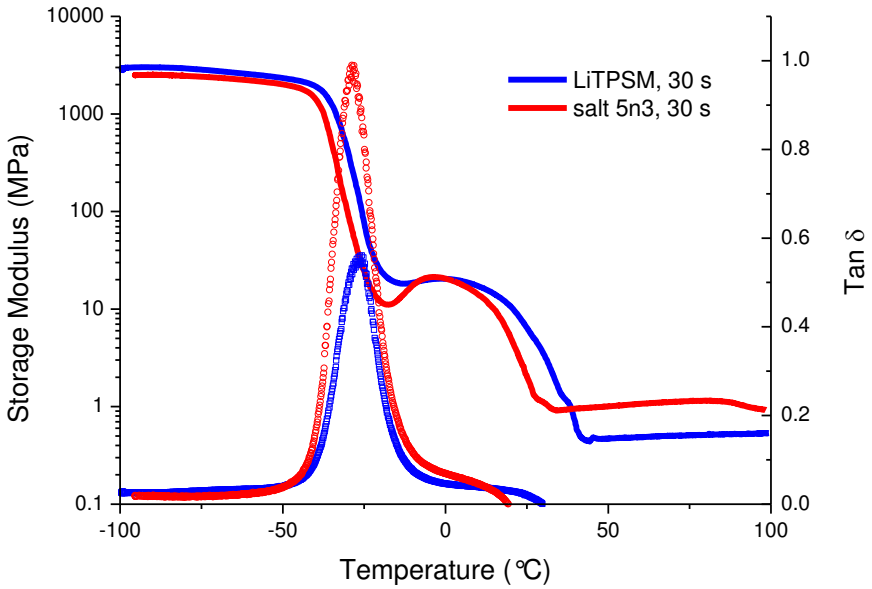

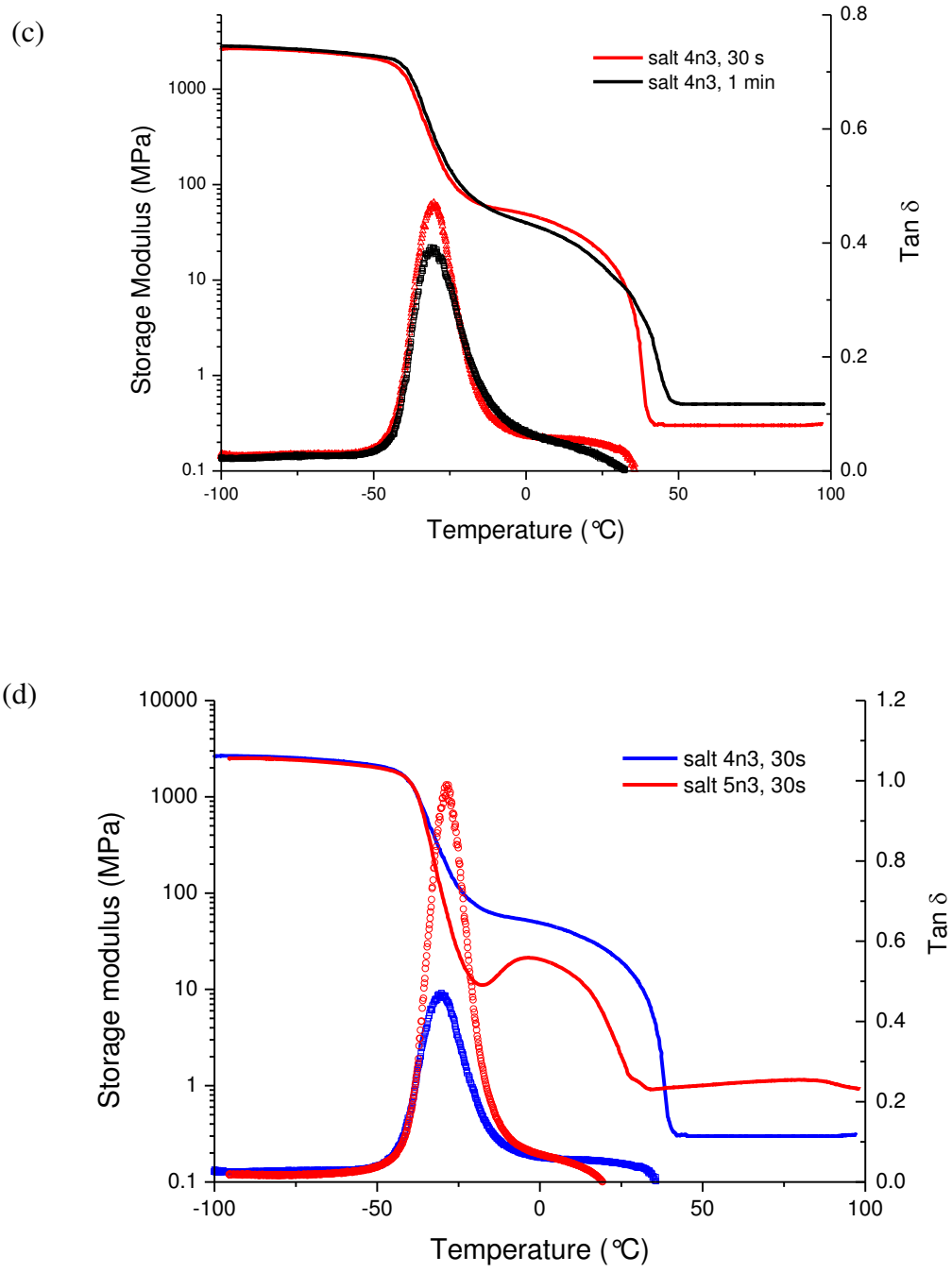

Figure 3.31. Storage modulus vs temperature for various polymer electrolytes based on NPC host polymer at O/Li= 30 in different crosslinking times.

(a) NPC/LiTPSN and NPC/**salt 4n3** for ratio O/Li= 30, irradiation time 30 s, (b) NPC/LiTPSM and NPC/**salt 5n3** for ratio O/Li= 30, irradiation time 30 s, (c) NPC/**salt 4** n3 and NPC/**salt 5n3** O/Li=30, irradiation time 30 s and 1 min (d) NPC/**salt 4n3** and NPC/**salt 5n3** O/Li=30, irradiation time 30s.

With regard to the difference of anion function, the T_α of NPC/**salt 5n3** is less than that of NPC/**salt 4n3** and this in agreement with the T_g obtained by DSC on the first heating. However after the T_α an increase of storage modulus is observed for the electrolyte NPC+**salt5n3,** due to the membrane recrystallization. The storage modulus on the rubbery plateau is higher for the electrolyte based on **salt 5n3** due probably to the higher crosslinking degree. This behavior (recrystallization + higher storage modulus on rubbery plateau) can explain why the T_{g2} measured by DSC is higher for the polymer electrolytes based on **salt 5n3** as compared to **salt 4n3** why for the polymer electrolytes irradiated 30 s the reverse was observed.

III.5.3.Conductivity

Host polymer

The effects of the host polymer (POE, NPC) on the conductivities of the electrolytes, based on **salt 4n3** and **salt 5n3**, are compared in figure 3.32. The conductivities of the electrolytes based on **salt 4n3 +** POE and **salt 5n3 + POE** are slightly higher than those of membranes based on NPC above the melting temperature, T_m, while, below Tm, the conductivities of NPC based electrolytes are roughly 10 times higher. The much lower crystallinity and T_m of NPC explain this conductivity gain at low temperatures.

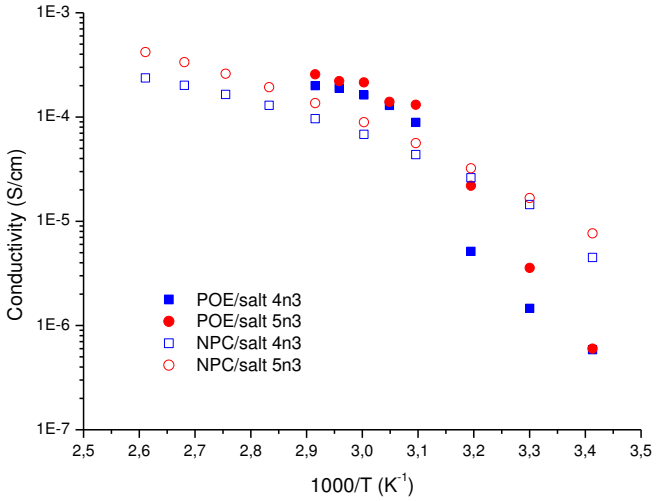

Figure 3.32. Comparison of conductivity between **salt 4n3** and **salt 5n3** in POE and NPC matrix.

Impact of mPEG

To evidence the impact of the mPEG on the conductivity the NPC electrolytes based on the LiTPSN, LiTPSM, **salt 4n3** and **salt 5n3** at O/Li=20 are drawn on the figure 3.33. The bonding the mPEG chain on LiTPSN and LiTPSM show two opposite effects. Thus in the case of anion LiTPSN the conductivity increase when mPEG is added to the anion. This result is similar to that obtained with POE host polymer electrolytes. Contrarily, the adding of mPEG to LiTPSM seems to decrease the conductivity and this result is opposite to that observed on this anion in POE host polymer electrolytes. One explanation on this opposite behavior could be the higher crosslinking degree of the film based on **salt 5n3** as compared to the film based LiTPSM and a decrease of POE chain mobility how prove the DMA analysis. The higher crosslinking degree can induce conductivity decreasing.

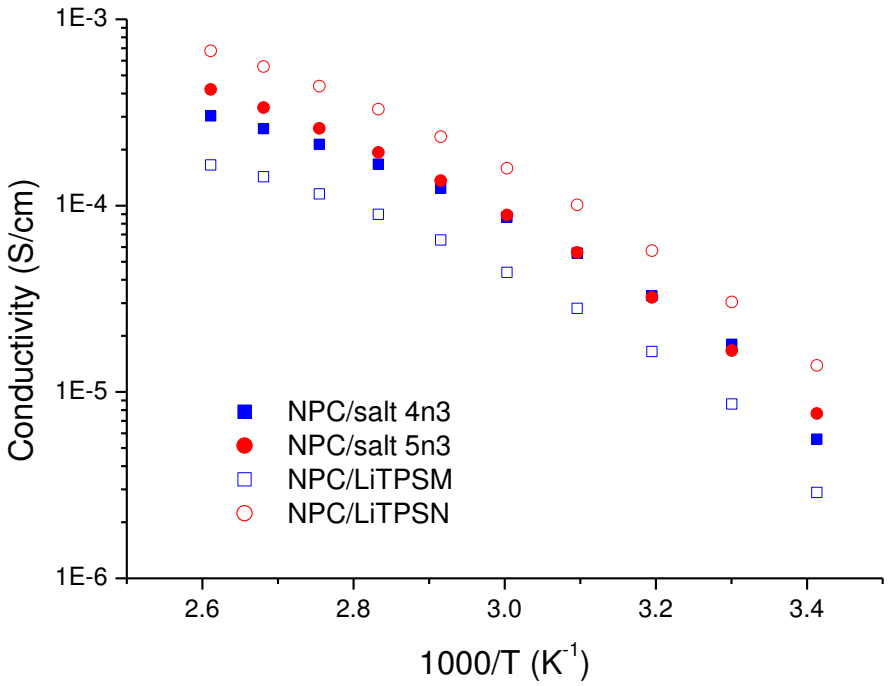

Figure 3.33. Conductivity of **salt 4n3** and **salt 5n3** compared with LiTPSN and LiTPSM in NPCmembranes (O/Li=20)

Impact of irradiation time

From the figure 3.34, which represents the influence of the irradiation time on the conductivity, a conductivity decrease can be observed upon an increase in irradiation time that can be ascribed to an increase of crosslink density.

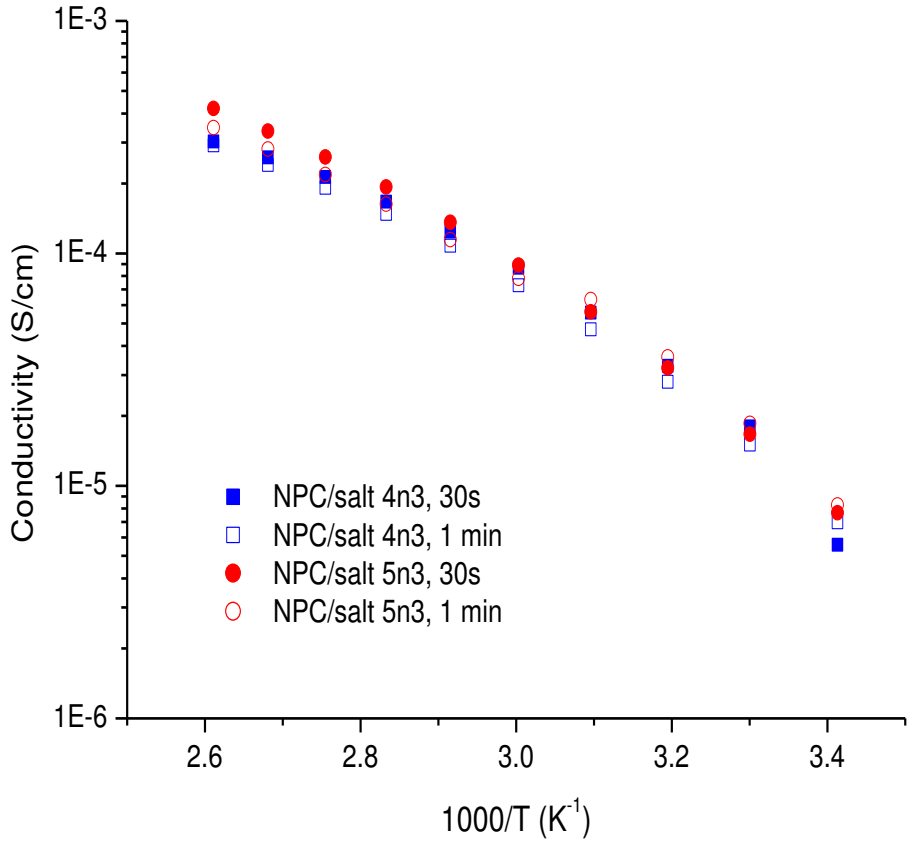

Figure 3.34. Conductivity of **salt 4n3** and **salt 5n3** in NPC with different crosslinking time 30 seconds and 1 minute, O/Li=20.

In figure 3.35 the Arrhenius plots of two electrolytes, i.e NPC/**salt 2n3** and NPC/**salt 4n3** are represented. Both salts contain the same mPEG (n =3) bonded to perfluorosulfonate anion. The electrolytes of **salt 4n3** exhibit at least 2 times higher conductivities than polymer electrolyte of **salt 2n3**. These results are similar with those obtained on polymer electrolytes based on these salts and POE and point out the presence of aromatic ring in the structure of

the salt might increase the viscosity of the polymer electrolyte and the salt dissociation degree and thus decrease the conductivities.

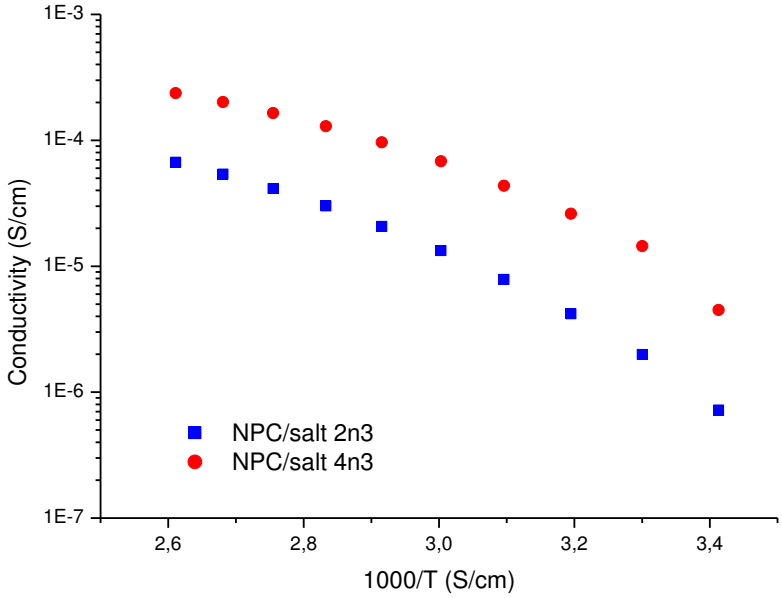

Figure 3.35. Comparison of conductivity between **salt 2n3** and **salt 4n3** in NPC matrix at O/Li=20.

III.6. Conclusion

The chapter 3 addresses both the new Li-conducting oligo(oxyethylene) salts and their blends with 2 types of host polymers i.e. linear (POE) and cross-linked (NPC) . The conclusions will therefore be shared into salts and polymer electrolytes.

Dealing with the salts

- Perfluoroalkanesulfonimide and perfluoroalkanesulfonate lithium salts endowed with a flexible ether moiety were synthesized.
- Perfluoroalkanesulfonimide and perfluoroalkanesulfonate modified with mPEG with 1 and 3 OE units were successfully obtained
- The addition of iodoperfluoroalkyl to an allylic bond was for the first time used for the synthesis of lithium salt

- The addition reactions and $Me_3Si)_3SiH$-mediated intermolecular perfluoroalkylation of alkenes are quantitative, however many problems were met during the purification steps.
- The aliphatic salt, **salt 4** and **salt 5** are thermally more stable than that of aromatic one.
- The salts are amorphous at room temperature at n (from mPEG) =3 while in the case of **salt 2** only from n>7.
- High oxidation potentials were obtained for all the salts

Dealing with the membranes

- The adding of mPEG on LiTPSN has a significant impact on mechanical properties, especially in POE polymer electrolytes.
- In the case of POE electrolytes, the increase of the mPEG lengths of the salt induce:
    - a T_g decrease,
    - a conductivity increase ,
    - a T^+ increase (determined by PFG NMR)
    - an increase of the salt dissociation
- As compared to the aromatic salt, the aliphatic salts:
    - Plasticize better the POE host polymer
    - give better conductivities in POE and NPC
    - have comparable or higher cationic transference number in POE
    - have higher dissociation degree in POE

- The polymer electrolytes based on mPEG sulfonimide aliphatic salts (**salt 5n3**) are the best in term of conductivity.
- The conductivity of NPC electrolytes is 10 times higher at low temperature than the POE ones while at high temperature they are 2 times lower.
- The irradiation time improve the mechanical properties; however the crosslinking degree depends on the salt structure and salt concentration.

III.7. References

[1] E. Paillard, F. Toulgoat, C. Iojoiu, F. Alloin, J. Guindet, M. Medebielle, et al., J. Fluor. Chem. 134 (2012) 72 – 76.
[2] E. Paillard, Thesis, Institut Polytechnique de Grenoble, 2008.
[3] H. Zhang, C. Liu, L. Zheng, F. Xu, W. Feng, H. Li, et al., Electrochimica Acta. 133 (2014) 529 – 538.
[4] F. Alloin, D. Benrabah, J.-Y. Sanchez, J. Power Sources. 68 (1997) 372 – 376.
[5] S. Barata-Vallejo, A. Postigo, Eur. J. Org. Chem. (2012) 1889–1899.
[6] W. Qiu, D.J. Burton, J Fluor. Chem. 62 (1993) 273–281.
[7] L.F. Chen, J. Mohtasham, G.L. Gard, J Fluor. Chem. 43 (1989) 329–347.
[8] T. Takagi, T. Kanamori, J. Fluor. Chem. 132 (2011) 427 – 429.
[9] T. Yajima, K. Yamaguchi, R. Hirokane, E. Nogami, J Fluor. Chem. 150 (2013) 1–7.
[10] M. Slodowicz, S. Barata-Vallejo, A. Vazquez, N. Sbarbati Nudelman, A. Postigo, J Fluor. Chem. 135 (2012) 137–143.
[11] M. Mortimer, P. Taylor, Chemical Kinetics and Mechanism, in: The Open University, 2002: p. 212.
[12] S. Barata-Vallejo, A. Postigo, J Org Chem. 75 (2010) 6141–6148.
[13] W.R. Dolbier, X.X. Rong, Tetrahedron Lett. 35 (1994) 6225–6228.
[14] A.E. Feiring, E.R. Wonchoba, J. Fluor. Chem. 105 (2000) 129 – 135.
[15] C.G. Cho, Y.S. Kim, X. Yu, M. Hill, J.E. Mcgrath, J. Polymer Science: Part A: Polymer Chemistry (2006) 6007-6014.
[16] C. Chauvin, X. Ollivrin, F. Alloina, J.-F. LeNest, J.-Y. Sanchez, Electrochimica Acta. 50 (2005) 3843 – 3852.
[17] C. Chauvin, Thesis, Institut Polytechnique de Grenoble, 2005.
[18] M. Erceg, D. Jozić, I. Banovac, S. Perinović, S. Bernstorff, Thermochim. Acta. 579 (2014) 86 – 92.
[19] P.R Soeresen, T. Jacobsen, Electrochimica Acta. 27 (1982) 1671–1675.

IV. Experimental Part

This chapter will focus on the synthesis protocols of each salt and the characterization procedure used in this research work. The detail has been divided into three main sections as follows:

- The first section will be focused on the synthesis procedures of all lithium salts, the linear polycondensat (LPC1000) for crosslinking the network polycondensat (NPC1000) including the characterization of salts and polymer synthesized and also LiTPSM salt (commercially available but it is used as one of the main products for chapter III.2)

- The second section contains the detail about the film preparation and salt concentration calculation.

- The last section, the characterization for the performance investigation of those membranes will be performed.

IV.1. Synthesis procedure of salts, linear polycondensat (LPC1000) and their characterization methods

a) Chromatographic purification

Crude products were purified by flash column chromatography with different column size of silica gel (stationary phase) and organic solvent system (movable phase) depending on the polarity of product. For chromatographic purification, reagent grade solvents were used as received.

Reactions were monitored by thin layer chromatography (TLC) using aluminiumbacked silica gel plates (Merck, Kieselgel 60 F254). Two techniques used to investigate TLC spots are (i) viewing under ultraviolet light at short wavelength of 254 nm and (ii) reacting with $KMnO_4$ solution.

b) Nuclear Magnetic Resonance (NMR)

NMR spectra were obtained on a Bruker AVANCE 300 NMR spectrometer at frequencies of 300.12 MHz for ^{1}H, 75 MHz for ^{13}C and 282.39 MHz for ^{19}F. The chemical shift (δ) is measured in the unit of part per million (ppm). The coupling constant (J) was expressed in Hertz (Hz). The deuterated solvent used was $(CD_3)_2SO$-d_6 (δ_H = 2.50 ppm, δ_C = 39.52 ppm). The substitution pattern of the different carbons was determined by a "DEPT135" sequence. Multiplicities are reported as follows: s = singlet, d = doublet, t = triplet, q = quadruplet, m = multiplet, dd = doublet of doublet, ddd = doublet of doublet of doublet, td = triplet of doublet.

c) Elemental analysis

All samples were characterized the elemental analysis by Service Central d'Analyse-Institute des Sciences Analytiques, Villeurbanne, France.

IV.1.1.Salt synthesis

Lithium perfluorosulfonate salt

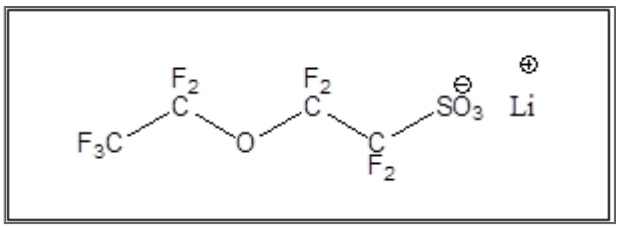

Product name: lithium 1,1,2,2-tetrafluoro-2-(perfluoroethoxy)ethanesulfonate (**LiTPSN**)

Formula: $C_4F_9LiO_4S$

Molecular weight: 322.03

Synthesis protocol:

Perfluoro(2-ethoxyethane) sulfonic acid (from Fluorochem) (20 mmol, 3.3 ml) was added in an aqueous solution of lithium hydroxide monohydrate (Alfa Aesar) (60 mmol, 25 ml). The mixture was stirred at room temperature for 2 h. After the solvent removal, the residue was dissolved in acetonitrile (Sigma Aldrich), filtered and concentrated under vacuum to afford 5.35 g of **LiTPSN** salt as a white solid. **LiTPSN** salts were further dried at 80°C for 48 h under vacuum before storing in a dry glove box.

% yield: 83%

Characterization:

^{19}F NMR $(CD_3)_2SO_2$-d6): -83.30 (t, J= 16 Hz., 2F), -87.91 (s, 3F), -89.39 (t, J= 16Hz., 2F), -119.33 (s, 2F)

Anal. Calcd.: C, 14.92; F, 53.10; Li, 2.16; S, 9.96

Found: C, 15.08; F, 49.92; Li, 2.15; S, 9.44

Lithium perfluorosulfonimide salt

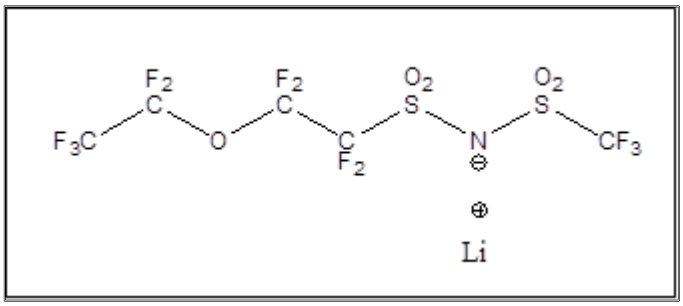

Product name: Lithium[tetrafluoro-2-(pentafluoroethoxy)ethane]-trifluoromethanesulfonimide (**LiTPSM**)

Formula: $C_5F_{12}LiNO_5S_2$

Molecular weight: 453.11

Synthesis protocol:

To a solution of anhydrous 1,2-dichloroethane and perfluoro(2-ethoxyethane) sulfonyl fluorides (13 mmol, 4.14 g) under inert atmosphere, was added freshly distilled benzylamine (65 mmol, 7.1 ml). The mixtrure was stirred at 50 °C during 20 h and was followed by thin layer chromatography (TLC) and ^{19}F NMR until sulfonyl fluoride completely disappeared. At room temperature, an aqueous HCl solution (10%) was added, and the mixture was extracted with dichloromethane. The organic phases were dried over $MgSO_4$, filtered and evaporated. The residue was purified by column chromatography on silica gel with gradient eluent (Pentane/AcOEt 1/0 to 4/1) to obtain a benzyl sulfonamide (13 mmol, 5.27 g). The second step, a solution of dichloromethane and benzyl sulfonamide, under inert atmosphere, was added DIEA (13 mmol, 2.3 ml) Then triflic anhydride (19.5 mmol, 3.3 ml) was added at 0°C, the mixture was stirred for 30 min at constant temperature then 1 h at room temperature (followed by TLC and ^{19}F NMR). Then the products were evaporated, and the residue was dissolved in hot pentane and the supernatant was isolated. The solvent was evaporated and the benzyl trifluoromethanesulfonamide was obtained. The third step, a suspension of benzyl trifluoromethanesulfonamide (12.8 mmol, 6.88 g) in ethanol (60 ml) was stirred during 8 h at room temperature until the solution was completely soluble. An aqueous solution of lithium hydroxide monohydrate (12.87 mmol, 540 mg) was added and the mixture was stirred at room temperature overnight. After the solvent removal, the white residue was dissolved in diethyl ether, filtered and concentrated under vacuum. The residue was washed with cyclohexane,

filtered and concentrated under vacuum to afford 4.5 g of LiTPSM salt as solid. LiTPSM salts was storing in a dry glove box.

% yield: 78%

Characterization:

^{19}F NMR $(CD_3)_2SO_2$): -79.08 (s, 3F), -81.52(t, J= 18 Hz, 2F), -86.34(s, 3F), -88.25(t, J=18 Hz, 2F), -117.29(s, 2F);

Anal. Calcd.: C, 13.25; F, 50.31; Li, 1.53; S, 14.15; N, 3.09
Found: C, 13.29; F, 47.48; Li, 1.52; S, 13.03; N, 3.16

Lithium aromatic perfluorosulfonate salts

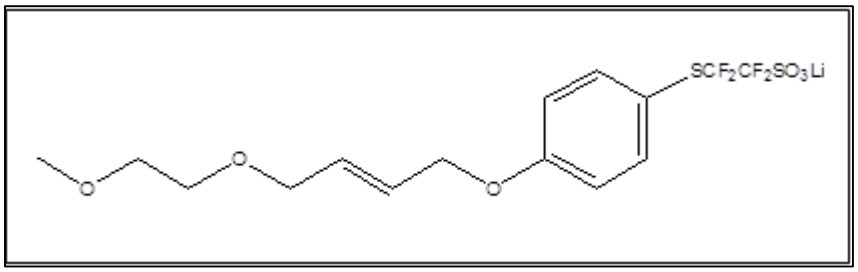

Product name: **salt 1**
Formula: $C_{15}H_{17}O_6F_4S_2Li$
Molecular weight: 440.36

Synthesis protocol:

A mixture of 2-Methoxyethanol (1 equiv.) and potassium hydroxide (3 equiv.) was dissolved in anhydrous dichloromethane. The reaction was stirred at the room temperature for 4 hours under an argon flow. Excess amount of (E)-1,4-dibromo-2-butene (3 equiv.) was added. The solution was then stirred for 24 hours. The resulting solution was extracted by

diethylether three times. The organic layer was concentrated under reduced pressure. The resulting residue was purified by silica gel column chromatography using 10% diethyl ether in CH_2Cl_2 as eluent to afford yellow oil (66 %). After that, the resulting yellow oil was added under an argon atmosphere to a magnetically stirred solution of LiPST (1 equiv.) in anhydrous THF (20 ml). The solution was heated to 60°C. The reaction progress was monitored by ^{19}F-NMR (appearance of C-H bonded peak of aromatic ring of **salt 1** at -84.98 and -112.32 ppm). After 72 hours, the progress was constant but it was not complete because of the hydrolyzed-LiPST. The reaction mixture had to be treated with quantitative amount of LiH that possibly reformed the LiPST hydrolyzed then reacted with the monobromo oligoether. After the solvent removal, the residue was purified by silica gel flash column chromatography using 5-10% of methanol in CH_2Cl_2 as eluent to eliminate unreacted substrates. The white powder was further dried at 80°C for 48 h under vacuum before it was stored in a dry glove box.

% yield: 63 %

Characterization:

^{1}H-NMR (DMSO-d6): 7.57 - 7.46 (m, 2H, ^{Ar}C<u>H</u>), 7.06 - 6.97 (m, 2H, ^{Ar}C<u>H</u>), 5.89 (td, J = 3.9Hz, J = 2.4 Hz, 2H, C<u>H</u>=C<u>H</u>), 4.64 - 4.56 (m, 2H, C<u>H</u>OAr), 4.00 - 3.91 (m, 2H, CHC<u>H$_2$</u>O), 3.51 - 3.39 (m, 4H, OC<u>H$_2$</u>C<u>H$_2$</u>), 3.23 (s, 3H, OC<u>H$_3$</u>)

^{13}C-NMR (DMSO-d6): 160.64 (s, <u>C</u>F$_2$SO$_3$), 139.06 (s, ^{Ar}<u>C</u>HO), 131.20 (s, <u>C</u>F$_2$S), 127.04 (s, ^{Ar}<u>C</u>HS), 116.14 (s, ^{Ar}<u>C</u>H), 115.08 (s, ^{Ar}<u>C</u>H), 71.70 (s, CH<u>C</u>H$_2$O), 70.60 (s, <u>C</u>H$_2$OCH$_3$), 69.30(m, CH<u>C</u>H$_2$O), 68.03 (s, <u>C</u>H$_2$O), 58.54 (s, CH$_3$O)

^{19}F-NMR (DMSO-d6): -84.89 (t, J= 7.2 Hz, 2F, C<u>F$_2$</u>S), -112.60 (t, J= 7.1 Hz, 2F, C<u>F$_2$</u>SO$_3$)

Anal. Calcd.: C, 40.91; H, 3.89; F, 17.26; Li, 1.58; S, 14.56

Found: C, 40.90; H, 3.91; F, 17.20; Li, 1.52; S, 14.30

Product name: salt 2

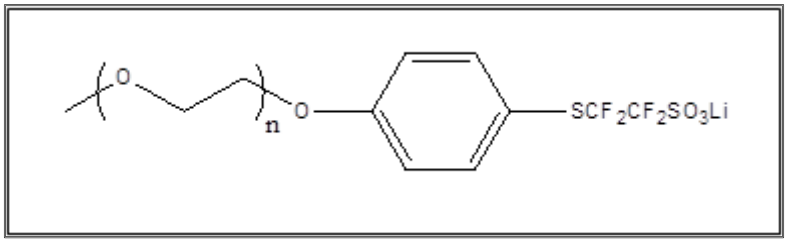

Synthesis protocol:

Each different length of methoxy polyethylene glycol (mPEG) (n=1, 3, 7.2, 16.3) (1 equiv.) was dissolved in anhydrous dichloromethane (30 ml) under an argon flow in the presence of Amberlyst 21® resin. Trifluoromethanesulfonic anhydride (1.2 equiv.) was added slowly, at 0°C. The reaction was monitored by ^{1}H and ^{19}F-NMR (appearance of CH_2 signals at 4.55 and 3.64 ppm for ^{1}H-NMR and CF_3 signal at -74.7 ppm in case of ^{19}F-NMR). After the reaction was complete, the solvent was removed by the rotary evaporator. The $CH_3(OCH_2CH_2)_nOSO_2CF_3$, resulting product was then added drop-wise to a solution of LiPST (1 equiv.) in anhydrous acetonitrile (20 ml) at ambient temperature. After stirring for 1 hour, the residue was concentrated under vacuum and was then purified by silica gel flash column chromatography using 20-100% of acetonitrile in dichloromethane as eluent. The white powder or yellow viscous liquid product was further dried at 80°C for 48 h under vacuum before it was stored in a dry glove box.

Table 5.1 Summary of the percentage of yield for each salt in a family of **salt 2**

n	1	3	7.2	16.3
% yield	56	90	67	50

n = repeating oxyethylene unit

<u>With n = 1</u>

Product name: **salt 2n1**

Formula: $C_{11}H_{11}O_5F_4S_2Li$

Molecular weight: 370.27

Characterization:

^{1}H-NMR (DMSO-d6)	7.57 - 7.48 (m, 2H, ^{Ar}C<u>H</u>), 7.07 - 6.99 (m, 2H, ^{Ar}C<u>H</u>), 4.15 (dd, J = 5.4 Hz, 3.7 Hz, 2H, C<u>H$_2$</u>OAr), 3.62 (dd, J = 5.4 Hz, 3.8 Hz, 2H, C<u>H$_2$</u>OCH$_3$), 3.32 (s, 3H, OC<u>H$_3$</u>)
^{13}C-NMR (DMSO-d6)	160.94 (s, <u>C</u>F$_2$SO$_3$), 139.07 (s, ^{Ar}<u>C</u>HO), 126.98 (s,CF$_2$S), 124.10 (s, ^{Ar}<u>C</u>HS), 117.77 (s, ^{Ar}<u>C</u>H), 115.22 (s, ^{Ar}<u>C</u>H), 115.05(s, ^{Ar}<u>C</u>H), 114.90 (s, ^{Ar}<u>C</u>H), 70.67 (s, <u>C</u>H$_2$OCH$_3$), 67.65 (s, CH$_2$O), 58.62 (s, <u>C</u>H$_3$O)
^{19}F-NMR (DMSO-d6)	-84.89 (t, J = 7.2 Hz, C<u>F$_2$</u>S), -112.57 (t, J = 7.1 Hz,C<u>F$_2$</u>SO$_3$)
Anal. Calcd.:	C, 35.68; H, 2.99; F, 20.52; Li, 1.87; S, 17.32
Found:	C, 35.37; H, 2.90; F, 20.84; Li, 1.80; S, 17.64

<u>With n = 3</u>

Product name:	**salt 2n3**
Formula:	$C_{15}H_{19}O_7F_4S_2Li$
Molecular weight:	458.37

Characterization:

^{1}H-NMR (DMSO-d6)	7.51 (d, J = 8.4 Hz, 2H, ^{Ar}C<u>H</u>), 7.03 (d, J= 8.5 Hz, 2H, ^{Ar}C<u>H</u>), 4.14 (s, 2H, C<u>H$_2$</u>OAr), 3.75 - 3.34 (m, 12H, OC<u>H$_2$</u>C<u>H$_2$</u>OCH$_3$), 3.23 (s, 3H, OC<u>H$_3$</u>)
^{19}F-NMR (DMSO-d6)	-84.93 (t, J = 7.1 Hz, C<u>F$_2$</u>S), -112.64 (t, J = 7.0 Hz,C<u>F$_2$</u>SO$_3$)

<u>With n = 7.2</u>

Product name:	**salt 2n7**
Formula:	$CH_3(OCH_2CH_2)_{7.2}OC_6H_4SCF_2CF_2SO_3Li$
Molecular weight:	643

Characterization:

^{1}H-NMR (DMSO-d6)	7.56 - 7.45 (m, 2H, ^{Ar}C<u>H</u>), 7.06 - 6.98 (m, 2H, ^{Ar}C<u>H</u>), 4.16 - 4.12 (m, 2H, C<u>H$_2$</u>OAr), 3.64 - 3.36 (m, 28H, OC<u>H$_2$</u>C<u>H$_2$</u>OCH$_3$), 3.22 (s, 3H, OC<u>H$_3$</u>)
^{13}C-NMR (DMSO-d6)	160.94 (s, CF_2SO_3), 139.06 (s, ^{Ar}<u>C</u>HO), 124.16 (s, CF_2S), 115.97 (s, ^{Ar}<u>C</u>HS), 115.05 (s, ^{Ar}<u>C</u>H), 71.74 (s, <u>C</u>H$_2$OCH$_3$), 70.25 (t, J=60 Hz, J=84 Hz, CH_2O), 69.24 (s, <u>C</u>H$_2$O), 67.90 (s, CH_2O), 58.51 (s, CH_3O)
^{19}F-NMR (DMSO-d6)	-84.90 (t, J = 7.2 Hz, C<u>F$_2$</u>S), -112.60 (t, J = 7.1 Hz,C<u>F$_2$</u>SO$_3$)
Anal. Calcd.:	C, 43.67; H, 5.57; F, 11.82; Li, 1.09; S, 9.95
Found:	C, 43.57; H, 5.44; F, 11.54; Li, 1.07; S, 9.13

<u>With n = 16.3</u>

Product name:	**salt 2n16**
Formula:	$CH_3(OCH_2CH_2)_{16.3}OC_6H_4SCF_2CF_2SO_3Li$
Molecular weight:	1043

Characterization:

^{1}H-NMR (DMSO-d6)	7.55 - 7.45 (m, 2H, ^{Ar}C<u>H</u>), 7.06 - 6.96 (m, 2H, ^{Ar}C<u>H</u>), 4.13 (dd, J = 5.4 Hz, J = 3.8, 2H, C<u>H$_2$</u>OAr), 3.74 (dd, J = 5.3 Hz, J = 3.9 Hz, 2H, C<u>H$_2$</u>OCH$_3$), 3.61 - 3.37 (m, 61H, OC<u>H$_2$</u>C<u>H$_2$</u>OCH$_3$), 3.23 (s, 3H, OC<u>H$_3$</u>)
^{13}C-NMR (DMSO-d6)	160.94 (s, CF_2SO_3), 139.06 (s, ^{Ar}<u>C</u>HO), 124.10 (s, CF_2S), 115.97 (s, ^{Ar}<u>C</u>HS), 115.05 (s, ^{Ar}<u>C</u>H), 71.76 (s, <u>C</u>H$_2$OCH$_3$), 70.26 (t, J= 56 Hz, J=84 Hz, CH_2O), 69.24 (s, <u>C</u>H$_2$O), 67.90 (s, CH_2O), 58.51 (s, CH_3O)
^{19}F-NMR (DMSO-d6)	-84.90 (t, J = 7.2 Hz, C<u>F$_2$</u>S), -112.60 (t, J = 7.1 Hz,C<u>F$_2$</u>SO$_3$)
Anal. Calcd.:	C, 47.86; H, 6.92; F, 7.29; Li, 0.67; S, 6.14
Found:	C, 47.75; H, 7.06; F, 7.33; Li, 0.57; S, 5.93

Lithium aliphatic perfluorosulfonate salts

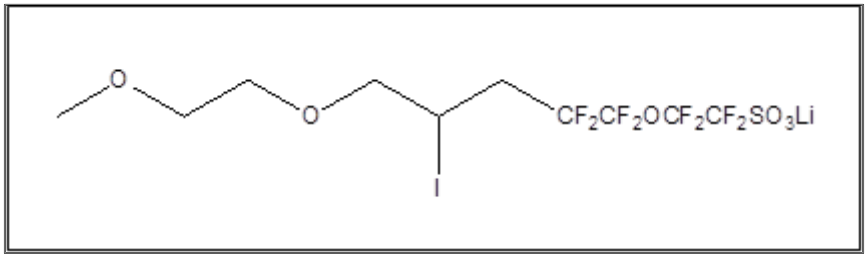

Product name: **salt 3**

Formula: $C_{10}H_{12}O_6F_8SILi$

Molecular weight: 546.10

Synthesis protocol

A mixture consisting of 2-Methoxyethanol (1 equiv.) and potassium hydroxide (3 equiv.) in dry dichloromethane was stirred at room temperature for 4 h under argon atmosphere. Allylbromide was added dropwise at 0°C and the reaction was stirred overnight. The crude product was washed by distilled water to remove a by-product and unreacted substrate. The pure product was carried out by the distillation as the colourless liquid. Next step, the mixture of allyl oligoether, benzoyl peroxide and 5-Iodoperfluoro-3-oxapentanesuolfonyl fluoride was stirred at 80°C for 24 h. Flash column chromatography on silica gel with hexane and dichloromethane (1:1) gave the compound containing the $OCF_2CF_2SO_2F$ group as light yellow liquid. In order to transform $–SO_2F$ group to $–SO_3Li$ group, LiOH was dissolved in THF and then, the resulting $OCF_2CF_2SO_2F$ compound was added at room temperature. The mixture was stirred overnight. After THF removal, the residue was dissolved in acetonitrile. LiF and LiOH in excess were removed by filtration and the crude product was then concentrated under vacuum to give a yellow viscous liquid. The product was further dried at 80°C for 48 h under vacuum before it was stored in a dry glove box.

% yield 67 %

Characterization:

^{1}H-NMR (DMSO-d6)	4.41 - 4.34 (m, C<u>H</u>I), 3.73 - 3.63 (m, CH_2CHI), 3.62 - 3.60 (m, CH_2O), 3.48 - 3.46 (m, CH_2O), 3.27 (s, CH_3O), 3.11 - 2.96 (m, CH_2CF_2), 2.79 - 2.63 (m, CH_2CF_2)
^{13}C-NMR (DMSO-d6)	75.84 (s, CH_2CHICF_2), 71.65 (s, CH_2OCF_3), 69.99 (s, CH_2O), 58.58 (s, CH_3O), 36.61-36.20 (t, J=96 Hz, CH_2CF_2), 17.00 (s, CHI)
^{19}F-NMR (DMSO-d6)	-83.61- -83.70 (m, 2F, $OC\underline{F_2}CF_2$), -88.78- -89.86 (m, 2F, $CH_2CF_2C\underline{F_2}O$), -118.48- -118.61 (m, 2F, CH_2CF_2), -119.21 (s, 2F, CF_2SO_3Li).
Anal. Calcd.:	C, 21.99; H, 2.21; F, 27.83; Li, 1.27; S, 5.87; I, 23.24
Found:	C, 22.02; H, 2.60; F, 27.89; Li, 1.10; S, 5.65; I, 23.55

Product name: salt 4

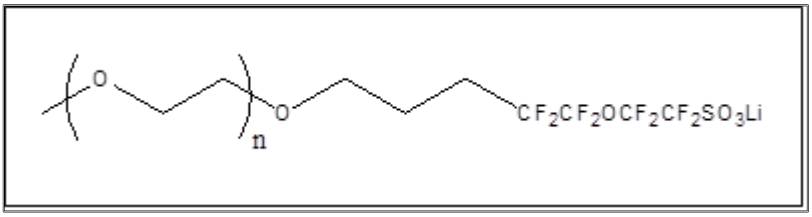

<u>With n = 1</u>

Product name: **salt 4n1**

Formula: $C_{10}H_{13}O_6F_8SLi$

Molecular weight: 420.20

Synthesis protocol

The allyl oligoether was prepared by stirring 2-Methoxyethanol (1 equiv.) and potassium hydroxide (3 equiv.) in dry dichloromethane at room temperature for 4 h under argon atmosphere. The resulting solution was cooled to 0°C and the allylbromide (2 equiv.) was added dropwise, following complete addition, the reaction was stirred overnight. The crude product was washed by distilled water to remove a by-product and unreacted substrate. The pure product was carried out by the distillation as the colourless liquid. Then, one-pot

reaction was done by adding the allyl oligoether (n = 1) to a solution of 5-Iodoperfluoro-3-oxapentanesuolfonyl fluoride (1.2 equiv), benzoyl peroxide (0.25 equiv.) and tris(trimethylsilyl)silane (1.2 equiv.) in dried toluene (15 ml). The solution was heated to 80°C and stirred for 36 h. After solvent removal, the crude solution was used as the substrate for the following step without the isolation, it was added to a solution of LiOH in dried THF and then, stirred at room temperature for 12 h. The reaction was monitored by ^{19}F-NMR (disappearance of signal around 46 ppm). After THF removal, the residue was dissolved in acetonitrile. LiF and LiOH in excess were removed by filtration. The resulting crude was purified by column chromatography on silica gel (CH_2Cl_2: ACN / 3:7) to afford the **salt 4n1,** as a white solid.

% yield 30 %

Characterization:

^{1}H-NMR (DMSO-d6) 3.55 – 3.45 (m, 4H, CH_2O), 3.23 (s, 3H, CH_3O), 2.15 (dd, J = 22.6 Hz, J = 14 Hz, 2H, CH_2CF_2), 1.74 (dt, J = 12.3 Hz, J = 6.1 Hz, 2H, CH_2).

^{19}F-NMR (DMSO-d6) -82.58 – -82.64 (m, 2F, $OC\underline{F_2}CF_2$), -88.01 – -88,14 (m, 2F, $CH_2CF_2C\underline{F_2}O$), -117.52 (t, J = 20 Hz, 2F, CF_2SO_3Li), -118.31 (s, 2F, CH_2CF_2).

Anal. Calcd.: C, 28.58; H, 3.12; F, 36.17; Li, 1.65; S, 7.63

Found: C, 28.48; H, 3.14; F, 34.63; Li, 1.65; S, 7.53

With n = 3

Product name: **salt 4n3**

Formula: $C_{14}H_{21}O_8F_8SLi$

Molecular weight: 508.30

Synthesis protocol

Triethylene glycol monomethylether (n = 3) was used as a substrate, the allyl oligoether was prepared by the following method. The alcohol substrate (1 equiv.) was stirred

with sodium hydride (3 equiv.) in anhydrous THF (20 ml) at ambient temperature for 1h. Allylbromide was then added dropwise and the mixture was heated to 40°C and stirred overnight. After THF removal, the resulting product was washed by water and extracted by diethylether to obtain the desired allyl oligoether as a pale yellow liquid. Allyl oligoether synthesized (n=3) was reacted with a solution of 5-Iodoperfluoro-3-oxapentanesuolfonyl fluoride (1.2 equiv.) and benzoyl peroxide (0.25 equiv.). The solution was stirred at 80°C for 36 h. The resulting crude was purified by flash column chromatography on silica gel (hexane : CH_2Cl_2 / 1:1) to afford iodoperfluoro oxapentanesulfonyl fluoride oligoether as a yellow liquid.

The following step, the dehalogenation was done by adding tris(trimethylsilyl)silane as a radical-based reducing agent to the dry toluene solution of previous resulting product and benzoyl peroxide at 80°C. The solution was stirred for 36 h. After solvent removal, the crude product was concentrated. Purification by column chromatography (hexane : diethyl ether / 2 : 3) afforded the desired product as a yellow viscous liquid.

To carry out the **salt 4n3**, the yellow viscous product from previous step was added to a solution of LiOH in dry THF at ambient temperature and the solution was stirred overnight. The reaction was monitored by ^{19}F-NMR (disappearance of signal around 46 ppm). After THF removal, the residue was dissolved in acetonitrile. LiF and LiOH in excess were removed by filtration. The **salt 4n3** was then concentrated and further dried at 80°C for 48 h under vacuum before it was stored in a dry glove box.

Overall percentage yield 52 %

Characterization:

^{1}H-NMR (DMSO-d6) 3.53 – 3.43 (m, 14H, CH_2O), 3.24 (s, 3H, CH_3O), 2.14 (dd, J = 22.8 Hz, J = 14.2 Hz, 2H, CH_2CF_2), 1.71 (dt, J = 12.4 Hz, J = 6.1 Hz, 2H, CH_2).

^{13}C-NMR (DMSO-d6) 117.87 (s, $\underline{C}F_2S$), 117.53 (s, $\underline{C}F_2CH_2$), 117.19 (s, CF_2O), 112.33 (s, $O\underline{C}F_2CF_2$), 71.73 (s, $\underline{C}H_2OCF_3$), 70.23 (t, CH_2O), 70.04 (s, CH_2O), 69.92 (s, CH_2O), 69.17 (s, CH_2O), 58.48 (s, CH_3O), 27.11 (t, J=88 Hz, $\underline{C}H_2CF_2$), 21.01 (s, $CH_2\underline{C}H_2CH_2$)

^{19}F-NMR (DMSO-d6)	-82.51 – -82.63 (m, 2F, $OC\underline{F_2}CF_2$), -87.97 – -88,04 (m, 2F, $CH_2CF_2C\underline{F_2}O$), -117.16 (t, J = 24 Hz, 2F, CF_2SO_3Li), -118.20 (s, 2F, CH_2CF_2).
Anal. Calcd.:	C, 33.08; H, 4.16; F, 29.90; Li, 1.37; S, 6.31
Found:	C, 31.44; H, 4.65; F, 26.33; Li, 1.24; S, 5.28

Lithium aliphatic perfluorosulfonimide salt

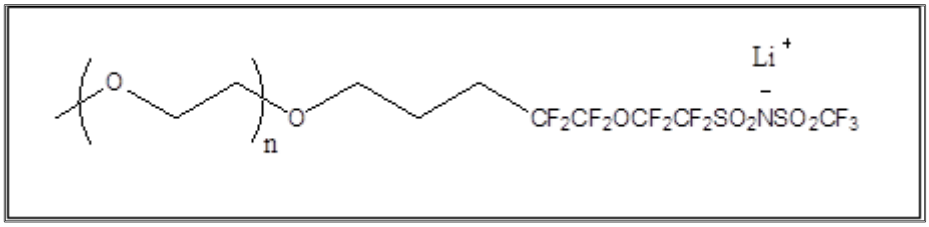

Product name: **salt 5n3**

Formula: $C_{15}H_{21}O_9F_{11}S_2NLi$

Molecular weight: 639.38

Synthesis protocol:

After the dehalogenation, perfluoro sulfonyl fluoride oligoether ($mPEGSO_2F$, n = 3) obtained was used as the substrate for this functional modification reaction. Firstly, trifluoromethanesulfonamide and dry triethylamine were dissolved in anhydrous acetonitrile at 40°C, then cooled to room temperature. The sulfonyl fluoride substrate was added and the solution was heated at 50°C for 16 h. The reaction was monitored by ^{19}F-NMR (disappearance of signal around 46 ppm). The solvent was evaporated under vacuum. The residue was dissolved in dichloromethane, washed several times by distilled water and concentrated under vacuum to yield the triethylammonium salt of the title product. This salt was added to the solution of aqueous LiOH in THF and the mixture solution was stirred at 40°C for 2 h. After THF removal, the residue was dissolved in acetonitrile, the LiOH excess was eliminated by filtration, then, the resulting solution was concentrated giving the title salt. The salt was further dried at 80°C for 48 h under vacuum before it was stored in a dry glove box.

Overall percentage yield 41 %

Characterization:

^{1}H-NMR (DMSO-d6) 3.52 – 3.44 (m, 14H, CH_2O), 3.34 (s, 3H,CH_3O), 2.26 (dd, J = 21.9 Hz, J = 13.4 Hz, 2H, CH_2CF_2), 1.90 – 1.74 (m, 2H, $CH_2CH_2CF_2$).

^{13}C-NMR (DMSO-d6) 121.60 (s, CF_3SO_2), 118.40 (s, CF_2S), 117.31 (s, $CF_2\underline{C}F_2O$), 117.20 (s, $O\underline{C}F_2CF_2$), 116.71 (s, $O\underline{C}F_2CF_2$), 112.00 (s, $O\underline{C}F_2CF_2$), 71.3 (s, $\underline{C}H_2OCF_3$), 70.22 (s, CH_2O), 70.03 (s, CH_2O), 69.62 (s, CH_2O), 69.05 (s, CH_2O), 58.46 (s, CH_3O), 26.76 (t, J= 88 Hz, $\underline{C}H_2CF_2$), 20.96 (s, $CH_2\underline{C}H_2CH_2$)

^{19}F-NMR (DMSO-d6) -78.63 (s, 3F, $C\underline{F}_3$-SO_2), -81.46 (m, 2F, $C\underline{F}_2$-SO_2), -87.86 (t, J= 12 Hz, 2F, CF_3-$C\underline{F}_2$-O), -116.94 (s, 2F, O-$C\underline{F}_2$-CF_2), -117.22 (t, J = 19.5 Hz, 2F, $C\underline{F}_2$-CH_2).

Anal. Calcd.: C, 28.18; H, 3.31; F, 32.69; Li, 1.09; S, 10.03; N, 2.19

Found: C, 28.75; H, 3.70; F, 30.13; Li, 0.90; S, 8.33; N, 2.28

IV.1.2.Linear polycondensat (LPC1000) preparation

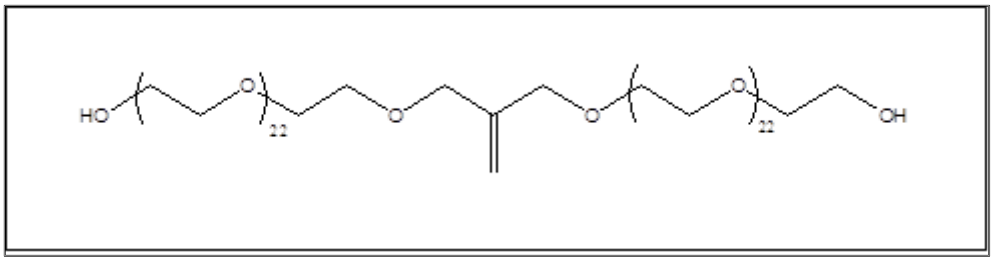

Synthesis protocol:

The mixture of polyethylene glycol (PEG) with M_w = 1000 and a four-fold excess of ground KOH were stirred at 40°C for 4 hours and 3-chloro-2-chloromethyl-1-propene (CCMP) was then added dropwise. After stirring for 48 hours, the resulting solution was dissolved in deionized water and neutralized by concentrated HCl solution until pH = 7. The inorganic by-products (KOH, KCl) were eliminated by the ultrafiltration and the water was removed by lyophilization for 3 days. The polycondensate obtained was further characterized and kept in the glove box.

Characterization:

$\overline{M_n}$ = 2.674×10^4 (±8.759%)

$\overline{M_w}$ = 7.347×10^4 (±3.123%)

Polydispersity (I) = 2.748 (±9.299%)

IV.1.3.Salt and LPC1000 characterization

a) Thermal analysis

The thermal properties of salts and the related membranes were determined while consecutively performing thermal gravimetric analysis (TGA/SDTA Mettler-Toledo STARe software version 12.10) and differential scanning calorimetry (DSC 1- Mettler -Toledo). For glass transition temperature (T_g) and melting temperature (T_m) measurements as in a typical procedure, samples were heated from -100 ° C to 150-200 °C (depending on the sample) with a heating rate of 10 °C / min. The oscillation period was 60 s and amplitude was ±1 °C. The TGA measurement was carried out at a heating rate of 5 °C/ min under nitrogen atmosphere and from 25 °C to 500 °C. An amount of approximately 10 mg of sample was prepared on a particular plate.

b) Conductivity measurements

Conductivities were measured by electrochemical impedance spectroscopy using an HP 4192A Impedance Analyzer in the low frequency range 5 Hz – 13 MHz. The ionic liquid lithium salts were placed in a dip-type glass cell with two platinum electrodes at a constant distance. Measurements were done on successive increase and decrease of temperature in the range 20 °C - 110 °C. The temperature was equilibrated for 1 hour before each measurement. The cell constant was determined by using a 0.1 M KCl solution.

c) Cyclic voltammetry

Cyclic voltammograms (CV) were recorded at room temperature in a glove box. The counter electrode was a Pt wire, and the working electrode was Pt with a diameter of 2 mm. The scan rate used was 10 mVs^{-1}. The reference electrode was an Ag wire in 10 mM $AgNO_3$ in acetronitrile + 0.1 M tetraethylammonium borofluoride ($TEABF_4$). Potential can be

converted to the NHE scale by adding 0.542 [1]. The ACN + $TEABF_4$ 0.1 M electrolyte exhibits a large electrochemical stability, with oxidation and reduction potentials at 2.6 V vs Ag/Ag^+ and −2.4 V vs Ag/Ag^+ respectively. These limits in potential were associated, in the studies, to the oxidation and reduction of the BF_4^- [2] and [3].

d) Diffusion coefficient and cationic transference number

The self-diffusion measurements were performed with the pulsed field gradient stimulated echo and LED sequence using 2 spoil gradients (PFG NMR) [4]. The magnitude of the pulsed field gradient was varied between 0 and 40 G cm^{-1}, the diffusion time, Δ, between two pulses was fixed at 100 ms and the gradient pulse duration, δ, was set between 3 ms and 18 ms, depending on the diffusion coefficient of mobile species, D. This allowed to observe the attenuation of spin echo amplitude over a range of at least 2 decades leading to good accuracy (<5%) of the self-diffusion coefficient values. They were determined from the relationship $\ln(I/I_0) = -Dg^2\gamma^2\delta^2(\Delta - \delta/3)$, where g is the magnitude of the two gradient pulses, γ is the gyromagnetic ratio of the nucleus under study and I and I_0 are respectively the area of the signal obtained with or without gradient pulses, D the diffusion coefficient, δ the gradient pulse duration and Δ the diffusion time. The measurement was carried out at high temperatures of 110 °C. The cation transference number is obtained from this relationship:

$$T^+ = \frac{D_+}{D_+ + D_-}$$

where D_+ is the self diffusiton coefficient of the cation and D_- the self-diffusion coefficient of the anion.

The sample investigated the diffusion coefficient by PFG-NMR technique was prepared by containing into the small tube in the glove box for preventing the humidity. The tube was subsequently closed and put in the NMR test tube before measuring by NMR instrument.

e) Freeze dryer or lyophilization

The LPC1000 dissolved in deionized water was dried by the lyophilization instrument. The solution was poured into the freeze drying flask and rotated the flask in a liquid nitrogen bath for few minutes. The solution flask was connected to the freeze drying machine. The lyophilization usually spent at least 3 days (depending on the water content inside the material) and the freezing temperature was -100°C.

f) Gel Permeation Chromatography (GPC)

GPC measurement was performed in a Waters 515 HPLC, equipped with a differential refractometer SOPARES RI2000 and WYATT DAWN EOS at 690nm. A column Couplage 10: AGILENT 2xPLgel-Mixed-D was used with DMF (Alfa aesar – HPLC grade 99.7%) + 0.1 M $NaNO_3$ flow rate of 1ml/min to analyse the sample. Molecular weight was calculated in polystyrene equivalents

IV.2. Membrane preparation and salt concentration calculation

IV.2.1.Membrane preparation

In our work, we study the performance of the salts in two different types of host polymer. The first one is linear POE (M_w =300,000 g/mol) from Acros Organics and another one is cross-linked POE (NPC). The former electrolyte was prepared in a glove box by dissolving both POE (0.3 g) and the salt (mass calculated by the following equation) in acetonitrile (8 ml). The resulting solution was stirred overnight and subsequently casted on a Teflon plate (diameter of 4 cm). Solvent evaporation process was done in the glove box for 18 h. The membrane was then dried under vacuum at 50°C for 48 h and further stored in the glove box under argon.

For the film processing of NPC, the electrolytes were prepared in the glove box by dissolving the salt (mass calculated by the following equation), LPC (0.3 g) and the initiator (IRGACURE® 2959, CIBA) (5 % of NPC mass) in acetonitrile (8 ml) and allowed to stir overnight. The resulting electrolyte was poured into a Teflon plate. After the solvent evaporation, the cross-linking under UV radiation (0.866 mW) was carried out for 30 seconds and 1 minute. The resulted NPC membranes were then dried under vacuum at 60°C for 72 h and carefully stored in the glove box.

IV.2.2.Calculation of salt concentration

The lithium salt concentration in the film is indicated by the number x = O/Li, which actually corresponds to the oxyethylene/lithium molar ratio.

The quantity of salt incorporated is calculated from these equations:

For POE host polymer $$\frac{O}{Li} = \frac{m_{POE}}{m_{salt}}\frac{M}{44} + n$$

For NPC1000 host polymer $$\frac{O}{Li} = \frac{m_{POE}}{m_{salt}}\frac{M}{46.4} + n$$

where m_{POE} = mass of polymer used

m_{salt} = mass of salt incorporated

M = theoretical molecular weight of salt

$M_{CH_2CH_2O}$ = 44 g/mol for POE and 46.4 g/mol for NPC1000

n = the number of oxyethylene repeating unit in lithium salt

IV.3. Membrane characterization

IV.3.1.Thermal analysis

The thermal properties of salts and the related membranes were determined while consecutively performing thermal gravimetric analysis (TGA/SDTA Mettler-Toledo STARe software version 12.10) and differential scanning calorimetry (DSC 1- Mettler -Toledo).

In the case of POE/salt samples, the glass transition temperature (T_g) and melting temperature (T_m) measurements was investigated with a typical procedure, two series of data can be obtained. For the first data series, samples were heated from -100 °C to 100 °C with a heating rate of 10°C / min, the T_{g1}, T_{m1}, ΔH_{m1} were measured, the membranes were cooled down at -100 °C with a ramp of 20 °C/min and heated once again to 100 °C (T_{g2}, T_{m2}, ΔH_{m2}). In the second ones, the samples were quenched, therefore the pans containing the samples places in a well closed recipient. They were heated at 80 °C on a heater outside of the DSC device and, after 10 min, the pans were put again in the DSC at -100 °C to get the characteristic temperature of the quenched samples (T_{gq}, T_{mq}, ΔH_{mq}).

For NPC/salt complexes, samples were heated to 60 °C with a heating rate of 10 °C/min and then quenched to -100 °C with a cooling rate of 50 °C/min. The samples were heated up again to 60 °C. The oscillation period was 60 s and amplitude was ±1 °C.

The TGA measurement was carried out at a heating rate of 5 °C/ min under nitrogen and from 25 °C to 500 °C. An amount of approximately 10 mg of sample was prepared on a particular plate.

IV.3.2.Dynamic mechanical analysis

The thermo-mechanical properties of the different membranes were determined using a TA Instruments DMA2980. The setup measured the complex tensile modulus E*, i.e. the storage component E' and the loss component E", as well as the ratio of the two component, i.e. tan δ (=E'/E"). Measurements were performed in isochronal conditions at the frequency of 1 Hz. Strain magnitude was fixed at 0.01% of the sample length, 150% force track. The temperature was varied in the temperature range of -100 °C - 100 °C at a heating rate of 3 °C / min. The film sample used should have the size of 5×10 mm^2 approximately and it should be measured immediately after taking out from the glove box for avoiding the humidity.

IV.3.3.Conductivity measurements

Conductivities were measured by electrochemical impedance spectroscopy using an HP 4192A Impedance Analyzer in the low frequency range 5 Hz – 13 MHz. The membrane with the diameter of 9 mm was placed between two stainless steel electrodes in a Swagelok cell with Teflon o-rings and spacers. The sample preparation step should take place in the glove box for avoiding the contamination of humidity. Measurements were done on successive increase and decrease of temperature in the range 20 °C - 70 °C (from 20 °C – 110 °C for NPC/salt complex). The temperature was equilibrated for 1 hour before each measurement. The ionic conductivity was calculated from

$$\sigma = \frac{L}{RS} \qquad (S.cm^{-1})$$

where σ is the ionic conductivity, R is the bulk resistance, L is the thickness of the polymer membrane and S is the area of the stainless steel electrode.

IV.3.4.Diffusion coefficient and transference number

The transference number was estimated from two methods; an electrochemical impedance spectroscopy technique (EIS) and diffusion coefficients. For the former technique, a sample was sandwiched between two metallic lithium electrodes. This cell was carefully prepared in an argon glove box in order to avoid degradations of lithium metal foil and the presence of humidity in the electrolyte. Both electrodes (anode and cathode) are made of thin

lithium foils which have a thickness of approximately 65 µm, while a polypropylene layer was used as insulator. Also the polymer electrolyte thickness (l), important, must be known before and after the impedance measurements. The cell elaboration (the lamination process) and further impedance measurements modify the membrane thickness. The value of diffusion coefficient can be easily detected while using the characteristic (solid state) diffusion time τ

$$\tau = l^2 / D$$

where l is the inter-electrode distance (polymer electrolyte thickness) and D is the ambipolar diffusion coefficient.

In the case of symmetrical electrochemical cells, Li/electrolyte/Li, the lithium metal electrodes are considered as blocking electrodes for the anion and non-blocking for the lithium cation. For this reason, the diffusion impedance (Warburg diffusion, W_d) is given by:

$$W_d = R_e \mu_2/\mu_1$$

Where μ_1 is the lithium cation mobility, μ_2 is the anion mobility and R_e is the electrolyte resistance. This leads to the final equation for transference number, T^+:

$$T^+ = R_e / (R_e + W_d)$$

The polarization voltage was kept at 40 mV using a computer-monitored Solartron 1470 battery test unit. The Nyquist plot obtained from EIS method was shown as follows.

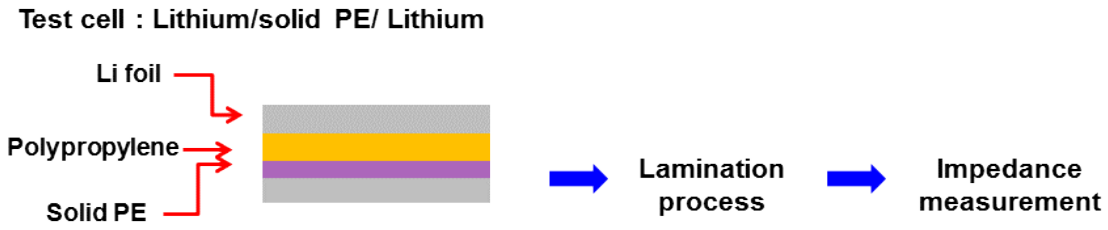

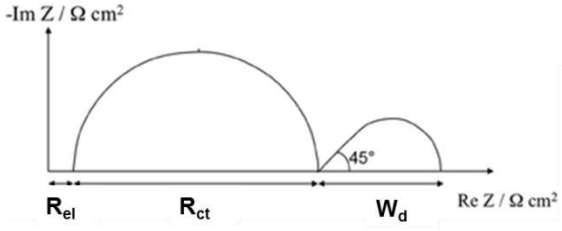

Nyquist diagram

The latter one, diffusion coefficient was determined by pulsed field gradient (PFG)-NMR. The magnitude of the pulsed field gradient was varied between 0 and 55 G cm^{-1} (sinus shaped pulsed gradient); the diffusion time Δ between two pulses was fixed at 500 ms and the gradient pulse duration δ was set between 3 and 22 ms depending on the diffusion coefficient of mobile species. This allowed us to observe the attenuation of spin echo amplitude over a range of at least 2 decades leading to a good accuracy (≤5%) of the self-diffusion coefficient values. They were determined from the classic relationship $\ln(I/I_0) = \gamma^2 D g^2 \delta^2 (\Delta - \delta/3)$ where g is the magnitude of the two gradient pulses, γ is the gyromagnetic ratio of the nucleus under study and I and I_0 are respectively the area of the signal obtained with or without gradient pulses. The measurement was carried out at high temperatures of 110°C. The cation transference number is obtained from this relationship:

$$T^+ = \frac{D_+}{D_+ + D_-}$$

where D_+ is the self-diffusion coefficient of the cation and D_- the self-diffusion coefficient of the anion.

IV.4. References

[1] V.V. Pavilishchuk, A.W. Addison, Inorg. Chim. Acta, 298 (2000) 97-102.

[2] P.A.Z. Suarez, V.M. Selbach, J.E.L. Dullius, S. Einloft, C.M.S. Piatnicki, D. Azambuja, R.F. deSouza, J. Dupont, Electrochim. Acta, 42 (1997) 2533-2535.

[3] E. Peled, D. Golodnitsky, C. Menachem, D. Bar-Tow, J. Electrochem. Soc., 145 (1998) 3482-3486.

[4] S. Altieri, D.P. Hinton, R.A.J. Byrd, J. Am. Chem. Soc., 117 (1995) 7566-7567.

General conclusion and prospects

This research targeted the syntheses and assessments of new lithium salts intended to be used, in a first stage, in solvent-free polymer electrolytes.

Once selected the suitable host polymer, macromolecular ionic solutions face two main issues as: 1) low cationic transference numbers T^+ and 2) a progressive stiffening of the polymer electrolytes with the increase in salt concentration, detrimental to the ionic conductivity. This stiffening results from the intra-chain and, above all, inter-chains solvation of Li^+ that induces physical cross-links, sometimes called transient cross-links. If the use of volatile, and then flammable, organic solvents, is discarded, one solution is to swell the polymer electrolytes with ionic liquids. These one, based on quaternary ammonium allow decreasing the glass transition temperatures thus increasing conductivities but are costly and don't participate to the reactions at the electrodes. Furthermore the T^+ of lithium is fairly low in these commercial ionic liquids.

Our target was to prepare multifunctional salts endowed with a plasticizing, a solvating and an ionic function. These materials, indeed Lithium-conducting ionic liquids, have 2 additional functions with regard to current ionic liquids i.e. lithium conductivity and Li^+ solvation.

For that purpose salts having an oligomeric tail i.e. oligo(oxyethylene) end-capped by perfluorinated or perfluorosulfonimide lithium salts were prepared. The ionic groups were spaced from the oligomeric tail either by a, aryl moiety or by an alkyl one. The results, which are promising both in terms of conductivity and of cationic transference numbers, can be still optimized and improved by monitoring the length of the oligomeric tail.

The new Li-conducting ionic liquids were characterized, alone (when possible) and in blend with 2 host polymers i.e. a linear commercial POE and a cross-linked polycondensate. The former, which is unsuited for the application, owing to its high crystallinity and to its very poor mechanical performances, was used because it allows a good comparison with a lot of literature data to be performed. The later provides much higher conductivities at ambient temperature and much higher storage modulus.

High cation transference numbers were obtained in both host polymers, and its values increase with the lengthening of the mPEG. The adding of mPEG chain on the anion leads,

generally to greater conductivity of polymer electrolytes and its conductivities increase with the increase of mPEG lengths.

The salts where the ionic groups were spaced from the oligomeric tail by an alkyl give polymer electrolytes with better properties in term of conductivity, cationic transference number, dissociation degree as compared with those of the salts spaces with an aryl moiety. Some questions are still pending. This is the case for the presence with the ionic liquid (**salt2n16**) of 2 T_g or 2 T_α obtained respectively by DSC and DMA and might reflect a phase or microphase separation. This ionic liquid seems to be prone to induce a self-solvation of the lithium cation, suppressing the increase compatibilization expected from the cation interaction with both hosts.

Prospects

- From the synthesis point of view, due to the difficulty in the salt purification step, a family of aliphatic lithium salts with four different number of oxyethylene units for both sulfonate and sulfonimide function was not completely carried out like the aromatic one as it was expected. It will be interesting if such salts can be purified by a green process in water i.e. ultrafiltration to make easier the full synthesis protocol but at this time we didn't find ultrafiltration membranes with a cut-off lower than 1,000 Dalton (g/mole). End-capping oligomers by two ionic groups will allow salts having molar mass much higher than 1,000 g/mole paving the route for an efficient ultrafiltration purification process.

- If, some of the oligomeric salts weaken the NPC electrolytes, the use of Nano Crystalline Cellulose will allow a huge improvement of the resulting nanocomposite NPC electrolytes while unaffecting the conductivities.

- Salts of Na and of alkaline-earth as Mg and Ca could be easily prepared and should be useful for the cation transport of electrolytes for post-lithium batteries. Last the best salts could be used as Li-ion electrolytes in solution in organic solvent mixtures.

- A more deep study has to be conduct in order to understand the differences between the cation transference numbers obtained by two methods.

Contexte

Actuellement, les prévisions de croissance du marché du transport électrique - electric vehicles, EV, hybrid electric vehicles, HEV, Plug-in hybrid electric vehicles, PHEV, motivent une recherche de nette amélioration de la sécurité par rapport aux batteries commercialisées pour les marchés des applications 4C (ordinateur, téléphone cellulaire, caméscopes, outils sans fil). Ainsi, les batteries sans solvant retrouvent actuellement un regain d'attention. C'est le cas des batteries tout- solide, aux composants solides inorganiques, et des batteries utilisant des électrolytes polymères sans solvant moléculaire liquide.

En ce qui concerne les problèmes de sécurité, les électrolytes polymères à solvant macromoléculaire permettant une élaboration en forme de films minces sont très intéressants, n particulier ceux préparés à partir du polymère hôte, le poly (oxyéthylène) (POE). Grâce au haut DN du POE, lié à la présence de paire d'électrons sur l'atome d'oxygène, le POE a une capacité exceptionnelle à solvater le cation lithium. La chaîne POE présente également une grande flexibilité et la mobilité des cations lithium, au-dessus de la température de fusion, s'effectue par le mouvement de segments de polymère. Il souffre cependant de divers handicaps, à savoir (i) une cristallinité élevée qui pénalise la conductivité de l'électrolyte en dessous de la température de fusion (ii) une résistance mécanique qui disparaît après la fusion de l'électrolyte de polymère et (iii) une stabilité à l'oxydation limitée à environ 3,9 V vs Li / Li^+. Outre des performances élevées en termes de propriétés électrochimiques, thermomécaniques, chimiques, une attention particulière doit être accordée au transport d'ions. Le fonctionnement d'une batterie à électrolyte polymère est en partie conditionné par sa température de fusion, Tf, car la conductivité est principalement obtenue à l'état amorphe. Mais le module de stockage, E', chute complètement à T > Tf avec un risque d'un court-circuit. La croissance de dendrites dépend de la mobilité de l'anion et serait donc favorisée par un faible nombre de transport cationique (T^+) pour les mélanges de POE et de sel. Ce nombre de transport bas est lié aux interactions faibles entre l'anion et les segments POE qui mènent à des coefficients de diffusion des anions très supérieurs à celui du cation lithium qui est lui fortement solvaté par les atomes d'oxygène du POE. Par conséquent, l'interaction entre les deux espèces doit être améliorée en modifiant l'anion. De plus, la modification de l'architecture du POE est l'une des voies pour améliorer les propriétés mécaniques après le point de fusion des membranes.

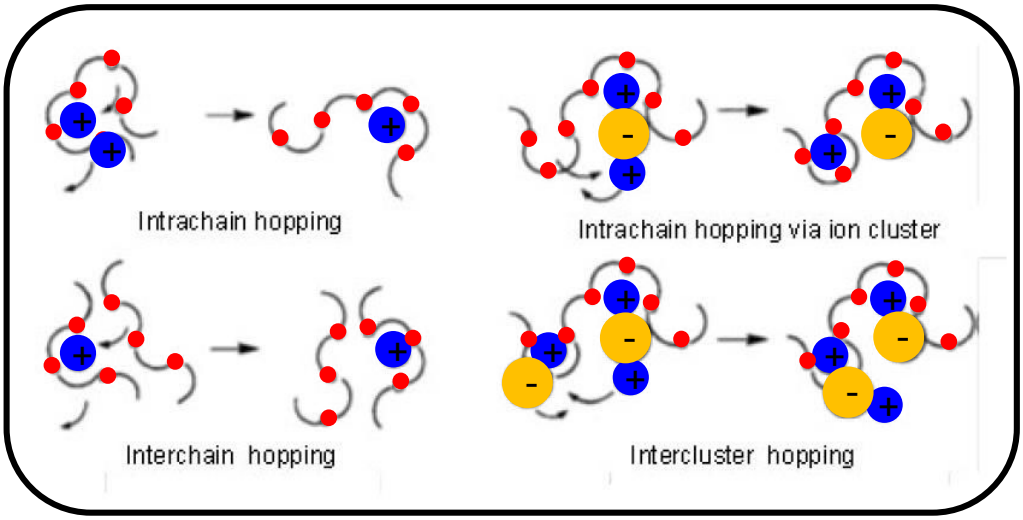

Figure 1. Ion mouvement en polymère hôte.

L'utilisation de liquides ioniques commerciaux est une des voies pour obtenir une conductivité suffisante aux basses températures mais, encore une fois, T^+ reste faible. De plus, ces liquides ioniques, qui bénéficient à la conductivité, sont basés sur des cations tétraalkyl ammonium qui ne participent pas aux réactions d'électrodes.

En pratique, le transport de cations lithium est couplé au mouvement du squelette du polymère ou de la mobilité segmentaire de la chaîne de polymère en coordonnant les interactions des mobiles Li^+ à l'oxygène de l'éther tandis que les anions ayant des interactions plus faibles avec des chaînes principales, sont beaucoup plus mobiles. Cela se traduit par un inconvénient majeur : un nombre de transport cationique faible. En outre, l'accumulation de ces anions à l''anode et un faible coefficient de diffusion des cations Li provoquent des gradients de concentration en sel qui favorisent une polarisation de concentration et donc une mauvaise performance de la cellule [120]. Afin d'atteindre un nombre de transport cationique élevé égal à l'unité, en théorie, un conducteur cationique unipolaire doit être préparé, dans lequel les anions sont immobilisés via des liaisons covalentes les liant aux chaînes polymères [121]. Ce concept a donné lieu à plusieurs contributions [118-121]. Les sels de lithium à anions imidure polymères dont les charges négatives sont délocalisées ont été étudiés par Watanabe et al. [123], [124]. La longueur de l'espace entre charges anioniques influence la conductivité et la dissociation de sels. Ces sels peuvent augmenter le nombre de transport cationique. Bouchet et al. [125], [126] ont préparé les alliages de polymères de mélange POE avec de lithium poly (4-styrènesulfonyle (trifluorométhylsulfonyl) imide polyélectrolyte. La conductivité est très faible (7.94×10^{-7} S/cm à 40 °C) pour une utilisation pratique dans les batteries Li-ion, même à travers ce polyanion

contient le caractère souple et délocalisée de la $-SO_2-N-SO_2-CF_3$ fournissant région plus amorphe matrice polymère. D'autre part, le nombre de transport lithium-ion est presque unité ($T^+ = 0,92$) à 60 ° C. Ces résultats sont très inférieurs à ceux obtenus précédemment, dans des réseaux POE par fixation d'anion perfluorosulfonate qui avaient abouti à une conductivité de 0,1 mS à 86°C pour un $T^+ =1$ par construction : réseau tri-dimensionnel extrait pour éliminer toutes traces de sel non-lié à la chaîne polymère [131]. Des oligomères porteurs de groupes perfluorosulfonimidure ont également été étudiés par Desmarteau et al. [127], [128]. Des oligomères à anions sulfonimidure aliphatiques et aromatiques ont été caractérisés : la plus haute conductivité à température ambiante est ~ 10^{-6} S/cm et atteint entre 10^{-4} et 10^{-3} S/cm à 120 °C Même si, les nombres de transport n'ont pas été déterminés, des gradients de polarisation de concentration n'ont pas été détectés par des études galvanostatiques. Outre des anions sulfonimidures, des oligoéthers ont également fonctionnalisés avec d'autres groupes terminaux ioniques tels que carboxylate, sulfonate et sulfate qui ont été présentés dans la recherche bibliographique de la manière suivante.

Deux démarches ont été entreprises pour se rapprocher d'un nombre de transport cationique = 1 : l'utilisation de polymères ioniques ou ioniques de haute masse ou réticulés, des oligomères porteurs de fonctions ioniques en bout de chaîne. Seuls les premiers garantissent un $T^+ =1$ si le polymère ionique est réticulé.

Ainsi les précurseurs, Bannister et al. ont préparé un conducteur unipolaire cationique à anion perfluorocarboxylate mais ce sel de lithium n'étant pas suffisamment dissocié dans la matrice de polyéther fournit de faibles conductivités [129]. D.Benrabah et al. ont immobilisé des anions perfluorosulfonates dans des réseaux polyéther et ont obtenu une conductivité purement cationique égale à 0,1 mS/cm à 86°C. [131]. Afin de diminuer la mobilité anionique et, d'atteindre le nombre élevé de transfert qui fermeture à l'unité, T. Hamaide et C. Le Deore ont utilisé des perfluorosulfonate de lithium à longue chaîne ($C_8F_{17}SO_3Li$) mais cela ne conduit pas à des $T^+ =1$ [130]. K. Ito et al. ont rapporté la synthèse de PEG, PPG et PEGME terminés par un benzènesulfonate de lithium [132]. W. Xu et al. ont préparé différentes longueurs de chaînes de PEG portant à leur extrémité un groupe sulfonate de benzoyle (EO_nPSLi). [133]. X. Ollivrin a synthétisé les PEG attachés par le lithium perfluorosulfonate et a obtenu de hautes valeur de conductivité lorsque les sels de lithium ont été incorporés dans le POE (10^{-3} S/cm à 78 ° C) [134]. Des mono et di-sel de lithium à base de sulfate oligoéther ont été réalisés par C. Chauvin et al. La conductivité atteint 6 x 10^{-5} S/cm à 70°C et est proche de 10^{-5} S/cm à 30° C pour le sel de lithium mono pur alors que les di-sels de lithium pur ont atteint des conductivités

de 8×10^{-5} S/cm à 70° C et de 2×10^{-5} S/cm à 30° C. Les nombres de transport cationique de ces deux sels étaient voisins de l'unité à 70° C [135].

Nous avons donc axé nos recherches vers les sels de lithium pouvant améliorer l'interaction entre les anions et les segments de polymère afin de diminuer la mobilité des anions. Ainsi, ce travail de thèse se propose d'aborder ces questions en concevant de nouveaux sels de lithium qui sont des liquides ioniques contenant les groupements oxyéthylène et les anions perfluorosulfonate /perfluorosulfonimidure. Le groupement oxyéthylène (CH_2-CH_2-O-) doit plastifier la chaîne polymère pour réduire la cristallinité et augmenter la mobilité segmentaire tout en améliorant l'interaction anion - segments polymères. En outre les motifs oligo(oxyethylène) peuvent contribuer à la solvatation des cations lithium. Par conséquent, l'influence (i) du nombre d'unités oxyéthylène (ii) des différentes structures chimiques et (iii) de la nature de l'anion sur leurs performances intrinsèques et sur celles de leurs complexes avec du POE (linéaire ou réticulé) ont été étudiées.

Résultats et discussion

Les résultats de mes travaux de thèse sont présentés à travers deux chapitres principaux.

Le Chapitre II est consacré à la synthèse et la caractérisation de sels de lithium à base de perfluorosulfonates aromatiques greffés sur des chaînes de PEG de longueur différente (n = 1, 3, 7 et 16) et le sel de lithium avec une double liaison dans la molécule afin d'étudier l'impact de la longueur de la chaîne de mPEG et de la structure chimique.

Le Chapitre III concerne des électrolytes à base d'anions perfluorosulfonates et perfluorosulfonimidures de lithium aliphatiques. Ce chapitre est divisé en deux parties. La première partie, présente la synthèse et la caractérisation de nouveaux perfluorosulfonate et perfluorosulfonimidure de lithium, destinés à être-fixés à une chaîne PEG afin de connaître les performances intrinsèques de ces sels. Les deux anions ont en commun la présence d'une fonction perfluoroéther qui devrait assurer une plus grande flexibilité des anions et l'anion perfluorosulfonimidure est dissymétrique.

La deuxième partie est consacrée aux synthèses et caractérisations d'oligoéthers (PEGs) porteurs des précédents sels de lithium. Pour réaliser l'électrolyte polymère, tous les sels

synthétisés ont été incorporés dans deux polymères hôte différents du POE linéaire et du POE réticulé. Leurs performances ont été comparées à celles des oligoéthers ioniques du chapitre II.

Chapitre II : Synthèse et caractérisation d'une famille d'oligoéthers terminés par un aryl perfluorosulfonate de lithium

L'objectif était l'évaluation de l'impact de la longueur de mPEG sur les oligoéthers à fonction aryl perfluorosulfonate de lithium sur les propriétés chimiques, mécaniques, électrochimiques, particulièrement, la conductivité et le nombre de transport cationique.

La première partie ce chapitre est consacrée à la synthèse et la caractérisation de ces sels. Dans la deuxième partie les nouveaux sels ont été incorporés dans du POE de masse 300000 g/mole ou dans une matrice POE réticulée, les films résultants étant évalués en termes de propriétés électrochimiques, thermiques, thermomécanique. Les conductivités ont été mesurées par spectroscopie d'impédance et leurs nombres de transport cationique par spectroscopies d'impédance électrochimique et de RMN à Gradient de champ pulsé (PFG-RMN).

Nous avons fixé les sels $PhSCF_2CF_2SO_3Li$ à une courte chaîne POE (méthoxy polyéthylène glycol, MPEG). Le cycle aromatique de $PhSCF_2CF_2SO_3Li$ a l'avantage d'être facilement modifié pour permettre son couplage avec les dérivés MPEG. En fixant le mPEG à l'anion du sel de lithium, on pourrait s'attendre (i) à une amélioration de la compatibilité entre l'anion et la matrice POE et donc à une augmentation du nombre de transport cationique, (ii) à une diminution de la cristallinité de la matrice POE (iii) à bénéficier d'une auto-solvatation de Li^+ par la chaîne oligomère et (iv) à une plastification de l'électrolyte polymère augmentant la mobilité de Li^+. Ainsi, dans ce travail, les PEG de différentes longueurs (n= 1, 3,7 et 16) terminés par la fonction sel ont été synthétisés.

Table 1 Sels de lithium aromatiques étudiés dans ce chapitre

Structures chimiques	Sel de lithium
Sel de lithium aryl perfluorosulfonate oligooxyéthylène 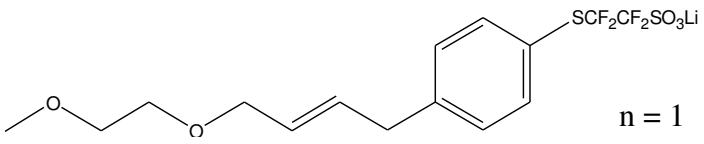	**Sel 1**
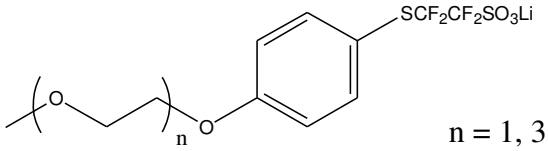	**Sel 2**

Synthèses

Deux protocoles de synthèse ont été utilisés:

1) la substitution nucléophile de LiPST sur mPEG portant un bromure d'allyle (**sel 1**) (Schème 1).

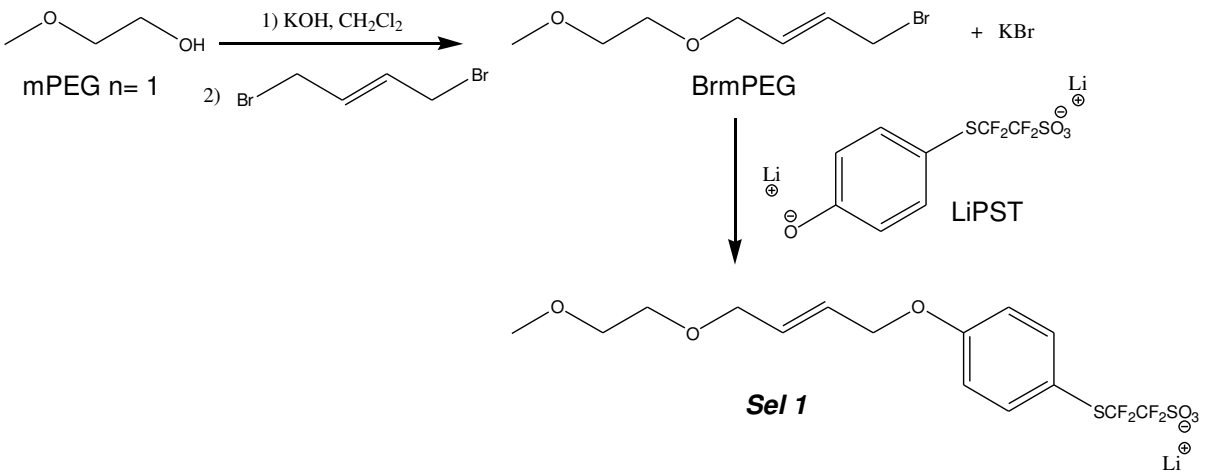

Schème 1. Synthèse du **sel 1**.

2) la substitution nucléophile de LiPST sur trifluorométhanesulfonate de mPEG (**sel 2**) (Schème 2). Du fait du caractère très nucléofuge du trifluorométhanesulfonate, les temps de réaction sont plus courts avec des rendements > 50 % qui dépendent de la longueur des mPEG.

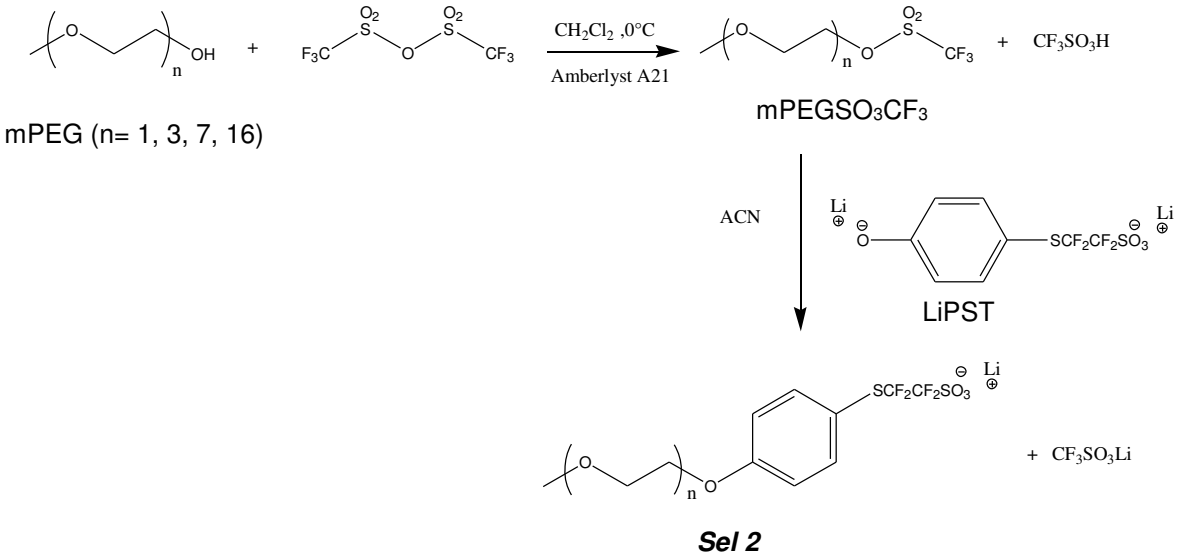

Schème 2. Synthèse du **sel 2** (n= 1, 3, 7, 16).

Caractérisations

Sel de lithium

Les composés obtenus ont été caractérisés par DSC, qui montre l'influence de la tête ionique sur les phases amorphes et cristallines.

- Les T_f du **sel 2n7** e_t du **sel 2n16** ne sont pas observées mais ils sont amorphes à la température ambiante et répondent donc aux caractéristiques des liquides ioniques. Il est connu que cinq atomes d'oxygène sont nécessaires pour la solvatation de Li^+. Dans les **sels 2n7** et **n16**, 2 et 11 atomes d'oxygène sont respectivement en excès. Nous supposons donc que la chaîne mPEG peut s'organiser différemment et conduire à des matériaux amorphes.
- La T_g du **sel 1** et du **sel 2n1** était impossible à mesurer, même après fusion et trempe, probablement en raison de l'aptitude des sels à recristalliser. Pour les autres sels 2 avec $n \geq 3$, la liaison du LiPST sur le mPEG conduit à une augmentation importante de la température de transition vitreuse (T_g) vs le mPEG pur. Cependant leurs T_g sont beaucoup plus basses que celle du sel de lithium aromatique, $PhSCF_2CF_2SO_3Li$ non-fixé sur mPEG et diminuent avec l'augmentation de n.

L'ATG montre que la dégradation du sel 2 ayant un n faible commence à la même température que celle du sel non-fixé sur mPEG (T_d = 210°C) et augmente avec n. Elle reste cependant

inférieure à celle du mPEG n = 16. Nous supposons donc que la dégradation se produit au niveau de la liaison C-S de l'anion.

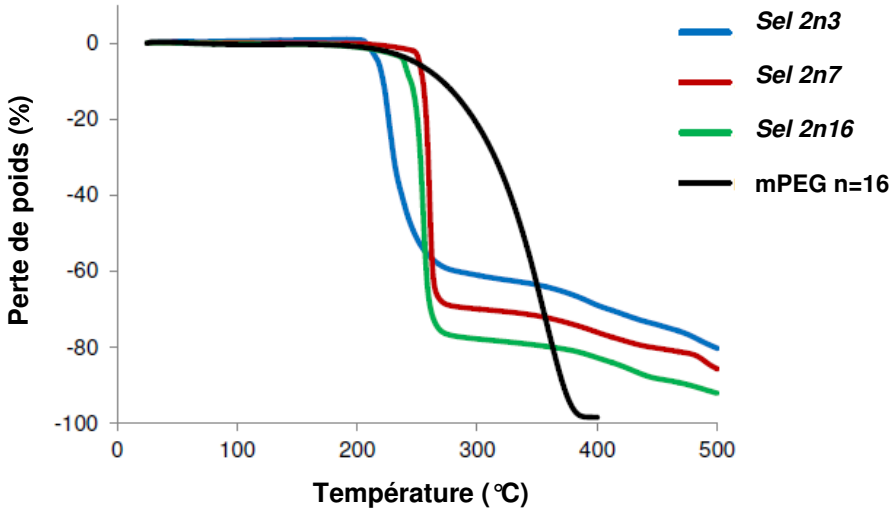

Figure 2. ATG des sels de lithium aromatiques.

La conductivité de **sel 2n16** est supérieure à celle du **sel 2n7**. L'augmentation du rapport molaire O/Li contribue à la fois (i) à la solvatation de Li^+, et donc à l'augmentation de la dissociation, et (ii) à l'augmentation de la mobilité des ions, en accord avec la T_g plus basse du **sel 2n16**.

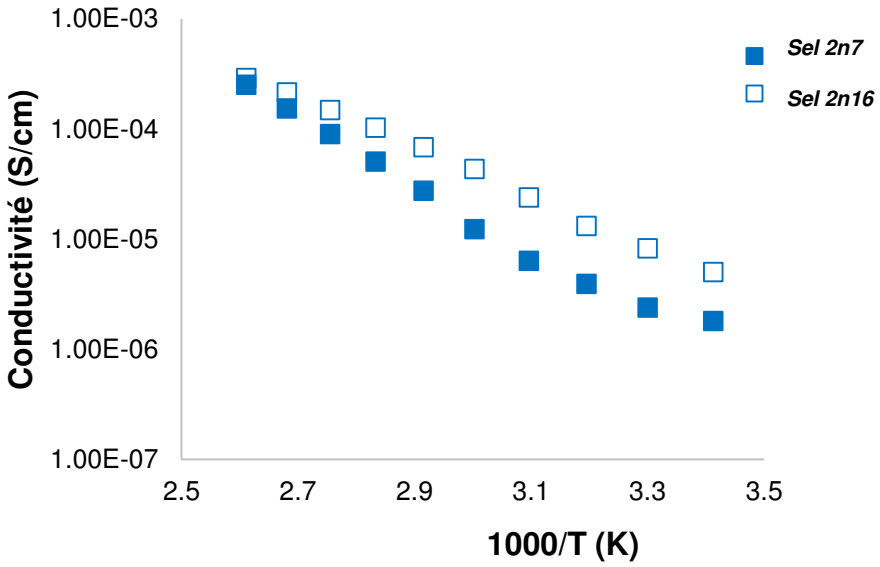

Figure 3. Conductivité des **sel 2n7** et **sel 2n16**.

Les coefficients de diffusion des anions (^{19}D) et de Li^+ (^{7}D) des **sels 2n7, 2n16**, est obtenu par PFG-RMN (^{7}Li et ^{19}F). On constate que les coefficients de diffusion des anions sont inférieurs à celui du lithium pour les deux sels. La comparaison des coefficients de diffusion des deux sels montre que ceux des anions (^{19}D) sont très proches alors qu'un facteur supérieur à 2, sépare les coefficients de diffusion du lithium (^{7}D). On peut supposer que la viscosité du sel **2n16** est inférieure à celle du **sel 2n7**. La valeur élevée du coefficient de diffusion du lithium dans le **sel 2n16** est en raison d'une plus grande flexibilité et du mouvement de la chaîne de segment mPEG par rapport à ceux de mPEG du **sel 2n7**.

Le nombre de transport du **sel 2n16** ($T^+ = 0,72$) présente une valeur supérieure à celle du **sel 2n7** ($T^+ = 0,64$).

Le mur d'oxydation du **sel 2** commence à 4,25 V par rapport à Li/Li^+ et semble être indépendant de la longueur de chaîne de mPEG et très proche de celui de $PhSCF_2CF_2SO_3Li$ (4,3 V). En outre, la stabilité semble être légèrement supérieure à celle du POE qui est connu pour être proche de 3,9 V par rapport à Li/Li^+. En ce qui concerne le **sel 1** sa stabilité semble être légèrement plus faible, un premier épaulement apparaît à 3,9 V par rapport à Li/Li^+ probablement dû à l'oxydation de la double liaison.

POE+Sel de lithium aromatique

Le sel oligomère a été incorporé dans le POE linéaire. La comparaison entre les électrolytes polymères conduit à plusieurs conclusions :

- L'augmentation classique de la T_g avec l'addition de sel dans la matrice POE, en raison de l'interaction entre les chaînes du POE hôte et le sel, une T_g qui décroît lorsque la longueur de chaîne de mPEG augmente. En outre, la DMA corrobore les résultats de DSC. Ainsi, la température de relaxation diminue avec l'augmentation de longueur de chaîne (figure 4 (a)). Toutefois, dans le cas de POE + **sel 2n16**, on observe une séparation de phase avec l'apparition de deux T_g en DSC et de deux T_α en DMA (figure 4 (b)).

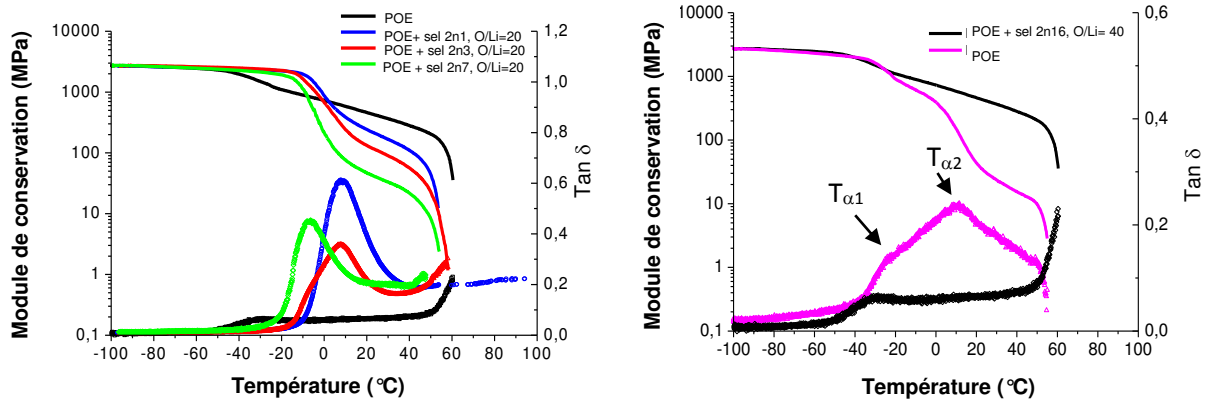

Figure 4. Propriétés mécaniques des sels de lithium aromatiques (module de conservation et Tan δ) (a) POE+**sel 2**, O/Li= 20 et (b) POE+**sel 2n16**, O/Li= 40.

➢ Toutes les courbes de conductivité montrent une forme classique pour l'électrolyte POE, c'est-à-dire qu'en dessous du point de fusion, T_f, la conductivité suit la loi d'Arrhenius, avec augmentation très nette de la conductivité au niveau de T_f et une loi de comportement de type VTF. Les conductivités des deux membranes (POE+**sel 1** et POE+**sel 2n1**) sont semblables au-dessus de T_f, pour $T < T_f$ les valeurs sont plus faibles pour l'électrolyte POE + **sel 2n1** (figure 5 (a)). Une augmentation régulière de la conductivité a été observée avec l'augmentation de la longueur de mPEG (figure 5 (b)), un écart qui diminue lorsque $T > T_f$. Nous supposons que cette augmentation est due à la double contribution des EO de mPEG en termes de solvatation et de mobilité des cations Li^+.

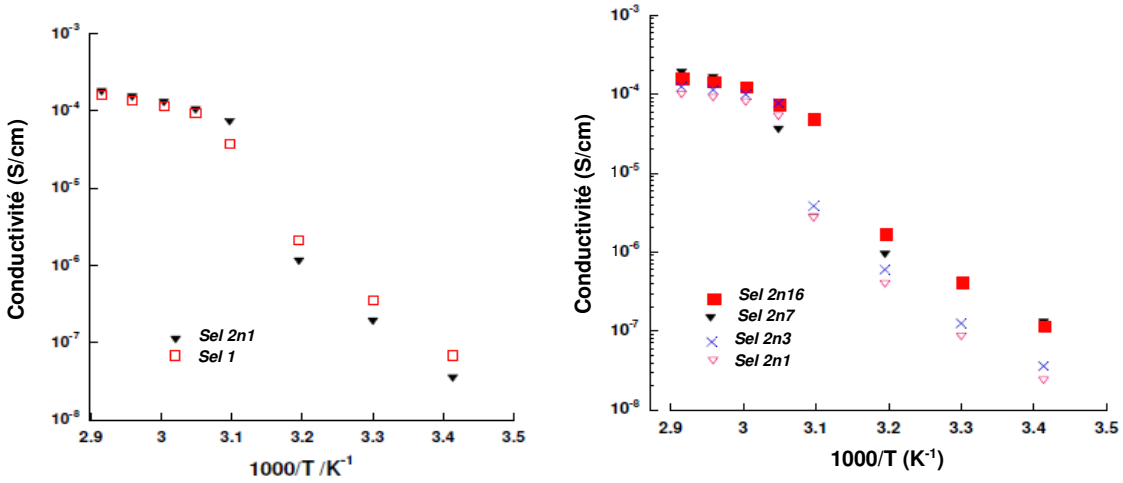

Figure 5. (a) conductivité de POE+ **sel 1** vs POE+ **sel 2n1**, O/Li =20, (b) comparaison de la conductivité de POE / **sel 2** avec différentes longueurs de chaîne mPEG, O/Li= 30 pour **sel 2n1**, **sel 2n3**, **sel 2n7** et O/Li= 40 pour **sel 2n16**.

Les coefficients de diffusion d'anions et Li^+ sont plus faibles pour POE + **sel 1** par rapport à POE + **sel 2**. Toutefois, il a été montré précédemment que les conductivités sont très proches à des températures supérieures à la température de fusion de l'électrolyte POE à la même concentration. En ce qui concerne l'anion du **sel 2**, ses coefficients de diffusion diminuent avec l'augmentation de la longueur de chaîne mPEG (à partir de n = 1 à n = 16). Au contraire, les coefficients de diffusion de Li^+ augmentent avec l'augmentation de longueur de chaîne mPEG : ceci tient probablement à l'auto-solvatation du cation Li^+ et à une plus grande mobilité des sels auto-solvatés par rapport aux cations solvatés par les grandes chaînes de POE.

Les valeurs de T^+ mesurées par PFG-RMN se situent entre 0,42 et 0,59. Tous les électrolytes POE / **sel 1** et **2** présentent des T^+ plus élevés que ceux obtenus avec des électrolytes POE/LiTFSI. Dans le cas du **sel 2**, l'allongement de mPEG induit une augmentation de T^+. Toutefois, l'incorporation des **sel 2n7** et **sel 2n16** dans le POE se traduit par des T^+ inférieurs à ceux des sels utilisés à l'état pur (sans POE). Dans le cas des sels purs l'auto-solvatation est possible pour les **sel 2n7** et **sel 2n16**. Leur dilution dans le POE se traduit par une compétition entre auto-solvatation et solvatation partielle ou totale par les grandes chaînes POE, donc à une diminution de la mobilité de Li^+. Sauf pour le **sel 2n7**, T^+ obtenus par EIS technique sont proches de 0,5 (entre 0,5 et 0,55) et pour les **sel 1**, **sel 2n1**, **sel 2n3**, les valeurs sont plus élevées que celles obtenues par PFG-RMN.

NPC+Sel de lithium aromatique

Tout électrolyte polymère à base de POE subit une nette dégradation des propriétés mécaniques au-dessus de la température de fusion (~60 °C). Par conséquent, afin d'améliorer la tenue mécanique, ces sels ont été incorporés dans une matrice de POE réticulé.

Après l'élaboration de films de sel de lithium et de polycondensat linéaire (LPC), les double liaisons du LPC ont été réticulées par irradiation UV pour former le POE réticulé ou NPC.

A même concentration en sel et pour des temps d'irradiation identiques nous n'avons pas observé une évolution importante et cohérente de T_g avec l'augmentation de la longueur de chaîne de mPEG n = 1 à n = 7 ou avec l'augmentation du rapport O/Li. Toutefois, pour les NPC + **sel 2n16**, un comportement similaire POE + **sel 2n16** a été observé. Ainsi, l'obtention de deux T_gs (en DSC) et deux T_αs (en DMA) confirment l'existence d'une séparation de phase (figure 6).

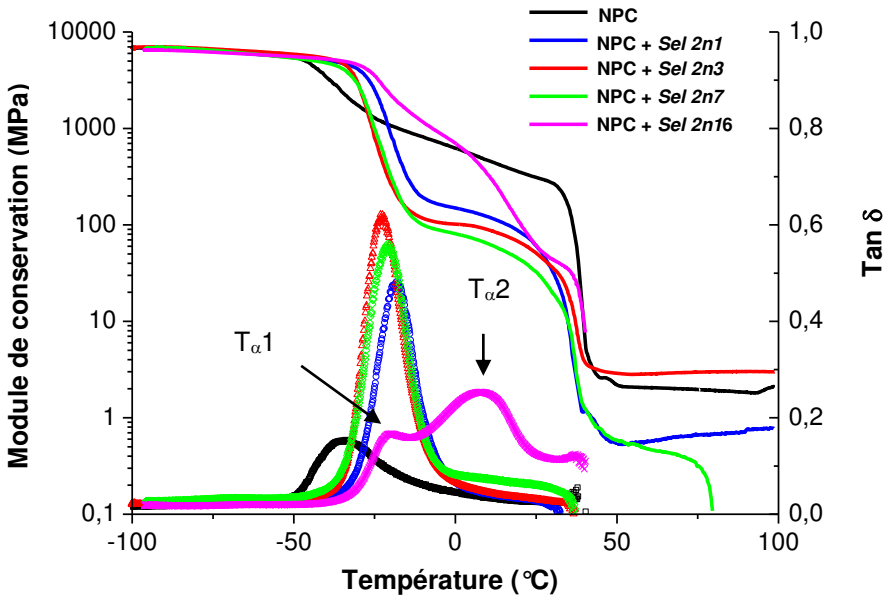

Figure 6. Module de stockage vs température pour divers sel 2 incorporés dans NPC hôte polymère à O / Li = 30, temps d'irradiation 30 secondes et leurs Tan δ.

En ce qui concerne l'effet du temps de l'irradiation sur NPC + **sel 2** complexes, une légère augmentation de T_g, attribuable à une augmentation de la densité de réticulation, est observée pour l'échantillon irradié 1 min par rapport à ceux irradiés pendant 30 secondes.

Les T_α du NPC + **sel 2n3** et **2n7** sont inférieures à celles des NPC + **sel 2n1**. En outre, les pics correspondant aux relaxations α sont très intenses et minces dans le cas des films à base de **sel 2n1, sel 2n3** et **sel 2n7** par rapport à la membrane NPC. Ces résultats indiquent une plus grande teneur en phase amorphe avec des tailles de domaines plus homogènes dans les électrolytes NPC par rapport à NPC pur. En outre, la présence du plateau caoutchouteux après la température de fusion démontre l'amélioration des propriétés mécaniques de ces films.

Les conductivités des électrolytes à base de POE + **sel 2n16** sont légèrement supérieures à celles des électrolytes à base de NPC-dessus de la température de fusion T_f tandis que, en dessous de T_f, les conductivités des électrolytes à base NPC sont à peu près 10 fois plus élevées (figure 7 (a)). La cristallinité et le T_f beaucoup plus faibles de NPC expliquent ce gain de conductivité à basse température.

Les conductivités sont proches, dans toute la gamme de température, pour tous les électrolytes quels que soient les longueurs de mPEG (figure 7 (b)).

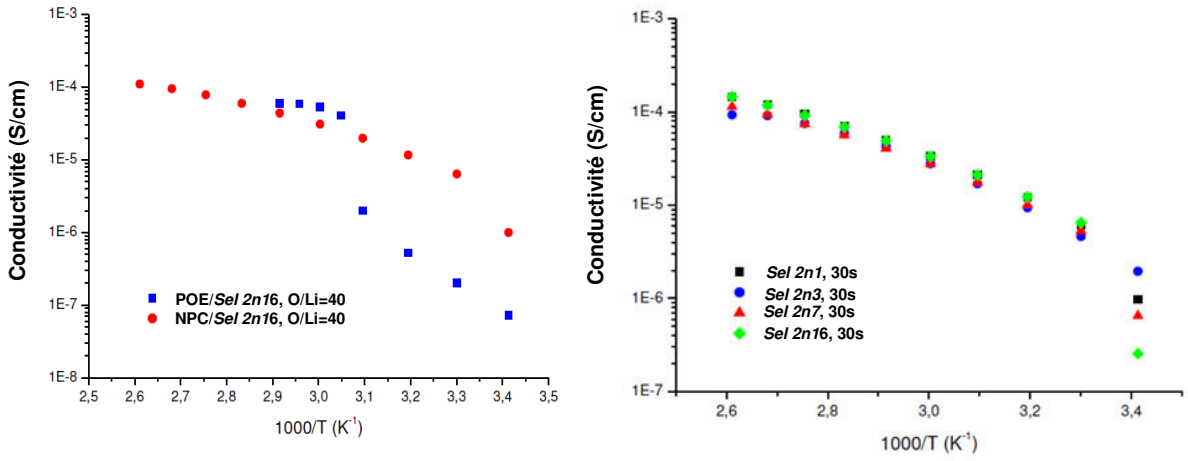

Figure 7. (a) Conductivités vs 1000/T pour le **sel 2n16** O/Li = 40 dans POE et NPC matrice et (b) Conductivité vs température réciproque des différentes longueurs de chaîne de **sel 2** dans le matrice NPC à la concentration O/Li = 30 avec des temps d'irradiation de 30 secondes.

.

T^+ ainsi que les valeurs des coefficients de diffusion sont plus élevés pour tous les électrolytes à base de NPC + sels par rapport à ceux des électrolytes POE + sels tandis que les conductivités, à 110°C sont plus faibles.

Chapitre III : Sels aliphatiques oligoéther de lithium à base de perfluorosulfonate et de perfluorosulfonimidure

Objectif :

Dans le chapitre précédent, une famille de sels de lithium aryle-perfluorosulfonate fixée sur oligoéther (mPEG) a été étudiée. La présence de mPEG dans la structure du sel a un impact modéré sur le degré de cristallinité du polymère hôte mais améliore les T^+ des électrolytes polymères et les conductivités cationiques par rapport au sel non-fixé sur mPEG. La présence du cycle aromatique dans la structure du sel généralement (i) augmente la viscosité du sel et (ii) pourrait modifier l'interaction du sel avec le polymère hôte par rapport aux sels aliphatiques. Par la suite, nous avons conçu des sels aliphatiques fixés sur mPEG et étudié l'impact de la fixation de mPEG sur les anions et sur les performances des électrolytes polymères.

Ce chapitre est divisé en deux parties: (i) dans la première partie, nous présentons comme une publication la caractérisation de deux sels, c'est à dire LiTPSM et LiTPSN dans des électrolytes polymères à base de POE linéaire et réticulé NPC. (ii) dans la deuxième partie les anions de LiTPSM et LiTPSN ont été modifiés pour les fixer sur des oligoéthers mPEG de différentes longueurs.

Table 2 Sels de lithium aliphatiques étudiés dans la première partie de ce chapitre

Structures chimiques	Sel de lithium
Sel de lithium perfluoro alkyl sulfonimidure 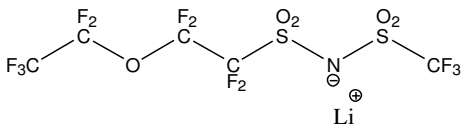	**LiTPSM**
Sel de lithium perfluoro alkylsulfonate 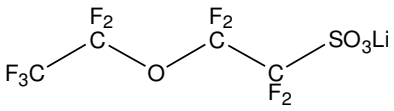	**LiTPSN**

Synthèse

- LiTPSN a été réalisé par la neutralisation de l'acide perfluoro (2-éthoxyéthane) sulfonique en solution aqueuse avec de l'hydroxyde de lithium (Schème 3).

Schème 3. Synthèse de LiTPSN.

- La synthèse de LiTPSM a été réalisée en trois étapes (schéme 4).

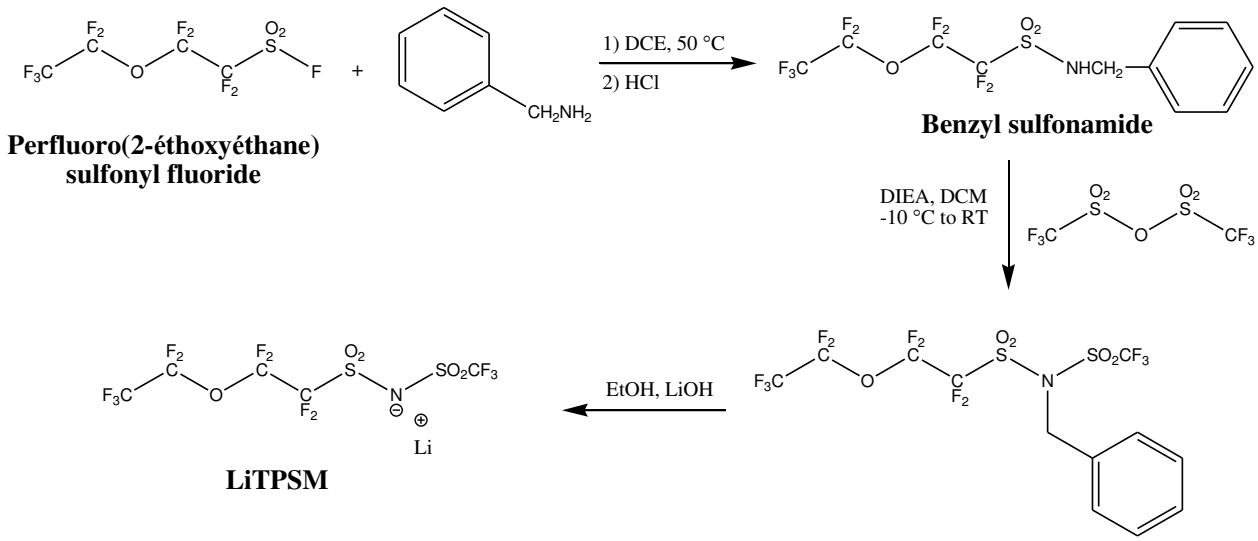

Schème 4. Synthèse de LiTPSM.

Caractérisations

POE+ LiTPSM ou LiTPSN

LiTPSN induit ni une diminution significante de la cristallinité, ni une diminution des températures de fusion. Au contraire, LiTPSM a un effet plus important à la fois sur la cristallinité, sur T_f et sur T_g.

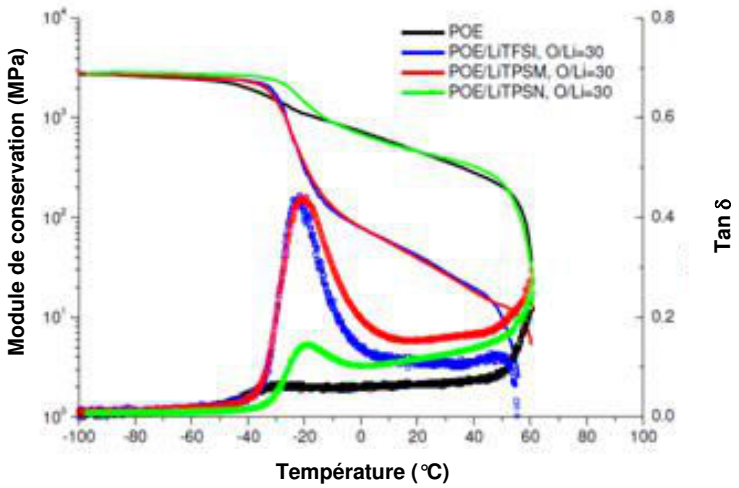

Figure 8. Module de stockage en traction (E') et Tan δ vs température à 1 Hz pour POE, POE/LiTPSM, POE/LiTPSN et POE/LiTFSI électrolytes à O/Li = 30.

Les courbes de DMA montrent que E' diminue fortement au-dessus de la température de fusion des échantillons. LiTPSM et LiTFSI impactent davantage la phase cristalline que LiTPSN : la baisse de E' à la T_α des électrolytes est beaucoup plus prononcée ainsi que la pente d (E')/dT sur le plateau cristallin.

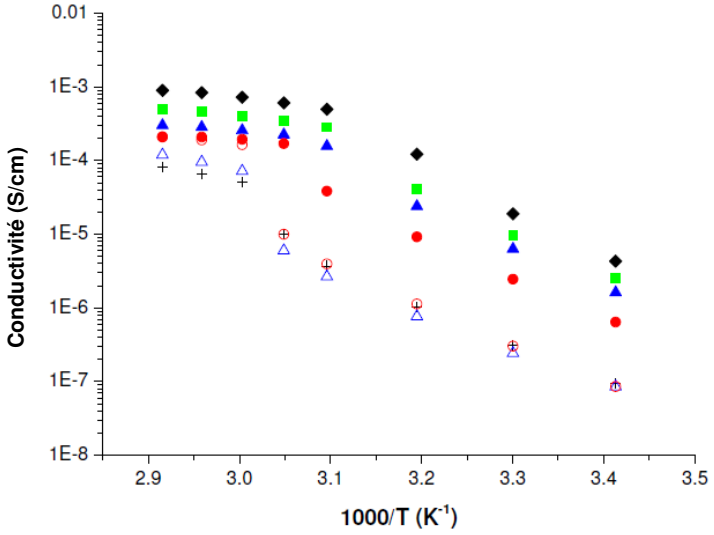

Figure 9. Comparaison de la conductivité en fonction de la concentration de sel dans POE/LiTPSM: (■) O/Li = 16, (▲) O/Li = 20, (●) O/Li = 30 et POE/LiTPSN: (+) O/Li = 12, (△) O / Li = 20, (○) O / Li = 30 par rapport à POE/LiTFSI (◆) O / Li = 20.

Les conductivités les plus élevées, 5×10^{-4} S/cm à 70 °C et $2{,}6\times10^{-6}$ S/cm à 20 °C, ont été obtenues avec POE/LiTPSM à O/Li = 16. A la même concentration (O/Li = 20), POE/LiTPSM

a montré les conductivités plus élevées que celles obtenues pour POE/LiTPSN mais toujours légèrement inférieures à celles obtenues pour POE/LiTFSI.

Les nombres de transports cationiques T^+ sont inférieurs à 0,5 pour les deux sels lorsque les sels sont dissous dans le POE.

NPC+ LiTPSM ou LiTPSN

Grâce à la faible cristallinité et T_f de NPC, le LiTPSN peut conduire à électrolytes polymères amorphes entre 29 et 34 °C, en fonction de la concentration de sel. LiTPSM, encore une fois, a fourni des cristallinités et T_f proches de celles obtenues avec LiTFSI.

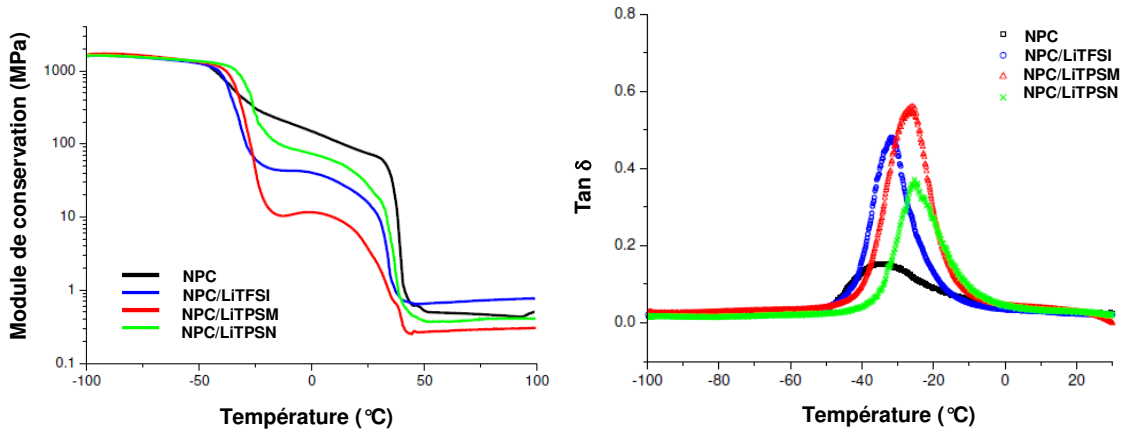

Figure 10. (a) Module de stockage en traction (E') et (b) Tan δ vs température à 1 Hz pour NPC, NPC/LiTPSM, NPC/LiTPSN et NPC/LiTFSI électrolytes à O/Li = 30.

Une T_α légèrement plus élevée est obtenue pour les électrolytes NPC/LiTPSN par rapport à NPC/LiTPSM ~ LiTFSI. La baisse de E' à T_α est beaucoup plus prononcée pour LiTPSM.

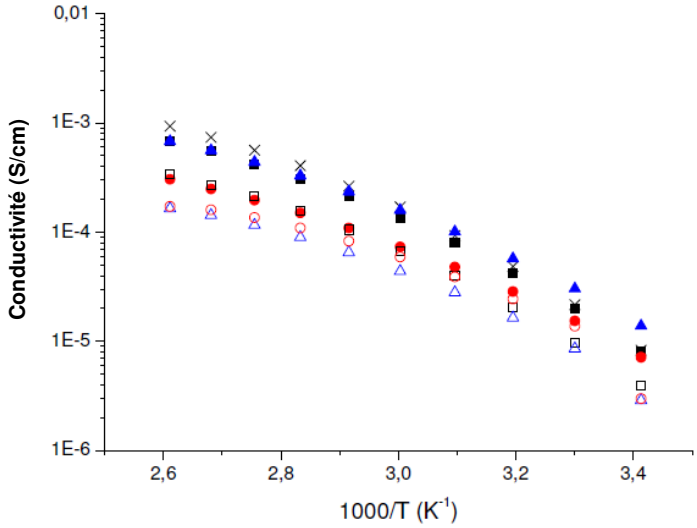

Figure 11. Comparaison de la conductivité en fonction de la concentration de sel dans NPC/LiTPSM: (■) O/Li = 12, (▲) O/Li = 20, (●) O/Li = 30 et NPC/LiTPSN: (□) O/Li = 12, (△) O / Li = 20, (○) O / Li = 30 par rapport à NPC/LiTFSI (×) O / Li = 12.

Les meilleures conductivités atteignant à 20°C, $1{,}6\times10^{-5}$ S/cm et à 110 °C, $7{,}2\times10^{-4}$ S/cm ont été obtenues pour la composition O/Li = 20 de NPC/LiTPSM électrolyte.

Les T^{+} sont plus élevés avec des électrolytes à base de LiTPSN qu'avec ceux à base de LiTPSM avec les deux techniques (PFG-NMR et EIS).

Afin d'étudier les performances des sels de lithium basé sur les 2 précédents sels à anions sulfonate /sulfonylimidure fixés sur mPEG et de les comparer avec les sels LiTPSM et LiTPSN nous avons modifié le 1,1,2,2, -tetrafluoro-2- (1,1,2,2, -tetrafluoro-2-iodoéthoxy) éthane fluorure de sulfonyle. Il est bien connu que le iodoperfluoalkyle est capable de s'additionner sur une double liaison allylique. Ensuite le SO_2F de R_F peut être transformé en SO_3Li par hydrolyse en présence de lithine ou en sulfonimidure de Li. La partie fluorée de ces sels est très proche de celle des sels LiTPSM et LiTPSN.

Ces sels sont présentés dans la Table 3.

Table 3 Sels de lithium aliphatiques étudiés dans la deuxième partie de ce chapitre

Structures chimiques	Sel de lithium
Sel de lithium alkyl perfluorosulfonate oligooxyéthylène 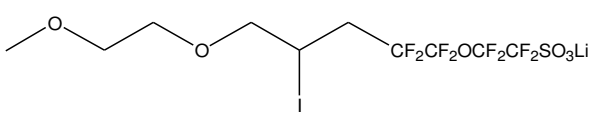	**Sel 3**
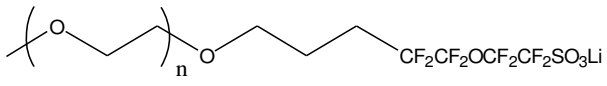 n=1 et 3	**Sel 4**
Sel de lithium alkyl perfluorosulfonimidure oligooxyéthylène 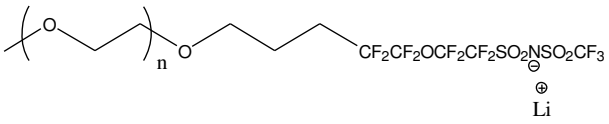 n=3	**Sel 5**

Synthèse

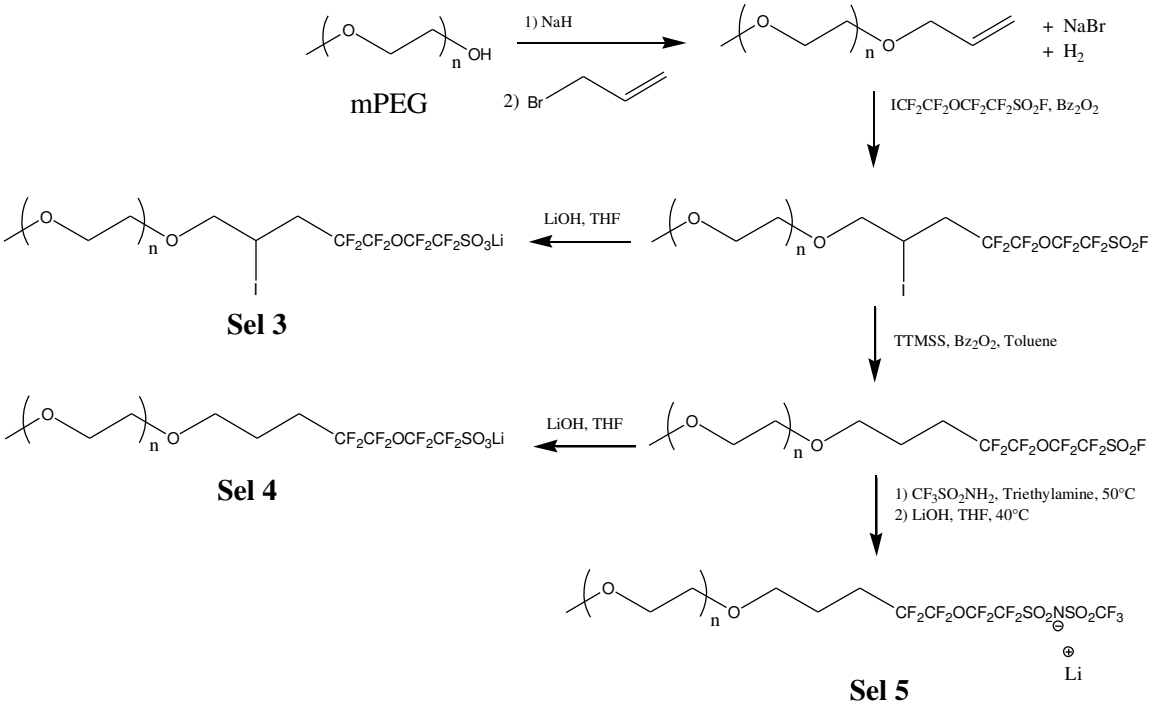

Schème 5. Synthèse de sels de lithium aliphatiques.

Caractérisations

Sels de lithium

Les composés obtenus sont caractérisés par DSC.

En ce qui concerne les sels sulfonés, la fixation d'un mPEG à l'anion perfluorosulfoné conduit à une diminution importante des valeurs de T_g et T_f. La présence d'iode volumineux et polaire dans la structure du sel semble augmenter la T_g (**sel 3n1**) par rapport au **sel 4n1** où l'iode a été remplacé par H (**sel 4n1**) alors que le point de fusion et le ΔH de fusion sont plus élevés pour ce dernier. La présence de I peut augmenter la viscosité du sel et empêcher son organisation. Cependant, l'augmentation de n de 1 à 3 (**sel 4n3**) conduit à une diminution importante de T_g, T_f ainsi que de ΔH de fusion.

En ce qui concerne les sels à base de sulfonimidure la fixation de mPEG n = 3 à l'anion conduit à un sel complètement amorphe. C'est contraire aux résultats obtenus avec les sels de référence, où le sel LiTPSM a une T_f plus élevée que LiTPSN. Pour le **sel 5n3**, nous supposons que l'ajout de mPEG, crée le désordre en raison de l'interaction de Li^+ avec le O de mPEG, et que ce désordre devrait être plus important que dans le **sel 4n3** en raison de l'asymétrie de l'anion. Par rapport au sel **2n3** (chapitre 2) les T_g sont beaucoup plus faibles pour les sels perfluorosulfonate aliphatiques, (**sel 4n1** vs **sel 2n1**, **sel 4n3** vs **sel 2n3**).

La présence de I dans la structure du **sel 3n1** diminue considérablement la stabilité thermique par rapport au **sel 4n1** (lorsque le I a été remplacé par H). Toutefois, l'apparition de la perte de poids est légèrement supérieure à celui du sel aromatique (par exemple le **sel 2n3**). En ce qui concerne l'impact de la mPEG lié à l'anion sur la stabilité du sel, nous pouvons voir, en comparant les courbes ATG de LiTPSN et LiTPSM avec celles des **sel 4n3** et le **sel 5n3**, que les seuils de perte de poids sont plus bas dans le cas des sels **4n3** et **5n3** mais qu'ils sont supérieurs à celui de mPEG. Par conséquent, nous pouvons en conclure que les pertes en poids des **sels 4n1**, **4n3** et **5n3** démarrent après la dégradation de mPEG. Les fragments formés doivent interagir avec le Li^+ retardant le début de perte de masse par rapport à celui du PEG non-ionique : mPEG n16.

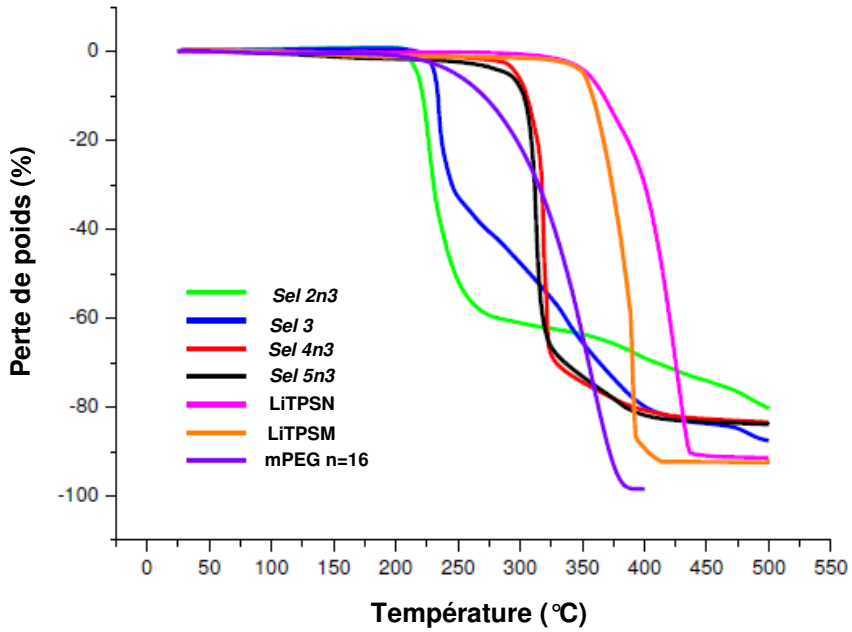

Figure 12. ATG des sels de lithium aliphatiques.

En comparant le **sel 4n3** et le **sel 5n3** ayant le même n de mPEG, le sel à anion sulfonimidure (**sel 5n3**) est plus conducteur que son homologue à anion sulfonate (**sel 4n3**). Ce résultat peut être expliqué par la faible viscosité des sels, c'est-à-dire une plus grande mobilité, comme le montre la DSC (T_g inférieure), mais aussi par une meilleure dissociation du sel à anion sulfonimidure.

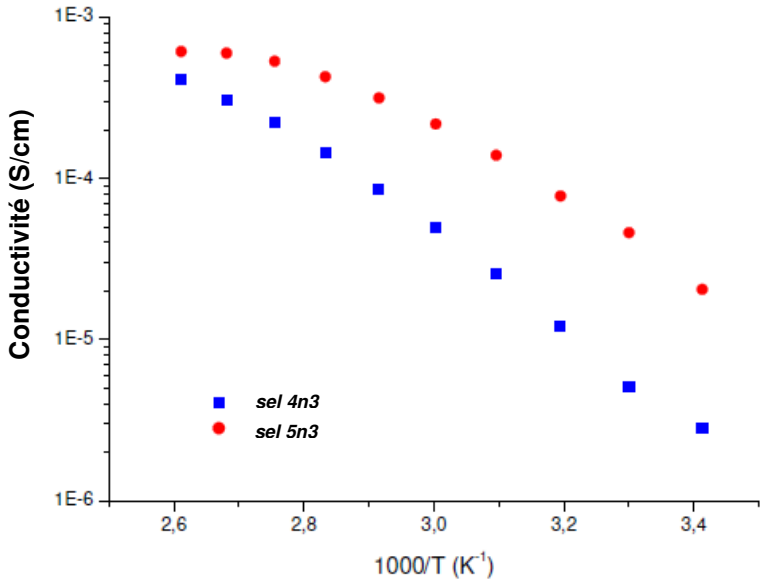

Figure 13. Conductivités des sels de lithium aliphatiques.

Le coefficient de diffusion ^{7}D du **sel 5n3** est supérieur à celui du **sel 4n3**. On peut supposer que la viscosité du **sel 5n3** est inférieure. Un plus faible degré de dissociation est obtenu pour le **sel 4n3** par rapport au **sel 5n3**.

Le nombre de transport cationique, T^{+}, du **sel 5n3** est supérieur à celui du **sel 4n3** et pourrait s'expliquer par une plus forte dissociation du **sel 5n3**.

Le **sel 3** a une plus faible stabilité en oxydation. Le mur d'oxydation du **sel 3** commence à 4,5 V et est inférieur à celles du sel LiTPSN (4,9 V). Le remplacement de I par H induit une augmentation du potentiel d'oxydation de 0,3 V qui le rapproche de LiTPSN et montre l'instabilité en oxydation générée par l'atome d'iode (rupture radicalaire de la liaison C-I ?).

Les longueurs de chaîne de mPEG n'exercent aucun effet sur le potentiel d'oxydation. En effet, à ces potentiels, les PEG ne sont pas stables. Le potentiel d'oxydation du **sel 5n3** (4,7 V) est légèrement inférieur à celle du **sel 4n3**.

POE+ Sel de lithium aliphatique

Caractérisations

En ce qui concerne l'impact de la taille de l'anion, pour la même concentration O/Li, on observe une légère diminution de T_g avec l'augmentation de la longueur de chaîne mPEG (**sel 4** n = 1 et n = 3), ce résultat est similaire à ceux rapportés sur le **sel 2** (chapitre 2). Comme pour le **sel 2** une augmentation de T_f et de cristallinité est observée lorsque la valeur n du PEG augmente. Les T_f et cristallinité les plus basses ont été obtenues pour le **sel 5n3**.

Toutes les observations en DMA amènent à la conclusion que la fixation d'un mPEG sur des anions change considérablement les interactions entre le sel et le polymère hôte (POE). La diminution dramatique du module de stockage après T_α peut être expliquée par une plus forte teneur en phase amorphe en raison de la contribution du sel.

Les résultats corroborent ceux obtenus par DSC dans le premier balayage en température, où la T_g du POE <POE+LiTPSN <POE + **sel 4n1** <POE+**sel 4n3** alors que T_f et le ΔH de fusion varient en sens opposé (POE> POE +LiTPSN> POE+**sel 4n1**> POE+**sel 4n3**) (figure 14 (a).).

Si l'on compare les électrolytes POE+**sel 2n3** (aromatique), POE+**sel 4n3** (aliphatique) et POE+**sel5n3** (aliphatique), on observe que la T_α du sel de lithium aromatique est supérieure à celles des sels de lithium aliphatiques. Ce comportement indique que la présence du noyau

aromatique dans le sel induit à la fois (i) une plus grande rigidité du complexe (POE/sel) et (ii) réduit l'impact du sel sur le degré de cristallisation du polymère hôte (POE) (figure 14 (b)).

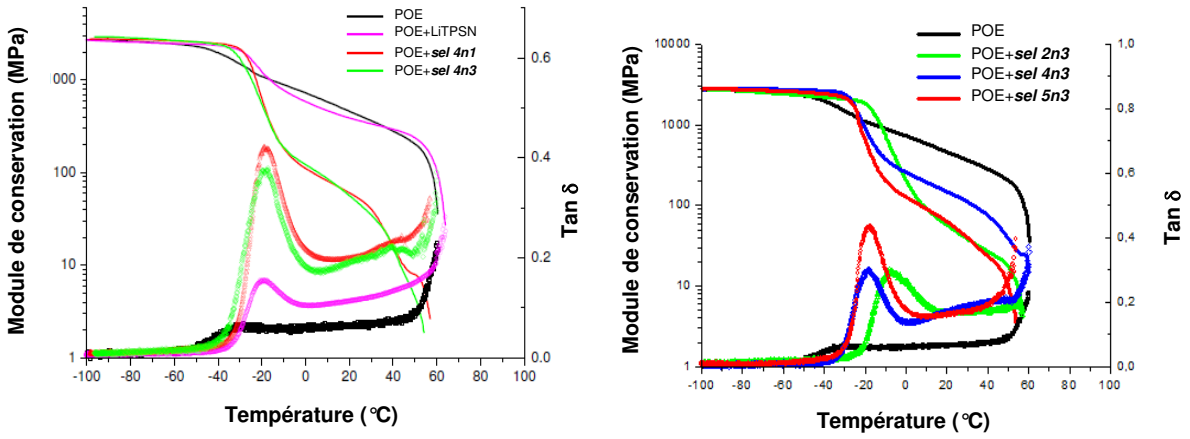

Figure 14. Comparaison des propriétés mécaniques du **sel 2n3** (aromatique) et des sels de lithium aliphatiques à la concentration O/Li= 20.

Les conductivités des électrolytes polymères à base de mPEG aliphatique, sulfonimidure (**sel 5n3**), aliphatique sulfonate (**sel 4n3**) et aromatique sulfonate (**sel 2n3**), et de POE ont été comparées, le premier électrolyte s'avérant le plus conducteur dans toute la gamme de températures explorée (figure 15).

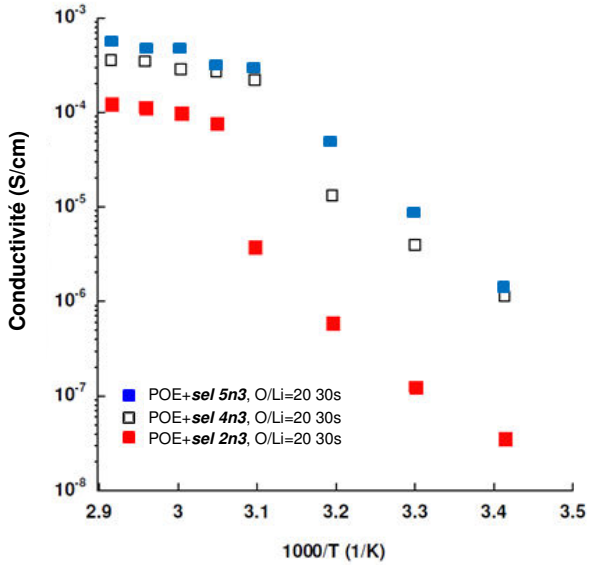

Figure 15. Comparaison des conductivités des électrolytes polymères : POE/**sel 2n3**, POE/**sel 4n3** et POE/**sel 5n3**, O/Li=20.

Les conductivités de l'électrolyte à base de **sel 4n3** ne sont pour autant pas négligeables. Ainsi ses conductivités sont au moins deux fois plus élevées que celles de l'électrolyte polymère du **sel 2n3**. Ce résultat indique que la présence d'un cycle aromatique augmente la rigidité et la viscosité de l'électrolyte polymère. Cette hypothèse est confortée par les résultats de DSC et de DMA.

Les coefficients de diffusion des anions sont plus élevés que ceux de Li^+ pour tous les sels. Toutefois, ils sont plus faibles que ceux des anions de LiTPSM ou de LiTPSN.

Le coefficient de diffusion plus faible de l'anion dans le cas d'électrolytes polymères à base de **sel 3n1** est probablement dû à l'interaction de Li^+ avec I qui porte une charge partielle δ. Il est surprenant d'observer que les valeurs de ^7D pour les **sel 4n1**, **sel 4n3** et **sel 5n3** sont très proches.

Ce résultat souligne que ^7D est indépendant de la longueur et de la nature des anions discutés ici (sulfonate ou sulfoimidure). D'autre part les sels à base d'anion aliphatique ont des coefficients de diffusion, anion et cation, supérieurs à ceux des sels incorporant un cycle aromatique.

Dans le cas de l'anion sulfonate, T^+ augmente avec l'augmentation du n de mPEG. Cependant, malgré la masse molaire supérieure de l'anion du **sel 3n1**, son T^+ est inférieur à celui du **sel 4n1**. En outre, le T^+ du **sel 3n1** obtenu par des mesures électrochimiques est inférieur à celui du LiTPSN. La présence d'iode dans la structure de sel doit ralentir la migration de Li^+. Nous pouvons noter également que les valeurs de T^+ de LiTPSN et du **sel 4n3** sont plus élevées quand ils sont calculés à partir des mesures électrochimiques, tandis que pour le LiTPSM et le **sel 5n3**, des résultats inverses sont obtenus. La fixation de l'anion mPEG conduit à des électrolytes polymères ayant de meilleures conductivités cationiques et il semble que les valeurs soient proches ou supérieures à celles obtenues pour POE/LiTFSI ($1{,}74 \times 10^{-4}$ S/cm).

NPC+ Sel de lithium aliphatique

Caractérisations

Les valeurs de T_g et T_f d'électrolytes (NPC+sel) sont, malgré l'effet plastifiant des anions, plus élevées que celles de la matrice hôte NPC. En ce qui concerne le temps d'irradiation (30s vs 1 min), les membranes qui ont été réticulées pendant 1 mn ont de plus faible T_g et T_f que celles irradiées pendant 30s. Un temps d'irradiation plus long devrait améliorer la densité

de réticulation qui induit généralement une augmentation de T_g. Dans notre cas, l'obtention de T_g plus basses peut s'expliquer par la diminution significative de cristallinité (phase cristalline contraint la phase amorphe), qui contrebalance la rigidification produite par une densité de réticulation plus élevée. En effet, la formation des ponts de réticulation crée du désordre et empêche la cristallisation des segments de NPC.

L'évolution de la T_g avec la concentration ne suit pas la même tendance que pour les électrolytes à base de POE, à savoir augmentation de la T_g avec la diminution de O/Li. Cela peut être expliqué par le fait que la densité de réticulation peut être affectée par la concentration en sel.

En ce qui concerne les propriétés mécaniques, nous avons observé que la fixation de mPEG à l'anion de LiTPSN, induit une diminution 1) du module de stockage après la T_α, 2) de la valeur de T_α 3) du module de stockage sur le plateau (après la fusion de NPC). L'impact sur T_α et sur le module de stockage avant le point de fusion est similaire à celui du POE, cependant l'effet du mPEG fixé à l'anion est moins spectaculaire. Cependant, la T_f ne semble pas être affectée par la présence de mPEG (figure 16 (a)).

Concernant l'impact de mPEG sur le comportement mécanique des électrolytes à base de LiTPSM (figure 16 (b)) anion les courbes sont très similaires avant le plateau caoutchouteux. Sur le plateau caoutchouteux le module de conservation est à peu près 0,5 MPa pour l'électrolyte NPC+LiTPSM tandis que pour NPC+**sel 5n3** il est supérieur à 1 MPa. Ainsi, pour les électrolytes polymères à base de **sel 5n3** nous pouvons supposer un degré de réticulation plus élevé.

Si l'on compare les temps d'irradiation, les membranes irradiées 1 mn ont un module de stockage après fusion i.e.sur le plateau caoutchouteux) plus élevé en relation avec un degré de réticulation plus élevé (figure 16 (c)).

En ce qui concerne l'influence de l'anion perfluorée, la T_α de NPC+**sel 5n3** est inférieure à celle de NPC+**sel 4n3**, en accord avec les T_g obtenues par DSC lors du premier balayage en température. Cependant, au-dessus de T_α on observe une augmentation du module de stockage pour l'électrolyte NPC+**sel 5n3**, en raison de la recristallisation de la membrane. Le module de stockage sur le plateau caoutchouteux est plus élevé pour l'électrolyte à base de **sel 5n3** probablement en raison du degré de réticulation plus élevé.

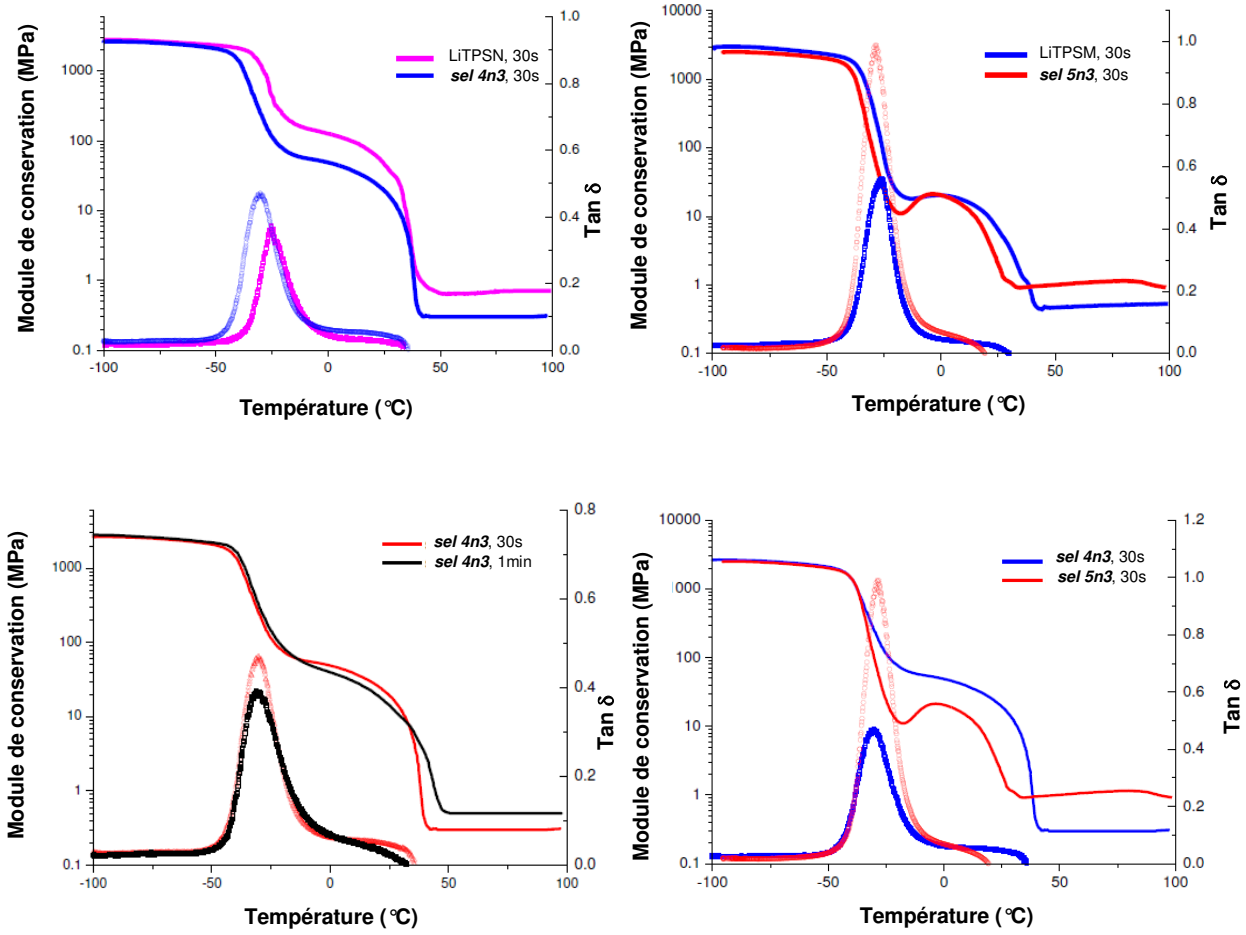

Figure 16. Module de stockage en fonction de la température pour différents électrolytes polymères à base du polymère hôte NPC à O/Li = 30 et à différents temps d'irradiation.

(a) NPC+LiTPSN et NPC+**sel 4n3**, O/Li= 30, 30 s, (b) NPC+LiTPSM et NPC+**sel 5n3**, O/Li= 30, 30 s, (c) NPC+**sel 4 n3** et NPC+**sel5n3**, O/Li = 30, 30 s et 1 min (d) NPC+**sel4n3** et NPC+**sel 5n3**, O/Li = 30, 30s.

Les effets du polymère hôte (POE, NPC) sur les conductivités des électrolytes, basée sur les **sels 4n3, 5n3**, sont comparées dans la figure 17. Les conductivités des électrolytes à base de **sel 4n3** + POE et de **sel 5n3** + POE sont légèrement supérieures à celles des membranes à base de NPC au-dessus de la température de fusion, T_f, tandis qu'en dessous de T_f, les conductivités des électrolytes à base NPC sont environ 10 fois plus élevées. La cristallinité et T_f beaucoup plus faibles de NPC expliquent ce gain de conductivité à basse température.

La fixation de la chaîne mPEG sur les anions de LiTPSN et LiTPSM permet de pointer deux effets opposés. Ainsi, dans le cas d'anions $TPSN^-$ la conductivité augmente lors de sa

fixation sur mPEG ; un résultat similaire à celui obtenu avec des électrolytes polymères à base de POE. Au contraire, la fixation de mPEG à TPSM- semble diminuer la conductivité ; un résultat opposé à celui observé pour ce sel en solution dans POE. Une explication de ce comportement opposé pourrait être le degré de réticulation du film à base de **sel 5n3** plus élevée par rapport au film à base LiTPSM et une diminution de la mobilité des chaînes POE comme l'établit l'analyse DMA.

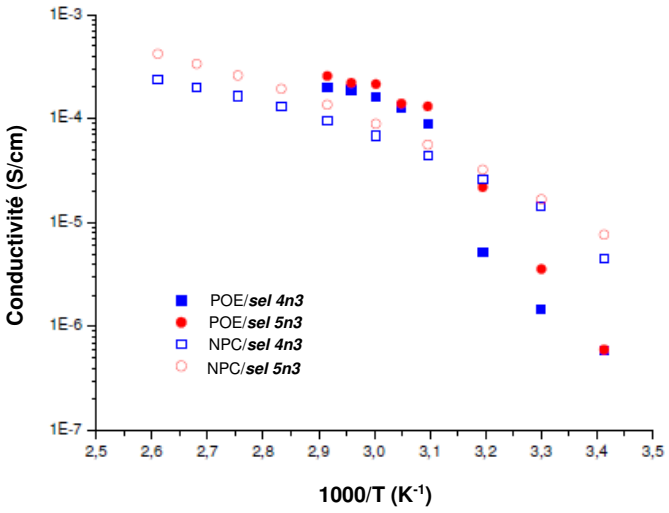

Figure 17. Comparaison des conductivités entre le **sel 4n3** et le **sel 5n3** dans les matrices POE et NPC.

Abstract

The new families of lithium-conducting ionic liquids; aromatic and aliphatic lithium salts based on perfluorosulfonate and perfluorosulfonylimide anions attached to an oligoether (methoxy polyethylene glycol mPEG) with different lengths were synthesized and characterized with the aim to improve the salt interaction with the host polymer's POE chains while keeping a high segmental mobility. They allowed obtaining membranes with lower crystallization degree and higher cationic transport number as compared with benchmarked salts. Their properties as lithium salts were investigated in two types of host polymers i.e. a linear polyether (POE) and a cross-linked polyether prepared by a 'GREEN' process. Their oligooxyethylene moieties improve the lithium cation solvation leading to an increase in cationic transference numbers. Their electrochemical and thermal stabilities are suitable for lithium battery application.

Key words: PEO; POE; Lithium salt; Polymer electrolyte; Ionic conductivity; Transference numbers

Résumé

De nouvelles familles de liquides ioniques conducteurs par ion lithium; à anions aromatiques et aliphatiques de type perfluorosulfonate perfluorosulfonylimidure attachés à des oligoéthers (méthoxy polyéthylène glycol mPEG) de longueurs différentes ont été synthétisées et caractérisées dans le but d'améliorer l'interaction entre les chaînes de POE et les sels de lithium en améliorant la mobilité segmentaire. Ainsi différentes membranes amorphes ou peu cristallines améliorent le transport cationique par rapport aux électrolytes polymères usuels. Leurs propriétés ont été évaluées dans deux types de polymères hôtes : un polyéther linéaire (POE) et un polyéther réticulé préparé par un procédé "VERT". Leurs parties oligooxyéthylène aident à la solvatation des cations lithium et conduisent à l'augmentation des propriétés de transport; c'est à dire la conductivité cationique et le nombre de transport. Leurs stabilités thermiques et électrochimiques sont adaptées à l'application batterie lithium-polymère.

Mots-clés : PEO; POE; sel de lithium; Electrolyte polymère; Conductivité ionique; Nombre de transport.